The Role of the General Circulation in Western Pacific Tropical Cyclone Genesis

by
Geoff Love

P.I. William M. Gray

Department of Atmospheric Science
Colorado State University
Fort Collins, Colorado

NSF ATM-7923591

Colorado State University

Department of Atmospheric Science

Paper No. 340

THE ROLE OF THE GENERAL CIRCULATION IN WESTERN PACIFIC TROPICAL CYCLONE GENESIS

By

Geoff Love

Atmospheric Science Department

Colorado State University

Fort Collins, Colorado

March, 1982

Atmospheric Science Paper No. 340

ABSTRACT

This study investigates the role that large scale circulation patterns play in tropical cyclone genesis. The data available for this study were largely from stations within the eastern hemisphere, accordingly the paper addresses the problem of defining the important flow features observed prior to cyclone genesis in the northwest Pacific and Australian region. A combination of case study and compositing has been used to identify those weather systems which interact with a pregenesis tropical cloud cluster, enhancing its development potential.

A comparison of pre cyclone genesis conditions with those observed during non cyclone genesis periods reveals more vigorous Hadley circulations between the subtropical ridges in both hemispheres and the ITCZ. The acceleration of the winter hemisphere Hadley cell in response to cold surge forcing appears to be very dominant.

In order to better understand the planetary scale adjustment processes resulting from these winter hemisphere surge situations, a series of simple numerical model experiments have been carried out. The shallow water equations have been solved for an arbitrary time dependent forcing in either wind or height field. Spherical geometry and a realistic pole to pole zonal wind profile have been used.

These experiments indicate that energy propagation from the midlatitudes to the deep tropics is dependent upon the scale of the forcing and the background wind field. For northern hemisphere midlatitude forcings which are equivalent barotropic in nature, it is possible to generate large amplitude responses in the southern hemisphere regardless of the intervening wind fields.

An important role of the tropics in all simulations appears to be to provide a region where 'down the pressure gradient' flow may readily occur, assisting in the adjustment processes to planetary scale forcings.

TABLE OF CONTENTS

TABLE OF CONTENTS (cont'd)

$\mathbb{V}_{AT}$	Antitriptic wind vector
$\mathbb{V}_g$	Geostrophic wind vector
V_R	Radial wind component
V_T	Tangential wind component
w	Vertical velocity = dz/dt
x	Eastward distance
y	Northward distance
z	Upward distance
α	Specific volume (also time constant in Chapters 7 and 8)
β	$\partial f/\partial y$
γ	Constant = $\sqrt{gh/2\Omega}$
δ	A small increment
ζ	Relative vorticity
θ	Potential temperature
θ_e	Equivalent potential temperature
λ	Longitude positive eastward
ρ	Density
ρ_W	Density of water
σ	Frequency
ϕ	Latitude, positive northwards
Ψ, ψ	Streamfunction
Ω	Angular speed of rotation of earth.

LIST OF SYMBOLS

a	Radius of the earth
c	Phase speed
C_D	Drag coefficient
C_g	Group velocity
C_W	Specific heat of water
f	Coriolis parameter = $2\ \Omega \sin \phi$
g	Gravity
h	Depth of fluid
h_e	Equivalent depth
H	Humidity parameter
$H(\phi)$	Depth of fluid in gradient wind balance
k	Zonal wavenumber
$\hat{k}$	Unit vector in local vertical
K	Guldburg-Mohn coefficient
ℓ	Meridional wavenumber
P	Pressure
R	Gas constant for dry air
r	Radius
r_e	e-folding radius
RH	Relative humidity
T	Temperature
t	Time
u	Zonal wind speed
v	Meridional wind speed
$\mathbb{V}$	Horizontal wind vector

1. INTRODUCTION

1.1 Background

For some considerable time there has been interest in the possible role that broad scale flow patterns play in tropical cyclone development. Some works relating to this area of research are: Ballenzweig (1956), Morgan (1965), Haggard (1965), Gray (1967), Carlson (1969), Namias (1969), Carlson (1969 and 1971), Namias (1973), Ramage (1974), Flohn (1975), Ding (1980a, 1980b and 1981) and many others for too numerous to detail. A review of these papers reveals that due to the complex interaction between the developing vortex and its environment, both the dynamic and thermodynamic large scale fields are believed to be important. Less well documented is the feeling among forecasters of the Australian, Chinese and Indian meteorological services, that what occurs in the Inter-Tropical Convergence Zone (ITCZ) is determined in some way by events in both winter and summer hemispheres. As most storms in the eastern hemisphere form close to the ITCZ, it may be conjectured that the climatology of these storms is related to the flow regimes of both hemispheres.

A study by Gray (1979) of the temporal distribution of storm genesis events for twenty seasons in both Northern and Southern Hemispheres reveals the presence of quiet periods, with little or no cyclone genesis followed by active periods with a number of genesis events. Figures 1 and 2 show the temporal distributions of genesis events for twenty years. It may be noted that while there is considerable variability in the length of quiet and active periods, they are of the order of two weeks or so. These data also provide additional circumstantial evidence that the environment in which a cloud cluster is

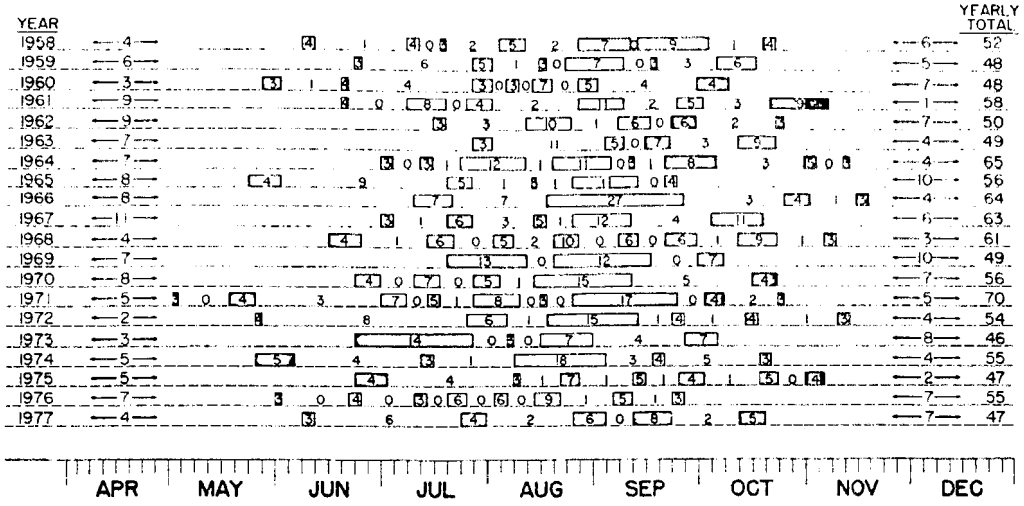

Fig. 1. Time and space clustering of Northern Hemisphere cyclone genesis. Numbers in shaded areas give the numbers of tropical cyclone formations during active genesis periods. Numbers of formations during inactive periods are also shown in areas without shading. Numbers between arrows indicate the numbers of cyclone formations before and after the active genesis periods. (After Gray, 1978).

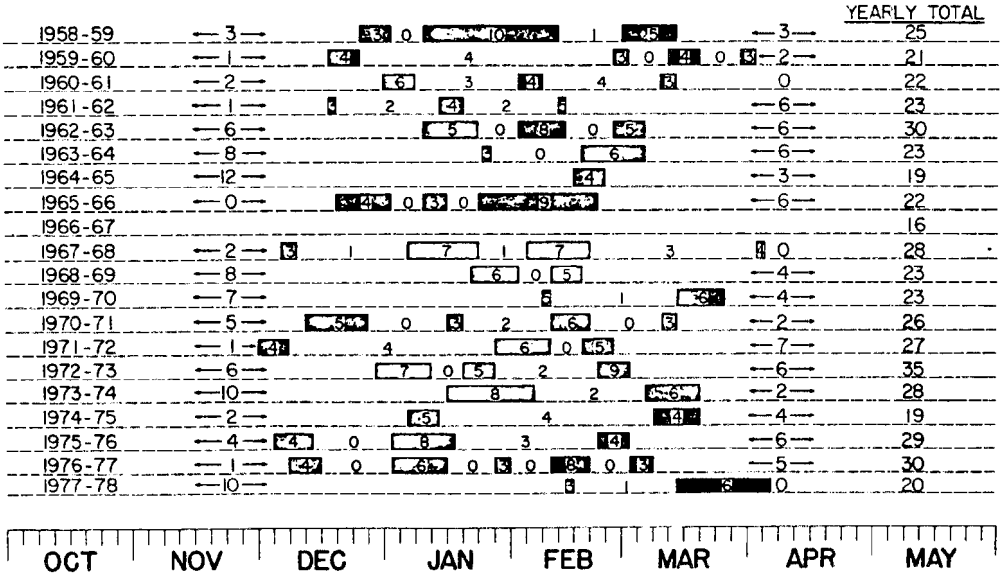

Fig. 2. As for Fig. 1, except for the Southern Hemisphere.

embedded plays a part in determining its future. It has been noted by Gray (1979) that while clusters propagate through the area of possible genesis every four or five days, only in certain periods do clusters develop into tropical storms. Assuming that each cluster has similar internal structure, its environment must then be a crucial factor in its development.

An analysis of the large scale dynamic and thermodynamic parameters relating to tropical cyclone genesis by Gray (1975) indicates that while the thermodynamic fields are relatively slowly changing the dynamic (wind) fields show much shorter time scale changes. However, for cyclone genesis to occur a favorable dynamic and thermodynamic environment is required. Figure 3 shows schematically how these dynamic and thermodynamic parameters combine to lead to conditions favorable for cyclone genesis. Favorable conditions may be expected to arise when the sum of the dynamic and thermodynamic genesis potential parameters exceed some critical level. The thermodynamic potential changes slowly, reaching a maximum sometime in summer. The dynamic potential changes on a time scale of days, leading to the quiet and active periods observed in the cyclone genesis time series. As will be seen from the analyses presented in this paper, an important modulator of the dynamic genesis potential parameter is the midlatitude weather systems.

1.2 Towards a Theory for Tropical Cyclone Genesis

Before proceeding to study the large scale circulation patterns for recurring features preceeding tropical cyclone genesis, it is useful to have some understanding of how tropical cyclone genesis proceeds. With such an understanding, the investigator may concentrate on those atmospheric fields important in the genesis process.

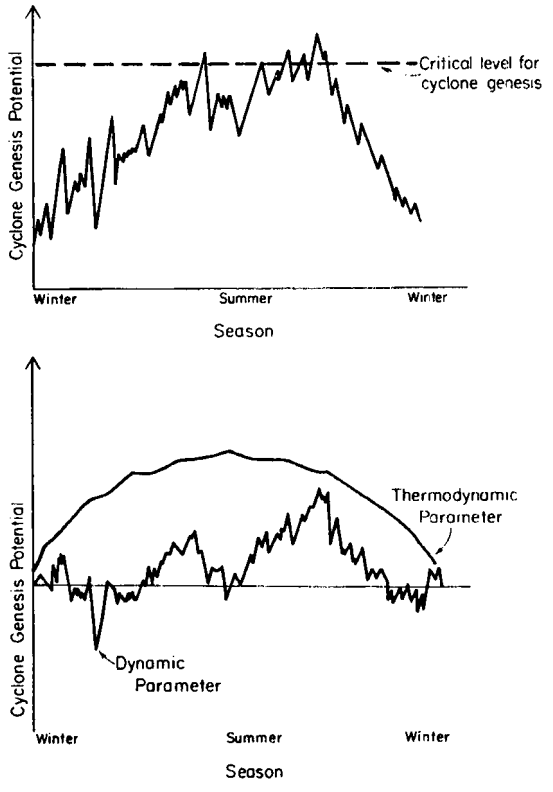

Fig. 3. An idealized picture of how the large scale dynamic and thermodynamic parameters interact to bring about conditions favorable for tropical cyclone genesis.

Studies by Gray (1968, 1975 and 1981), Frank (1977a, 1977b), McBride (1981a, b, c), Lee (1981) and Holland (1981) have done much to define the requirements, both dynamic and thermodynamic, of a developing tropical cloud cluster, modeling studies by Ooyama (1964 and 1969), Charney and Eliassen (1964), Silva Dias and Schubert (1979), Fingerhut (1981) and Hack and Schubert (1981) and others have contributed to the understanding of the basic physical processes of tropical weather systems. However, there is still no generally accepted genesis theory, and so it is not possible to specify precisely how the energy and angular momentum requirements of a tropical cloud cluster 'spinning up' to tropical storm intensity are met.

The observational studies of Riehl and Malkus (1961) and others have shown that the energy to drive tropical cyclones is derived from the release of latent heat in deep cumulus convection. The moisture required by these systems comes from evaporation at the sea surface and import from the environment surrounding the area of convection. The work of McBride (1981c), following that of Gray (1973) and Yanai et al. (1973) reveals that all classes of tropical maritime weather systems are large exporters of moist static energy. In order then that the energy budget be balanced there is a required large flux of energy from the sea surface to the tropospheric circulation. For intensifying cloud clusters there is an energy accumulation within the system and an export. In order to meet these additional energy accumulation requirements, there must be higher ocean to atmosphere energy fluxes in intensifying systems than in steady state or decaying systems. Gray (1981) has speculated that convection embedded in the strongly sheared environment of a developing cloud cluster more efficiently promotes the upward energy flux from the sea surface than convection embedded in the weakly sheared non-developing cluster environment. The data considered in later chapters of this paper have a spatial resolution of the order of five degrees which is far too coarse to resolve cumulus scale events. Questions concerning the nature of the interaction between cumulus dynamics and synoptic scale flow fields are not addressed, rather, the role the planetary scale flow fields play in genesis establishing the observed strongly sheared pregenesis environment is investigated.

McBride (1981b, 1981c) has noted that developing systems have greater outer radius low level cyclonic and upper level anticyclonic surrounding tangential wind fields. Furthermore, he notes the angular

momentum budgets differ greatly between these systems. Holland (1981) presents a detailed analysis of the angular momentum budgets for four categories of northwest Pacific composite tropical cyclones. To the full extent of the composite grid used in the study, inward transports of cyclonic angular momentum are required to balance the losses due to frictional dissipation at the surface. The apparent source region of relative angular momentum is not contained within a ten degree radius of the composite grid. Thus, it must be inferred that the weather systems, at radii greater than 10^{o} are arranged in such a fashion to permit these favorable transports. Holland (1981) following the work of Palmen and Riehl (1957), Pfeffer (1958) and others calculates the shear generation by differential angular momentum transports. A generation of anticyclonic shear, with anticyclonic flow above low level cyclonic flow, is associated with intensifying cyclonic weather systems. For intensifying systems, the horizontal transports of angular momentum lead to anticyclonic shear generation to a radius of 10^{o}. For decaying systems the transports are uniformly inadequate, to a radius of ten degrees, to support increased shears within four degrees.

It is thus apparent that both energy and angular momentum requirements of a system must be met if intensification is to occur. If the cloud cluster cannot provide the moisture for its convective elements, then the necessary latent heat release to drive the system cannot be met. If the large scale angular momentum transports into the system do not balance the surface loss, the system must spin down.

From the work of McBride (1981b) it would appear that if a cloud cluster is to undergo tropical cyclone genesis, a crucial factor is the generation of differential shear at large radii, far beyond the extent

of cloudiness (which typically extends to about 4^{o} radius (Arnold, 1977)). If this is so, then the question remains: what are the basic physics behind the individual genesis event? How is it that certain systems retain more of the energy released internally than others? One may speculate that in a pre genesis cluster, because its radius is much less than the Rossby radius of deformation, the inner region temperature anomaly is proportional to the vertical distribution of shear in the tangential wind field. Anticyclonic shear generation, by large scale circulation features, in the tangential wind field (in the early stages) will lead to greater heat retention in the inner core. As the vorticity rises, so the efficiency of partitioning the released latent heat energy to the tangential wind field, rather than gravity wave field, increases. And so, for intensification, the ability of the system to enhance the surface energy flux within the cloudiness region may be crucial.

The problem of where intensification starts and genesis ends is not addressed in this paper, rather, the large scale fields are studied to detect changes in organization which lead to increased shears around ITCZ disturbances. As the data of Gray (1981), McBride (1981b) and Holland (1981) indicate, the dynamic influences extend beyond the fifteen degrees radius of the composite grid, an area of 100^{o} latitude by 90^{o} longitude has been studied. The resolution of the data used has been such that the cloud cluster is only crudely resolved. Questions of how the cumulus scale processes interact with the synoptic scale are not addressed within the paper. The complex questions concerning the nature of changes in the thermodynamic structure during tropical cyclone genesis have been left to other workers.

In summary then, those data analyzed by Gray and others indicate that the thermodynamic environment of a cluster changes on a relatively long time scale. The dynamic fields, such as wind shear, are influenced greatly by events outside the cloudiness region, in fact by events outside the composite grid outer radius and appear to change on a much shorter time scale than the thermodynamic parameters. This paper describes in detail the type of flow fields which induce favorable shears about an ITCZ disturbance and attempts to deduce the physical mechanisms of large scale interactions.

1.3 Structure of the Paper

The aim of this paper is to document how the weather systems surrounding a cloud cluster in the ITCZ trough bring about the environment of increased tangential vertical wind shear which is necessary for tropical cyclone genesis. The majority of ITCZ type storms form in the eastern hemisphere where there is an adequate network of Northern and Southern Hemisphere weather stations. Accordingly, this paper concentrates exclusively on tropical cyclone genesis in the eastern hemisphere.

Throughout the paper tropical cyclone genesis is defined as occurring when a cyclonic vortex over an ocean of sea surface temperature in excess of 26.5^{o}C is first analyzed, in a post analysis, to have gradient level winds equal or exceeding 34 kts. This definition is consistent with that used in tropical cyclone forecasting centers throughout the world (Pellissier, 1979, pg. I.2.1).

Chapter two deals with the global climatology of tropical storm occurrence. This provides a background for the more detailed eastern hemisphere case study and composite work. Two contrasting seasons are

studied which reveal that while storm genesis locations may differ greatly from year to year, the related thermodynamic parameters within the tropical genesis areas are little changed. Dynamic parameters do show considerable variability over quite large areas between the seasons, indicating the large scale dynamic forcings to be important. These data also hint at some of the flow changes which may be important to the changed storm genesis climatology.

In chapter three, two case studies are presented which illustrate the evolution of both winter and summer hemisphere flow fields prior to tropical cyclone genesis in the eastern hemisphere. These case studies suggest teleconnections are in effect over the region between the winter hemisphere subtropical ridge and ITCZ. In Chapter 4 the observed teleconnections are further investigated through the use of time series data.

Chapters 5 and 6 deal with the results obtained from compositing a large number of pre cyclone genesis days over an area of approximately 100^{o} latitude by 90^{o} longitude. These results are contrasted with similar 'quiet period' composites. These data reveal the Chapter 3 case studies to be typical of ITCZ tropical cyclone genesis events. The much greater data density in the composites compared to the case studies enables a detailed analysis of the pre genesis flow fields.

The data analyzed in the first six chapters indicate that a tropical response to a midlatitude forcing, on a time scale of several days, is occurring. In Chapters 7 and 8 the possibility of such rapid, large scale energy propagation is investigated through the use of a simple, linear, global model. Forcings are selected to resemble the essential features of those weather systems observed in earlier

chapters, and the subsequent adjustment of the model studied. Qualitative conclusions are drawn as to how the planetary scale adjustment processes proceed. One of the more striking results from these simulations is the ability of energy to propagate through regions of easterly flow, in the divergent, spherical geometry shallow water model.

2. TROPICAL CYCLONE CLIMATOLOGY

2.1 Introduction

In order to better understand how a particular weather event is related to the larger scale circulation patterns a knowledge of the climatology of the weather event and the dynamic and thermodynamic parameters relating to that event are useful. In this chapter a brief review of the global climatology of tropical cyclones is presented along with a discussion of the atmospheric conditions required for their genesis.

The locations of tropical storm genesis points and the subsequent movement of storms shows a great deal of variability from year to year. It is believed that those parameters which are related to genesis and which show considerable year to year variability may well be responsible for the annual differences in storm climatology. A comparison is made between some features of the tropospheric circulations during the tropical cyclone seasons of 1975 and 1977, for both the northern and southern hemispheres. In agreement with Gray's (1975) results, the data analyzed support the conclusion that there is more seasonal variability in dynamic parameters than in the thermodynamic parameters. It is also noted that the winter hemisphere flow regimes are very different during these two years, suggesting that cross-equatorial effects may be important. This interhemispheric interaction question is investigated in more detail in later chapters of this paper.

2.2 The Global Climatology of Tropical Storms

There are approximately eighty tropical storms with maximum sustained winds of at least 20 m s^{-1} over the globe per year. Table 1 gives the ocean basin breakdown of this annual number of genesis events

TABLE 1

Yearly Variation of Tropical Cyclones by Ocean Basin (Adapted from Gray, 1979).

Year	S. Hemp.	NW ATL	NE PAC	NW PAC	N INDIAN	S INDIAN	AUST	S PAC	TOTAL
1958	1958-59	12	13	22	5	11	11	7	81
1959	1959-60	11	13	18	6	6	13	2	69
1960	1960-61	6	10	28	4	6	8	8	70
1961	1969-62	11	12	29	6	12	7	4	81
1962	1962-63	6	9	30	5	8	17	3	78
1963	1963-64	9	9	25	6	9	7	7	72
1964	1964-65	13	6	39	7	6	9	4	84
1965	1965-66	5	11	34	6	12	7	4	79
1966	1966-67	11	13	31	9	5	5	6	80
1967	1967-68	8	14	35	6	11	9	8	91
1968	1968-69	7	20	27	7	8	7	8	84
1969	1969-70	14	10	19	6	10	7	6	72
1970	1970-71	8	18	23	7	11	12	3	82
1971	1971-72	14	16	34	6	7	14	6	97
1972	1972-73	4	14	28	6	13	12	10	88
1973	1973-74	7	12	21	6	4	16	8	74
1974	1974-75	8	17	23	7	6	10	3	74
1975	1975-76	8	16	17	6	8	16	5	76
1976	1976-77	8	18	24	5	9	12	9	85
1977	1977-78	6	17	19	5	6	7	7	67
TOTAL		176	268	526	121	168	206	118	1583
AVERAGE		8.8	13.4	26.3	6.0	8.4	10.3	5.9	79.1
S. DEV.		2.97	3.65	6.25	1.05	2.64	3.57	2.29	7.73
%VAR'N.		34	27	24	17	31	35	39	10

for a 20 year sample. The standard deviation of the annual number of storms when divided by the average can be used to give the percent variation of one standard deviation from the mean. It can be seen (in Table 1) that while globally there is only 10% variability per year, the individual basins have between 16% and 39% variability. Furthermore, the ratio of northern hemisphere to southern hemisphere genesis events varies from 1.5 to 4.0.

Figure 4 gives the mean latitudinal distribution of genesis points in six tropical ocean basins. The southern hemisphere storms show a very tight distribution around 13°S while genesis in the northern hemisphere may occur further poleward in the mean. Figure 5 showing the summer sea surface temperature distribution indicates why southern hemisphere storms rarely form poleward of 17°S. The lack of continents poleward of 35°S ensures polar waters may flow equatorwards maintaining cold sea surface temperatures relatively close to the equator when compared with the northern hemisphere. The need for sea surface temperatures in excess of 26.5°C (84°F) for tropical cyclone genesis is well known (Palmen, 1948).

About two thirds of all storms form in the northern hemisphere, similarly about two thirds form in the eastern hemisphere. This study concentrates on the eastern hemisphere, where nearly all southern hemisphere storms form and where a good distribution of tropical station data are available both north and south of the equator.

Gray (1968, 1975 and 1978) discusses in great depth the climatological controls which act upon tropical clusters to determine their future intensity. It appears that tropical cyclone frequency on a seasonal basis can be directly related to six parameters.

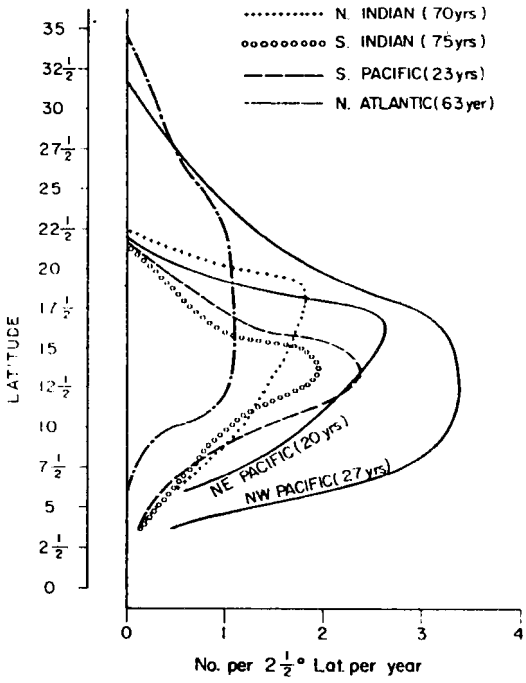

Fig. 4. Latitude at which initial disturbances which later become tropical cyclones were first detected for the six genesis areas. Number of years in data average in parenthesis. (After Gray, 1979).

i) The low level vorticity (ζ). Other conditions being favorable and remaining constant, the analysis of a great deal of data by Williams and Gray (1973) and McBride (1981b) shows that a deep layer of lower tropospheric cyclonic vorticity is favorable for cloud cluster 'spin-up' to tropical cyclone intensity.

ii) The earth's rotation (f). Cyclones rarely form within 4° latitude of the equator. It would appear the Coriolis parameter is too small.

iii) Zero vertical shear (S_z). McBride (1981b) has shown that the outer region vorticity shear between the surface and 200 mb is a maximum in developing clusters. For this to be so, an upper level anticyclone must overlie the low level cyclonic circulation. This being the case the zero shear lines of zonal and meridional winds will pass close to the center of the vortex.

iv) Ocean thermal energy (E). A number of studies, Malkus and Riehl (1960), Whitaker (1976), Frank (1977) and others have shown the ocean to be vital source of energy for the cyclone. The ocean thermal energy has been defined by Gray (1975) as:

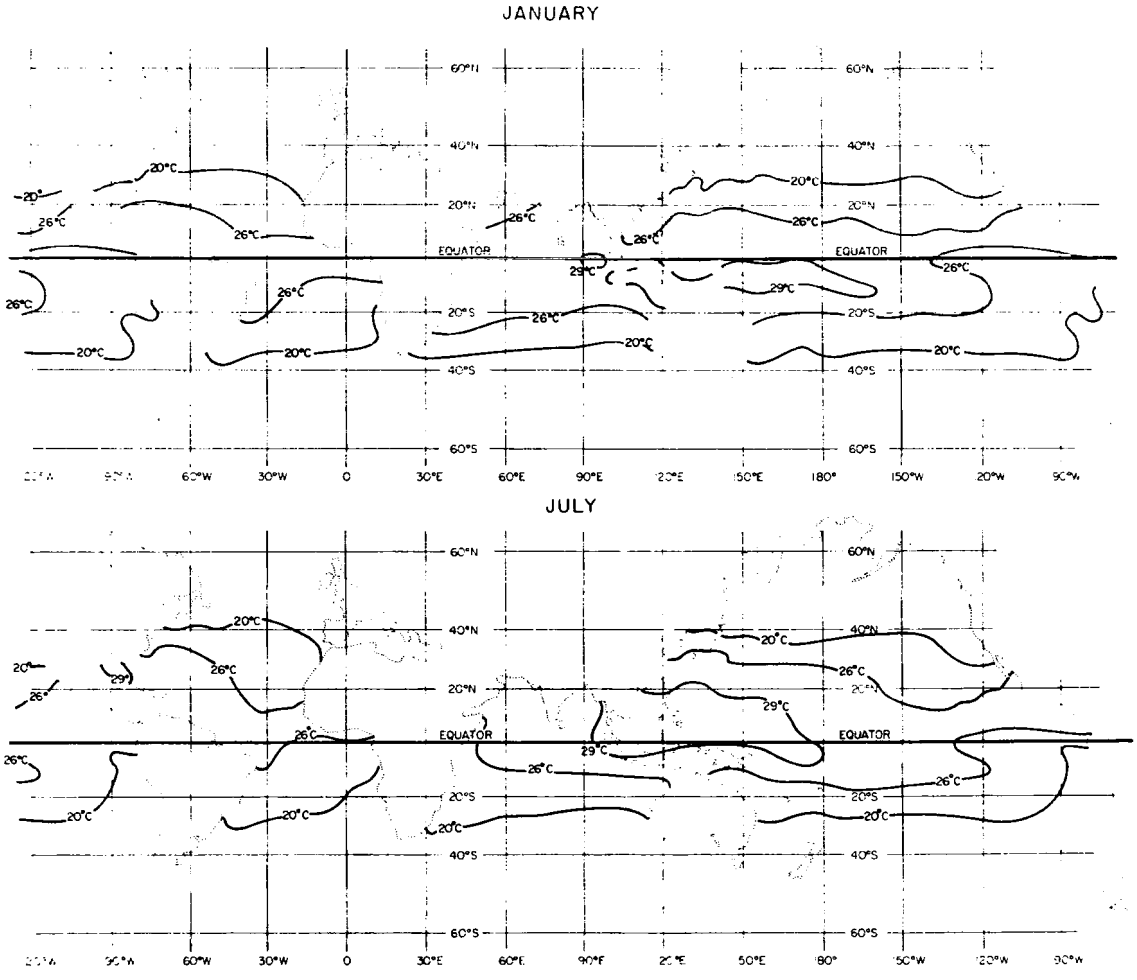

Fig. 5. Mean sea surface temperatures (^{o}C) for January and July. (After Gorshkov, 1974).

$$E = \int_{\text{surface}}^{60\text{ m depth}} \rho_W C_W \, (T-26) \, dz$$

With this variable positive, cyclone genesis is possible.

v) θ_e gradient. Gray (1975) has shown the surface to 500 mb θ_e gradient should exceed 10^{o}C. Generally this gradient is of the order of 15 to 20^{o}C which is adequate for storm development. Little daily variation is seen in $\partial\theta_e/\partial p$.

vi) Middle level humidity. Gray (1967) has defined a humidity parameter:

$$H = \begin{cases} \dfrac{(\overline{RH}-40)}{30} & RH > 40\% \\ 0 & RH < 40\% \end{cases}$$

where $\overline{RH}$ is the average 700 mb to 500 mb relative humidity. All other conditions being favorable, the higher the long term value of H for a region the more likely tropical cyclone occurrence.

The six genesis parameters may be combined to give a Seasonal Genesis Parameter:

S.G.P. = dynamic parameters x thermal parameters

$$= .\left(\zeta+5 \times f \times \frac{1}{S_z+3}\right) \times \left(E \times \frac{\partial\theta_e}{\partial p} \times \overline{RH}\right) \qquad [1]$$

Figure 6 shows the yearly genesis parameter as evaluated from the sum of the six parameters described above. This figure may be compared with Fig. 7 which shows the observed cyclone frequency. The good correlation between these figures lends strong support to the physical arguments used in justifying these parameters.

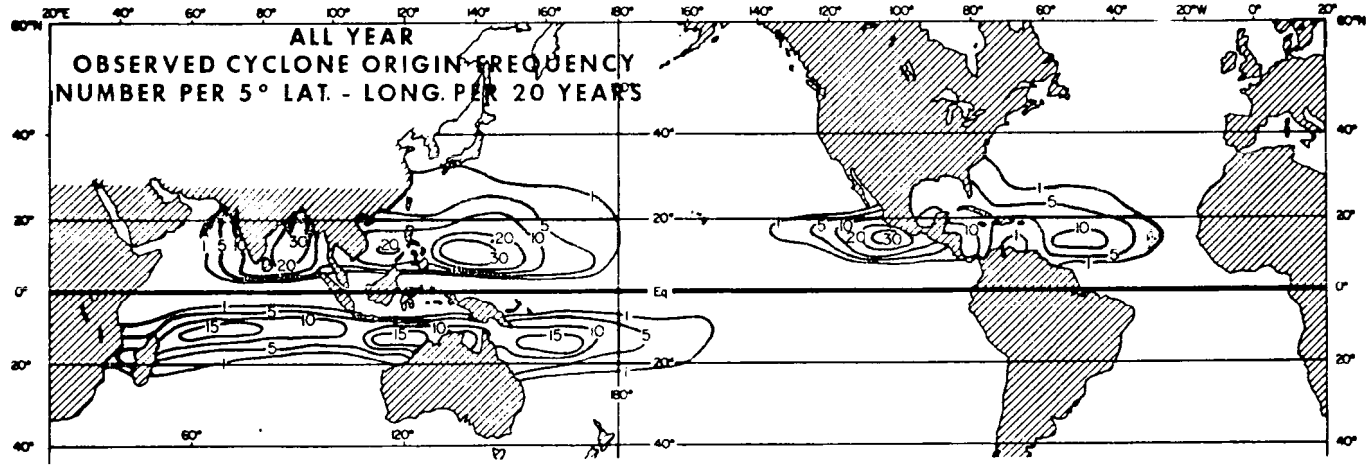

Fig. 6. The observed cyclone genesis frequency diagram for the same years as in Fig. 7. (After Gray, 1975).

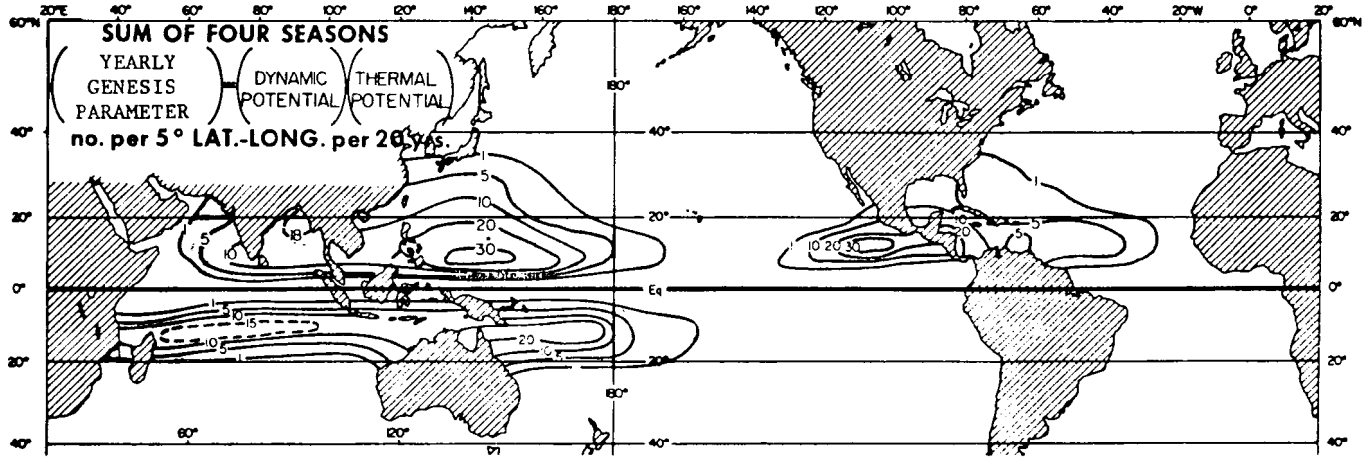

Fig. 7. Yearly genesis as evaluated from the sum of the six individual parameters. (After Gray, 1975).

2.3 Seasonal Variability of Genesis Parameters

While Fig. 7 depicts a regular pattern of cyclone occurrence on the long term, the interannual variability of the distribution of genesis locations is quite large. Figures 8 and 9 show the global cyclone tracks for the summer seasons of 1975 and 1977. During 1977, in the northwest Pacific there were more low latitude cyclone genesis events in the extreme eastern regions of that genesis area than in 1975. Similarly, in the southern hemisphere, the 1976-1977 season shows many more eastward genesis events than 1974-1975. Extreme differences between these seasons are also seen in the Atlantic and South Indian Ocean genesis areas.

The large changes in genesis locations between the seasons, which occur on a global scale, can only be related to changes in the general circulation. The 1976/77 season was a season of anomalously warm water and low M.S.L. pressure along the Peruvian coast. Following Bjerknes (1969), Julian and Chervin (1978) and others, the Easter Island minus Darwin monthly mean sea level pressure difference may be used as an index of the strength of the Walker Circulation. The more negative this number, the weaker the Walker Circulation. Figure 10 shows a plot of this index for the period 1973-1978. On Fig. 10 smooth curves have been drawn (dashed) connecting the December and June values of the pressure gradient. From these curves it can be seen that the Easter Island-Darwin pressure gradient is 2.5 mb greater in June 1975 than in June 1977 and also about 2.5 mb greater in December 1974 than in December 1976. 1977 was a year of weakened Walker circulation and this large scale circulation pattern change 'fed back' into the individual weather events to change the climatology of storm genesis, favoring mid Pacific

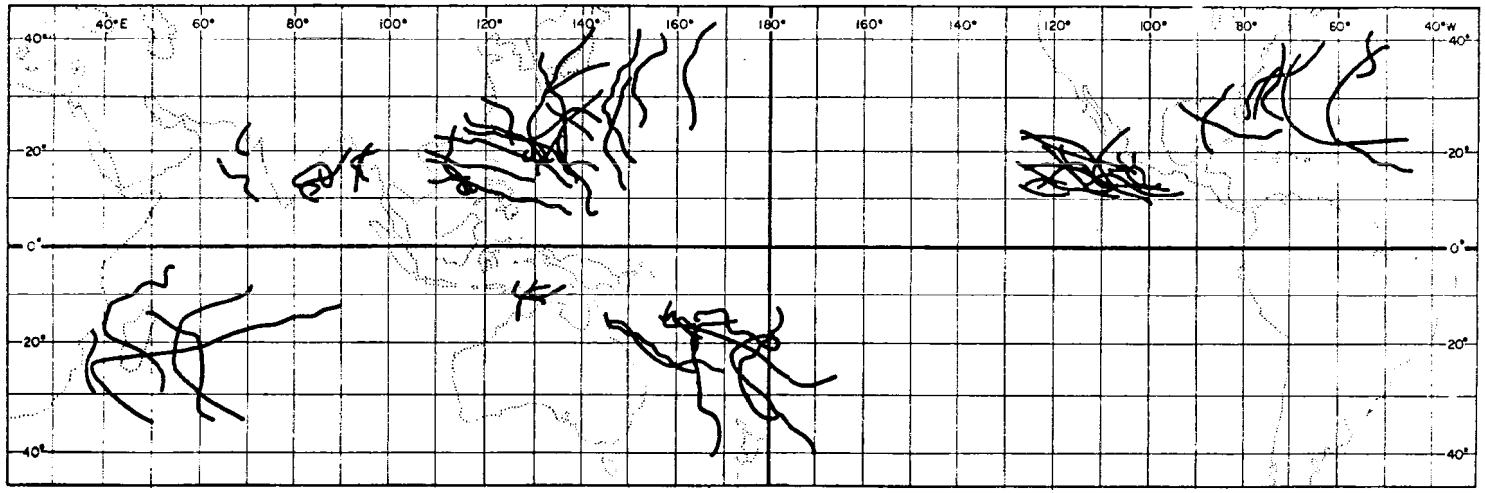

Fig. 8. Global cyclone tracks for southern hemisphere 1974/1975 and northern hemisphere 1975 season.

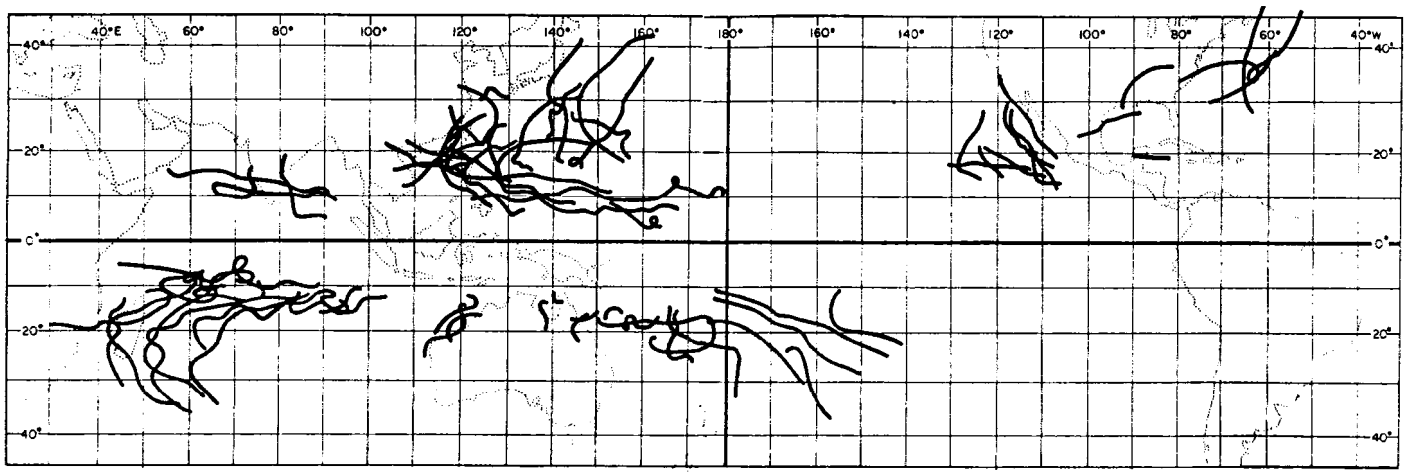

Fig. 9. As for Fig. 8, except for southern hemisphere 1976/1977 and northern hemisphere 1977 season.

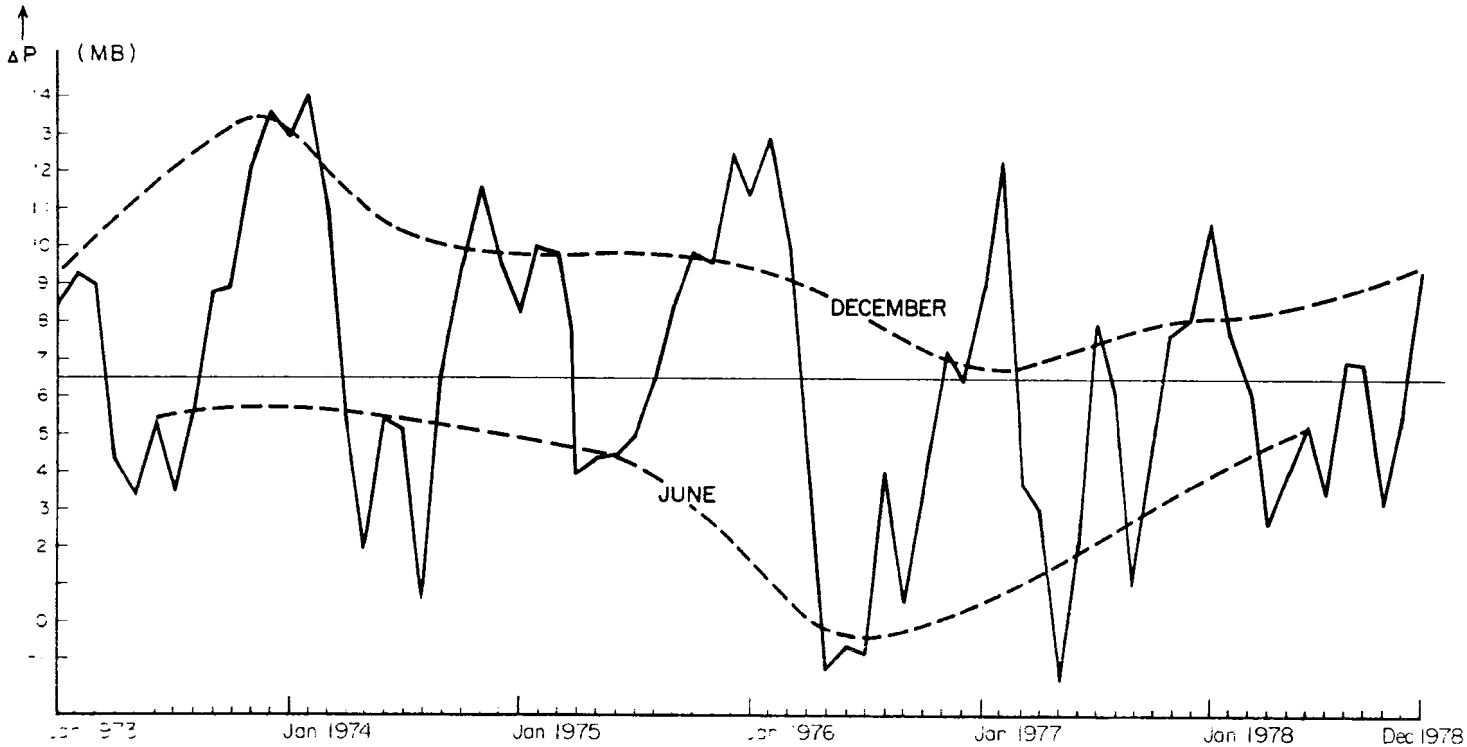

Fig. 10. Easter Island minus Darwin monthly mean sea level pressure fo the period January 1973 to December 1978. Dashed curves join the June and December pressure differences.

storm genesis. In the analysis which follows, both dynamic and thermodynamic parameters will be examined to determine those most changed by these large scale circulation changes.

To better understand the synoptic differences for 1975 and 1977 tropical cyclone seasons, a detailed study of them has been made. Bimonthly mean charts for January/February and July/August, for the latitude belt 30^{o}N to 30^{o}S for dynamic and thermodynamic parameters of Eq. 1 (zonal and meridional wind , vorticity, wind shear, θ_e at sfc, 700 mb, 500 mb and relative humidity at sfc, 700 mb, 500 mb and Sea Surface Temperature (SST)) have been prepared. Gray's (1975) six genesis parameters and an additional vorticity shear parameter $(\zeta_{200}-\zeta_{850})$ have been evaluated.

The data used were from a variety of sources. Australian region atmospheric data were obtained from the 'real time data set' described in Chapter 5 of this paper. Southern hemisphere sea surface temperature data were obtained from copies of the operational analyses routinely prepared by the Australian Bureau of Meteorology, National Meteorological Analysis Centre. Northern hemisphere sea surface temperatures are from the US Navy data tape held at the National Center for Atmospheric Research, Boulder, Colorado. All remaining data were obtained from the Monthly Climatic Data for the World, prepared by the US Department of Commerce.

There are two problems which arise from such an analysis. The first is caused by the way the data are interpreted. The usual inference drawn from general circulation differences between various seasonal mean charts are that these lead to different tropical storm climatologies. However, the presence of a different distribution of

storms will lead directly to different tropical circulation regimes, particularly in the upper levels where the upper anticyclones over tropical storms cover vast areas of the tropics. If large differences are noted in areas unperturbed by tropical storms, it would then appear quite reasonable to assume these differences were in some way related to the different seasonal storm climatologies. It will be shown in Chapters 4 and 5 that by careful stratification of the data, composite charts, with equal or greater data density than bimonthly means, can be constructed, which do not suffer from this problem.

The second problem which arises from such an analysis is that the events leading to storm genesis may differ vastly from the mean synoptic regime. This being the case, the means say little concerning why the distribution of storms differ from one season to the next.

Figure 11 shows the locations of the stations used in this study. The sparcity of stations in the Indian Ocean and northeast Pacific Ocean make it impossible to reach any meaningful conclusions concerning changed climatologies in these regions.

2.4 Comparison of the Summer Seasons of 1975 and 1977

The five basic parameters are used to compare these two contrasting seasons are listed below, along with a critical level for each parameter above which genesis is more likely to occur.

i) θ_e gradient 500 mb to the surface. A gradient of at least 10^{o}K appears necessary for genesis (Gray, 1975).

ii) Mean middle level relative humidity parameter:

$$\overline{RH} = (RH_{700}+RH_{500})/2.$$

An $\overline{RH}$ exceeding 40% appears necessary for genesis (Gray, 1975).

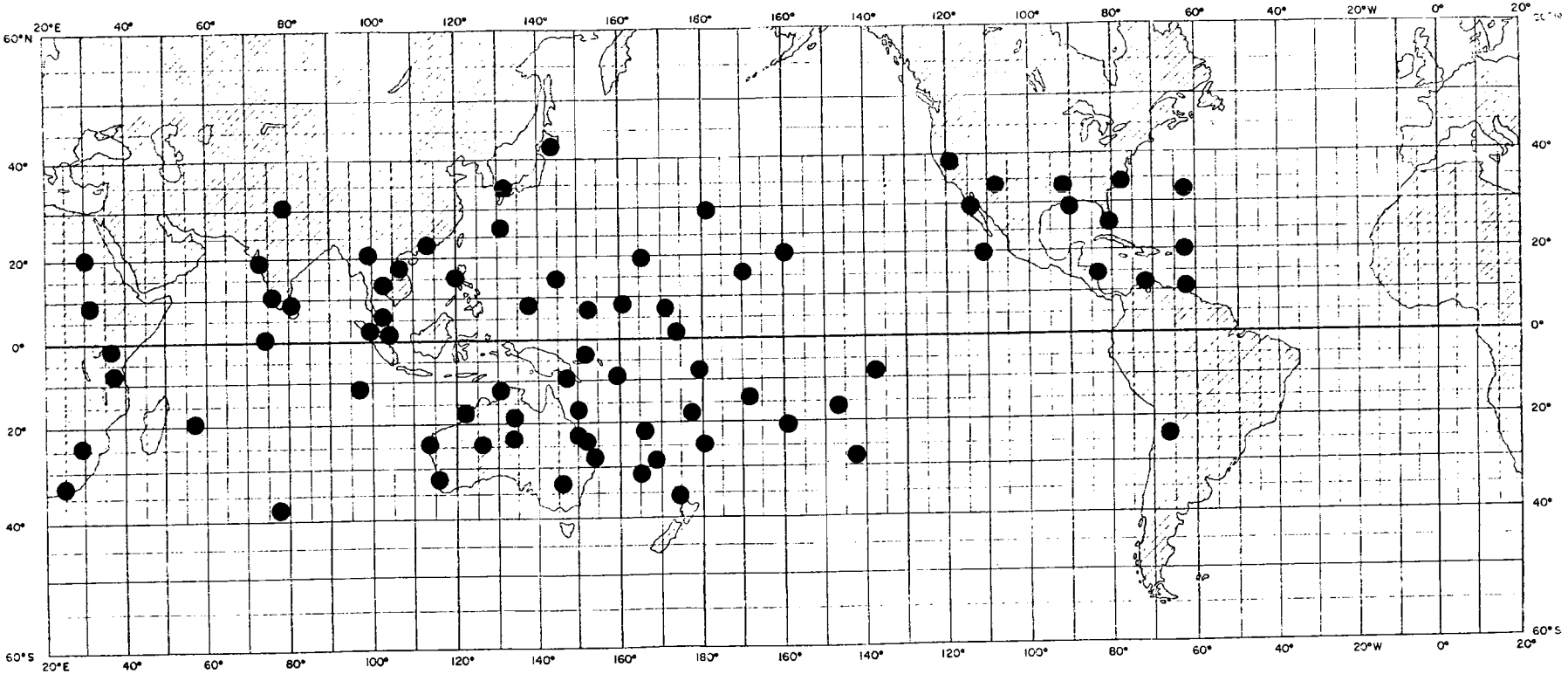

Fig. 11. Location of stations used in the comparative studies of two contrasting seasons.

iii) Sea Surface Temperature. A sea surface temperature exceeding 26.5°C has been suggested by Palmen (1948) as necessary for tropical cyclone genesis.

iv) The absolute shear of the wind through the troposphere.

$$|\partial V_h / \partial p|$$

In this analysis the shear between the 200 mb and 850 mb winds has been computed. A long term mean wind shear of less than 5 m s^{-1} per 650 mb appears necessary for storm genesis (Gray, 1975).

v) The shear of the vorticity between upper and lower layers of the troposphere. In the northern hemisphere this Genesis Parameter (after McBride, 1981b) has been defined as:

$$GP = \zeta_{850} - \zeta_{200} \quad (x10^{-6} sec^{-1})$$

while in the Southern Hemisphere as:

$$GP = \zeta_{200} - \zeta_{850} \quad (x10^{-6} sec^{-1})$$

Accordingly if the vorticity shear (Genesis Potential) parameter is positive and greater than a somewhat arbitrary value of 15 x 10^{-6} s^{-1} genesis is felt to be possible. The value 15 x 10^{-6} s^{-1} is consistent with that found by McBride (1981b) to be required for genesis in individual cloud clusters.

vi) The Coriolis parameter (f) does not change from season to season and so has not been calculated in this seasonal comparison.

By taking an area average of any parameter and subtracting the critical level of that parameter necessary for genesis, the result gives a number indicating how favorable the environmental conditions are for genesis. A large positive number will indicate exceedingly favorable conditions. By subtracting the 1975 bimonthly mean of a parameter from

its 1977 value, an indicator of how variable that parameter is for seasons of highly contrasting storm genesis climatologies results.

Table 2 shows these two numbers, written in fractional form for the five genesis parameters in the southern hemisphere summer, for three genesis regions. The numerator gives the changes between seasons, the denominator, the 1977 value minus the critical level of that parameter For all thermodynamic parameters in all genesis areas the variation between seasons is far less than the amount the 1977 value exceeds the minimum requirements. In general terms there were more storms in the South East Indian Ocean in 1975 than in 1977 and an opposite tendency in the South Pacific, east of 170°E and yet both θ_e gradient and $\overline{RH}$ show small changes which suggest a weak negative correlation with the number of storm genesis events. The dynamic parameters are all very close to the critical levels and the seasonal swings appear to be able to effect great changes on the storm genesis events of a region. It is noteworthy that the genesis potential parameter is less than the suggested value for the bimonthly means in two regions in 1977, and yet genesis events do occur. In this situation, transient changes to the large scale environment must occur which lead to much higher levels of vorticity shear for brief periods, otherwise the observed genesis events could not occur.

A similar analysis has been performed for the northern hemisphere summers of 1975 and 1977. The results are summarized in Table 3. Once again there is a weak, negative correlation between both θ_e gradient and $\overline{RH}$ and the number of genesis events in a particular ocean basin in a season. The variation between seasons in the thermodynamic parameters is insufficient to bring about a change in the environment from

TABLE 2

Climatological parameters for the southern hemisphere summer. The numerator of each fraction gives the parameter value in 1977 minus that in 1975. The denominator gives the 1977 value minus the required minimum value for genesis as specified by Gray (1975).

Genesis Area	South East Indian Ocean (East of 100 E)	South Pacific West of 170°E	South Pacific East of 170°E
Thermodynamic Parameter			
θ_e gradient (°K)	2/10	-1/5	-4/13
RH (%)	3/15	0/20	-10/15
S.S.T. (°C)	-0.5/2.8	.25/2.5	1.5/3.0
Dynamic Parameters			
$\lvert \partial \mathbb{V}_h / p \rvert$	2/3	0/-2	10/0
Genesis Potential ($\times 10^{-6}$ s^{-1})	-2/3	-2/-5	10/-2

TABLE 3

Climatological parameters for the northern hemisphere summer. The numerator of each fraction gives the parameter value in 1977 minus that in 1975. The denominator gives the 1977 value minus the required minimum value for genesis as specified by Gray (1975).

Genesis Area	North Indian Ocean	Northwest Pacific (West of 160°E)	Northwest Pacific (East of 160°E)	Atlantic/ Caribbean
Thermodynamic Parameter				
θ_e gradient (°K)	6/12	4/10	-5/8	3/11
RH (%)	-7/12	-5/20	-1/15	3/5
S.S.T. (°C)	*	0.6/2.5	0.0/2.8	*
Dynamic Parameters				
$\lvert \partial \mathbb{V}_h / p \rvert$	-5/30	2/3	-5/0	5/5
Genesis Potential ($\times 10^{-6}$ s^{-1})	-8/-7	-2/-12	10/-7	-5/-25

*Data Unavailable

favorable to cyclone genesis to unfavorable. The dynamic parameters show generally unfavorable values in 1977 with the required climatological variations being too small to produce long term highly favorable conditions. Once again, it is necessary to postulate the existence of transient states in which the dynamic conditions are favorably enhanced.

In order that a more comprehensive picture of the changes between the seasons may be obtained, analyses of the seasonal differences in each parameter have been included in Appendix A. Each analysis also shows the area for which that parameter exceeds the given critical level.

As noted previously, the 1976/77 season was one of low Easter Island - Darwin pressure gradient(an El Nino year). During such periods the equatorial sea surface temperatures near longitude 180^{o} are anomalously warm. The observation of more eastward genesis events in the South Pacific in 1976/77 raises questions concerning the role of air-sea interactions. The changes between the 1975 and 1977 seasons in sea surface temperature were greatest along the equator (see Fig. A3 Appendix A) west of 180^{o}. However, in the storm cyclone genesis belts of 5 to 15^{o}N and S, the anomalies are only 1^{o}C or less. Since the increased tropical cyclone activity is associated with stronger low level equatorial westerlies (as is shown in Chapter 3), it is unclear whether the higher equatorial sea surface temperatures lead to greater cyclone activity or the increased equatorial westerly winds associated with the tropical cyclones reduces the cold water upwelling. It is

noteworthy that the greatest anomalies are equatorward of the genesis areas, supporting in some way the latter conclusion.

Inspection of the dynamic parameter analyses in Appendix A (Figs. A4, A5, A8, A9) reveals that the greatest changes occur in the winter hemisphere, indicating that the global circulations are changed, as well as the cyclone genesis climatologies between seasons.

2.5 Conclusions

The global climatology of tropical cyclones reveals that while the annual number of such weather systems only varies by about 10% individual ocean basins may have nearly 40% variability. Using those parameters Gray (1975) has identified as being crucial in tropical cyclone genesis, an analysis of two years with markedly different distributions of cyclone genesis points was undertaken. The following conclusions may be drawn from the study:

i) The thermodynamic parameters such as θ_e gradient and middle level relative humidity changed little in the tropics between seasons. Larger changes were observed in the winter hemisphere, which appeared related to a changing distribution of ridge/trough systems.

ii) The cause/effect relationship between large scale sea surface temperature anomalies and changes in location of tropical cyclone genesis events has not been resolved. It does appear that changes in equatorial wind fields can explain the largest equatorial sea surface temperature anomalies which are some distance from the genesis areas. Within the genesis areas there does not appear to be a strong positive correlation between sea surface temperature and tropical cyclone genesis event climatology.

iii) The dynamic parameters show marked changes in the summer hemisphere tropics and the winter hemisphere midlatitudes. There is some circumstantial evidence that increased troughing occurs in the winter hemisphere in the longitudes of increased tropical cyclone genesis activity.

iv) The McBride (1979) genesis potential parameter is able to account for a good deal of the variability in

seasonal genesis patterns as well as serve as a forecast tool on a daily basis. There is, however, the problem that increased storm activity will lead to increased vorticity shear, such that when incorporated into a bimonthly mean, a more favorable genesis parameter results.

In some sense, the use of mean data to contrast seasons of different tropical storm climatologies represents a crude form of compositing. The major problem being that while it is desirable to have only those days in the composite which lead to the different genesis patterns, there are many days in the composite whose flow fields (particularly at upper levels) may be changed by the storm circulations. Furthermore, if the events which lead to storm genesis are transient in nature, lasting for a day or two, the bimonthly means will contain many days whose flow fields contribute nothing to the storm genesis dynamics.

Many of these objections to monthly mean studies can be overcome by careful selection of those events to be composited. However, before proceeding to composite studies, a more detailed analysis of pregenesis flows may be obtained through case studies. Chapter 3 describes two such case studies.

3. CASE STUDIES

3.1 Introduction

In this chapter two case studies are presented which illustrate the typical sequence meteorological events that precede the genesis of a tropical cyclone in the eastern hemisphere. The first genesis event occurs in the southern hemisphere around 120°E, the second in the northern hemisphere around 150°E. Both storms may be considered to be ITCZ type storms, that is they form in close proximity to the ITCZ. For both genesis events, cross equatorial forcing appears to play a major role. In order to assess the importance of a number of pregenesis, winter hemisphere events in the dynamics of genesis, a survey of some seventy-four events was made. The results indicate that for about 75% of all genesis events (in the longitudes 100°E to 180°E) there is an equatorwards surge of cold air in the winter hemisphere. This surge is accompanied by large scale equatorial pressure rises and followed by accelerated westerly flow on the equatorward side of the ITCZ.

These case studies suggest that two important large scale teleconnections are in operation. The first is the almost simultaneous changes in midlatitude and equatorial pressure fields. The second is the increased westerly flow accompanying the equatorial pressure rises.

3.2 The Genesis Event of March 1977

The following case study illustrates some processes which appear to be important in tropical cyclone genesis. Charts are presented every second day in order to illustrate how the large scale flow evolves. The charts used in the research contained a much greater density of data than those presented in this paper, not all available observations were

plotted in an attempt to prepare a legibile chart. Two sources of synoptic information were used:

i) The microfilmed analyses routinely prepared by the Australian Bureau of Meteorology, Tropical Analysis Centre, Darwin and

ii) Microfilms of the tropical strip surface charts produced by the US Weather Service.

The Mean Sea Level (M.S.L.) chart for March 3, 1977 (Fig. 12) shows an anticyclone moving eastwards away from the Australian continent, with a baroclinic zone moving towards the west Australian coast. In the northern hemisphere a cold front is moving out of China with a strong outbreak cold high following in its wake. Weak winds are observed in the belt 10^{o}S to 20^{o}N. At 500 mb (Fig. 13) the subtropical ridge of the northern hemisphere lies along 12^{o}N with westerlies poleward of it. In the southern hemisphere the subtropical ridge is broken near 140^{o}E with the western portion near 30^{o}S and the eastern portion near 20^{o}S. At 250 mb (Fig. 14) a cut-off low over southeastern Australia breaks the upper subtropical ridge. In the northern hemisphere a sloping subtropical ridge from 16^{o}N, 115^{o}E to 6^{o}N, 170^{o}E is seen. Poleward of the subtropical ridge the westelies are quite zonal in character.

By the 5th of March enhanced low level northwesterly flow is occurring through the Indonesia Archipelago (Fig. 15). The genesis of tropical cyclone 'Karen' occurred on this day, near 16^{o}S, 120^{o}E. The northern hemisphere cold outbreak high has moved equatorward, while the baroclinic system which spawned it is moving poleward to reinforce the Aleutian low. At 500 mb on the 5th (Fig. 16) stronger northwesterly

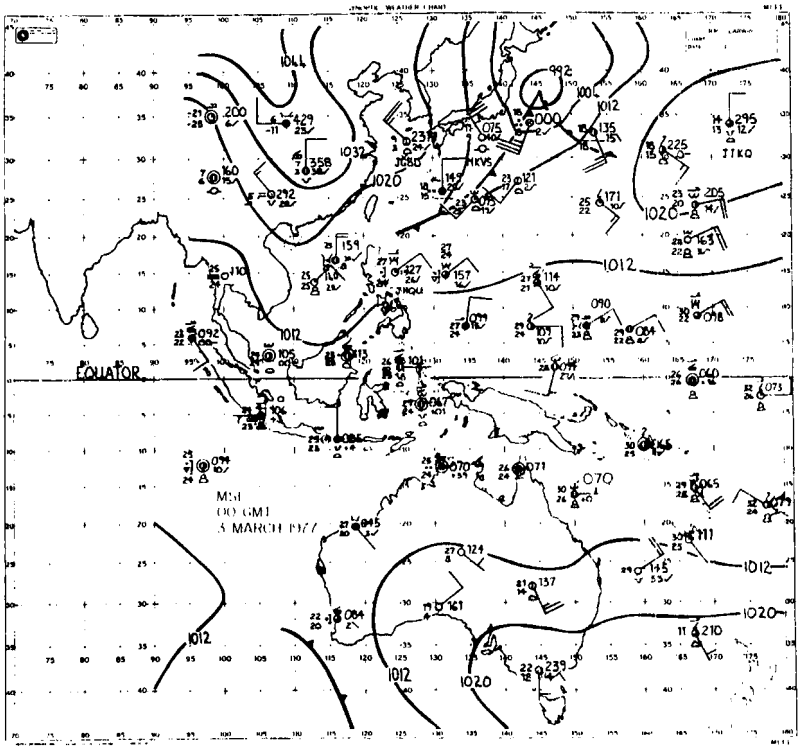

Fig. 12. Mean sea level pressure analysis. March 3, 1977. Wind speeds in knots, temperature in degrees celsius.

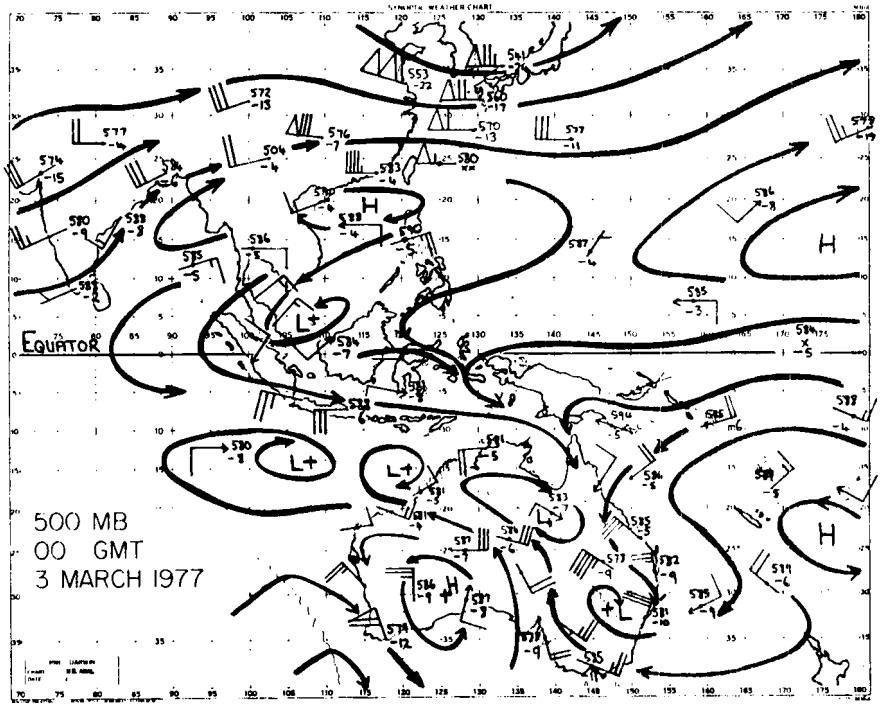

Fig. 13. 500 mb streamline analysis. March 3, 1977. Units as for Fig. 12.

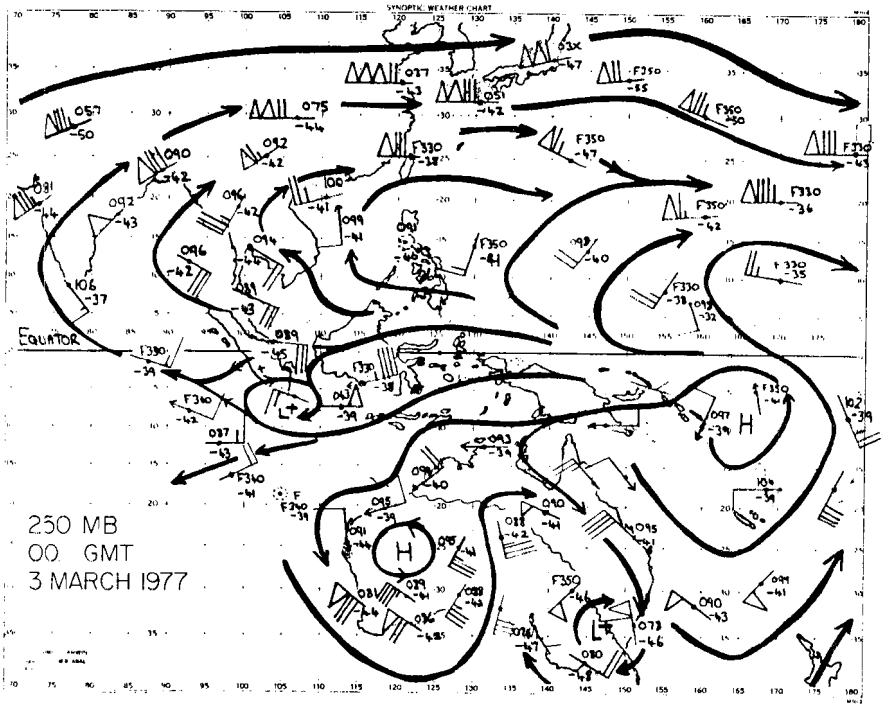

Fig. 14. 250 mb streamline analysis. March 3, 1977. Units are as for Fig. 12.

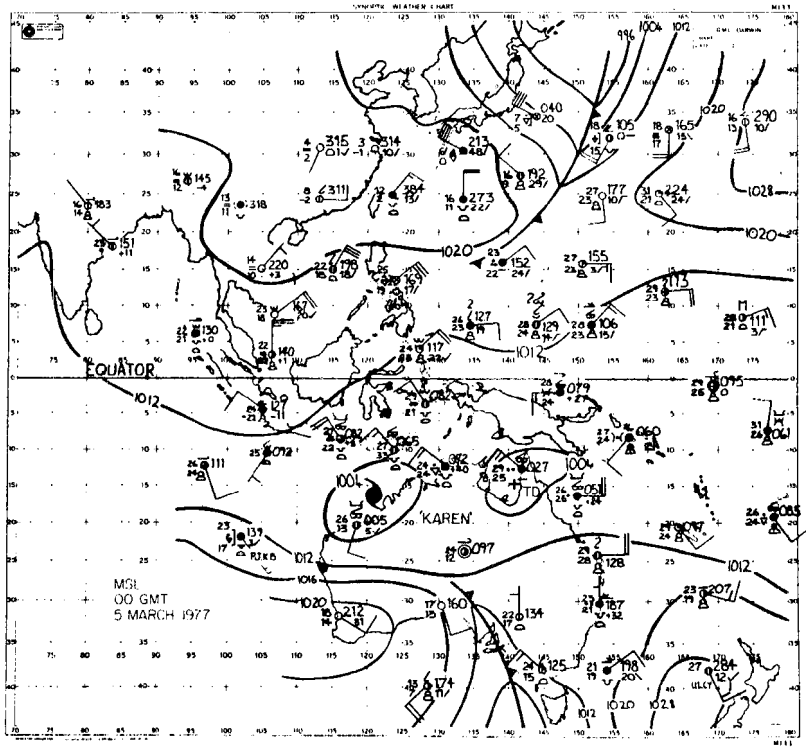

Fig. 15. Mean sea level pressure analysis. March 5, 1977. Units as for Fig. 12.

flow is evident over the Indonesian Islands, indicating that the mechanisms responsible for the monsoon flow are acting through a deep layer. Associated with the northern hemisphere baroclinic zone is a middle level (Fig. 16) and upper level (Fig. 17) trough over Japan. At 250 mb the geopotential heights have increased 40 to 70 gpm over Singapore and Clarke AFB (Phillipines) respectively. A new 250 mb high cell is evident over the Phillipines and the troughing over Australia has dissipated.

On the M.S.L. analysis of the 7th of March (Fig. 18) the cold outbreak high is seen to have broken away from its source region, the Siberian high, to reinforce the northwest Pacific subtropical ridge. The 1012 isobar has moved well down into the southern hemisphere from its initial position through the South China Sea. Tropical cyclone Karen is approaching landfall while two tropical depressions, one near $14^{o}S$, $140^{o}E$ the other near $18^{o}S$, $148^{o}E$ were intensifying only to dissipate as the ITCZ moved south over the Australian continent. This raises the important problem that not all surges may initiate tropical storms because the ITCZ may move over a landmass or other necessary conditions may not be present. Instead a so called burst in the monsoon occurs. Heavy rainfall over Northern Australia, associated with the steady deep northwesterly air flow occurs.

Webster and Chou (1977) and Webster et al. (1977) demonstrate that the surge/break oscillation of the monsoon can be attributed to changing levels of solar short wave radiation received at the earth's surface. During burst periods the increased cloudiness restricts the incoming solar short wave radiation and hence decreases the surface temperature. The burst weakens and break conditions become established. During break

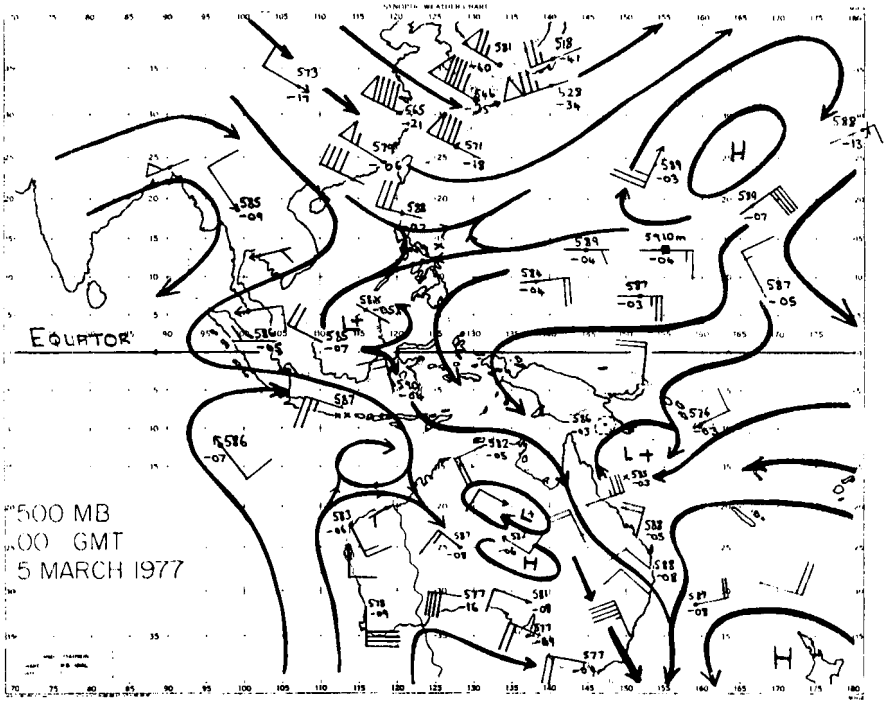

Fig. 16. 500 mb streamline analysis. March 5, 1977. Units as for Fig. 12.

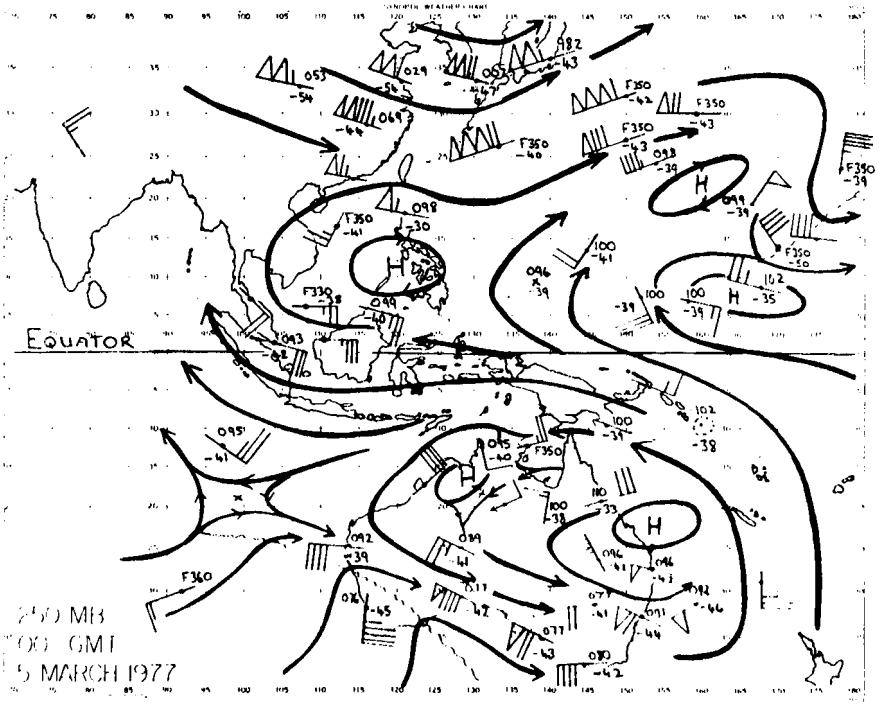

Fig. 17. 250 mb streamline analysis. March 5, 1977. Units as for Fig. 12.

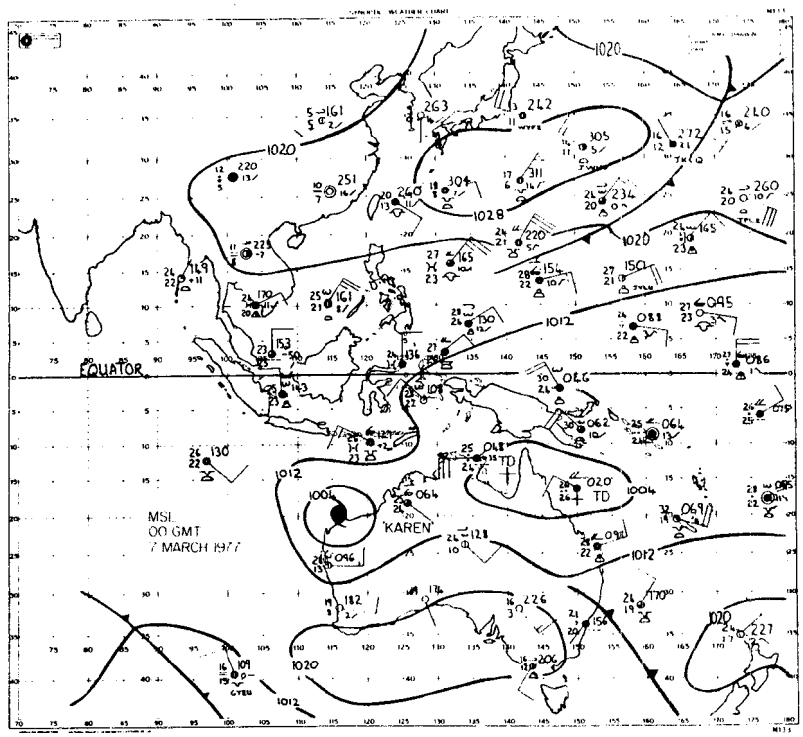

Fig. 18. Mean sea level pressure analysis. March 7, 1977. Units as for Fig. 12.

conditions relatively large amounts of solar short waves are received at the surface and the atmosphere tends back towards 'burst' conditions. The data considered in this paper suggest that second, extremely important modulation of the monsoon intensity is occurring, namely cross equatorial forcing.

At 500 mb on the 7th (Fig. 19) the flow from nothern to southern hemisphere appears to have weakened, though the available data were sparse. At 250 mb (Fig. 20) the main high cell has moved eastwards, while the flow returning to the northern hemisphere from the heavy convection in the Australian ITCZ is quite marked.

The changes in the surface level cross-equatorial wind field between the 3rd and 5th of March 1977 have been plotted in wind vector form on Fig. 21, along with streamlines of wind field change. The data

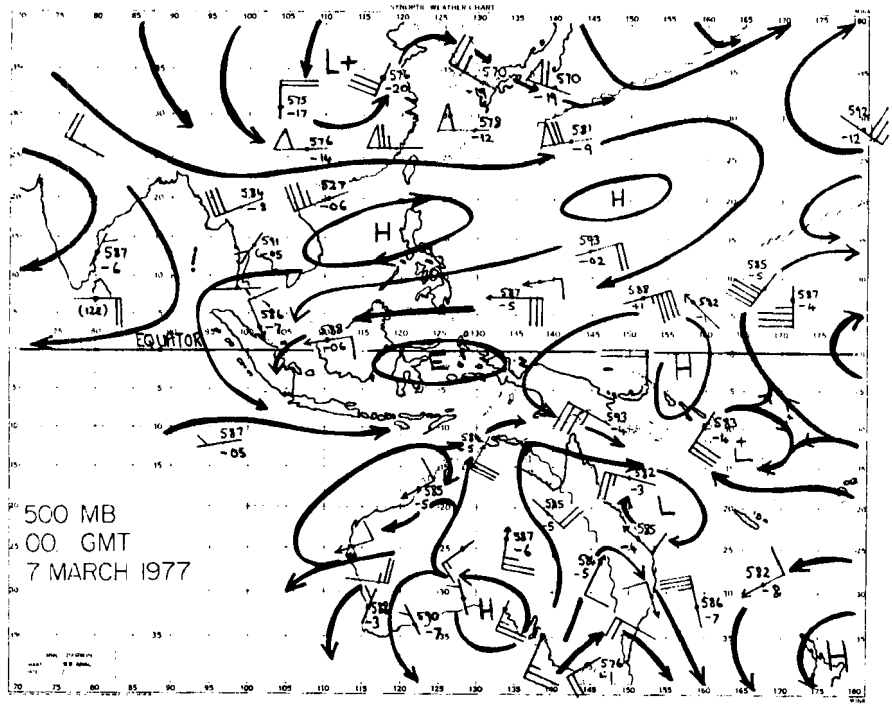

Fig. 19. 500 mb streamline analysis. March 7, 1977. Units as for Fig. 12.

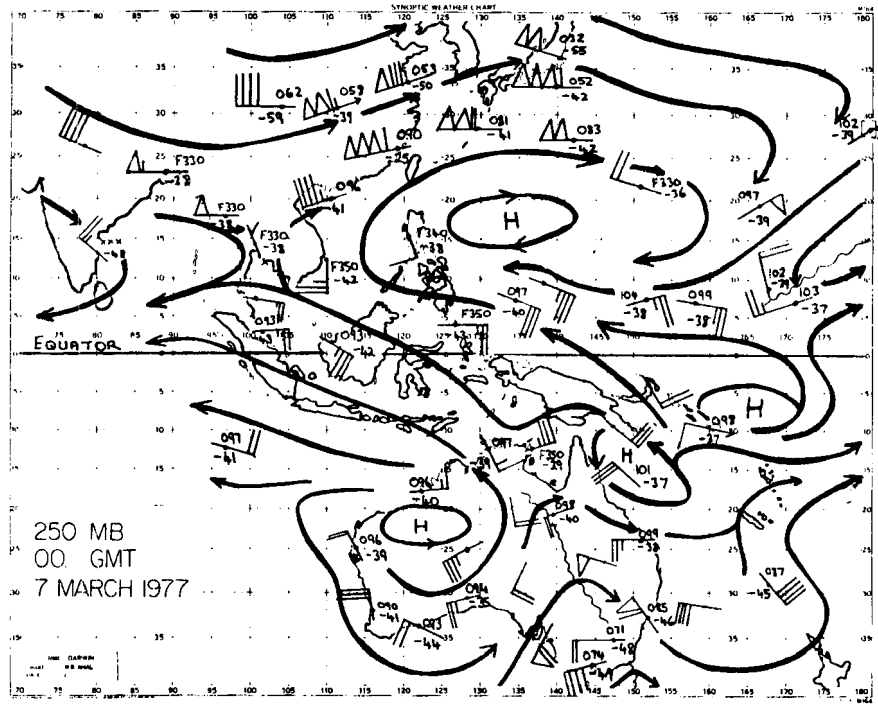

Fig. 20. 250 mb streamline analysis. March 7, 1977. Units as for Fig. 12.

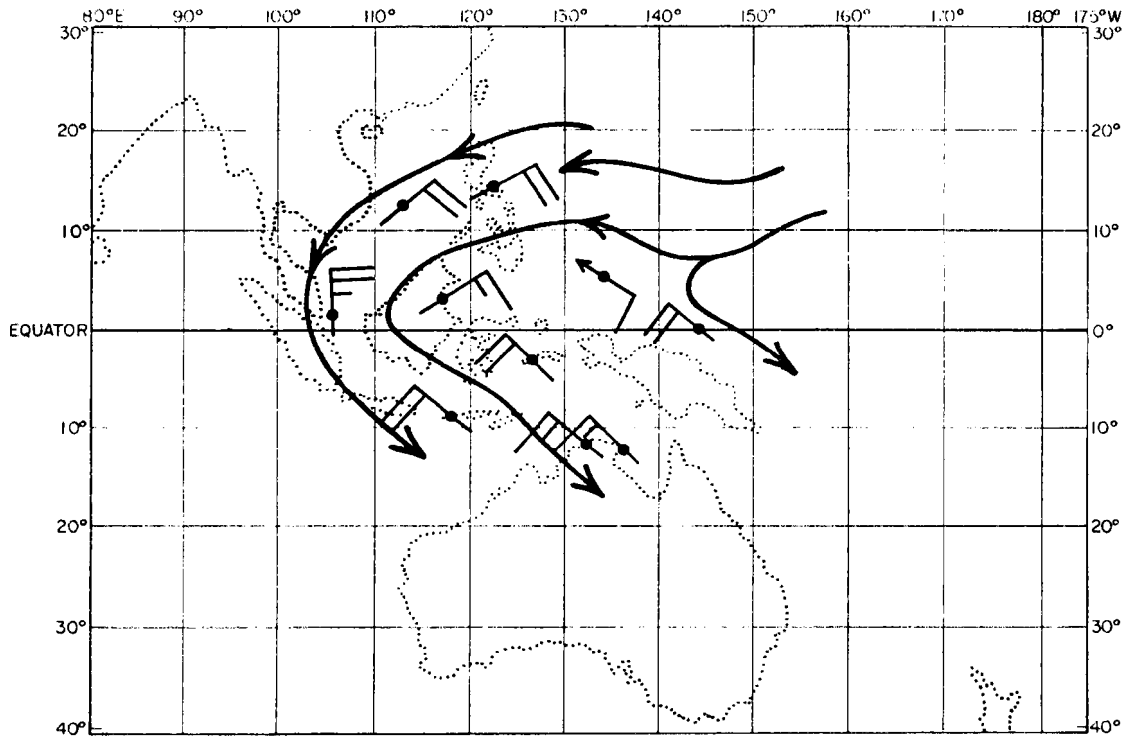

Fig. 21. Vector difference (knots) between surface winds, 5th minus the 3rd of March, 1977.

presented are the difference between station observations at 00 GMT on the 3rd and 5th of March. This figure reveals clearly the increased cross-equatorial convergence into the ITCZ between March 3rd and 5th. Figure 22 shows the difference field between the 5th and 7th of March. There is now a change in direction of the difference field, the surge has weakened around the time the ITCZ disturbances are becoming most intense, suggesting surges may be important in the initiation of vortices in the ITCZ but not so important in their maintenance.

Figure 23 shows the positions of the 1020 mb and 1012 mb isobars on each day, at 00 GMT, from 3rd March 1977 through to the 7th of March. Associated with the cold surge from the China Mainland there is a rising of pressures from 20°N to 10°S. Between the 3rd and the 4th and again between the 6th and the 7th, the 1012 mb line is seen to move

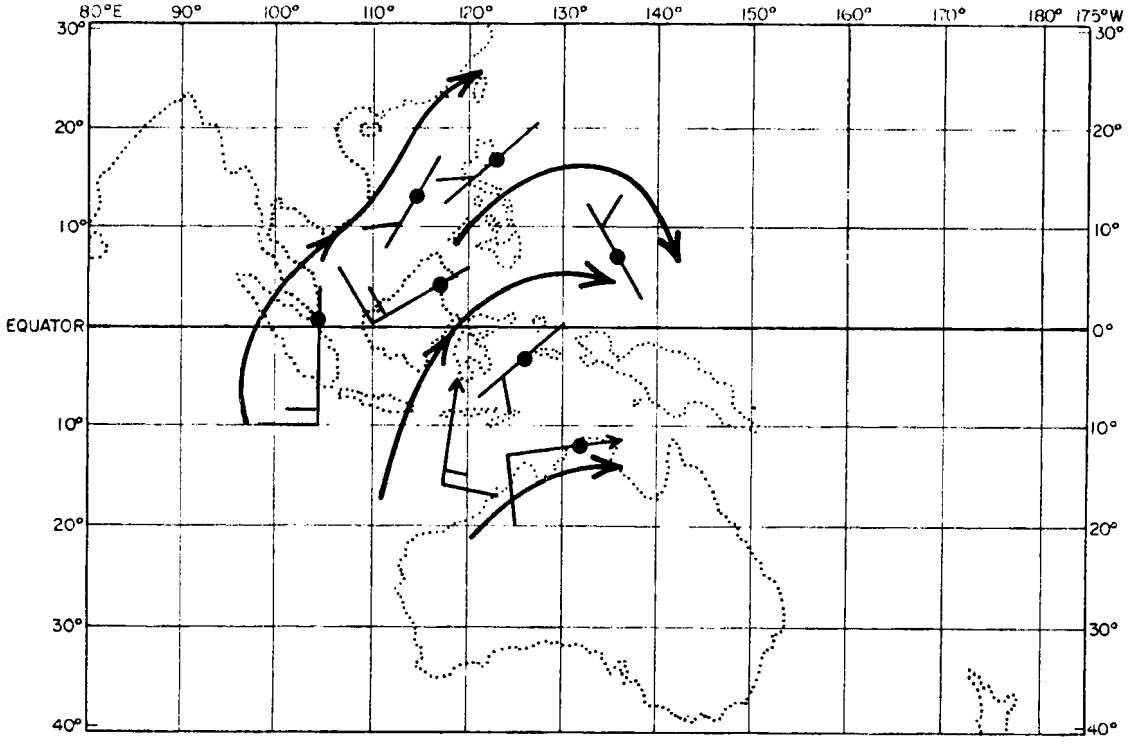

Fig. 22. Vector difference (knots) between surface winds, the 7th minus the 5th of March, 1977.

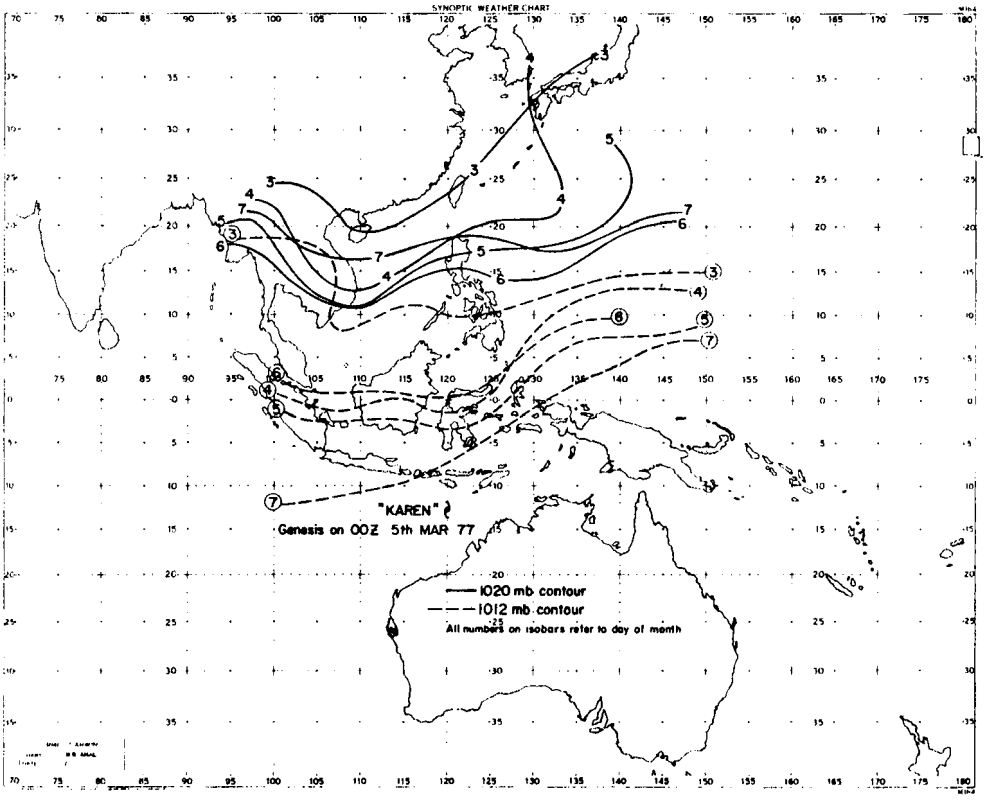

Fig. 23. Positions of 1012 mb and 1020 mb isobars at 00 GMT for 3 March through 7 March, 1977.

approximately 10^{o} of latitude southwards. Observations similar to these have been reported previously by Williams (1981).

Further indication that the "triggering impulse" for this cyclone genesis/monsoon burst is northern hemispheric in origin can be obtained by taking daily longitudinal strips of mercator projection satellite mosaics. Figure 24 shows the sequence starting the first of March and going through to the 11th for a 10^{o} wide belt centered on 150^{o}E. On the first of the month some isolated convection is evident around 5^{o}N to the equator. By the 4th the northern hemisphere frontal cloud band is evident, the area of southern hemisphere tropical cloudiness has broadened. By the 9th the cloudiness associated with the ITCZ has propagated to near 25^{o}S, which represents a rate of movement of about 300 km/d averaged over a nine day period. It is noteworthy that on the 3rd of March, at each synoptic level (including those not presented here), there is evidence of easterly winds in the belt 10^{o}S to 10^{o}N and yet there appears to be energy propagation through this belt from northern to southern hemispheres. Furthermore, this energy appears fundamentally related to such important events as tropical cyclone genesis and a burst in the Australian monsoon. The question of energy propagation through easterly wind regimes is addressed in later chapters of this paper.

3.3 The Genesis Event of August 1976

To demonstrate that the sequence of events described in section 3.2 are not peculiar to southern hemisphere ITCZ bursts, a study of northern hemisphere tropical cyclone genesis has been performed. Once again, the tropical cyclone forms in close proximity to the ITCZ.

Fig. 24. Daily, 10° wide longitudinal strips of satellite mosaics. The area covered is from 50°N to 50°S centered on 150°E.

On the first of August 1976, the M.S.L. analysis (Fig. 25) reveals a midlatitude cyclone at 42°S, 147°E which is deepening and moving rapidly to the south. The zone of maximum tropical cloudiness lies along 7°N between 130°E and 155°E, the observations on Fig. 25 indicate the ITCZ to be in this area. At 500 mb on the 1st, (Fig. 26), the trough associated with the surface front stretches from near Melbourne

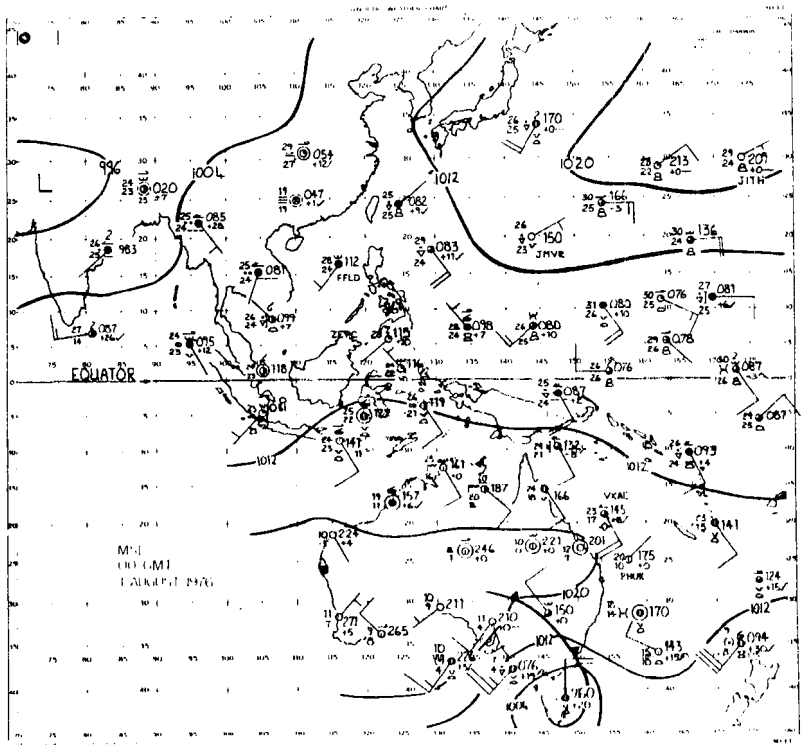

Fig. 25. Mean sea level pressure analysis, August 1, 1976. Wind speed in knots, temperatures in degrees celsius.

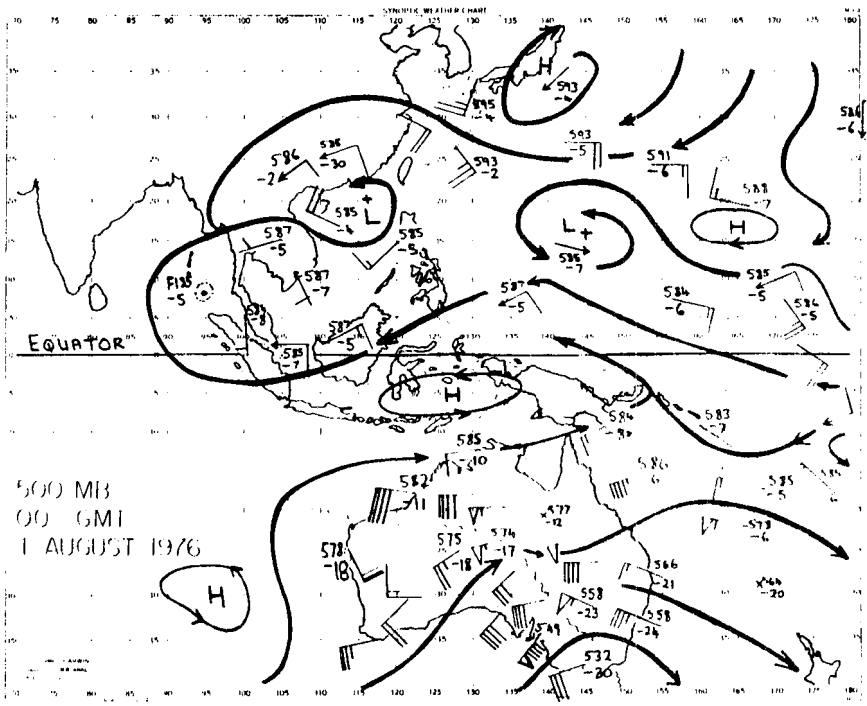

Fig. 26. 500 mb streamline analysis, August 1, 1976.

on the south coast to Port Hedland, Western Australia. Weak cross equatorial flow has been analyzed in the vicinity of Papua, New Guinea. At 250 mb (Fig. 27) a sloping trough is seen over Australia along with strong outflow from the Indian monsoon. A Tropical Upper Tropospheric Trough (TUTT) low is observed near20°N, 140°E.

The M.S.L. analysis (Fig. 28) on the 3rd of August shows the cold outbreak high to have moved north to become established over the Australian continent. The dew point temperature at Darwin, Australia has dropped from 16°C to 1°C indicating the passage of the dryline. The 1020 mb and 1012 mb contours both show about 5° latitude displacement northwards from their positions on the first. A tropical depression is noted near 13°N, 150°E which reached tropical storm intensity twelve hours later. The 500 mb analysis (Fig. 29), on the 3rd of August shows much stronger northward wind components in the belt 10°S to 5°N than two days earlier. At 250 mb (Fig. 30) all available observations indicate a much stronger return flow from the northern to southern hemisphere. Thus, the vertical wind shear in the equatorial belt, 10°S to 5°N appears to have increased substantially with the evolution of the southern hemisphere weather systems. This increased shear prior to genesis has been an important feature of both case studies and will be shown in Chapter 4 to be present in the composite of a large number of pre-cyclone genesis days.

By the 5th of August on the M.S.L. chart (Fig. 31) it can be seen that the Australian high has again been split by troughing action, the southeasterly winds between the equator and 20°S have weakened and the Darwin dew point has returned to a more normal dry season value of 10°C.

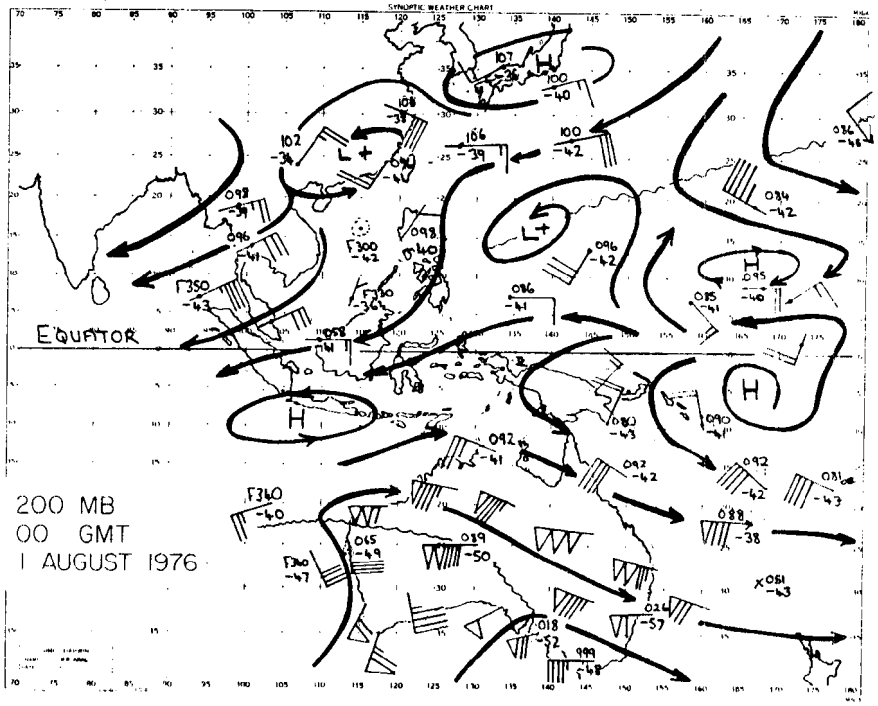

Fig. 27. 250 mb streamline analysis, August 1, 1977.

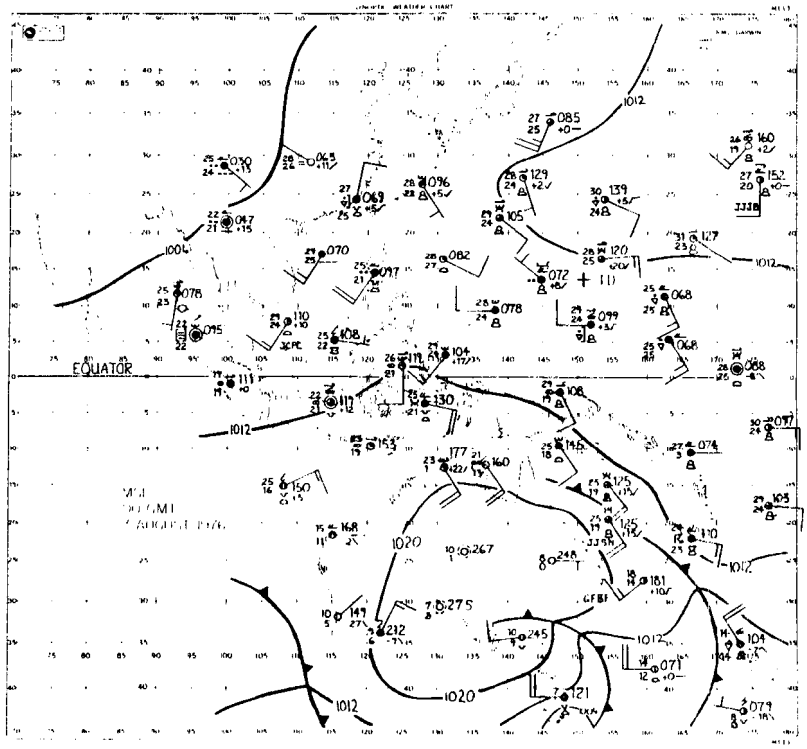

Fig. 28. Mean sea level pressure analysis, August 3, 1976.

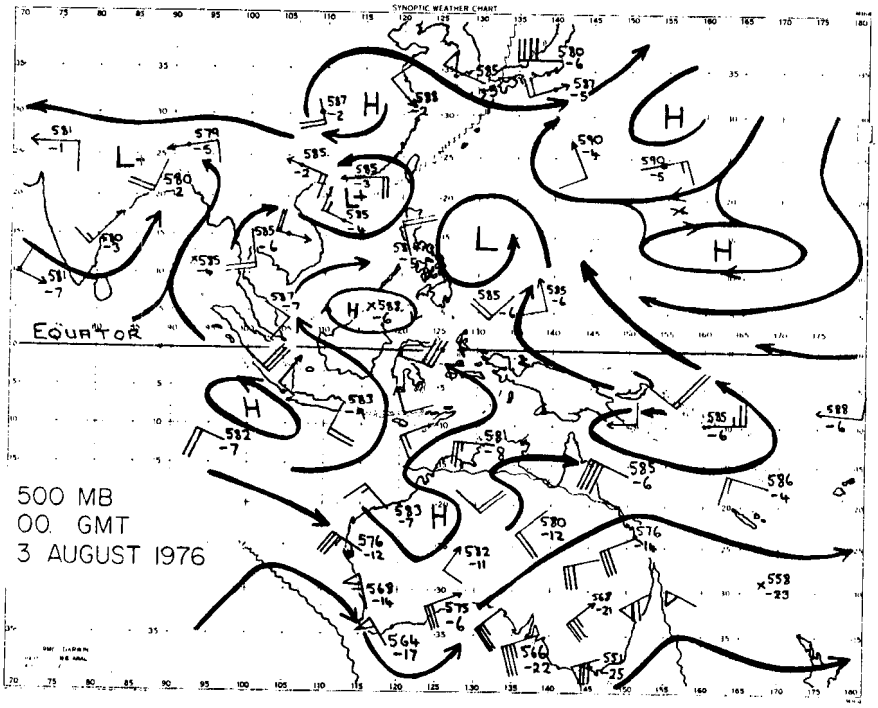

Fig. 29. 500 mb streamline analysis, August 3, 1976.

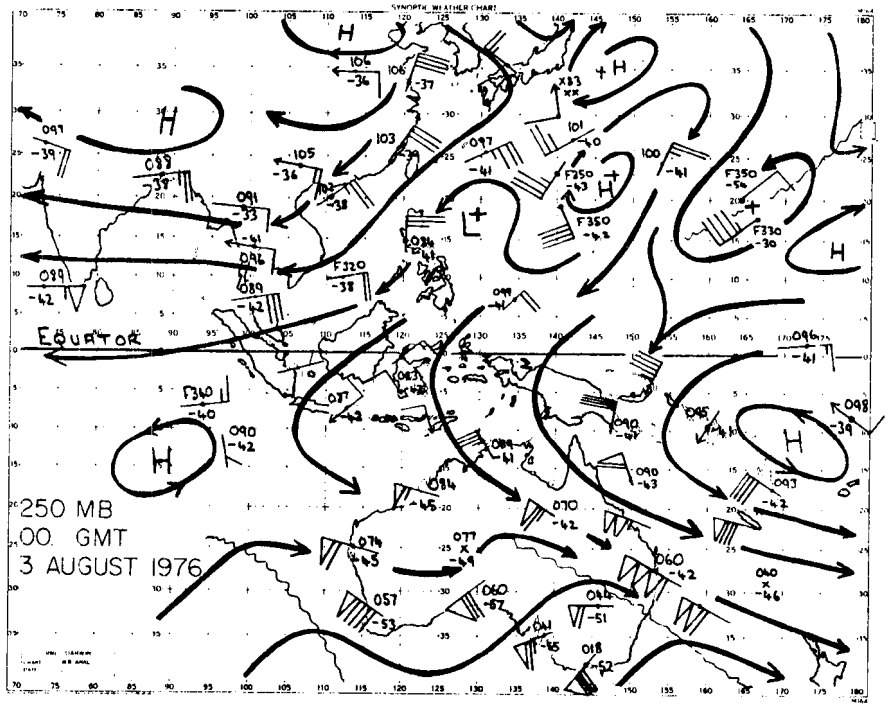

Fig. 30. 250 mb streamline analysis, August 3, 1976

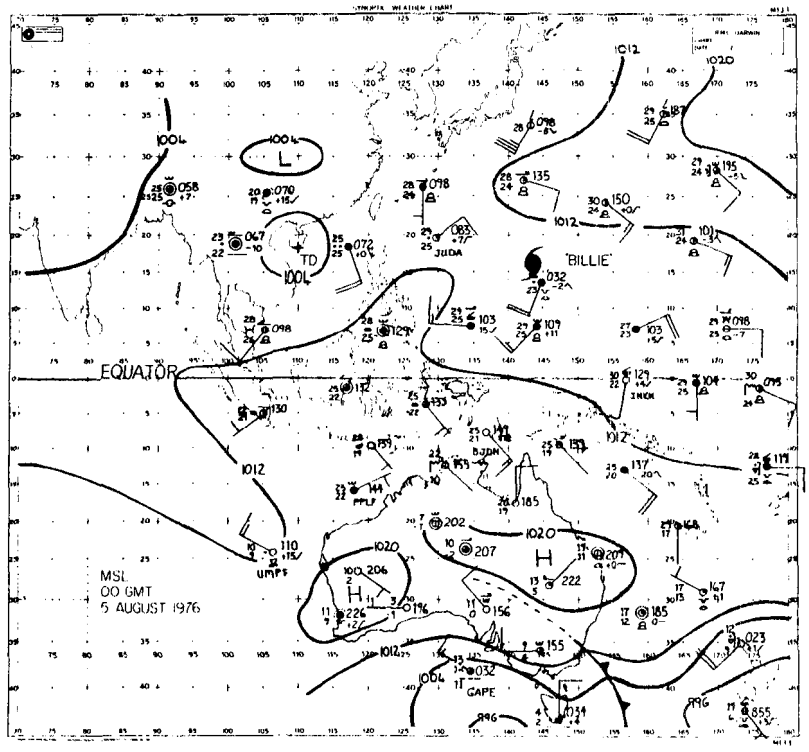

Fig. 31. Mean sea level pressure analysis, August 5, 1976.

The surging 1012 mb isobar has reached its maximum northern hemisphere penetration, with a number of ship observations east of the Phillipines (not plotted) indicating pressure around 1013 mb. At 500 mb, (Fig. 32), the southerly flow at the equator, east of 130°E, has been reversed while at 250 mb (Fig. 33) the northerly flow in this sector has been reduced. Thus, while increased shear in the equatorial winds were observed prior to genesis with the intensification of 'Billie' they fell back to the levels of the 1st of August.

As in the previous case study, large scale surface wind field difference charts have been prepared. The wind vectors are the differences between surface wind observations at stations at 00 GMT on the dates given, the streamlines give a subjective analysis of the difference flow field. Figure 34 shows the increased south to north cross-equatorial flow between the 1st and 3rd of August, 1976. This occurs prior to the genesis of 'Billie'. Figure 35 shows a reversal

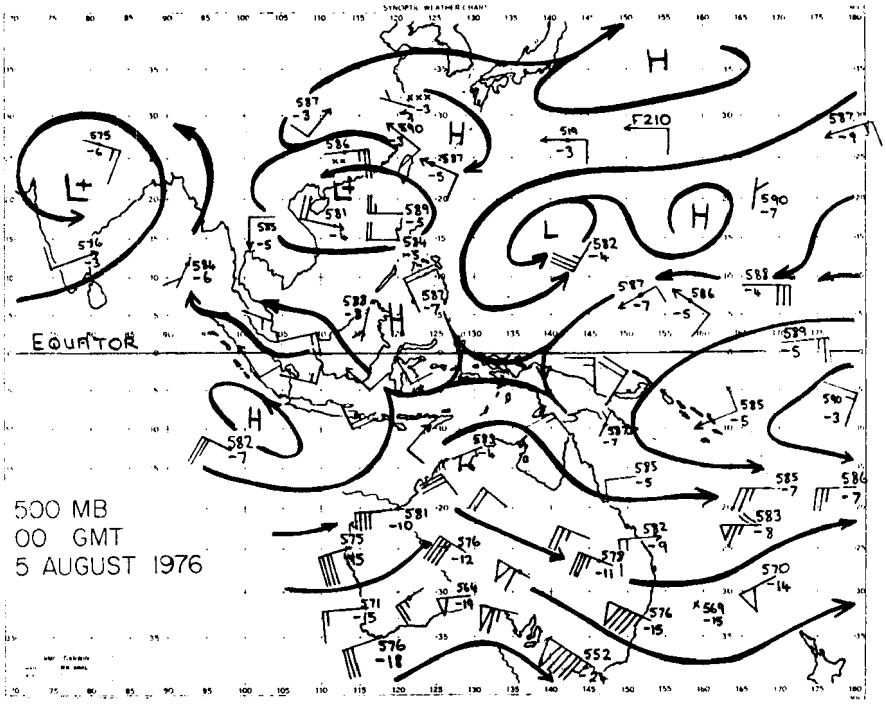

Fig. 32. 500 mb streamline analysis, August 5, 1976.

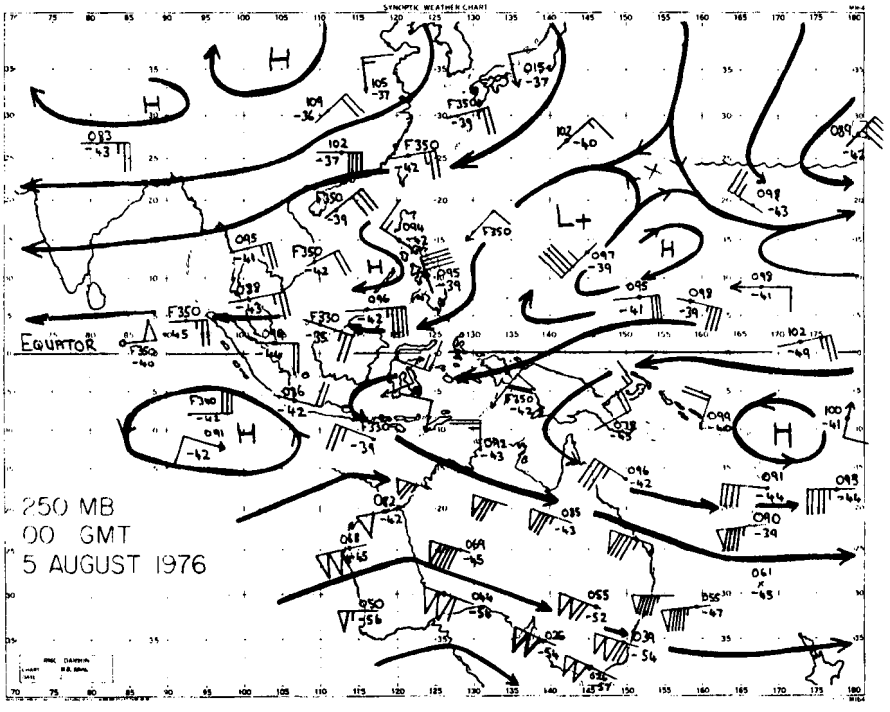

Fig. 33. 250 mb Streamline analysis, August 5, 1976.

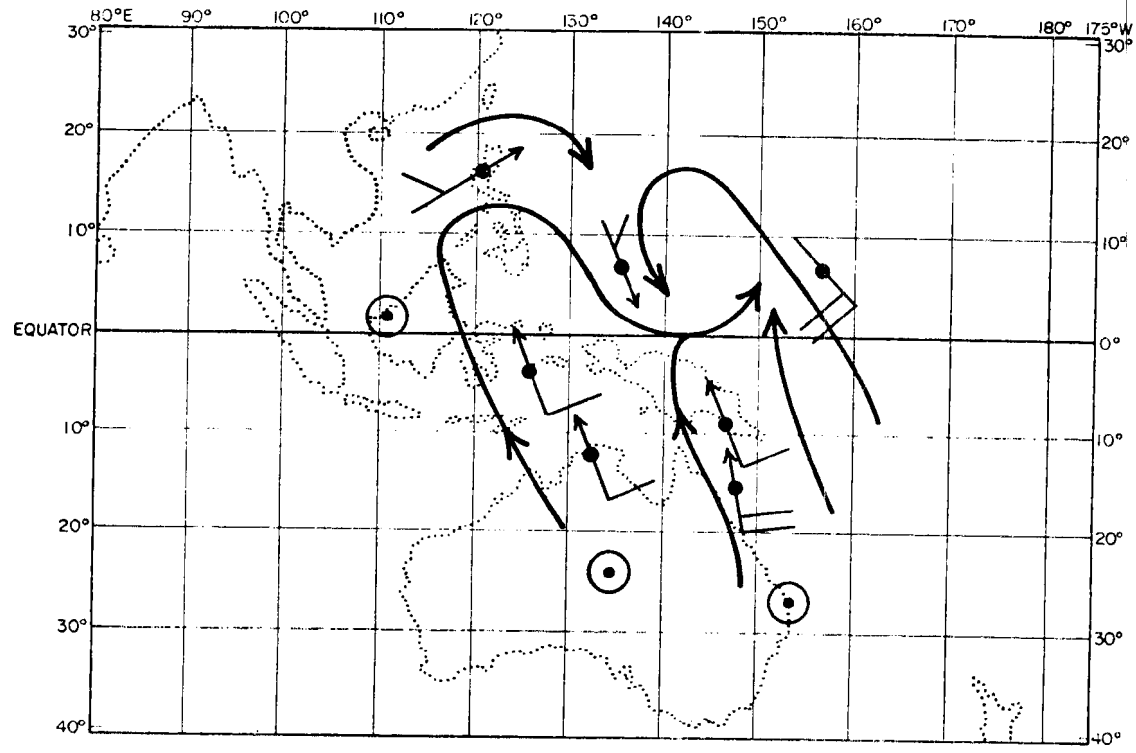

Fig. 34. Vector difference (knots) between surface winds, 3rd minus the 1st of August, 1976.

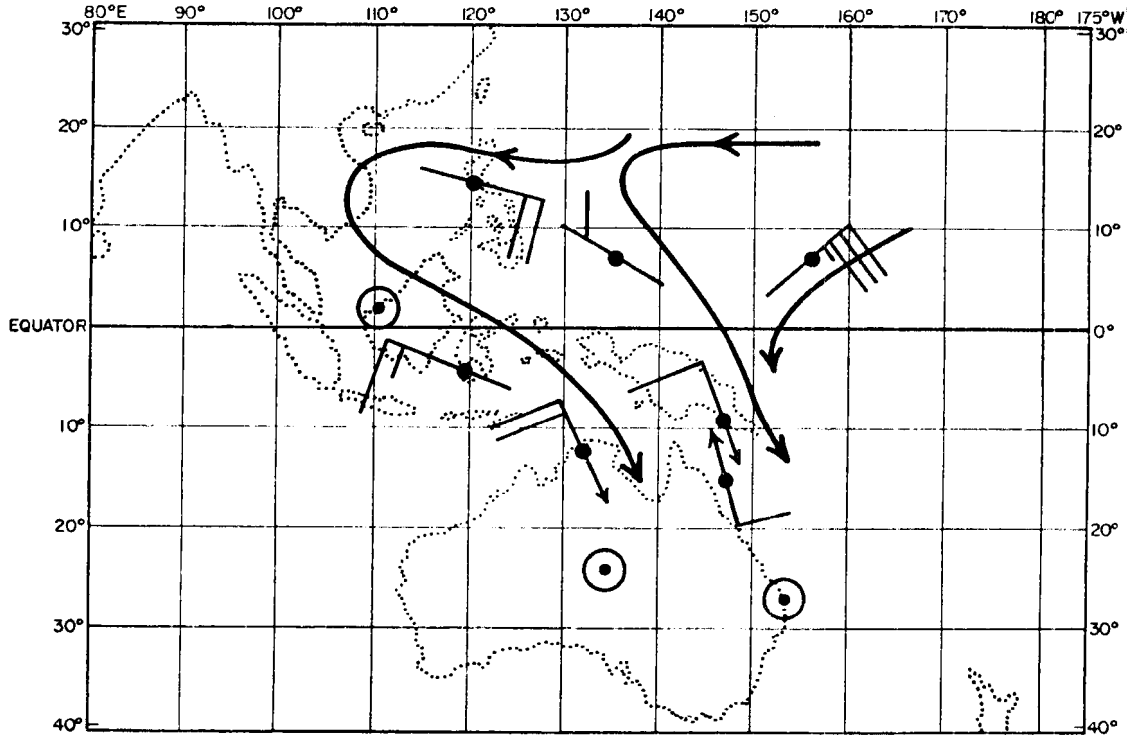

Fig. 35. Vector difference (knots) between surface winds, 5th minus the 3rd of August, 1976.

with the cross-equatorial flow weakened between the 3rd and 5th of August when compared with the earlier period. As with Figs. 21 and 22, these data seem to indicate the time scale of a surge is something less than 4 days. Furthermore, the surge is not required for the maintenance of a tropical storm, though it appears to assist in its formation

Once again the positions of the 1012 mb and 1020 mb isobars have been plotted for the days included in this case. As for the March 1977 case considered previously, Fig. 36 reveals the same equatorward surging isobars from the winter hemisphere. The maximum rate of northward motion of the isobars is around 10^{o} latitude/day (15 m/s) which far exceeds the observed meridional wind velocities. It is interesting to note that in both cases the highest equatorial pressures are in the

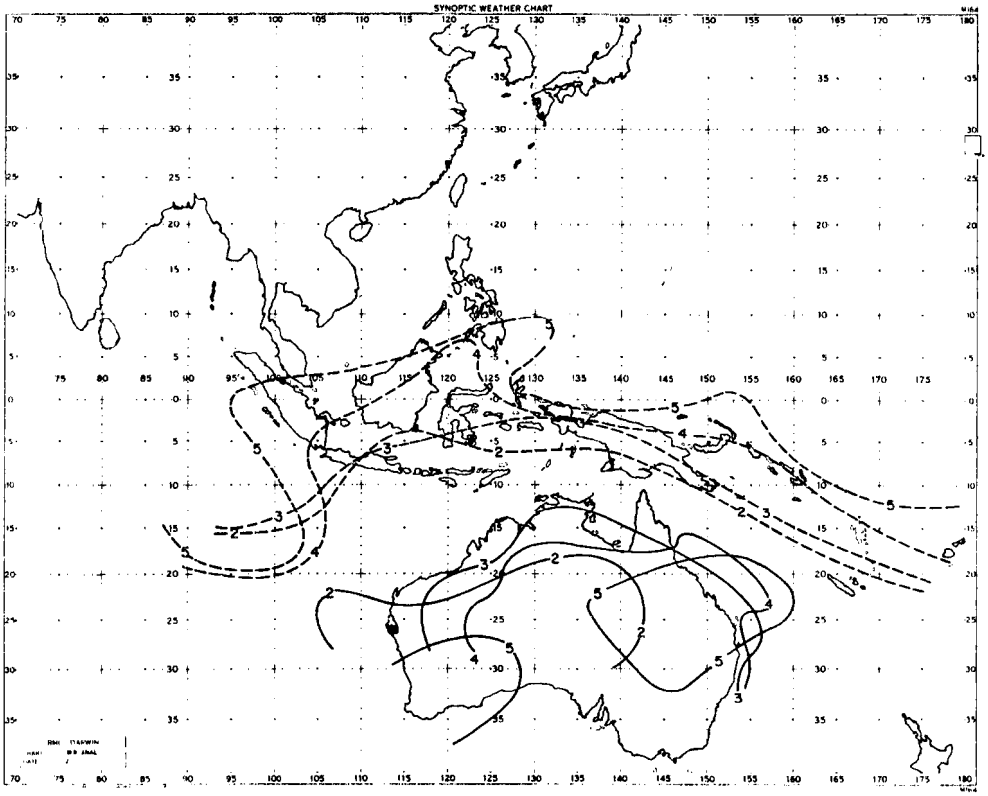

Fig. 36. Positions of 1012 mb and 1020 mb isobars at 00 GMT for 2 August, 1977.

vicinity of the Borneo/Celebes region. Inspection of the charts associated with more than seventy genesis cases reveals the region 100°E to 120°E on the equator to be in some type of preferred channel for surges from both hemispheres. This feature is further investigated in the remainder of this chapter.

As with the previous study, 10° wide longitudinal strips of satellite mosaics have been prepared to determine whether the cloud features of the northern hemisphere showed meridional propagation, with an equatorial origin, following the surge. Figure 37 depicts these data. There are the appearances of a minimum of convective cloudiness in the northern hemisphere through to the 5th of August, with the passage of the low level trough across the Australia coast on the 3rd and the 4th. On the 6th the convective activity increases on the equator and by the 13th convection appears around 22°N. Though less organized than the cloud fields in Fig. 24, those in Fig. 37 exhibit the same tendencies.

3.4 Summary of Results from Case Studies

The climatologies of the northern and southern hemispheres are sufficiently different in that in the longitude belt 70°E to 180°E March flow patterns are not the mirror image of August flow patterns. Despite asymmetries, the large scale pre-genesis situations show some striking similarities and suggest the presence of large scale teleconnections.

In both genesis events a winter hemisphere equatorwards surge of cold air led to rising pressures in the subtropical ridge of the winter hemisphere and strengthened easterly trade flow. Accompanying the

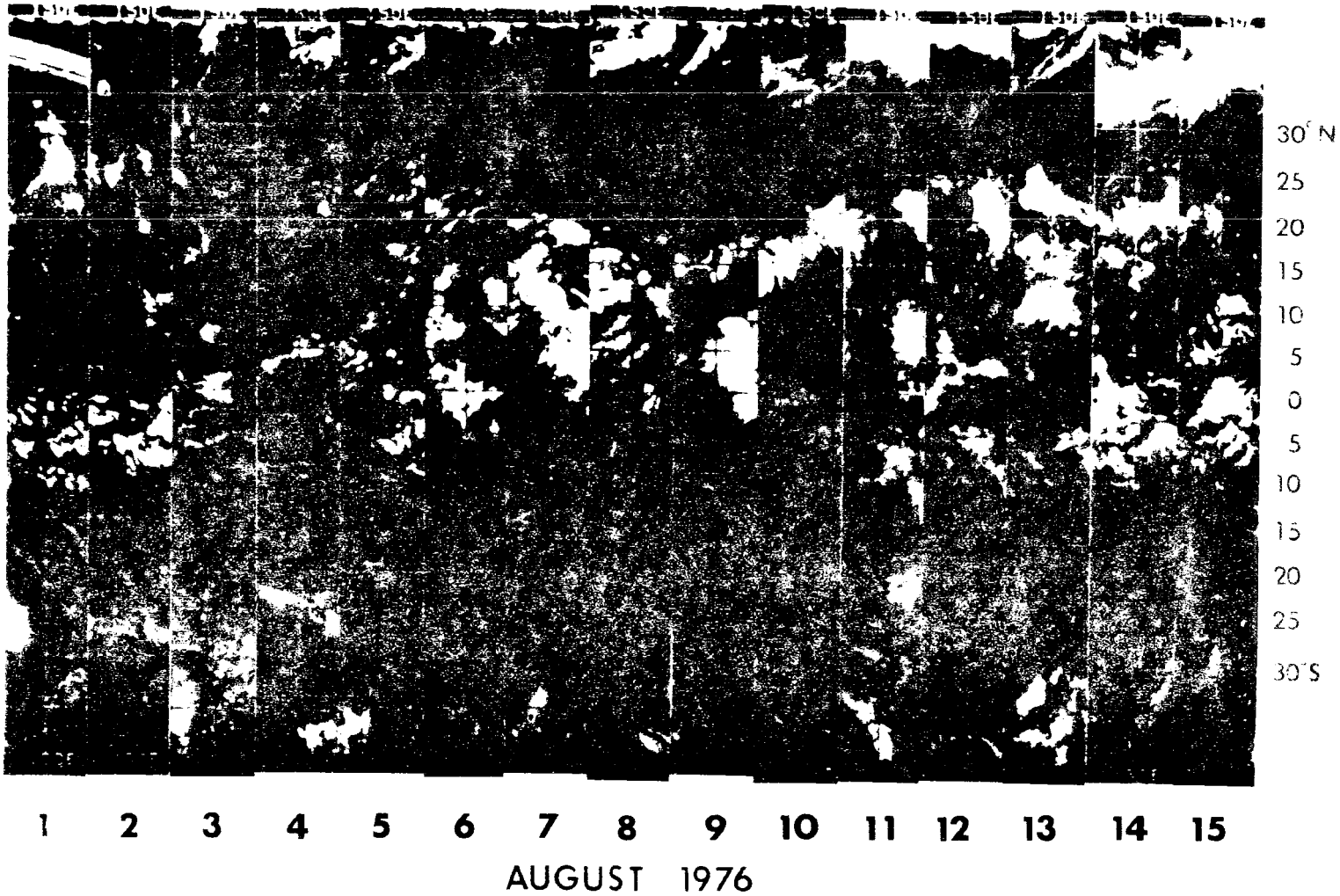

Fig. 37. Daily, 10° wide longitudinal strips of satellite masaics. The area covered is from 50°N to 50°S centered on 150°E.

midlatitude pressure rises were equatorial pressure rises suggesting cold air advection behind the cold front.

In both genesis events, the pre-genesis monsoon flow revealed stronger westerlies from the surface to 500 mb and stronger easterlies aloft. In each case, the surface pressure field in the vicinity of 0^{o}, 115^{o}E showed rises of the order of two millibars, thus establishing east-west pressure gradients close to the equator. The explanation for the enhanced westerlies may be that they are due to "down the gradient" (antitriptic) flow. In Chapter 4 the balance equation for antitriptic flow is written and an analysis of the observed flows made to ascertain whether this is an acceptable hypothesis.

The third notable feature of both studies is the apparent meridional propagation of convective areas in the summer hemisphere. Such convective activity originates close to the equator and propagates polewards. In each case the rate of cloud propagation is around 4 m/s. Similar time longitude sections of satellite mosaics have been constructed for a number of seasons, these indicate such events occur in all seasons studied. The energy source for these events appears to be in the baroclinic systems of the winter hemisphere. Furthermore, the effects in the summer hemisphere are appreciable, even when winds in the latitudes between the energy source and the tropics are easterly. This problem is addressed from a more theoretical point of view in Chapters 7 and 8.

3.5 A Survey of Many Storm Genesis Events

For the years 1974 through to 1978 a uniform data set in the form of microfilmed surface analyses, for the area 30^{o}N to 50^{o}S for the circumference of the earth, is available from the US National Weather

Service. From consideration of the case study data, five criteria for interhemispheric interactions during storm genesis have been tested. The criteria were not selected to be independent, in fact each is felt to be symptomatic of the same organized pattern of large scale circulation change. The survey is aimed at determining which provides the best forecast tool.

The five criteria are listed below with the rationale for their selection:

i) Greater than 5^{o} latitude or 10^{o} longitude displacement of the 1020 mb contour equatorwards/eastwards in the winter hemisphere, in a 24 hour period. This usually follows a cold front and is part of the cold air advection associated with a cold outbreak high.

ii) A surge of wind equatorward behind the winter hemisphere trough. Such a surge should be observed over a 10^{o} latitude longitude area (at least) for more than two days.

iii) A 10^{o} latitude displacement of the 1012 mb contour towards the ITCZ, from the winter hemisphere, in a 24 hour period. There may be multiple 1012 mb contour surges associated with the single 1020 mb contour surge.

iv) An increase in the pressure of at least 1 mb (within 5^{o} of the equator) over a region of 20^{o} longitude.

v) An increase in the winds in the belt equator to 10^{o} in the summer hemisphere. Generally speaking, winds equal to or exceeding 15 kts at the surface should be reported.

For some seventy-four tropical cyclone genesis events the tropical strip mean sea level pressure/wind charts were analyzed for fulfillment of one or more of these criteria. In not all cases, (due to poor data) could a confident assessment be made. Although difficulties were observed in about 5% of the cases, the correct change trend was often observed. Table 4 shows the percentage of time, for each hemisphere's genesis cases that each of the five criteria were met.

TABLE 4

Summary for a survey of cyclone genesis forecast parameters for seventy-four storms.

	1020 mb Isobar Movement	Winter Hemisphere Wind Surge	1012 mb Isobar Movement	Equatorial Pressure Rise	Summer Hemisphere Equatorial Winds
NH Genesis (40 cases)	51% Yes	77% Yes	56% Yes	71% Yes	70% Yes
SH Genesis (34 Cases)	83% Yes	85% Yes	65% Yes	79% Yes	74% Yes
Total Eastern Hemisphere	65% Yes	80% Yes	60% Yes	75% Yes	72% Yes

Clearly the technique works better in the northern to southern hemisphere forcing than vice versa. This may be a result of the baroclinic developments in the area east of the Asian Mainland producing more intense cold surges than their Australian counterparts.

Of the parameters chosen, the winter hemisphere wind surge provides the best forecast tool. The selection of the 1020 mb and 1012 mb isobars is overly restrictive. At times the 1024 mb and 1014 mb contours would have been more appropriate. The equatorial pressure rise is also a fairly consistent pregenesis precursor.

The difficulty with such a survey is that is doesn't address the null hypothesis, namely how often do surges occur and storms don't. Or perhaps more correctly, how often does a cloud cluster experience a surge/cross equatorial effect, and subsequently dissipate? This complementary survey has not been performed due to the lack of data on depressions which are in such favorable positions.

3.6 Discussion

The case studies presented at the beginning of this chapter indicated an organization of the large scale in such a fashion as to increase the large scale vertical wind shear in the wind field equatorward of the pregenesis cloud cluster. The sequence of events seen to occur in both cases began with the cold high behind a winter hemisphere baroclinic system initiating an equatorward surge of cold air. Pressure rises were observed to occur from the midlatitude subtropical ridge to the equatorial regions. In the summer hemisphere the monsoon westerly flow accelerated while the upper easterly flow also intensified. This shear generation was followed by storm genesis.

A survey of 74 genesis events was used to confirm that these observed large scale rearrangements occur in about 75% of all ITCZ tropical cyclone genesis events. The survey established that this particular sequence of events is neither a necessary nor sufficient condition for tropical storm genesis, but rather they provide a favorable environment.

Figure 38 shows schematically the organization of surface weather systems prior to tropical cyclone genesis in the southern hemisphere. The northern hemisphere cold outbreak high behind the eastward moving baroclinic zone is depicted, along with the equatorward surging 1012 mb isobar. In the equatorial regions enhance westerlies are shown while the steady trades of the southern hemisphere assist in enhancing convergence into the vicinity of the genesis point.

Figure 39 depicts schematically the arrangement of the surface weather systems prior to northern hemisphere genesis. There are several minor changes from Fig. 38. The area of equatorial pressure rises

appears less extensive in a longitudinal sense and closer to the genesis longitude. This reflects somewhat weaker surges of the southern hemisphere. It may also occur because the northwest Pacific clusters are moving westwards at around 8 m/s, they then 'feel' the surge effects when they are some distance east of the genesis longitude.

These idealizations of how the large scale sets up prior to genesis provide a genesis hypothesis which may be tested with composite studies. They also indicate inter-relationships between the large scale wind and pressure fields which can be further investigated with time series data.

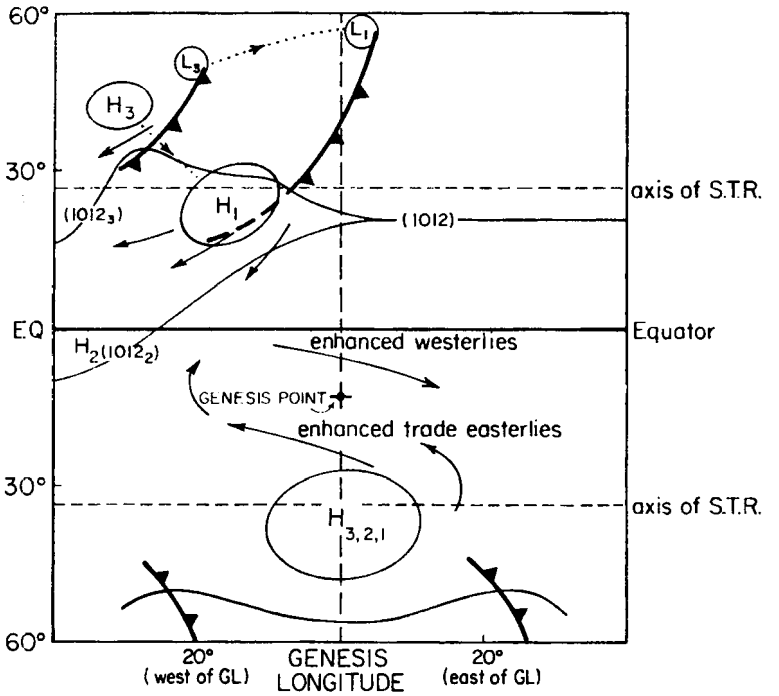

Fig. 38. Idealized surface chart showing the positions of important synoptic scale features 3 and 1 day before Southern Hemisphere tropical cyclone genesis. Subscripts denote day number before genesis.

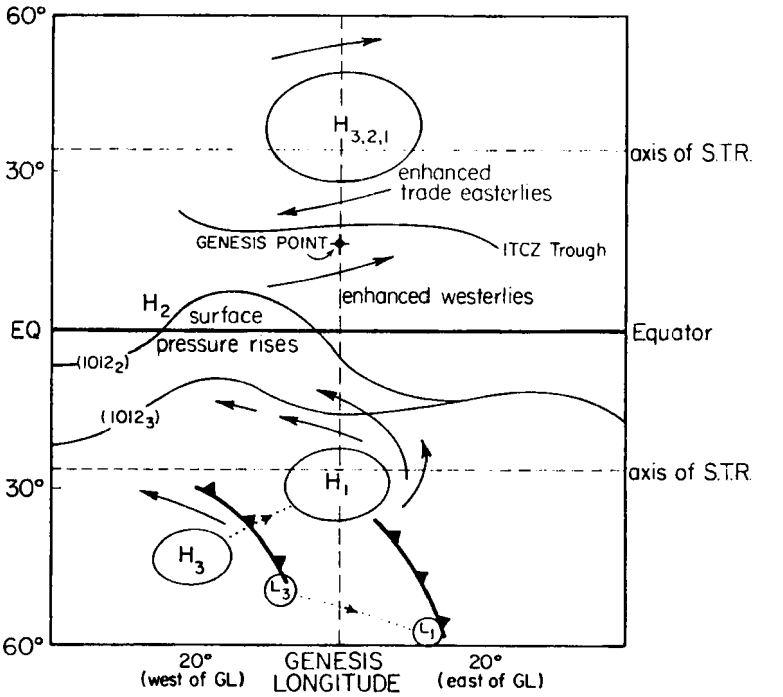

Fig. 39. Idealized picture chart showing the positions of important synoptic features 3 and 1 day before Nothern Hemisphere tropical genesis.

4. TELECONNECTIONS AND ANTITRIPTIC FLOW

4.1 Introduction

In a recent article by Wallace and Gutzler (1981), teleconnections have been defined as "contemporanous correlations between geopotential heights on a given pressure surface at widely separated points on earth". In this section the definition has been altered to include correlations between pressure fields on the surface of the earth and correlations between wind fields and pressure fields.

The case studies and subsequent survey of many storm genesis events in Chapter 3 revealed that pressure rises in the subtropics, associated with cold outbreak highs, were accompanied by pressure rises in the tropics. In this chapter it will be shown that the pressure fields of the deep tropics (within 5^{o} of the equator) are highly correlated with those of the subtropics.

An additional feature of the case study data was the observation of 'down the pressure gradient' (antitriptic) flow of the westerly winds equatorward of the ITCZ. Time series of wind fields and pressure gradients are analyzed in this chapter to determine how consistently such flows occur.

4.2 Teleconnections in the Large Scale Pressure Fields

In order to prepare time series of surface pressure data, two different sources were used. For the Borneo,China and Solomon Island areas mean surface pressures were computed daily by reading the pressure plotted at 5 or 6 stations in each area and taking an arithmetic average. The data were read from microfilmed tropical strip analyses. For stations over the Australian Mainland, in the vicinity of New Guinea and the northwest Pacific daily rawinsondes of height and temperature

were available at 900 mb, 700 mb and 500 mb. For these stations, the surface pressure was computed by use of the hypsometric equation, that is:

$$P_{surface} = P_{700} \exp\left(\frac{g\Delta z}{R\bar{T}}\right).$$

where Δz is the geopotential height in meters of the 700 mb pressure surface.

$\bar{T}$ is the mean layer temperature given by the empirical relation

$$\bar{T} = T_{900} - 0.5(T_{900} - T_{700})$$

where subscripts denote pressure levels.

The locations of the areas for which mean pressures were evaluated and stations for which it was calculated are shown on Fig. 40.

The time series of MSL area mean pressure for Borneo and China for the winter MONEX period (1st Dec. 1978 to 5th March 1979) are shown in Fig. 41. Also, plotted are the periods for which a northeasterly trade wind surge was observed to occur through longitude 120°E. The surges were defined as occurring in an area where three or more observations (usually ship observations) reported surface winds equal to or exceeding 25 knots. Furthermore, the area affected exceeded ten degrees longitude by five degrees latitude for at least two days. It can be seen (From Fig. 41) that the surges are associated with periods of high China pressure and are often followed by storm genesis in the southern hemisphere.

The two time series plotted on Fig. 41 show similar trends, the statistical significance of which may be determined through the evaluation of time lagged correlation coefficients. If the Borneo time series lags the the China time series by 12 days, then 11 and so on until it leads by 12 days, and the correlation coefficient evaluated for

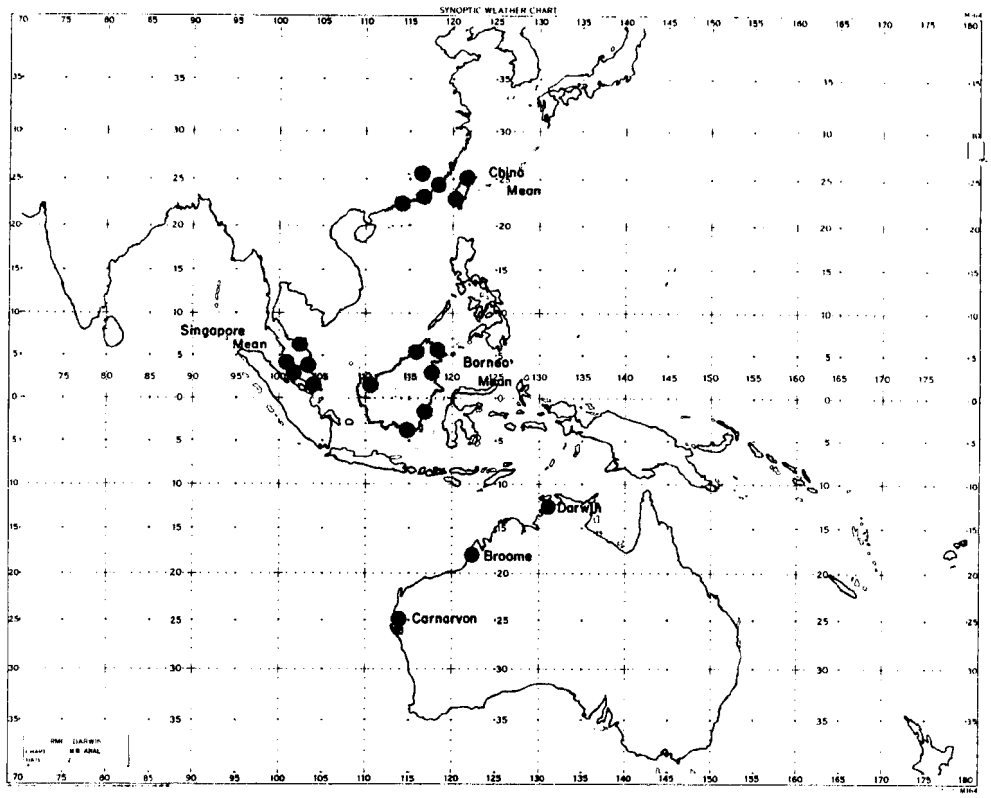

Fig. 40. Locations of stations used in time series analysis of large scale pressure fields.

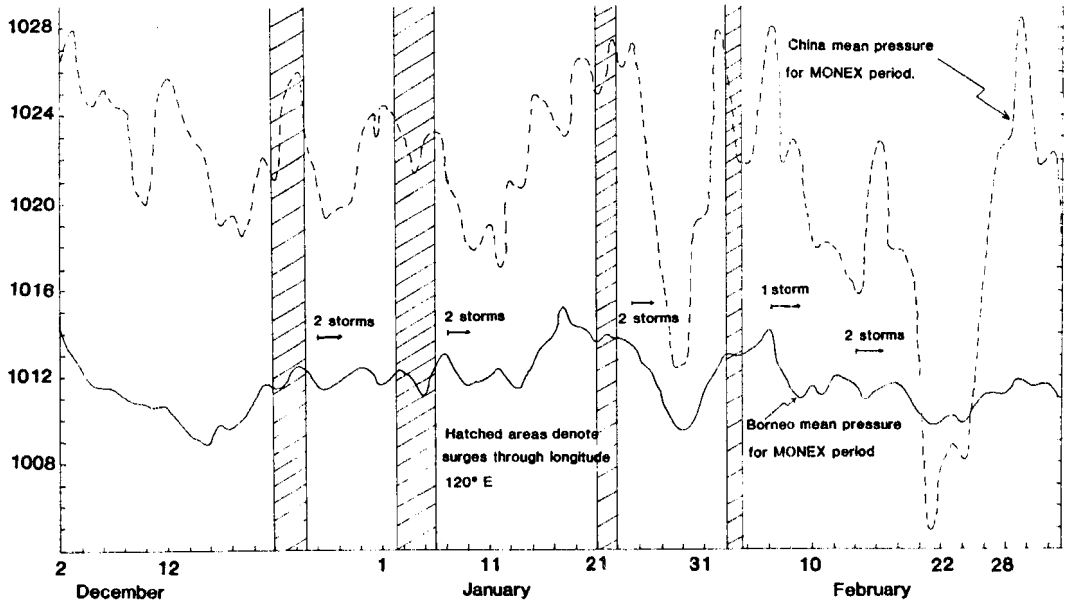

Fig. 41. Time series of Borneo and China pressures with times of Northern hemisphere cold surges and Southern Hemisphere tropical storm genesis.

each lag/lead, an appreciation of the time scale of the large scale pressure field changes can be obtained. Figure 42 shows such a time lagged correlation coefficients for the time series in Fig. 41. For a time series of 100 points a correlation coefficient of 0.25 is significant at the .01% level and .33 at the .001% level. It must be concluded from the correlation coefficient of 0.6 (on Fig. 42) that the correlation between the China and Borneo means is highly significant. If this time lagging procedure is repeated for two sine waves of equal frequency for a phase lead/lag of $\pi/2$ the correlation coefficient equals 0, at π it equals -1. Thus, it is possible that 5 days corresponds to 1/4 of the period of dominant forcing in the surface pressure field, however such a periodicity could be obtained from time lagging of two stationary series.

In order to determine whether the strong correlation between the Borneo and China mean pressures during 1978/79 occurs annually, similar time series were prepared for the 1974/75 and 1973/74 northern hemisphere winters. Table 5 shows the time lagged correlation coefficients for each of the three seasons. It is very obvious from this table that the 1978/79 season differed markedly from the two other seasons. Inspection of the synoptic charts for six winter seasons reveals that during 1978/79 the cold surges were much further east than usual. Figure 43 shows a histogram of the location of the western edge of the cold surges for the 1978/79 (year of the winter MONsoon EXperiment) season and a six season mean (which includes the MONEX season). From this figure it is quite apparent that the surges were further east than usual. Further examination of the synoptic charts revealed that in the years of many surges through the South China Sea

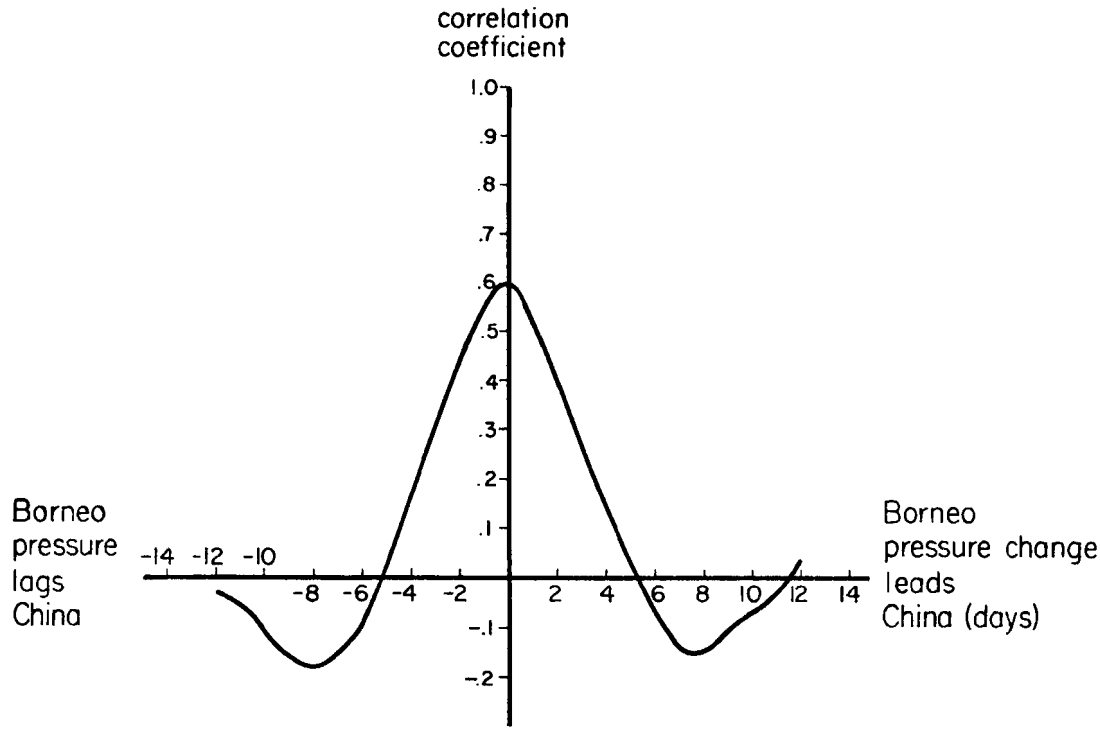

Fig. 42. Time lagged correlation between China and Borneo pressures series for the MONEX period.

TABLE 5

Hong Kong area mean pressure correlated with the Borneo mean pressure.

Lag (days)	-2	-1	0	1	2
Season					
1978/79 (MONEX)	.30	.52	.60	.56	.42
1974/75	-.06	.03	.05	.03	.01
1973/74	-.02	-.01	-.01	-.01	.02

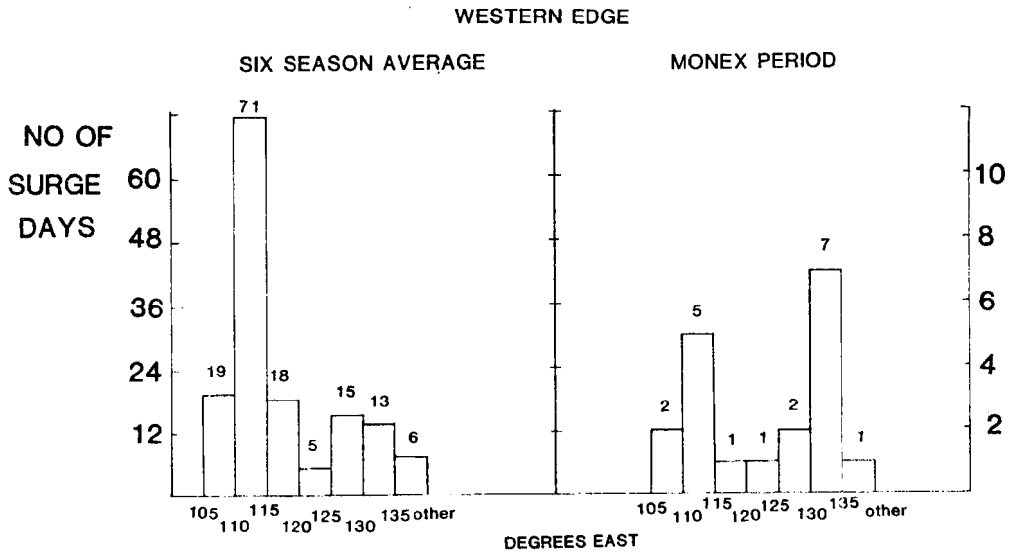

Fig. 43. Histograms giving the longitude belt in which the western edge of Northern Hemisphere, winter, cold surges were located. The long term (six season) distribution is contrasted with that for the MONEX period.

(longitudes 110°E to 120°E) small low pressure systems form in the vicinity of the Borneo northwest coast, leading to a regional lowering of the pressure at times of strong pressure rises over the Hong Kong area and thus giving rise to a negative correlation between China and Borneo area pressure fields.

It is possible to depict schematically the flow of the Borneo region in the MONEX period and contrast that with the two typical flow regimes more usually observed. Figure 44 shows the MONEX period cross-equatorial flow, with the surge zone for that season between longitudes 120°E and 150°E. Figure 45 depicts the six year mean surge zone and associated low level cross-equatorial flow. Figure 46 has the same surge zone as in Fig. 45, but now the flow around northwest Borneo is perturbed by a low. The more intense the surge, the stronger the low and hence a negative correlation between midlatitude pressure and Borneo pressure occurs for some periods while a positive correlation occurs at

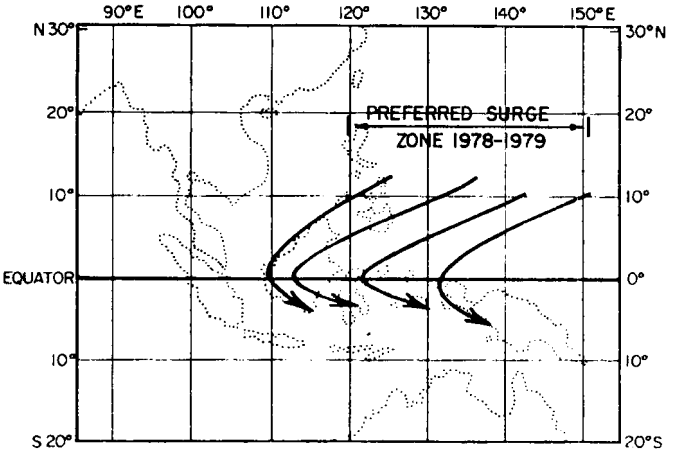

Fig. 44. Schematic chart showing the mean gradient level (300 m elevation) flow during the MONEX period, in the equatorial area around longitude 120°E.

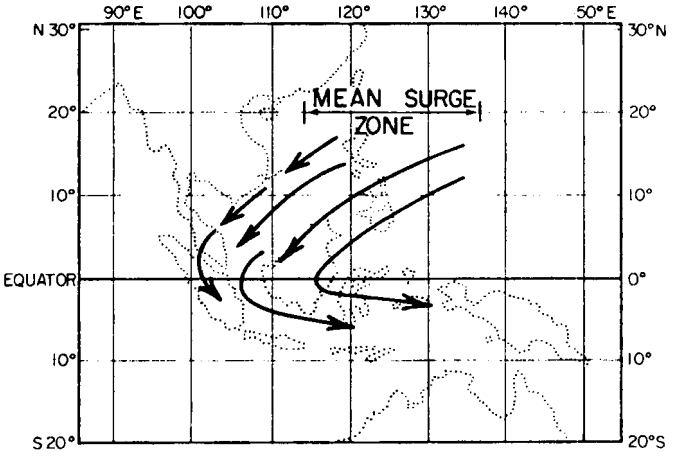

Fig. 45. Schematic chart showing the long term mean gradient level flow in the vicinity of 120°E with no Borneo low pressure system.

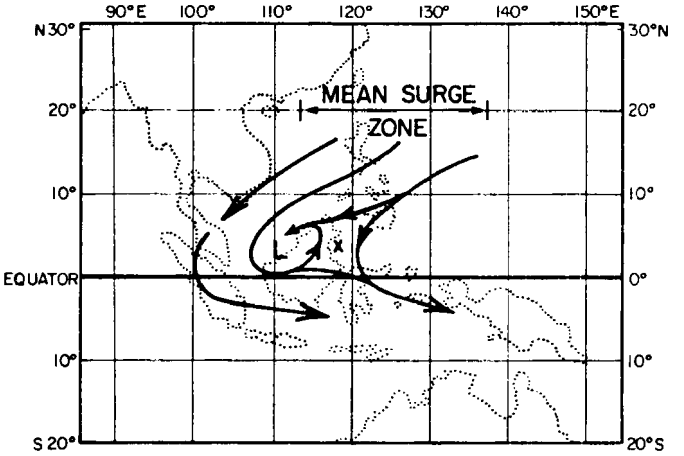

Fig. 46. Schematic chart showing the long term mean gradient level flow in the vicinity of 120°E. This chart depicts a Borneo low pressure system.

times when the flow is unperturbed by Borneo lows. Thus, when seeking to understand the large scale pressure field teleconnections, it is necessary to study the weather systems which occur within the region of study.

For the 1973/74 and 1974/75 seasons a mean pressure was evaluated for the Singapore area which appears to be uneffected by the Borneo lows. Table 6 shows the correlation coefficients for the time lagged correlation between the Hong Kong and Singapore mean pressures. It is quite apparent that the large scale pressure field teleconnections is in effect for the 1973/74 season, though the effect is reduced in 1974/75.

Chang and Lau (1980) and Chang et al. (1979) have studied those events wherein a cold surge through the South China Sea is associated with the development of a Borneo low. Chang and Lau show schematically that the enhanced convection in the Borneo area is the ascending branch of both the Hadley and Walker circulations. Analysis of the time series data and many cases suggests such circulation regimes occur around November and December. By January and February the ITCZ is well established in the Southern Hemisphere and the strongest ascending branch of the Hadley and Walker circulations is over the New Guinea highlands and Solomon Islands. During these periods the pressure fields over China and Borneo rise and fall in phase.

The same type of investigation has been carried out to determine whether during the southern hemisphere winter, the Borneo pressure field is highly correlated with the stations equatorward of the subtropical ridge in the southern hemisphere. The results of this study are given in Table 7, for the 1974 Austral winter and Table 8 for the 1975 Austral winter. The correlation coefficients are lower than in the Northern

TABLE 6

Hong Kong area mean pressure correlated with the Singapore area mean pressure.

Lag (days)	-2	-1	0	1	2
Season 1973/74	.49	.57	.50	.27	-.08
1974/75	.13	.19	.26	.22	.18

TABLE 7

Correlation coefficients for the correlation of Australian station surface pressures with the Borneo area mean surface pressure 1975.

	Day Before				
Year 1975 Station	-2	-1	0	1	2
Broome	.09	.08	.21	.32	.27
Carnarvon	-.03	.17	.25	.19	.15
Darwin	.05	.08	.32	.42	.32
Perth					

TABLE 8

Correlation coefficients for the correlation of Australia station surface pressures with the Borneo area mean surface pressure 1974.

	Day Before				
Year1974 Station	-2	-1	0	1	2
Broome	.14	.14	.23	.33	.23
Carnarvon	.08	-.02	-.03	-.07	-.03
Darwin	.02	.08	.25	.37	.27
Perth	.05	-.06	-.04	-.11	-.21

Hemisphere case yet still highly significant for the Australian station pressure lagging the Borneo pressure by about 1 day. The time lag may enter the system because the stations are located to the east of Borneo

while the pressure field forcing of the subtropical ridge generally occurs through its interaction with the eastward propagating weather systems of the westerly wind belt. The lower correlations may enter the system for one or more reasons. The computation of surface pressure downward may neglect the effect of cold air surges beneath the trade inversion. Or alternatively, the southern hemisphere surges may be less intense than their northern hemisphere counterparts, leading to weaker interactions between the subtropics and the equatorial regions.

The importance of the surges in maintaining high correlations may be assessed in a somewhat subjective manner. Inspection of the curves on Fig. 41 suggests that in early December the pressure fields are less highly correlated than after the first surge. Evaluating the correlation coefficient at zero time lag for the two series, from the first of January to 5 March yields a coefficient which has risen from 0.6 for the entire series to 0.78 for this partial series. Performing similar analyses on the other seasons indicates that after the first surge of each winter season the pressure fields have this strong tendency to oscillate together.

The poor correlation of Carnarvon (Table 8) (and all stations south) may be explained by noting the different climatologies of it from Broome and Darwin. Through the Austral winter, Broome and Darwin lie in the southeast trades exclusively. Carnarvon is effected (at times) by the passage of westerly troughs whose associated cold outbreak highs may perturb the subtropical ridge to a greater or lesser extent not well determined by the magnitude of the pressure change across the trough.

In summary, there appears to be a teleconnection between the winter hemisphere subtropical pressure fields and those in equatorial regions.

The deep equatorial pressure fields are observed to be 'beating in time' with those in the winter hemisphere midlatitudes. Furthermore, for stations on the same longitude, near simultaneity between midlatitude and equatorial pressure rises, are observed.

4.3 Antitriptic Flow

From inspection of case study data it would appear that the monsoon flow in the tropics has a component directed down the pressure gradient. In this section it will be shown from theoretical considerations that quite large deviations from geostrophy are to be expected in the deep tropics. Mahrt (1972) has shown that strong cross isobar flow in the boundary layer can be expected in a cross equatorial stream as the rapidly changing Coriolis with latitude is not compensated for by corresponding pressure gradient changes. This effect rapidly damps away from the equator, and would not appear to be observable more than 3^{o} downstream from the equator. It will be seen in Chapter 8 of this paper that strong cross isobar flow occurs in the absence of friction, however in this chapter an analysis is perfomed to identify cross isobar flow in the monsoon stream within 10^{o} of the equator, with friction playing a part in the observed processes. Time series of pressure gradient and wind data are examined for areas encompassing both northern and southern hemisphere monsoon westerlies.

Antitriptic flow has been defined by Saucier (1955, p. 242) as one characterized by a balance between Coriolis, pressure gradient and frictional forces. It is possible to parameterize the frictional force by assuming that it acts against the flow and is proportional to the wind speed. Following the analysis of Schaefer and Doswell (1980) the balance equation for antitriptic flow can be written:

$$-fk\mathbf{x}\,\mathbb{V}_{AT} - \alpha\nabla p - K\,\mathbb{V}_{AT} = 0 \qquad [2]$$

where K is the Guldburg-Mohn coefficient, and $\mathbb{V}_{AT}$ is the antitriptic wind vector.

An alternative definition for the antitriptic wind is found in the Glossary of Meteorology (1959 page 36). In this definition a two way balance between friction and pressure gradient is assumed and the examples of antitriptic flow given are mesoscale events where their time scale is much less than 1/f. However, in the tropics there remains the question of whether ($-f\hat{k}\mathbf{x}$ V) is of the same order of magnitude as ($\alpha \nabla$ P). Noting from Fig. 51 that (∇ P) is approximately 5 mb over 40^{o} longitude and $|\mathbb{V}|$ is approximately 5 m/s, a crude scale analysis reveals that for latitude less than 4^{o} latitude the balance in Eq. 2 is primarily between friction and the pressure gradient force. That is at very low latitudes winds adjust to east-west pressure gradients by running down the gradient. In the latitude belt 4^{o} to 20^{o} there is a three way balance between the pressure gradient, Coriolis and frictional forces.

It may be noted that in Eq. 2 the acceleration term has been neglected. The adjustment time for the pressure/wind fields coming to balance in the presence of unbalancing perturbations is given by Silva Dias and Schubert (1979) as:

$$T = r_e/C_g \qquad [3]$$

where r_e is the e-folding radius of the disturbance and C_g the group velocity of the gravity waves generated by the out of balance wind and pressure fields. For an equatorial pressure rise with r_e equal to 20^{o} longitude and a gravity wave group velocity of 56 m/s (which corresponds

to a two layer atmosphere (Silva Dias and Schubert, 1979) then on a time scale of about one half a day the wind and mass fields can be assumed to come to balance. If time series data are to be used to investigate the large scale, long term relationships between winds and pressure gradient, observations taken daily should be used to ensure that short term oscillations associated with adjustment processes do not contaminate the results.

Returning to Eq. 2 and noting that it is appropriate for large scale, slowly varying, straight flows at least 4^{o} from the equator, then by use of the geostrophic wind relationship the difference between this antitriptic wind and the geostrophic wind may be illustrated.

Substituting for the geostrophic wind

$$\mathbb{V}_g = \hat{k} \times \frac{a}{f} \nabla p \qquad [4]$$

in Eq. 2, and rearranging gives:

$$\mathbb{V}_{AT} = \frac{1}{(1 + K^2/f^2)} \left[\mathbb{V}_g - \frac{K}{f} \mathbb{V}_g \times \hat{k} \right] \qquad [5]$$

In order to solve (5) for the magnitude and speed of the antitriptic wind it is necessary to have a good estimate of K. In general, the flow is considered to be antitriptic in the boundary layer where the frictional dissipation of the wind is parameterized by:

$$\frac{C_D \rho \mathbb{V}^2}{Z} = K|\mathbb{V}| \qquad [6]$$

$$C_D = 4 \times 10^{-3}$$

$$\rho = 1.25 \text{ kg/m}^3$$

$$\mathbb{V}^2 = 10^2 \text{ m}^2/\text{s}^2$$

$$Z = 10^3 \text{ m}$$

substituting the typical values for the constants and solving (6) for K yields a value of 5×10^{-5} s^{-1} which is equal to that used by Schaefer and Doswell (1980). Above the boundary layer (K) is assumed to decrease rapidly reducing (2) to the geostrophic balance equation.

In the westerly monsoon stream equatorward of the ITCZ the effects of abundant tropical convection must be considered. If cumulus clouds rearrange momentum in the vertical, in a down gradient sense, they will decelerate the flow. In this situation the friction cannot be considered to go to zero above the boundary layer and the observations would be expected to show a deep layer of antitriptic flow.

Before solving Eq. 5 for the deep layer antitriptic flow an estimate of the deep layer deceleration due to convection is required. Lee (1981) has calculated the effect of subgrid processes (including convection) on the tangential momentum fields for a number of composite tropical cyclones in the north Atlantic and northwest Pacific oceans. Lee defines the total conective effect as that residual which results from evaluation of all the terms in the radially averaged tangential momentum equation except that of vertical advection of momentum. Figure 47 shows the acceleration of the tangential winds by this total convective effect for the composite Atlantic Tropical cyclone, Developing Stage 3 (ATD3). Below 600 mb there appears to be a deceleration of the tangential wind which suggests friction is not zero in this layer.

Figure 48 shows a vertical profile of the ATD3 radially averaged tangential wind and a vertical profile of the composite zonal component of the wind, one day before tropical cyclone genesis in the southern hemisphere in the westerly monsoon stream, 20^{o} northwest of the

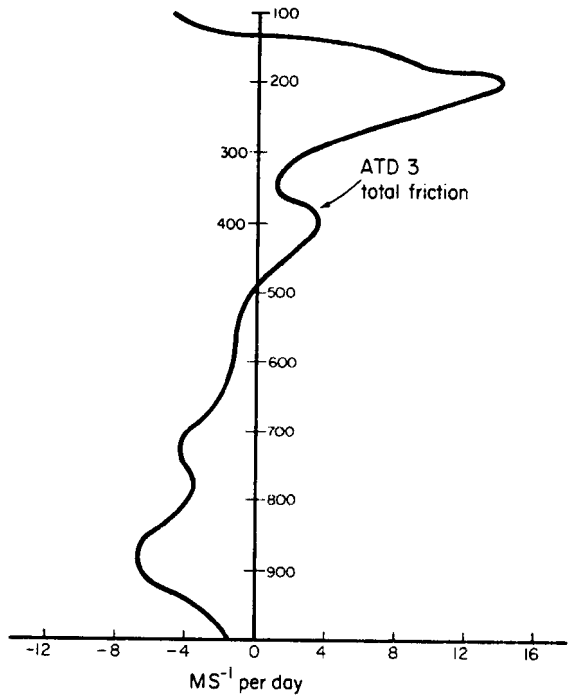

Fig. 47. 1-5° azimuthal average of the total convective effect for Atlantic developing tropical cyclone (ATD3). (After Lee, 1981).

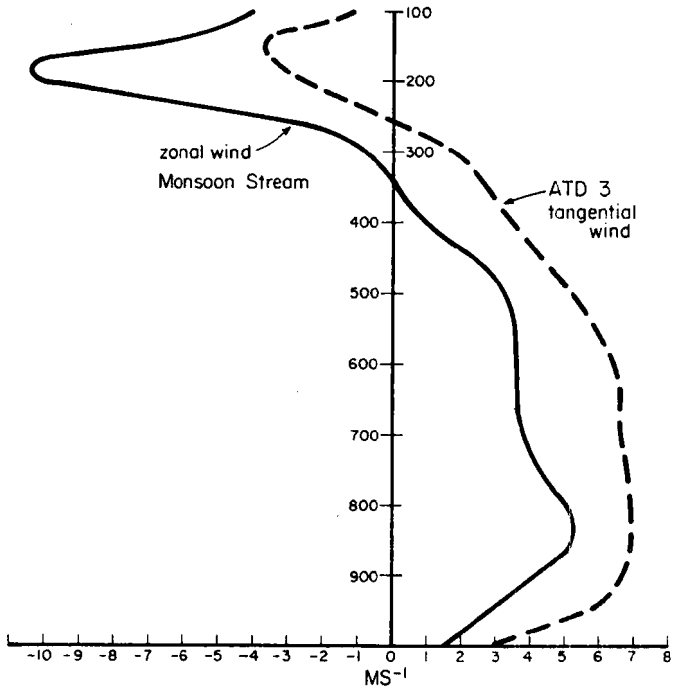

Fig. 48. Vertical profile of zonal wind one day before genesis in the northwest monsoonal stream and 4° radius profile of tangential wind in ATD3 system (dashed). Both data sets are for composites of many weather systems.

circulation center. (Further discussion of this data is left for Chapter 5). The curves have similar net shear and a similar profile, however, the cyclone tangential wind profile is displaced further to the right of the somewhat arbitrary origin. The similarities lend support to the contention that convection embedded in the monsoon current may modify the zonal momentum field in a similar fashion to the way convection in the ATD3 system modifies the tangential wind field. In order then to get a crude estimate of K in the monsoon westerlies it is possible to hypothesize that below 700 mb, the deceleration due to the total convective effect is of the order of 5 m/s/d acting on a wind of order 5 m/s. K is then equal to $1.2 \times 10^{-5} s^{-1}$.

Returning to Eq. 5 which is the equation for a circle of diameter $\mathbb{V}_g$ a graphical representation of the difference between $\mathbb{V}_{AT}$ and $\mathbb{V}_g$ may be plotted. The angle (θ) between $\mathbb{V}_g$ and $\mathbb{V}_{AT}$ is given by:

$$\theta = \tan^{-1} (K/f)$$

Using a value of $K = 1.2 \times 10^{-5}$ the $\mathbb{V}_{AT}$ vector, from 5° latitude to the pole, for each hemisphere has been plotted on Fig. 49. It must be remembered that as the Coriolis parameter becomes small, the veering angle will tend to 90°, with antitriptic winds running down the pressure gradient.

Rather than merely hypothesizing that in a monsoonal flow the convection acts to decelerate the lower levels of westerly flow, it is possible to make some crude calculations of (K), given time series of winds and pressure gradients. However, the space scale of such an investigation is an important parameter. Silva Dias and Schubert (1978) have shown that in the tropics the wind field can be expected to adjust

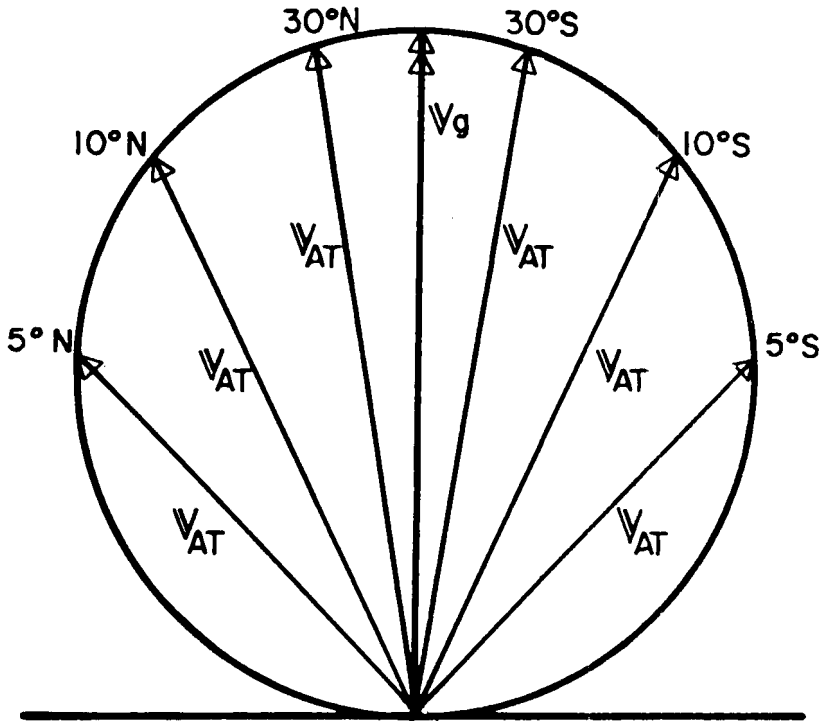

Fig. 49. Graphical representation of the relationship between V_{AT} and V_g at varying latitude, for $K = 1.2 \times 10^{-5} s^{-1}$.

to the pressure field in those situations where the pressure perturbation has a radius larger than the Rossby radius of deformation. At 5^{o} latitude, for a two layer atmosphere (with easterlies above westerlies, as shown in Fig. 48) the Rossby radius of deformation is about 1500 km (Silva Dias and Schubert, 1979). In investigating the degree of antitripicity of the large scale tropics it is necessary then to determine pressures over distances around 20^{o} of longitude (or greater).

Two large scale pressure gradients have been defined. The first from Borneo to the Solomon Islands, the second from Borneo to 5^{o}N, 165^{o}E. For each gradient, about 100 days of surface pressure gradient (Δp's) have been calculated and cross correlation coefficients between these and the winds at stations between the end points of the gradients calculated. Figure 50 shows the locations of these stations and areas.

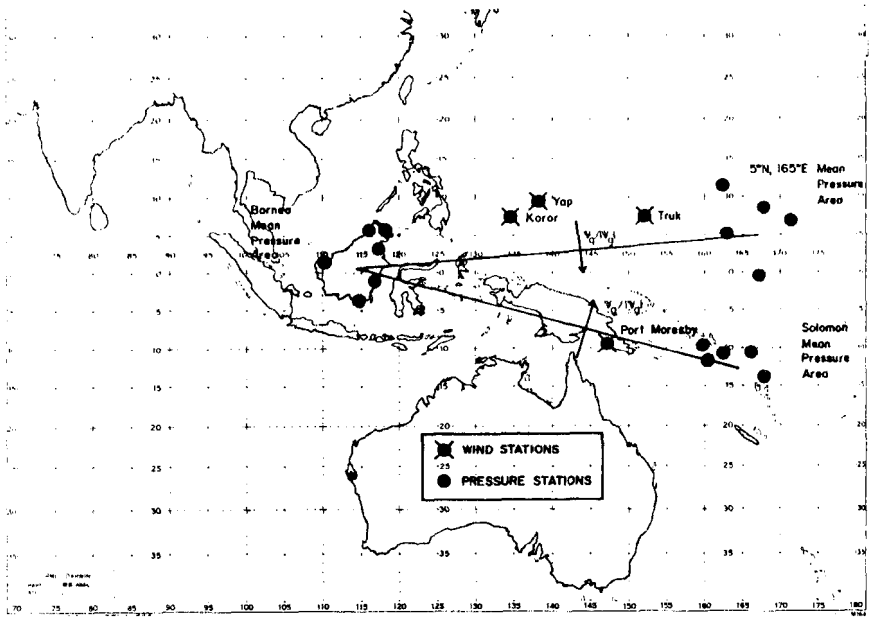

Fig. 50. Locations of areas for which large scale pressure gradients were calculated and intervening stations whose wind fields were cross correlated with the pressure gradient time series.

The wind field time series initially lags the pressure field by twelve days and then the lag is progressively reduced by one day until it leads by 12 days. By selecting the day of maximum correlation between the two, the response time of the antitriptic wind to the pressure gradient may be calculated. In order to calculate θ, the angle between $\mathbb{V}_g$ and $\mathbb{V}_{AT}$, the station wind field is resolved into components normal and parallel (v_1 and v_2 respectively) to $\mathbb{V}_g$, and the correlation coefficient between Δp and v_1 calculated. The wind field is then decomposed into components where v_1 is at 80° to $\mathbb{V}_g$ and the lag/lead correlation coefficients reevaluated. This procedure is repeated in 10° steps until v_1 is parallel to $\mathbb{V}_g$. The angle between $\mathbb{V}_{AT}$ and V_g is assumed to be that when the correlation between Δp and v_1 time series is greatest.

Figure 51 shows the 600 mb wind (v_1 component) at Port Moresby and the Borneo–Solomon Island pressure gradient for the Austral summer of

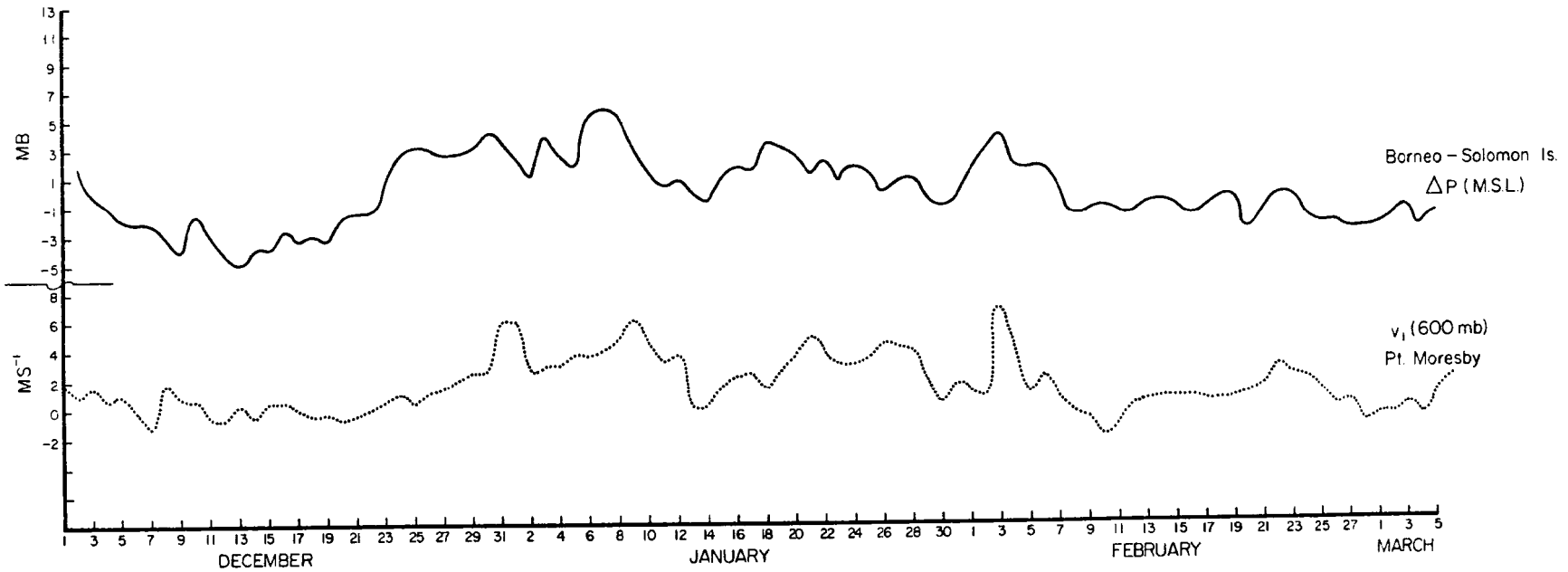

Fig. 51. The 600 mb V_1 component at Port Moresby and the Borneo Solomon Islands pressure gradient for the MONEX period. The angle between V_1 and V_g is 54°.

1978/79. The two curves appear similar and cross correlation coefficients support these similarities. Figure 52 shows several plots of the correlation coefficient between these series for lag of 12 days through to lead of 12 days, for differing angles between v_1 and Ψ_g. From these data it has been concluded that the angle between Ψ_{AT} and Ψ_g is 54^o. The time series for v_1 at 54^o is that plotted on Fig. 51. Figure 52 shows a similar trend to observed in all other time/angle lagged correlations. That is, for large angles between Ψ_g and v_1, the wind field lags the pressure gradient by relatively few days. Then as the angle between Ψ_g and v_1 decreases, the time lag between wind field pressure gradient maximum correlation increases. This suggests that with the establishment of an east-west equatorial pressure gradient the winds commence 'running down' the gradient. Then with an increasing number of days the winds begin veering towards geostrophic balance. That the time scale of this process is of the order of days is difficult to explain. Perhaps the intensity of convection decreases with time after a surge lowering K, leading to a tendency towards geostrophic balance.

Tables 9 and 10 carry data for these time/angle lagged calculations of correlation coefficient for two summer seasons in each hemisphere. The southern hemisphere monsoon most closely approximates a straight antitriptic stream (centrifugual forces have been neglected in (2)), perhaps explaining the higher correlation in Table 9 than in 10. The 950 mb data for the 1978/79 season gave the unusual result that the best correlation occurred at an angle of θ greater than 90^o. The data showed the correlation between Δp and v_1 to be high through to an angle of

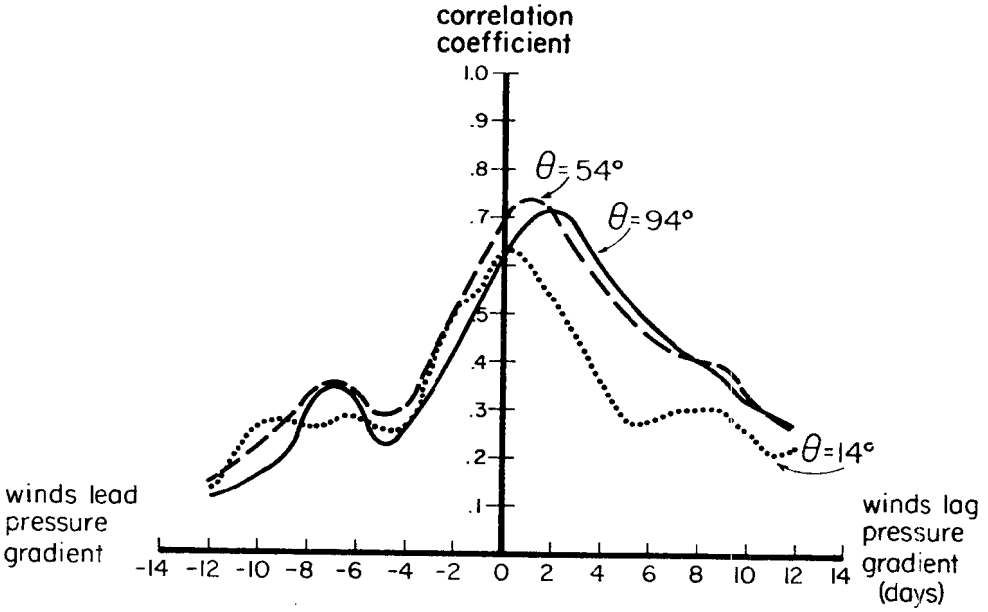

Fig. 52. Time lagged correlation coefficient for angles of 94°, 54° and 14° between V_1 and V_g, for 600 mb wind at Port Moresby during the MONEX period.

74° and then dropping off sharply. Accordingly 74° has been suggested as an appropriate θ.

Because of the extreme crudeness of this technique, it was felt that the arithmetic mean of the veering angles, substituted into (6) would be sufficient to give an order of magnitude estimate of K. For a latitude of 8° (which is close to the wind stations latitudes) for the norhern hemisphere $K = 3.5 \times 10^{-5} s^{-1}$ and for the southern, $K = 2.0 \times 10^{-5} s^{-1}$. These are slightly larger than the data of Lee (1981) would suggest, but not unreasonable considering the crude method of their determination.

4.4 Discussion and Conclusions

In Chapter 3 it was seen that associated with subtropical wind field surges in the winter hemisphere were pressure rises throughout the subtropics to equatorial regions. In this chapter time series of subtropical pressure fields were correlated with those of equatorial

TABLE 9

Correlation between Borneo mean pressure minus the Solomon mean pressure and the wind at Port Moresby southern hemisphere summers.

Year	Level	Maximum Corr. Coefficient	No. of Days Wind Lags Pressure	Angle Between V_g and V_{AT}
1975/76	900 mb	.60	4	34^o
	700 mb	.61	3	24^o
1978/79	950 m	.69(.74)	4(4)	$74^o(104^o)$
	600 mb	.73	1	54^o
				Mean 46^o

TABLE 10

Correlation between Borneo mean pressure minus 5^oN, 165^o mean pressure and northwest Pacific station winds, Northern hemisphere summer.

Year	Station	Level	Maximum Corr. Coefficient	No. of Days Wind Lags Pressure	Angle Between V_g and V_{AT}
1974	Koror	900 mb	.40	7	27.5^o
		700 mb	.46	5	77.5^o
	Yap	900 mb	.42	6	77.5^o
		700 mb	.51	5	77.5^o
	Truk	900 mb	.38	5	37.5^o
		700 mb	.38	5	37.5^o
1975	Koror	900 mb	.53	5	57.5^o
		700 mb	.45	5	57.5^o
	Yap	900 mb	.43	5	47.5^o
		700 mb	.42	5	67.5^o
	Truk	900 mb	.36	5	77.5^o
		700 mb	.34	4	77.5^o
					Mean 60^o

pressure fields. It was seen that the equatorial pressure fields move up and down in rythmn with the subtropical fields. The development of regional scale weather systems can obscure this relationship, but by selecting areas not affected by these systems the subtropical-equatorial connection can be shown to be present in all winter seasons.

It was also seen in Chapter 3 that winter hemisphere surge events can lead to east-west pressure gradients becoming established on the equator. In order to investigate how the observed wind fields relate to large scale equatorial pressure gradients four seasons of time series data were analyzed. In all cases the component of the wind which correlated most highly with the observed pressure gradient was at an angle to both the pressure gradient and the geostrophic wind vector. Using this angle a mean friction coefficient for each hemisphere was calculated, these were of a similar magnitude to that obtained by Lee (1981) in a much more sophisticated analysis. The intriguing result that it takes up to four or five days after establishment of a pressure gradient to observe the wind field which correlates most highly with it remains unexplained, though it may be related to changing levels of convection within the monsoonal stream. An alternative explanation could be that after the initial establishment of an equatorial east-west pressure gradient, the wind fields rapidly adjust. Accelerated monsoonal westerlies trigger ITCZ disturbances which further accelerate the westerlies over some longer time period, leading to high correlations at 4 days lag. In this latter situation the friction calculations would be invalid.

In conclusion, the time series analyzed have shown that winter hemisphere baroclinic actions constantly change the east-west equatorial

pressure gradients. They also reveal the winds to be substantially out of geostrophic balance, with a tendency for 'down the gradient' flow. However, the subsequent calculation of friction in the monsoon stream from the diagnosed veering angles must be treated with caution, and must further be investigated.

5. COMPOSITE MIDLATITUDE HEIGHT FIELDS

5.1 Introduction

In Chapter 2 it was shown that for months of differing tropical cyclone climatologies the large scale dynamic parameters were considerably altered, particularly in the winter hemisphere. Through the consideration of case study data in Chapter 3, it appeared that cold surges in the winter hemisphere can lead to increased equatorial westerly flow which assists in the tropical cyclone genesis process. A survey of seventy four cyclones revealed that the cross equatorial forcing was present in about 75% of all genesis events.

In this chapter a large number of days have been separated into four classes depending on where they appear to be in the tropical cyclone quiet/active cycle (described in Chapter 1). Composite midlatitude height fields are presented for each class, for an area 50^{o}N to 50^{o}S over a 90^{o} wide longitude belt. Using these data it is possible to obtain an appreciation of the midlatitude height anomalies preceeding tropical cyclone genesis without having to contend with the problem of cyclone circulations biaing the data. Unfortunately the analysis schemes used to prepare the data make it exceedingly difficult to draw conclusions on how the tropical flow fields evolve prior to storm genesis.

It will be seen that anomalies of the order of 50 GeoPotential Meters (GPM) do develop in both winter and summer hemispheres prior to genesis. The summer hemisphere anomaly is indicative of increased anticyclonicity poleward of the developing ITCZ system, the winter hemisphere anomaly suggests increased baroclinicity at all levels in the genesis longitudes. These conclusions are based on the analysis of data

for both northern and southern hemisphere summers in the eastern hemisphere.

5.2 Data Stratification Procedure

In order to investigate the interaction between midlatitude flow fields and the tropics, the quiet and active periods were defined more precisely. A quiet period is one for which no tropical cyclones occur within $\pm$ 4 days and is defined at a longitude for which no cyclones occur within $\pm$ 40^{o} (longitude). An active period commences on the day the responsible national tropical cyclone warning centre first analyzes (in their best track summary) a disturbance to have gradient level wind speeds in excess of 34 kts. The active period continues through to the dissipation of the last storm existing in that period.

A summary of the important large scale flow pattern differences between quiet and active periods can most effectively be made by compositing available synoptic data for a series of dates, stratified by their belonging to quiet or active periods.

The preparation of a composite analysis requires a point to be defined about which the data are composited. In analyzing the midlatitude flow patterns associated with active periods, data were composited about the longitude of storm genesis keeping latitude fixed. The contrasting quiet period sample was chosen to have the same longitude and Julian day number distribution, as the active sample. To more accurately specify the evolution of the midlatitudes in the period preceding tropical storm development, four data stratifications were composited:

i) 3 days prior to an active period (denoted -3)

ii) 1 day prior to an active period (denoted -1)

iii) During an active period (denoted A)

iv) During a quiet period (denoted Q).

Because of the relative abundance of active period days this sample was larger (but with approximately the same date longitude distribution) than the other samples.

Table 11 gives the number of charts in each of the four categories for southern and northern hemisphere genesis/nongenesis.

TABLE 11

Number of days composited in each category, in each hemisphere.

	Quiet	-3 days	-1 day	During
Northern Hemisphere	45	50	50	160
Southern Hemisphere	52	50	50	150

5.3 Description of Data Composited

The data used in compositing were the grid point hemispheric analyses of height, temperature and wind prepared routinely in the southern hemisphere by the Australian Numerical Modelling Research Centre (A.N.M.R.C.) and in the northern hemisphere by the United States National Weather Centre (N.W.C.). A comprehensive description of the N.W.C. product may be obtained from Cressman (1959), McDonell (1962) and Gustafson (1965). The Australian system is in broad detail quite similar to that used by the N.W.C. Gauntlett (1972) and Seaman (1977) provide a description of this analysis system with emphasis on the differences from the N.W.C. system which enable a more satisfactory treatment of the vast, data sparse, southern oceans.

The N.W.C. scheme uses the previous twelve-hour numerical prognosis as a first guess field and incorporates all available rawinsonde and Satellite Infrared Radiation Spectrometer (SIRS) data along with regression equations (climatology) in data sparse areas, to prepare the analyses. This scheme then uses the height fields to prepare gradient balanced wind fields (with some correction to allow for cyclostrophic accelerations). The A.N.M.R.C. scheme uses manual surface and 1000-500 mb thickness analyses as the first guess field poleward of 25°S equatorward of 15°S climatology is used and between 15°S and 25°S there is a progressively changing weighting between the two fields. No SIRS data is incorporated into the ANMRC System while all available wind data are transformed to height gradient information by use of a gradient/geostrophic balance scheme. Once again the final wind fields are then derived from height fields assuming gradient/geostrophic balance.

The composite analyses of height, wind and temperature fields from the grid point data summarize the important midlatitude synoptic differences between quiet and active periods. However, observational work by Nunez (1980) and theoretical work by Schubert et al. (1980) indicate that the essential physics of the tropic-midlatitude interaction involves the unbalancing of the wind and mass fields. Because of the assumed balance of these fields in these analysis schemes, a further analysis of tropical station data (where wind and height are measured independently) is needed to fully describe the tropical flow fields and specify the physics of the tropic-midlatitude interaction.

5.4 Results

As described earlier, composite charts have been produced for three days prior to genesis, one day prior to genesis, during active periods and during quiet periods, for quiet/active cycles in both the northern and the southern hemispheres. Each composite analysis covers the area 50^{o}N to 50^{o}S in a longitude belt 90^{o} wide centered on the longitude of genesis. Data fields composited are surface pressure, 1000 mb, 850 mb, 700 mb, 500 mb, 250 mb and 200 mb geopotential height, temperature and wind.

The most convenient way to depict the evolution of the large-scale flow fields to a situation favorable for tropical storm genesis is to subtract the quiet period charts from their respective -3, -1 and Active period charts. In doing so, a set of composite anomaly charts are produced. In all, some 350 composite charts and composite anomaly charts form this set of analyses, obviously all fields cannot be presented in the discussion which follows, accordingly only those data will be presented which are required to build a clear picture of the interactions occurring.

Figures 53 through 56 show the spatial distribution of points about which the quiet/active composites were prepared. Each dot in Figs. 54 and 55 represent the point in which the first tropical cyclone in an active period attained winds equal to or exceeding 17.5 m/s. These points were obtained from post analysis 'best tracks' from the Joint Typhoon Warning Center in Guam and for the Australian region from Lourensz (1977). The points in Figs. 53 and 56 were selected to have the same longitude/date distributions as samples in Figs. 54 and 55.

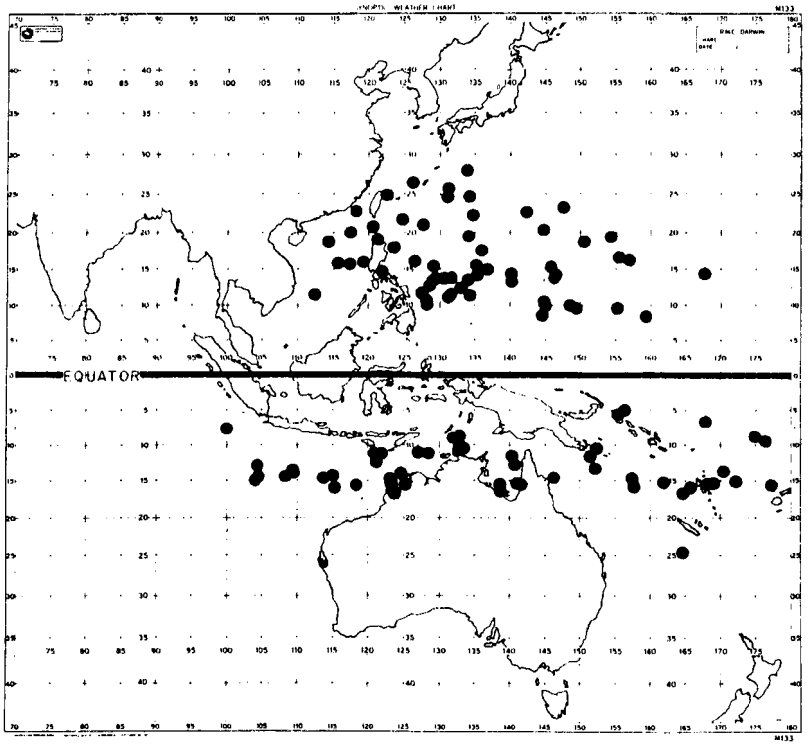

Fig. 53. Spatial distribution of points about which the 'Quiet' composite was made.

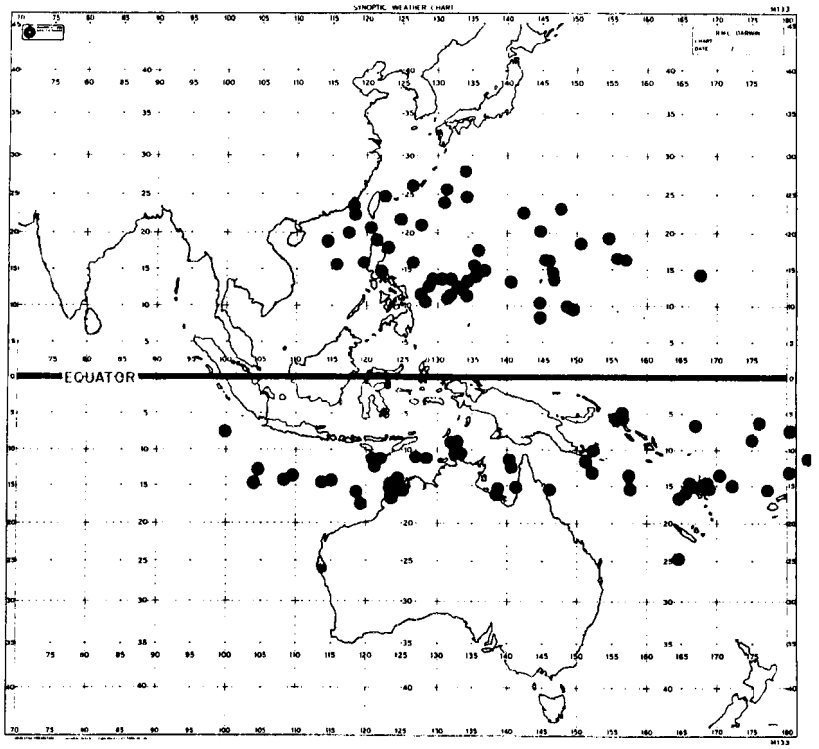

Fig. 54. Spatial distribution of points about which the -3 composite was made.

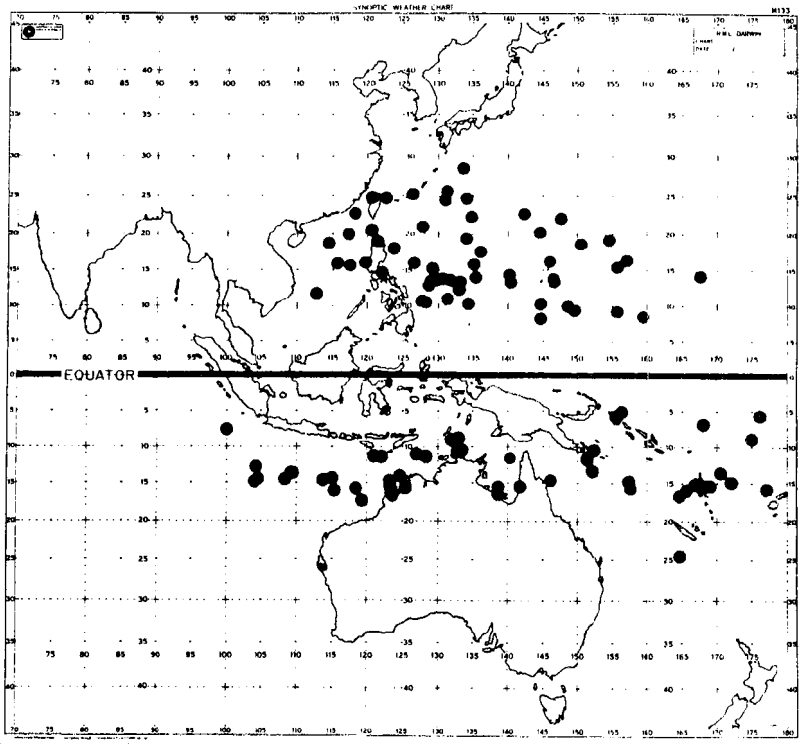

Fig. 55. Spatial distribution of points about which the −1 composite was made.

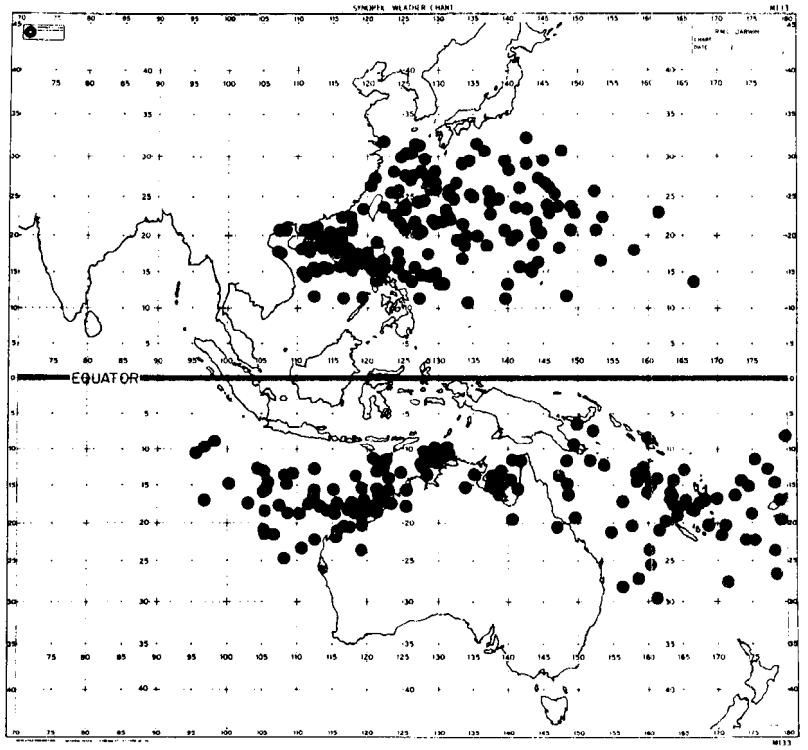

Fig. 56. Spatial distribution of points about which the Active composite was made.

Figure 57 is the quiet period mean sea level pressure composite analysis for the southern hemisphere. At 50°N and 30°E of the genesis longitude (marked on the longitude scale), the Aleutian low at about 1006 mb can be seen, while at the same latitude but 40°W of the genesis longitude, the composite Siberian high of 1023 mb is evident. At 30°S to 35°S the subtropical ridge extends across the analysis with minimum pressures around 1014 mb in the longitude of genesis, reflecting lower pressures over the heated Australian continent. At 5°S the monsoon trough with central pressures around 1008 mb extends across the whole composite. It is noteworthy that the low pressures in this trough fall to their lowest values northeast of where the Australian continent is located. This is about the area of the Solomon Islands. Thus, in the composite quiet conditions there is an east-west pressure gradient of 2 mb from 10°W of the genesis longitude to 35°E of the genesis longitude. Following the analysis of Chapter 3, this would be expected to lead to a steady state westerly antitriptic wind, accelerated by either pressure rises to the west or falls to the east.

Figure 58 shows the 500 mb height field composite for the same time periods as in Fig. 57. This field is relatively featureless compared to the previous mean sea-level pressure analysis. The usual gradient of height increasing from high latitudes to subtropical ridges located near 12°N and 20°S. Figure 59 is the 200 mb height composite for the same time period as in Figs. 57 and 58. Once again the height increases from high latitudes to the subtropical ridges now located equatorward of 10° in each hemisphere. These fields are very much as one would expect them

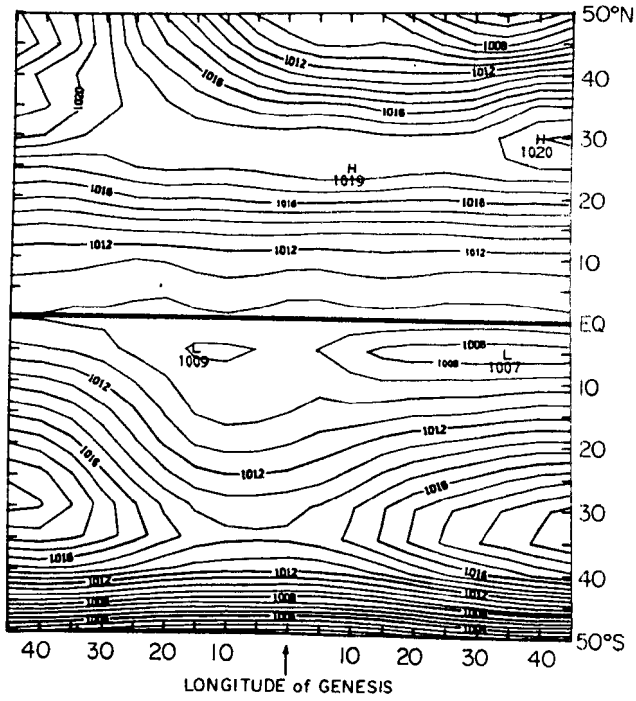

Fig. 57. Quiet period, mean sea level pressure composite analysis for the southern hemisphere summer (mb).

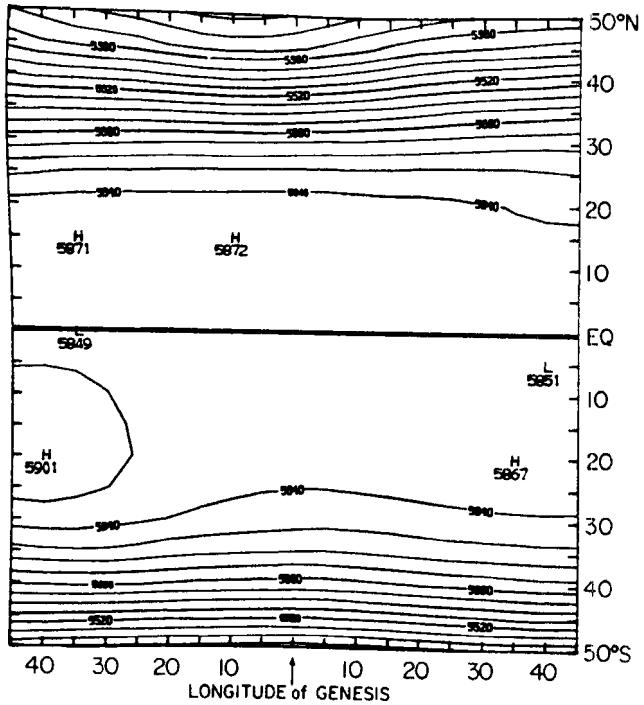

Fig. 58. Quiet period, 500 mb composite height field for the austral summer (GPM).

to be, reinforcing the belief that compositing the grid point height values leads to a meaningful analysis.

5.4.1 Southern Hemisphere Genesis Composite Height Anomaly Charts

Rather than present the composites of -3, -1 and A to compare with the Q charts of Figs. 57, 58, and 59, the anomaly charts for -3 minus Q, -1 minus Q and A minus Q have been computed. Figure 60 is the -3 minus Q 1000 mb height anomaly field for genesis occurring at the point +. The northern hemisphere positive height anomaly of 55 GPM near 45^{o}N on the genesis longitude represents a tendency for strong anticyclonicity around these latitudes preceding southern hemisphere genesis. However, between 25^{o}N and 15^{o}N there is a belt of negative anomalies implying that the baroclinic disturbances in the winter hemisphere westerlies have moved abut 15^{o} equatorward relative to their quiet positions three days before tropical cyclone genesis in the southern hemisphere. The equatorial regions west of the genesis longitude show weak, but positive pressure rises consistent with the case study data of Chapter 3. In the southern hemisphere of 45^{o}S and 15^{o}E of the genesis longitude is a positive height anomaly of 26 GPM. This reflects a reduction in baroclinic action poleward of the tropical depression prior to genesis. It is noteworthy that the northern hemisphere anomaly is nearly twice as great as that in the southern hemisphere. There are two possible explanations for this:

i) Greater variability of intensity of winter hemisphere systems inherently leads to larger anomalies

ii) The forcing from the northern hemisphere is more important than that from the southern hemisphere.

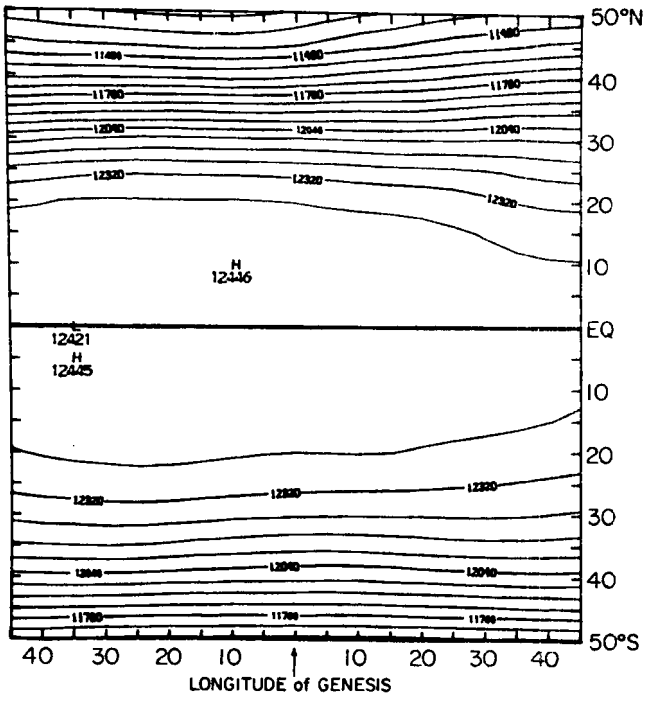

Fig. 59. Quiet period, 200 mb composite height field for the austral summer (GPM).

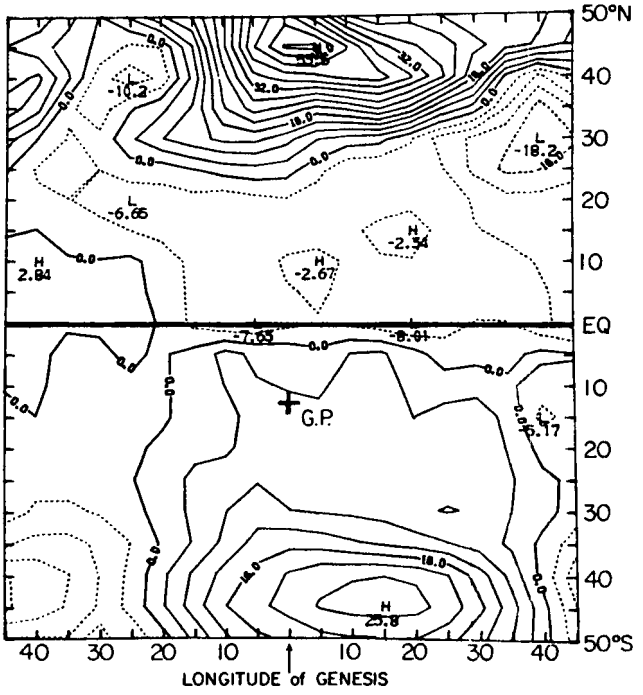

Fig. 60. 1000 mb height anomaly field for the southern hemisphere summer. -3 minus Q height difference (GPM).

As will be seen from a comparison with the analysis in section 5.4.2, the northern hemisphere winter anomalies do exceed those in the southern hemisphere winter, but not greatly. This suggests the cold surges of the China region are more intense than those of the Australian region. However, the summer hemisphere anomalies are generally weaker than those of the winter hemisphere.

The 1000 mb -1 minus Q composite given in Fig. 61 shows the northern hemisphere positive anomaly to be reduced to 29 GPM at its maximum with the 30^{o}N negative anomaly at 40^{o}E of the genesis longitude decreased from -18 GPM to -30 GPM. This suggests a rapid west to east translation of baroclinic systems. The positive equatorial anomaly remains, though diminished in magnitude. In the southern hemisphere, the 45^{o}S positive anomaly has remained of the same magnitude but moved slightly west to be very nearly on the genesis longitude. Figure 62 gives the A minus Q 1000 mb height anomaly. The northern hemisphere shows the now familiar picture of strong height rises from 50^{o}N to around 30^{o}N and falls equatorward of 30^{o}N. The weak equatorial anomaly has gone indicating the surging effect leading to equatorial rises does not persist through the lifetime of storms, but is a transient event present only at their genesis. The positive anomaly in the southern hemisphere is roughly half that of the -3 minus Q and -1 minus Q charts, but is displaced further equatorward.

Figure 63 shows the 500 mb -3 minus Q composite. In the winter (northern) hemisphere there is apparently stronger baroclinic action associated with the negative height anomalies in the belt running SW to NE from 25^{o}N 30^{o}W of genesis longitude to 50^{o}N 25^{o}E of genesis

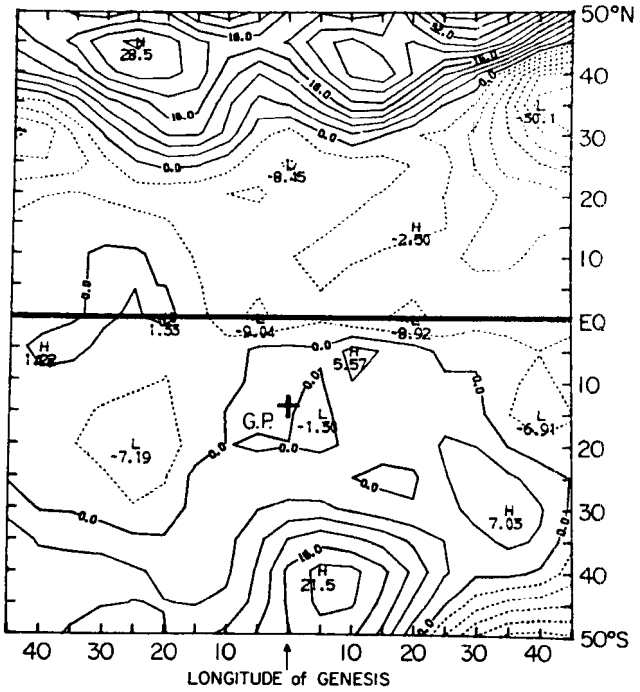

Fig. 61. 1000 mb height anomaly field for the southern hemisphere summer. -1 minus Q height difference (GPM).

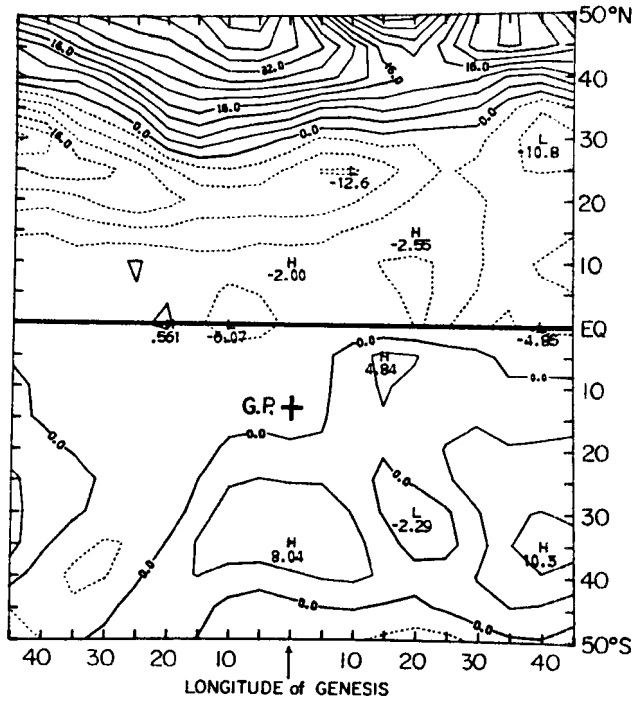

Fig. 62. 1000 mb height anomaly field for the southern hemisphere summer. A minus Q height difference (GPM).

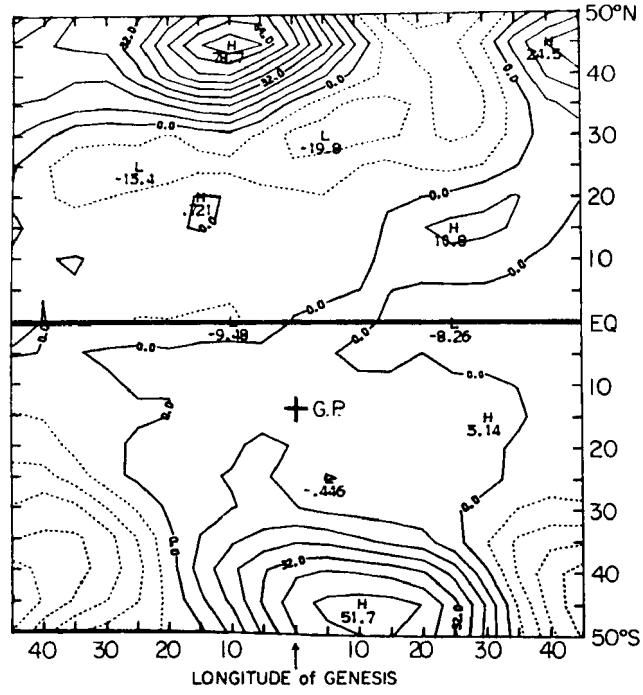

Fig. 63. 500 mb height anomaly field for the southern hemisphere summer. -3 minus Q height difference (GPM).

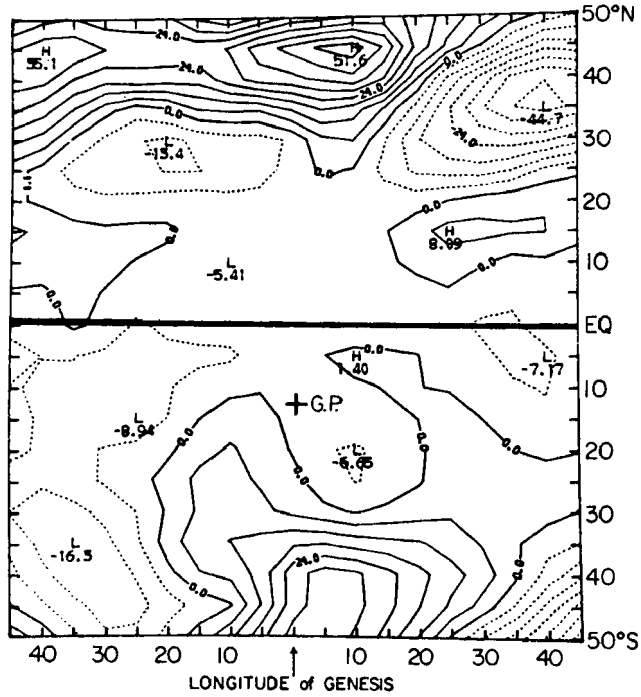

Fig. 64. 500 mb height anomaly field for the southern hemisphere summer. -1 minus Q height difference (GPM).

longitude, with evidence of a strong cold outbreak high in the wake of the baroclinic zone. A positive height anomaly in the southern hemisphere of 52 GPM lies nearly directly over its 1000 mb counterpart.

Figure 64 is the -1 minus Q 500 mb composite. The northern hemisphere positive anomaly has been reduced by one third and the apparent center of anomalously large baroclinic action has moved nearly to the eastern edge of the composite, once again suggesting rapid progression of the baroclinic centres of action. There is now a break in the subtropical negative anomalies indicating height rises moving equatorwards. In the southern hemisphere the positive height anomaly has remained in the same position though halved in magnitude.

On the 500 mb A minus Q in Fig. 65 the northern hemisphere now resembles -3 minus Q in Fig. 63, however, the negative anomaly is much greater near 50^{o}N showing the baroclinic low centers to be much more intense and much more poleward during southern hemisphere tropical cyclone active periods than at three days prior to the period. This suggests that at around three days before the commencement of a southern hemisphere active period the low centers of the northern hemisphere are at their most equatorward displacement, then by one day before, the height rises in the wake of the baroclinic zone have replaced falls. The cold surge is occurring. The southern hemisphere positive anomaly, as for the 1000 mb A minus Q composite shows a weakening and equatorward displacement.

Figures 66, 67, and 68 give the 200 mb height anomaly composites at -3 minus Q, -1 minus Q and A minus Q respectively. They demonstrate essentially the same features as their 1000 mb and 500 mb counterparts.

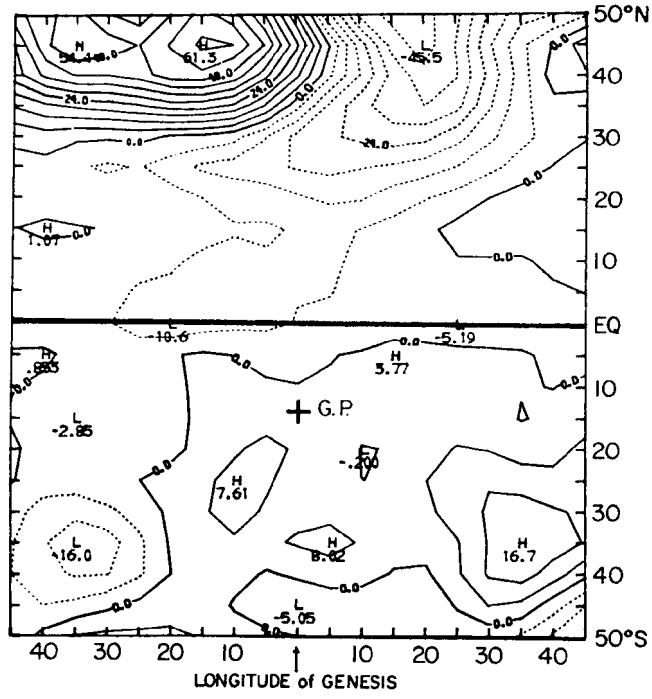

Fig. 65. 500 mb height anomaly field for the southern hemisphere summer. A minus Q height difference (GPM).

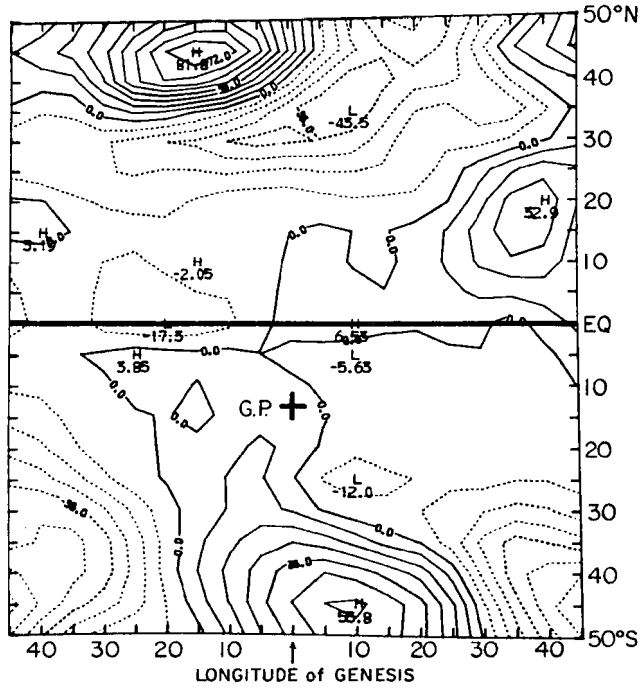

Fig. 66. 200 mb height anomaly field for the southern hemisphere summer. −3 minus Q height difference (GPM).

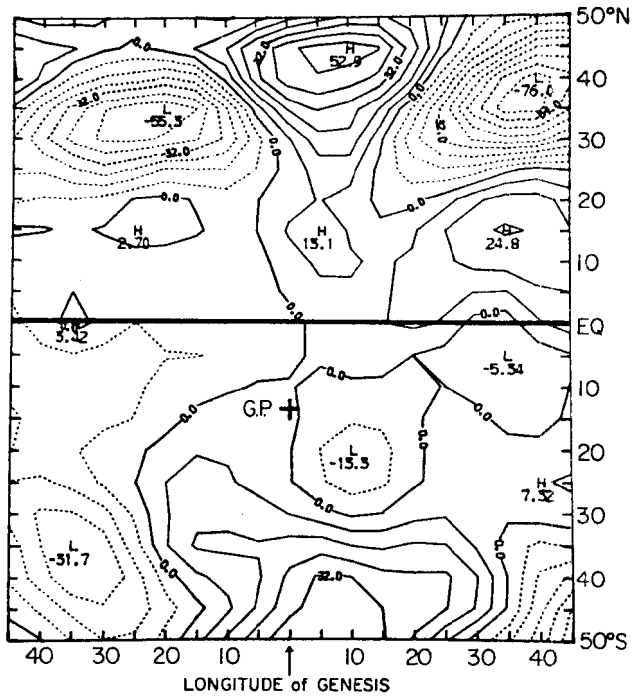

Fig. 67. 200 mb height anomaly field for the southern hemisphere summer. -1 minus Q height difference (GPM).

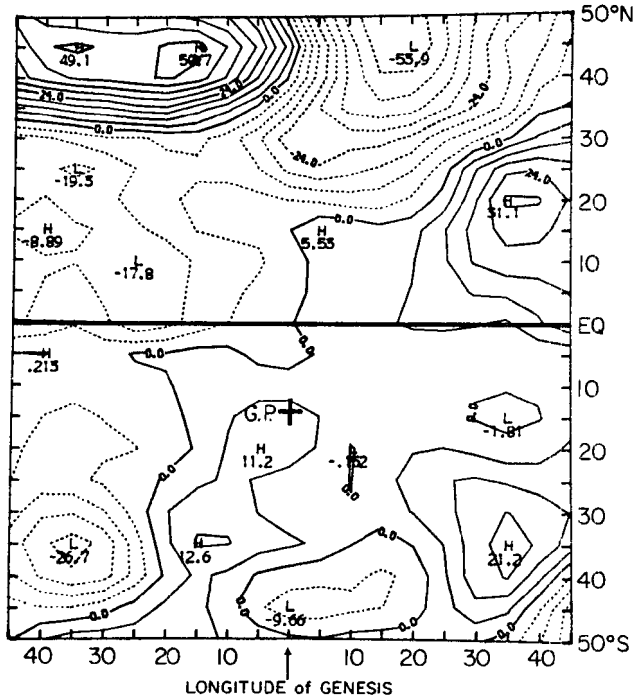

Fig. 68. 200 mb height anomaly field for the southern hemisphere summer. A minus Q height difference (GPM).

The positive anomalies in the southern hemisphere show a nearly vertical arrangement implying a tendency for "blocking" highs (and reduced baroclinic action) poleward of a developing tropical disturbance. However, the apparent weakening of these positive anomalies at all levels for the active case compared with -3 and -1 leads to the belief that the reduction in baroclinicity is only short lived in many cases. There is one feature seen in the 200 mb -3 minus Q not seen at the lowest levels, it is a NW to SE negative anomaly area representing an upper trough poleward, but very close to, the developing disturbance. This trough is not associated with lower level baroclinicity but would serve to intensify the westerly wind immediately poleward of the upper anticyclone above the developing disturbance. This feature is also evident at -1 minus Q but is gone by A minus Q implying the upper trough (TUTT) type systems may play an important role in genesis but are not so necessary for maintenance of the tropical storm.

The features felt to be important in these composites are the maximum equatorward displacement of the baroclinic systems at -3 days in the northern hemisphere with their progression north on -1 and the establishment of a zone of baroclinic activity through the 30°N to 45°N belt during cyclone activity. The cold outbreak high is most marked on day -1. In the southern hemisphere there is ridging poleward of the disturbance which decreases in amplitude during storm development but maintains itself in the genesis longitudes throughout. Finally, there is the upper trough unsupported by lower level baroclinicity which does not persist after the genesis period.

5.4.2 Northern Hemisphere Genesis Composite Charts

One test of these composite analyses for the southern hemisphere active/quiet cycle is to prepare a similar set of analyses for the northern hemisphere genesis cycle. The latitude longitude distribution of genesis points for this northern hemisphere composite set is given in Figs. 53 through 56. It can be seen that compared to the set of genesis points for the southern hemisphere this northwest Pacific set covers a smaller longitude range, accordingly a less diverse range of circulation systems are to be composited over, and a common physics between the two hemisphere sequences will lend support to the conclusions drawn.

For the northern hemisphere quiet/active cycle Figs. 69, 70 and 71 represent the quiet period mean sea level pressure, 500 mb height and 200 mb height analyses respectively. At MSL, the monsoon trough extending into the Pacific from Asia can be seen around 20^{o}N on the western side of the composite. The mid Pacific anticyclone can be seen around 30^{o}N on the eastern side of the composite. In the southern hemisphere the subtropical ridge lies along 30^{o}N, with an extremely strong poleward gradient of the MSL pressure. At 500 mb the subtropical ridges lie along 25^{o}N and $6-8^{o}$S. At 200 mb the subtropical ridges lie along 20^{o}N and 10^{o}S with evidence of an upper trough extending into the northern hemisphere tropics around 30^{o} to 40^{o}E of the genesis longitude. These upper charts also show a much stronger height gradient in the winter (southern) hemisphere.

Figures 72, 73, and 74 give the 1000 mb -3 minus Q, -1 minus Q and A minus Q composite height anomaly charts for the northern hemisphere active/quiet cycle. At -3 minus Q there is evidence that the baroclinicity poleward (northwards) of the genesis point is reduced.

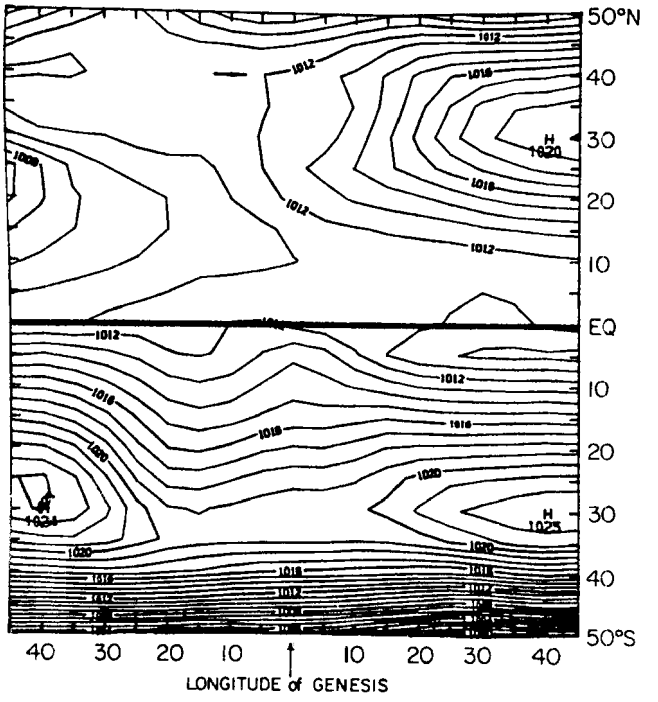

Fig. 69. Quiet period, mean sea level pressure composite analysis for the northern hemisphere summer (mb).

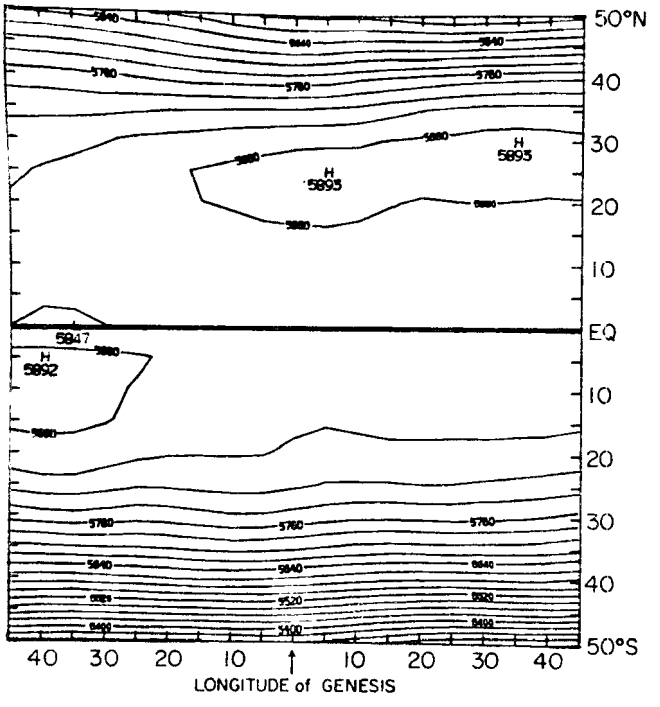

Fig. 70. Quiet period, 500 mb composite analysis for the northern hemisphere summer (GPM).

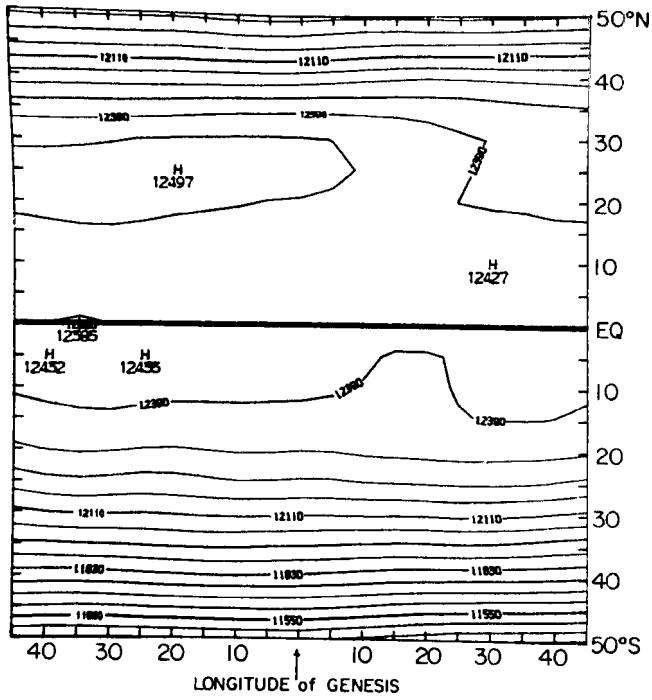

Fig. 71. Quiet period, 200 mb composite analysis for the northern hemisphere summer (GPM).

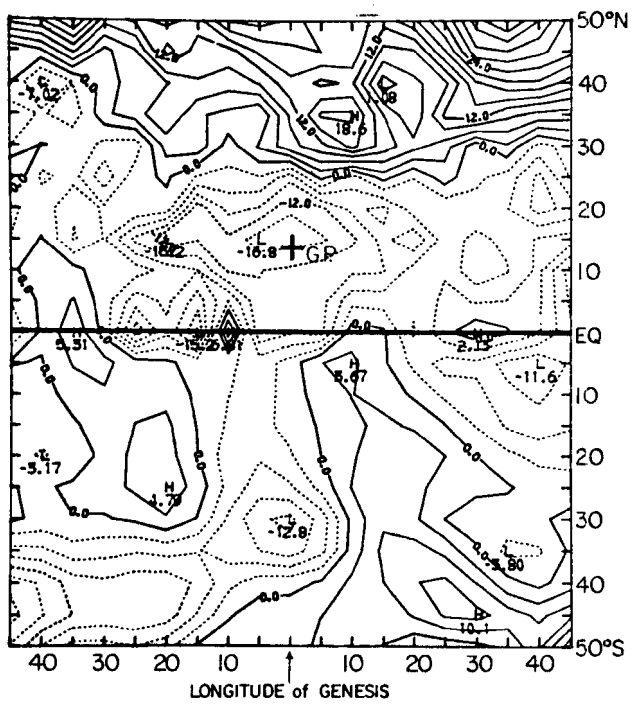

Fig. 72. 1000 mb height anomaly field for the northern hemisphere summer. −3 minus Q height difference (GPM).

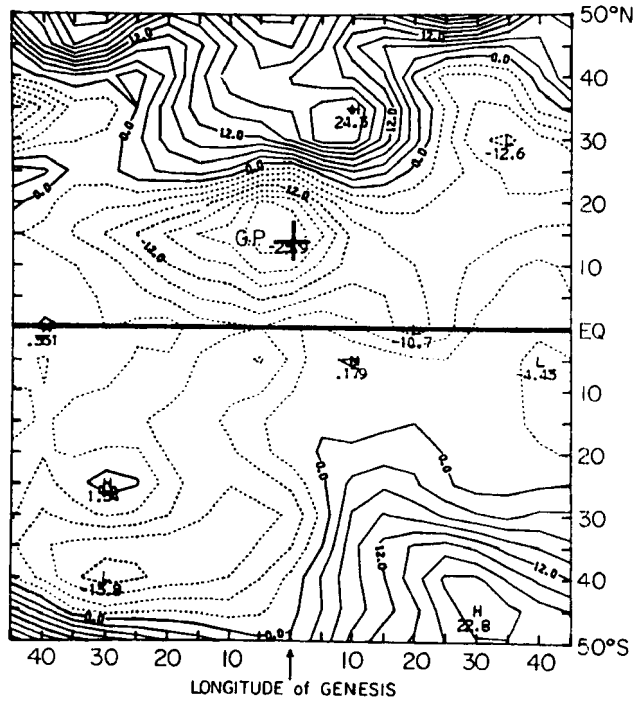

Fig. 73. 1000 mb height anomaly field for the northern hemisphere summer. -1 minus Q height difference (GPM).

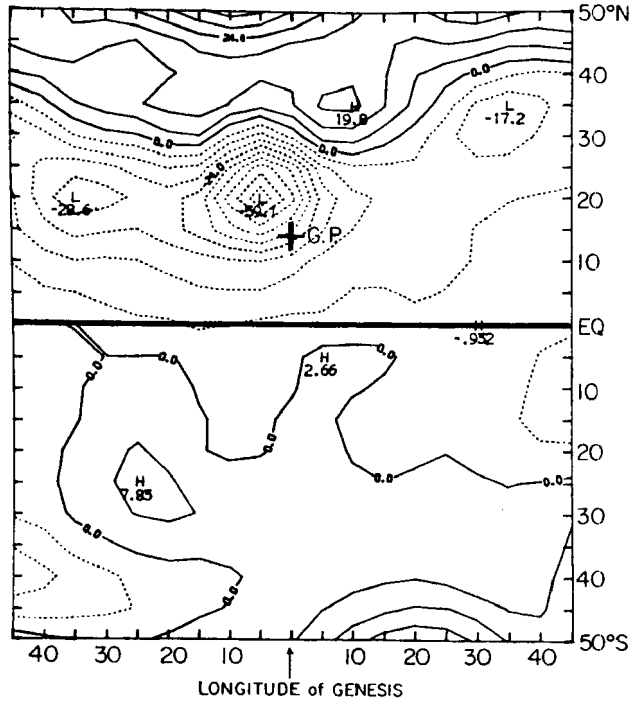

Fig. 74. 1000 mb height anomaly field for the northern hemisphere summer. A minus Q height difference (GPM).

The Asian monsoon trough is extending into the northwest Pacific lowering heights while in the southern hemisphere baroclinic activity has increased in the longitudes west of the genesis longitude and decreased to the east. On the −1 minus Q chart there is considerably less noise in the anomaly chart, the anomalies all show increased amplitude (the lows lower, highs higher). By A minus Q the anomalies still show good geographic organization but are reduced in amplitude. The largest changes are in the southern hemisphere where the baroclinic activity in the longitudes west of the genesis longitude has now dissipated.

Figures 75, 76 and 77 give the 500 mb height anomaly charts for −3 minus Q, −1 minus Q and A minus Q respectively. A qualitatively similar pattern to the 1000 mb sequence evolves. The midlatitudes poleward of the disturbance reveal higher heights prior to genesis with lower heights in the summer hemisphere tropics. Across the equator there is a greater level of baroclinic activity west of the genesis longitude and a small subtropical high is seen in the wake of the baroclinic zone. To the east of the genesis longitude the anomalies are positive. The winter hemisphere pattern becomes considerably more organized between −3 minus Q and −1 minus Q indicating that the winter hemisphere flow evolves rapidly (in about three days) to become favorable for tropical cyclone genesis. The southern hemisphere anomalies west of the genesis longitude change sign between −1 minus Q and A minus Q indicating that the pre-active period flows do not persist through the active period. The baroclinicity pushing through the subtropical ridge, equatorwards, has been reduced to below the quiet period levels.

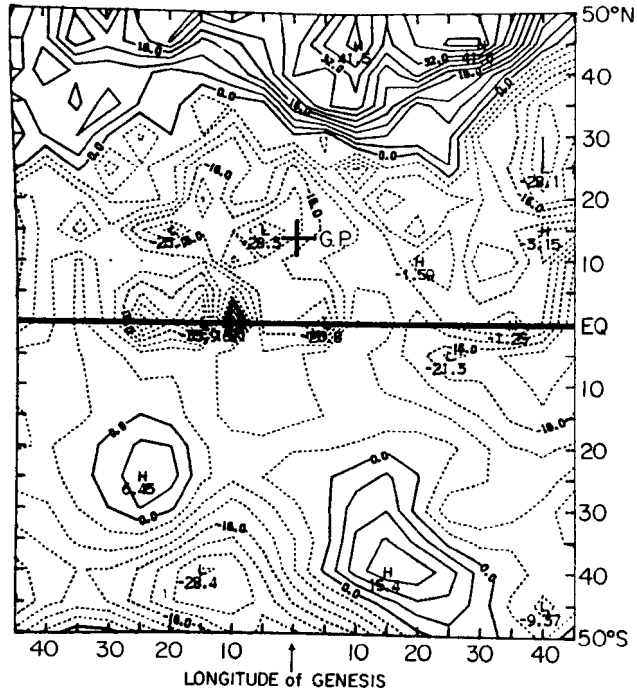

Fig. 75. 500 mb height field for the northern hemisphere summer. -3 minus Q height difference (GPM)

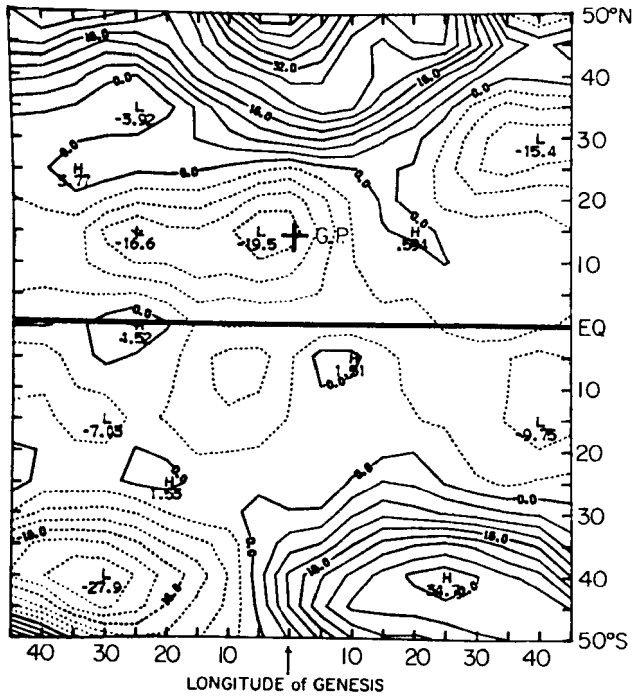

Fig. 76. 500 mb height field for the northern hemisphere summer. -1 minus Q height difference (GPM).

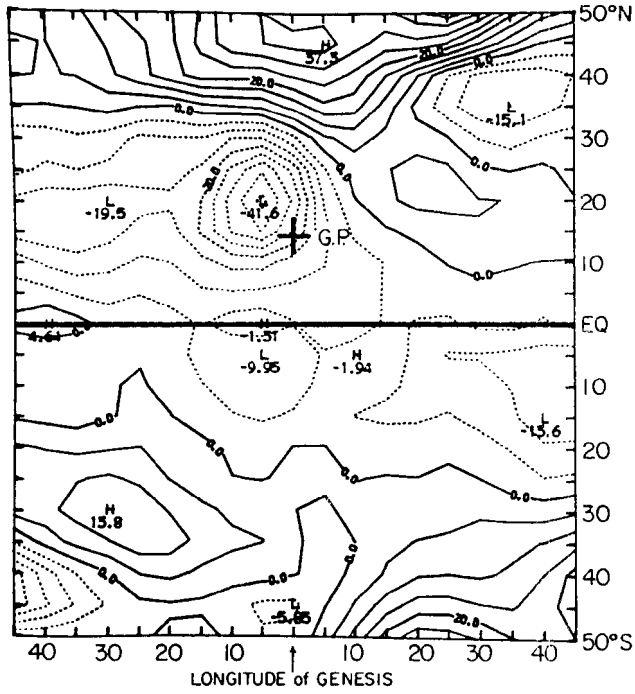

Fig. 77. 500 mb height field for the northern hemisphere summer. A minus Q height difference (GPM).

Finally, Figs. 78, 79 and 80 give the sequence of 200 mb height anomaly charts for -3 minus Q, -1 minus Q and A minus Q. Once again, a similar qualitative picture emerges consistent with the 500 mb sequence. Above the 1000 mb and 500 mb low summer hemisphere tropical heights, is a region of high 200 mb heights which reflects the strong anticyclone found above the composite tropical storm. However, between this tropical anticyclone and the high height anomaly of the reduced midlatitude baroclinic activity is a region of low heights representing the intrusion of a tropical upper tropospheric trough (TUTT) of much greater intensity than during the quiet periods. As with the southern hemisphere case, this serves to intensify the westerlies immediately poleward of the disturbance at upper levels but is not associated with strong lower level temperature gradients.

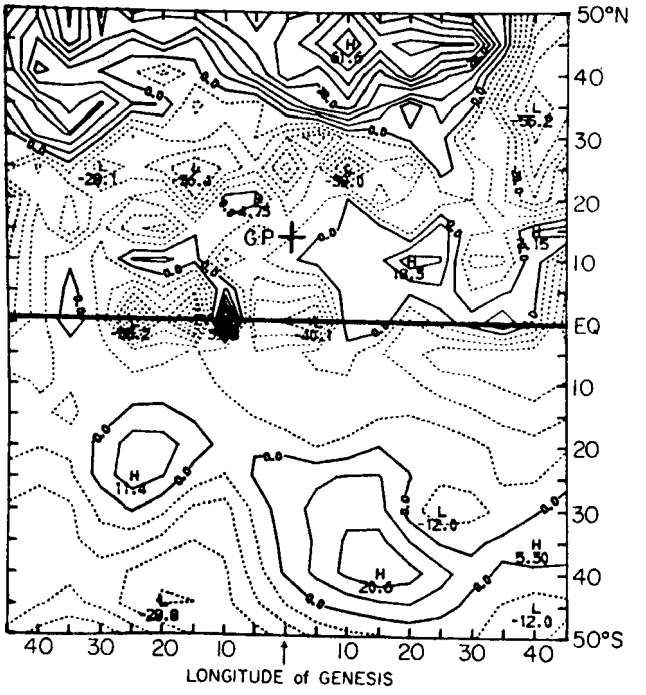

Fig. 78. 200 mb height anomaly field for the northern hemisphere summer. -3 minus Q height difference (GPM).

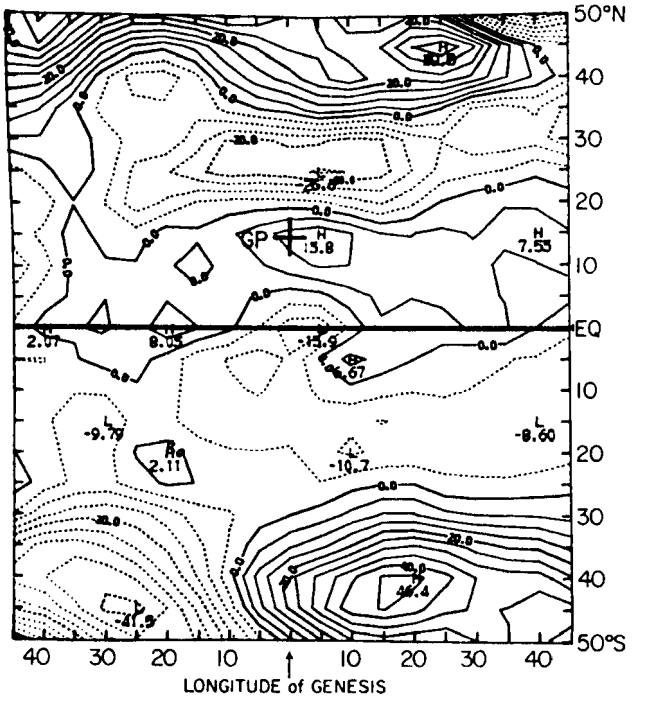

Fig. 79. 200 mb height anomaly field for the northern hemisphere summer. -1 minus Q height difference (GPM).

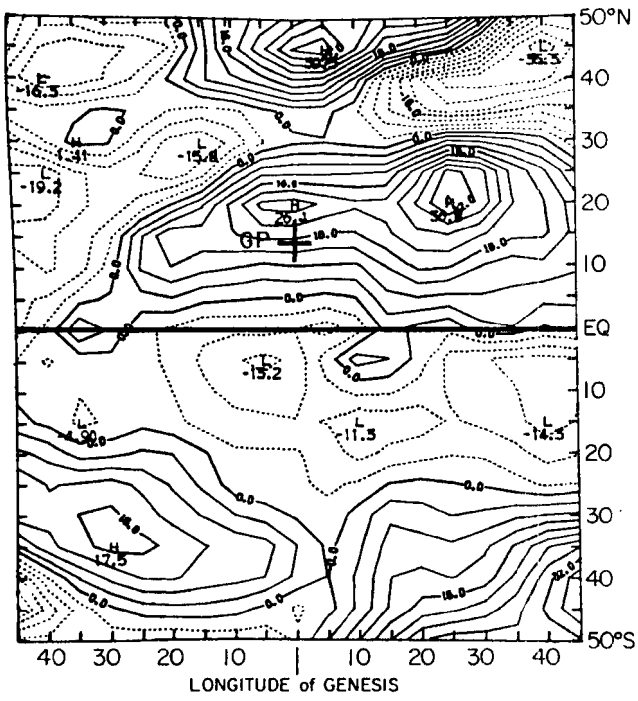

Fig. 80. 200 mb height anomaly field for the northern hemisphere summer. A minus Q height difference (GPM).

5.5 Conclusions

The height anomalies associated with the differences between quiet and active periods show that the tropical cloud cluster receives a similar forcing influence from the midlatitude circulation systems in both hemispheres. The more intense systems in the northern hemisphere winter yield slightly larger anomalies. These northern hemisphere systems show a slightly different geographic arrangement, but the essential physics of the interaction between midlatitudes and tropics remains the same.

A minimum of baroclinic action poleward of a developing disturbance is favorable, with a near vertical orientation of the positive height anomalies seen in the composites. These are the characteristics of a weak block, since it need not be maintained for more than several days. At 200 mb, between the positive height anomalies and the ITCZ

disturbance an upper trough is observed. An upper low is to be expected equatorward of a block, which is consistent with this feature.

A maximum of baroclinic action pushing towards the equator in the vicinity of the genesis longitude, in the winter hemisphere, is favorable. Case studies indicate such low latitude baroclinic developments are followed by cold surges which lead to pressure rises in equatorial regions. Even though the height data are most reliable in the midlatitudes rather than the tropics, these tendencies are seen in the composites.

6. TROPICAL COMPOSITE WIND ANALYSES

6.1 Introduction

In this chapter the differences in the tropical wind fields between quiet and active periods are determined through the use of composite analyses. The same four data stratifications as described in Chapter 4 are used with the same distribution of composite points as given in Figs. 53 through 56.

All stations used in the preparation of these composites lie in the area 30°N to 40°S between longitudes 90°E and 130°W. The data originate from two sources:

(i) The Australian Bureau of Meteorology

(ii) The National Center for Atmospheric Research, Boulder, CO.

The differences between pregenesis and quiet period wind fields are consistent with those of Chapter 5. The most striking features are the increased easterly vertical shear in the near equatorial wind field and the increased westerly shear poleward of the ITCZ just before tropical cyclone genesis. An enhanced meridional component of the wind directed equatorwards in the winter hemisphere before tropical cyclone genesis can also be seen in these data.

At the conclusion of this chapter, the results of this and the previous five chapters are integrated to present an idealized picture of how the large scale circulation fields typically evolve before genesis of ITCZ type storms.

6.2 Data Base

The locations of the pibal and rawinsonde stations used in the preparation of tropical wind field composites are shown in Figs. 81 and 82. These data were derived from two sources. For those stations in

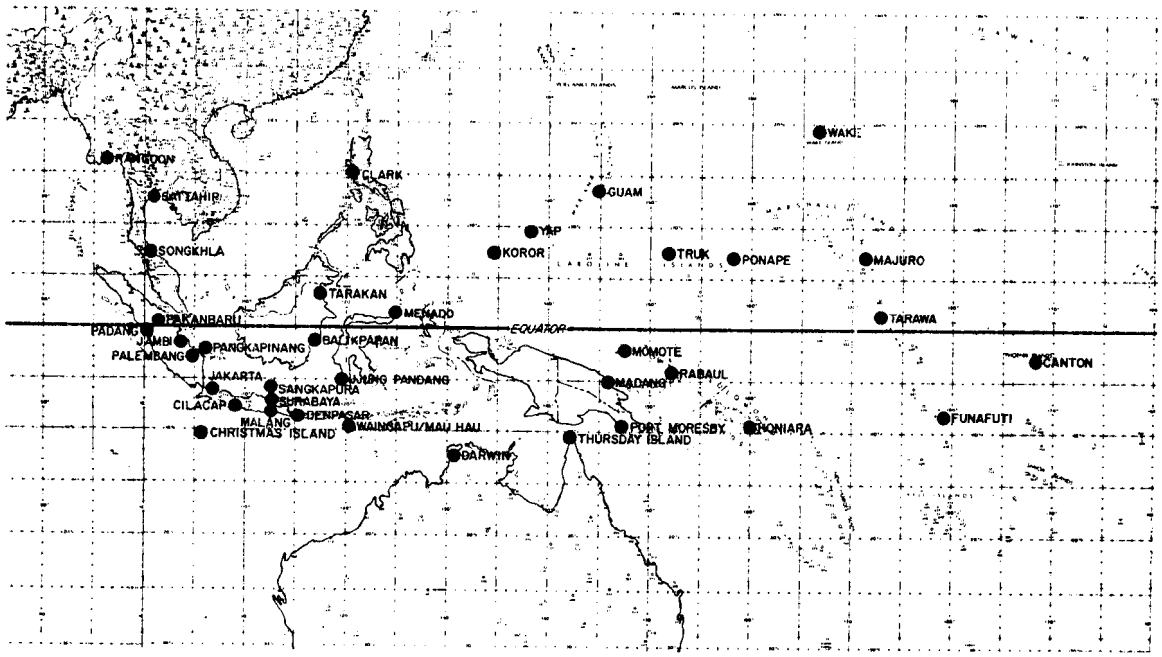

Fig. 81. Location of stations used to obtain composite wind fields for the northern hemisphere.

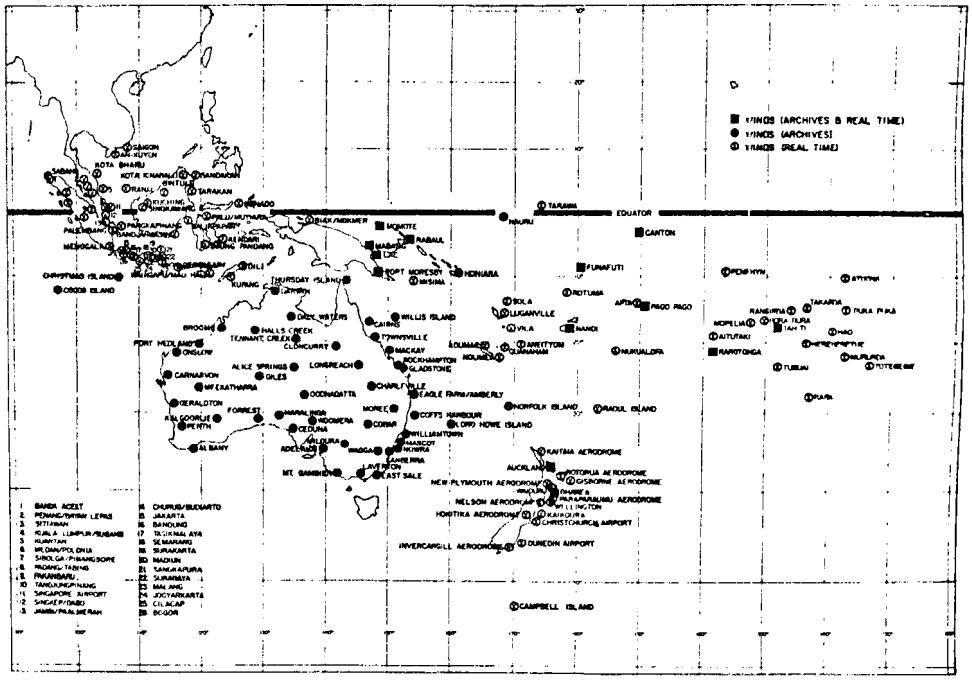

Fig. 82. Location of stations used to obtain composite wind fields for the southern hemisphere.

the northwest Pacific wind data were obtained from the National Center for Atmospheric Research data tapes. These data were available twice daily at 00 GMT and 12 GMT. For those stations in the southern hemisphere and those in the northern hemisphere west of 130°E, wind information through the troposphere was generally available four times daily, usually at 23, 05, 11 and 17 hour GMT. Height, temperature and moisture data are available once daily at 23 hour GMT. The source of these station data was the Australian Bureau of Meteorology archived data and a magnetic tape listing of all real time messages received in Australia on the World Meteorological Organization (W.M.O.) global telecommunications system. This Australian data set contains over 2 million wind flights and 300,000 thermodynamic flights.

6.3 Program Structure

A rectangular grid covering an area of 50 degrees latitude by 100 degrees longitude was centred upon a point about which it was desired to composite each day. The grid is subdivided into 5° latitude by 5° longitude boxes. A running total of all observations falling in each box is kept and at the completion of summing all available data a box average is calculated. From these composited (average) wind fields, analyses of kinetic energy, vorticity, divergence and vertical motion (by way of the continuity equation) have been performed. East-west and north-south cross-sections of these fields have also been prepared.

All available wind observations have been composited with respect to the genesis point in the summer hemisphere and with respect to the genesis longitude keeping latitude fixed in the winter hemisphere. The data during active tropical cyclone periods have been composited about

the storm center in the summer hemisphere and storm longitude in the winter hemisphere, again keeping the latitude fixed. This scheme allows for good resolution of those synoptic features in the winter hemisphere which tend to be latitudinally related and resolves the tropical flow features related to the developing vortex.

Figure 83 shows a typical plan view wind field output. Composite fields of the zonal (u), meridional (v) wind components in m/s, kinetic energy (WV2) in m^2/s^2 and number of observations in each grid box for the 900 mb level, one day before storm genesis in the southern hemisphere. Zero latitude on this output corresponds to 13.39°S and zero longitude to 144.53°E. On this and the next two figures, data points enclosed by the square boxes are at the genesis point. Figure 84 shows the plan view of wind speed and direction (DDD + VV) and divergence. Figure 85 shows the calculated vorticity and vertical motion for those wind data shown in Fig. 83. The vertical motion has been calculated using the continuity equation. Each vertical column of grid points has been divergence balanced such that the vertical motion at 100 mb is zero.

6.4 Southern Hemisphere Tropical Cyclone Genesis - Composite Wind Fields

Figures 86, 87, and 88 show the 1013 mb, 500 mb and 200 mb composite streamline/isotach analyses, one day before tropical cyclone genesis in the southern hemisphere. The location of the streamline/isotach fields relative to the geography is determined by the mean position of all those cases composited. The geography is included to give the reader a 'feel' for how the composite charts relate to daily weather maps.

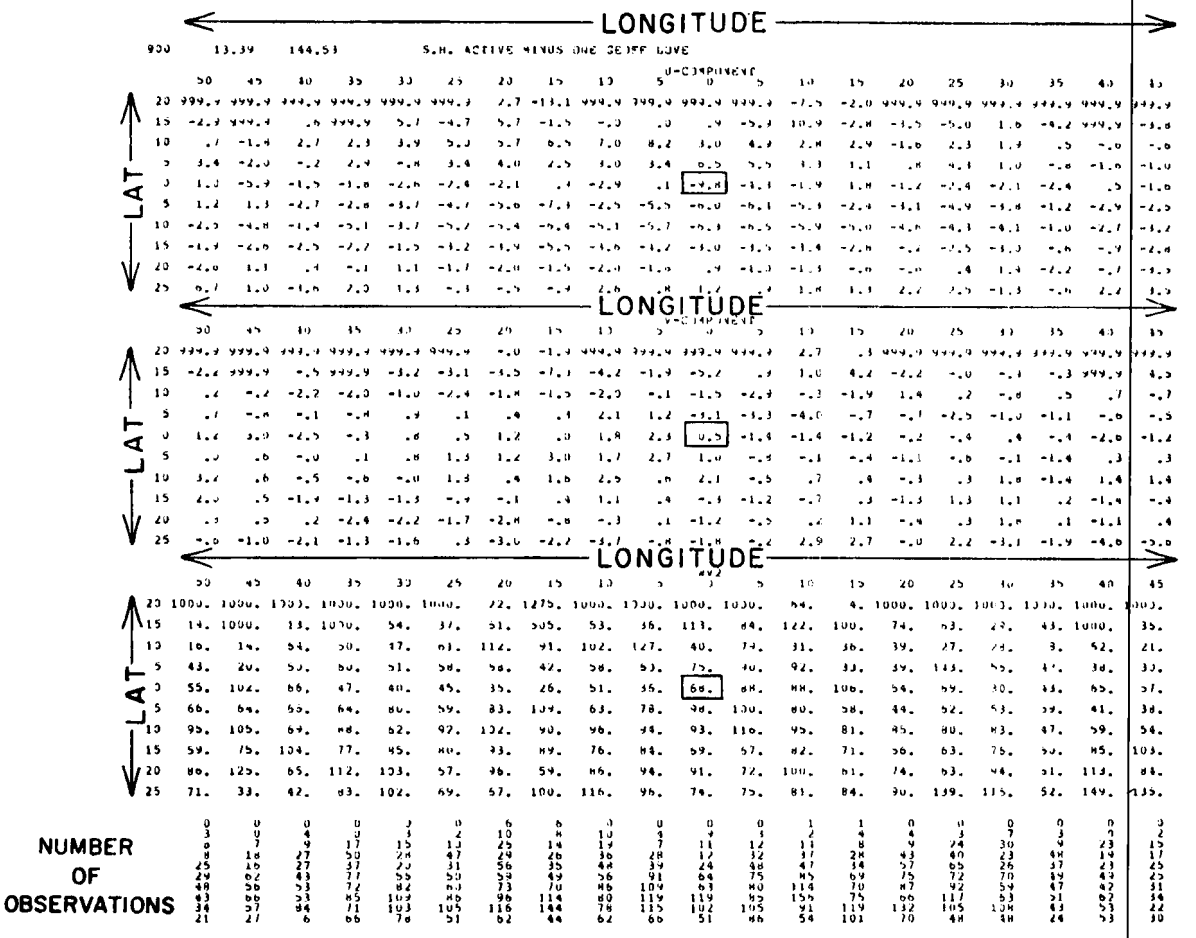

Fig. 83. Typical rectangular composite plan view output. The four data fields displayed are from top to bottom; zonal component of the wind (m/s), meridional component of the wind (m/s), kinetic energy per unit mass ($m^2 s^{-2}$) and the number of observations in each 5^o x 5^o grid box. The boxed value represents the point about which the data were composited.

Comparing Fig. 86 with the case study data presented in Chapter 3 the trade wind regimes and the monsoon trough resemble Fig. 15. The composite midlatitudes do not reveal the presence of sharp baroclinic troughs. These events have been smoothed out in the compositing process. However, the composite height fields of the previous chapter revealled the preferential locations of baroclinic westerly systems prior to tropical cyclone genesis.

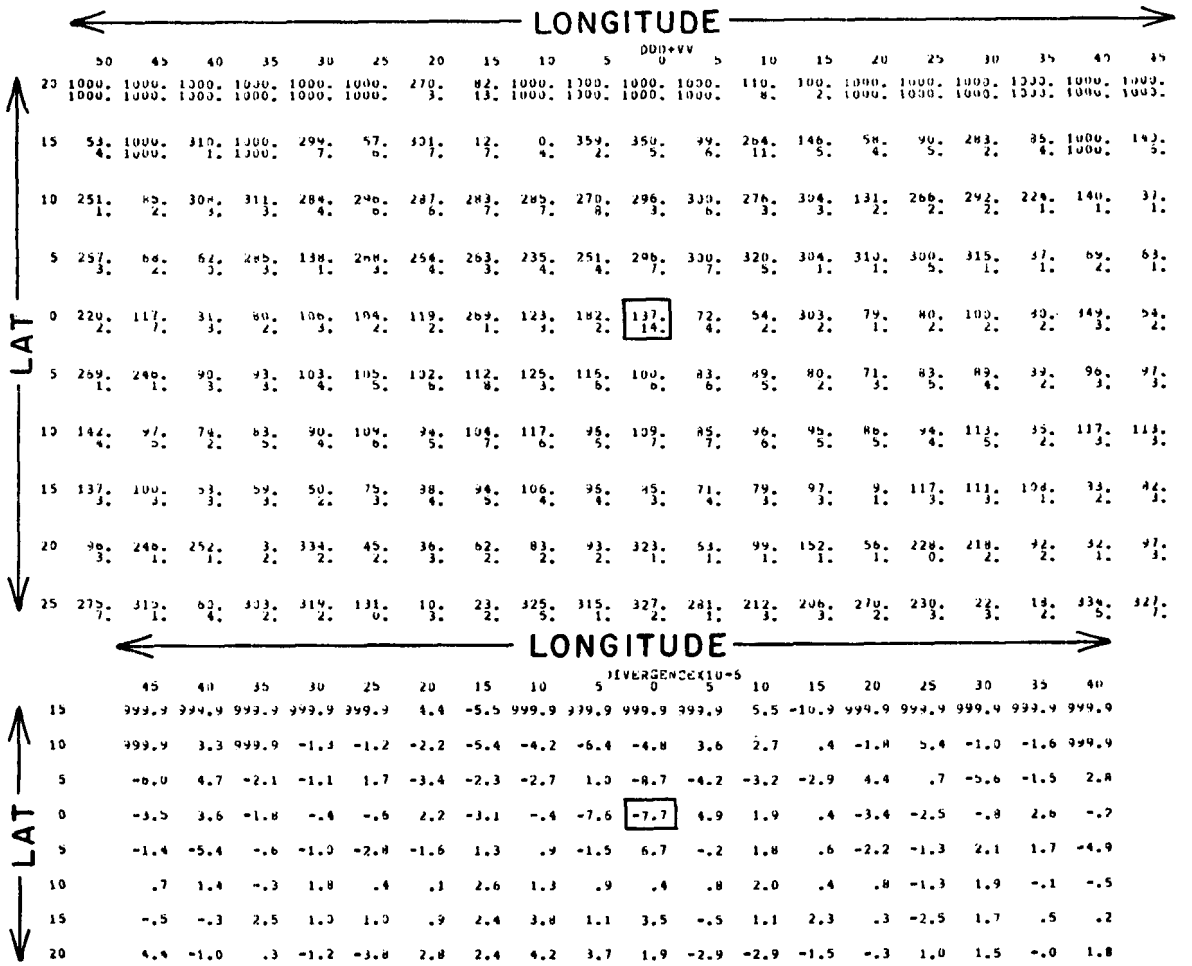

Fig. 84. A typical plan view output of the composite total wind (angle given in degrees from north, speed in m/s) field and divergence. Boxed values as in Fig. 83.

At 500 mb the similarities between the composite analysis (Fig. 87) and the case study charts are greatest in the tropics. The sharp westerly trough over the Australian continent seen in Figs. 13, 16, and 19 is not evident in the zonal westerly flow of Fig. 87. There is however a weak composite westerly trough in the same relative position as that seen in the case study 500 mb chart. The composite 500 mb charts also reveals cross equatorial flow into the pregenesis cluster. Inspection of the composite charts of every level from 1013 mb to 100 mb reveals this inflow to be present at all levels below 300 mb.

LONGITUDE

VORTICITYX10-6

LAT	45	40	35	30	25	20	15	10	5	0	5	10	15	20	25	30	35	40
15	999.9	999.9	999.9	999.9	999.9	-.8	17.0	999.9	999.9	999.9	999.9	12.3	1.4	999.9	999.9	999.9	999.9	999.9
10	999.9	-2.4	999.9	-6.2	6.7	-.8	3.5	4.0	3.4	2.4	11.4	-6.0	5.1	5.7	6.4	-.2	4.4	999.9
5	-4.4	-3.8	-2.6	-5.1	-7.1	-6.8	-3.5	-8.1	-12.0	-15.5	-9.1	-2.0	2.0	-1.2	-4.6	-2.2	-2.2	1.5
0	-.4	-5.3	-2.2	-1.8	-7.0	-9.1	-8.3	-2.9	-.3	[-14.6]	-21.5	-7.5	-2.1	-2.8	-7.7	-4.3	-3.0	-1.9
5	1.0	-.8	-2.2	.9	-7.2	-1.5	-6.1	-2.3	-5.9	-.0	-3.1	-3.2	-7.0	-3.3	-.8	-2.6	1.6	-1.3
10	-6.9	-.9	1.0	4.2	1.7	1.3	3.7	-2.0	.8	1.7	1.2	2.6	-1.3	2.5	4.0	-.8	.1	4.3
15	1.8	.8	5.1	4.7	4.2	4.2	5.5	2.8	2.5	5.0	4.7	5.5	4.4	4.5	5.4	4.0	-3.4	1.2
20	3.3	-3.5	1.5	3.2	2.1	3.9	6.4	6.4	3.7	3.2	5.2	6.2	3.2	1.5	5.6	1.3	-2.7	3.1

LONGITUDE

OMEGA

LAT	45	40	35	30	25	20	15	10	5	0	5	10	15	20	25	30	35	40
15	0.0	0.0	0.0	0.0	0.0	92.2	-41.5	0.0	0.0	0.0	0.0	16.9	-94.4	0.0	0.0	0.0	0.0	0.0
10	0.0	5.0	0.0	-14.6	-50.7	-2.9	-27.0	-33.9	-57.6	-50.1	49.0	2.0	8.8	6.3	6.8	14.8	2.8	0.0
5	-56.7	4.4	-15.8	-16.4	29.3	-32.0	-17.7	4.8	-23.9	-31.8	-29.6	-13.2	-10.7	6.1	-8.4	-7.6	-14.5	-33.3
0	-47.1	12.1	1.4	15.6	8.0	1.6	.6	3.7	-21.1	[-43.3]	-30.2	7.1	-18.3	-12.5	-19.9	-7.9	-17.2	17.0
5	13.2	-42.9	34.3	-19.0	6.3	-9.8	17.6	34.4	12.6	-6.4	1.1	1.6	-19.0	-17.1	-12.3	-47.1	.2	2.3
10	-23.1	-16.3	16.5	-18.2	-24.6	5.7	39.4	-1.4	-14.7	34.8	14.8	-36.5	12.3	22.3	-31.2	-34.7	-3.1	-31.1
15	-1.4	-9.0	9.1	11.5	35.4	1.5	-1.6	16.2	-22.1	23.1	9.9	12.9	-12.7	6.6	9.7	-28.4	-51.3	4.4
20	1.6	22.6	12.8	31.1	-3.3	13.7	19.6	-16.2	-36.9	-.7	39.5	21.9	16.5	18.4	40.9	-20.0	47.7	56.6

Fig. 85. A typical plan view output of vorticity (units of $10^{-6}s^{-1}$) and vertical motion (units of mb/d). Boxed values as in Fig. 83.

At 200 mb Fig. 88 shows the same return cross equatorial flow from south to north as seen in Figs. 14, 17, and 20. Once again the westerlies are more zonal in the composites than in the case study. Weak upper troughs east and west of the Australian continent are evident.

6.5 Anomaly Cross Sections for Southern Hemisphere Genesis

The most efficient way to depict the evolution of the atmosphere from quiet conditions to those preceeding tropical cyclone genesis is through the use of anomaly charts. Anomaly cross sections of the three days before genesis composite minus the quiet composite and the one day before genesis composite minus the quiet composite have been prepared for the zonal and meridional winds for storm genesis occurring at 13°S 140°E. North-south cross-sections of the mean wind field difference for 15° (longitude) wide belts centered on 125°E, 140°E and 155°E are

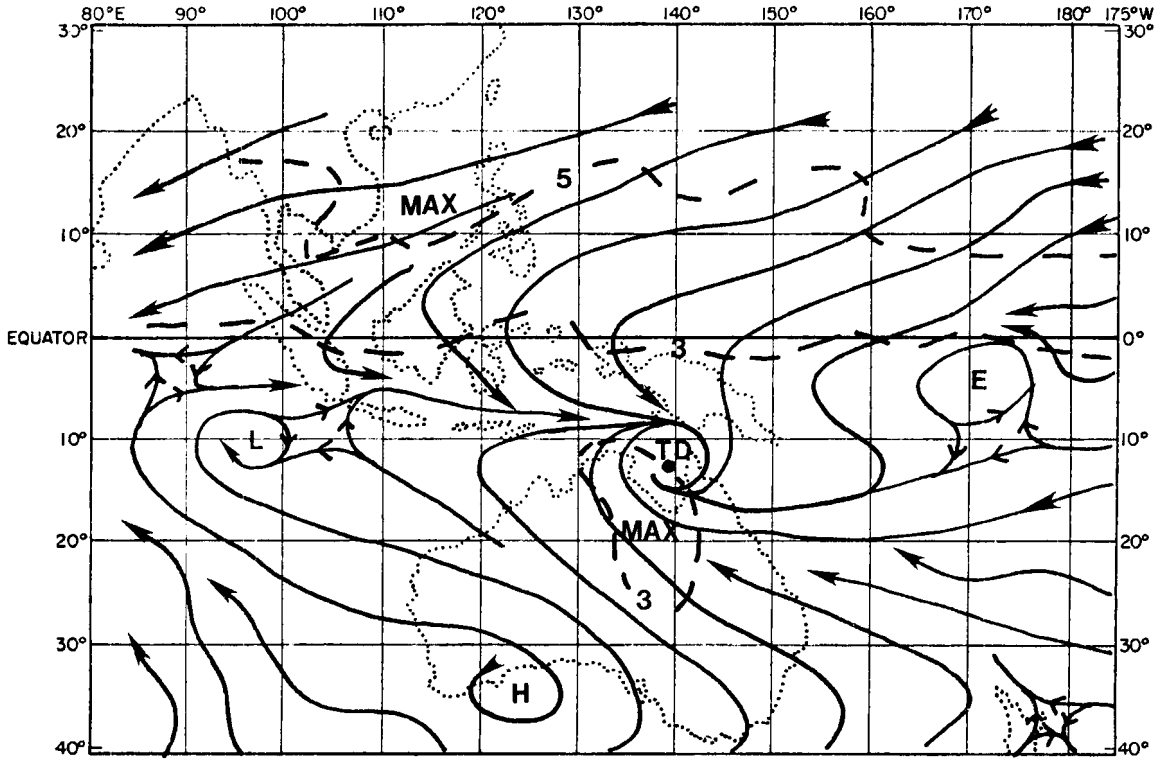

Fig. 86. Composite streamline/isotach analysis one day before tropical cyclone genesis in the southern hemisphere. 1013 mb level (isotachs in m/s).

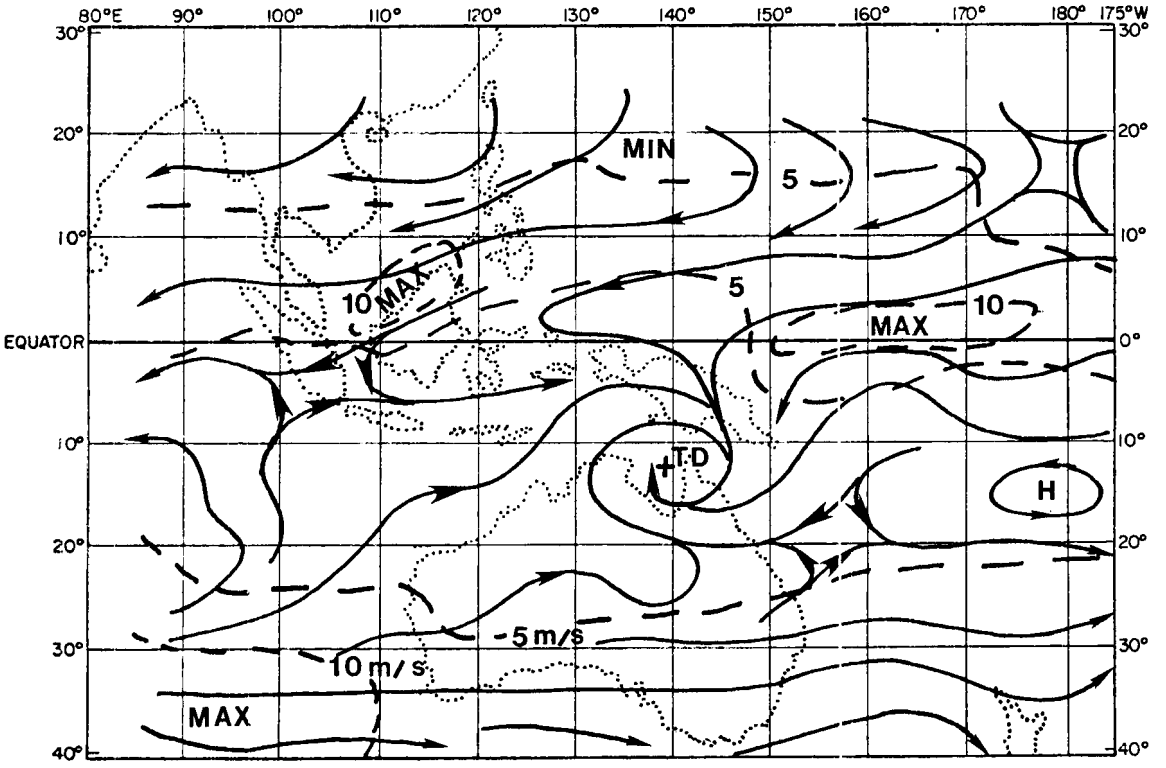

Fig. 87. Composite streamline/isotach analysis one day before tropical cyclone genesis in the southern hemisphere. 500 mb level (isotachs in m/s).

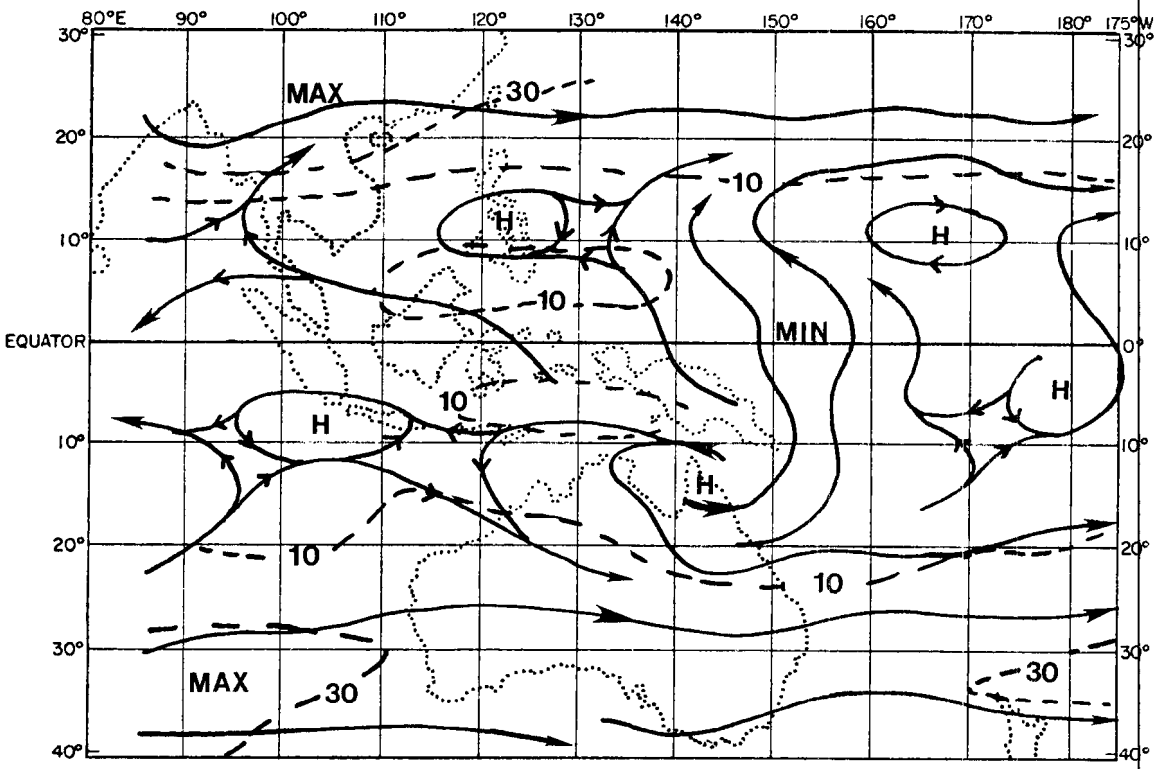

Fig. 88. Composite streamline/isotach anaysis one day before tropical cyclone genesis in the southern hemisphere. 200 mb level (isotachs in m/s).

presented in Figs. 89 through 94. In interpreting the anomaly cross-sections a positive change in the zonal component the wind implies stronger westerly (or weaker easterly) winds preceeding genesis than during the quiet period. A positive meridional wind anomaly implies a stronger southerly (or weaker northerly) wind in the pregenesis than quiet composite. Since the zonal winds are generally around 5 to 10 m/s (as seen in Figs. 86, 87 and 88) an anomaly of 5 m/s represents at least a 50% change in the winds. Similarly where the meridional wind anomalies exceed 2 m/s at least a 50% change in the winds between composite types is being observed. Heavy arrows on the meridional anomaly charts indicate the direction of increased flow.

Considering first the three days before genesis composite minus the quiet composite, some features of the zonal wind anomaly cross-section

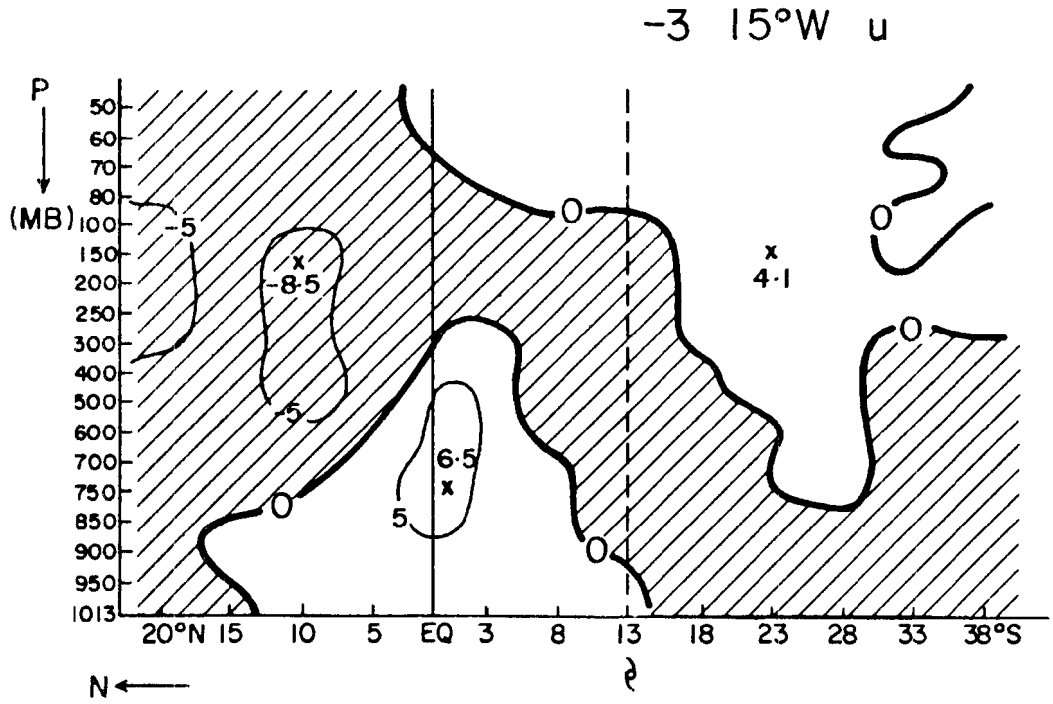

Fig. 89. Zonal wind field anomaly cross-section. -3 minus Q, 15° west of the genesis longitude for southern hemisphere genesis (m/s).

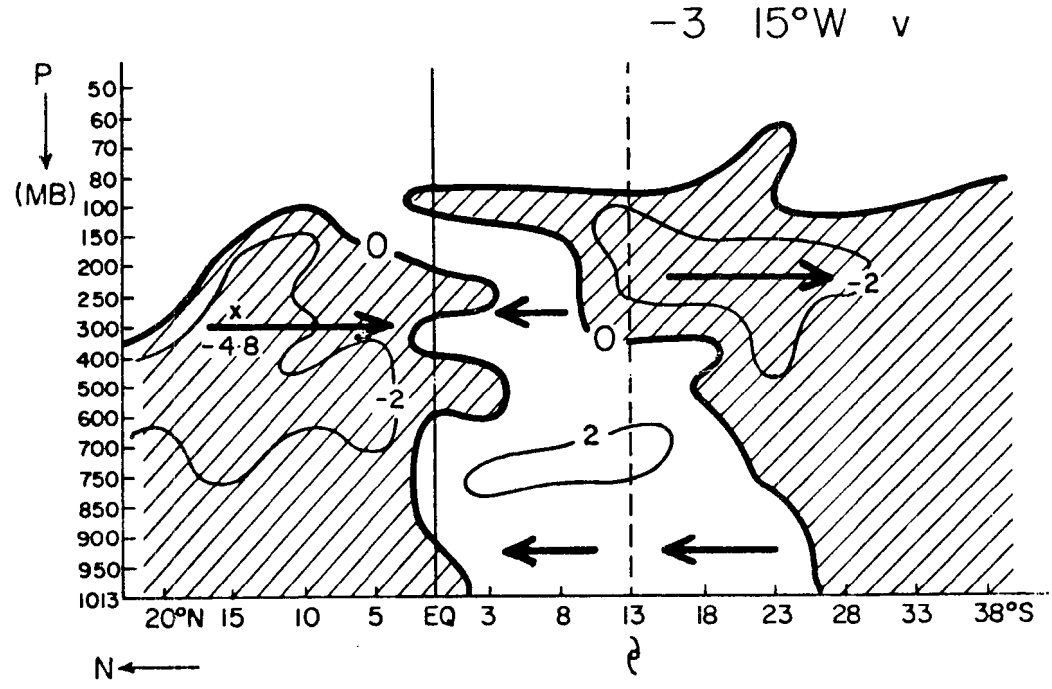

Fig. 90. Meridional wind field anomaly cross-section. -3 minus Q, 15° west of the genesis longitude for southern hemisphere genesis (m/s).

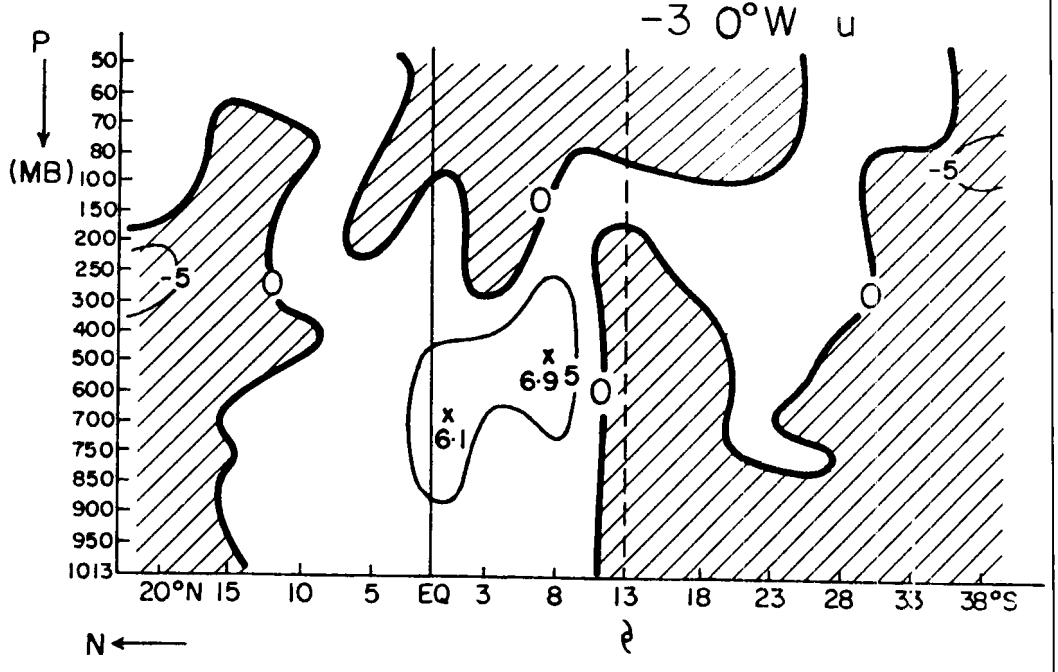

Fig. 91. Zonal wind field anomaly cross-section. -3 minus Q, at the genesis longitude for southern hemisphere genesis (m/s).

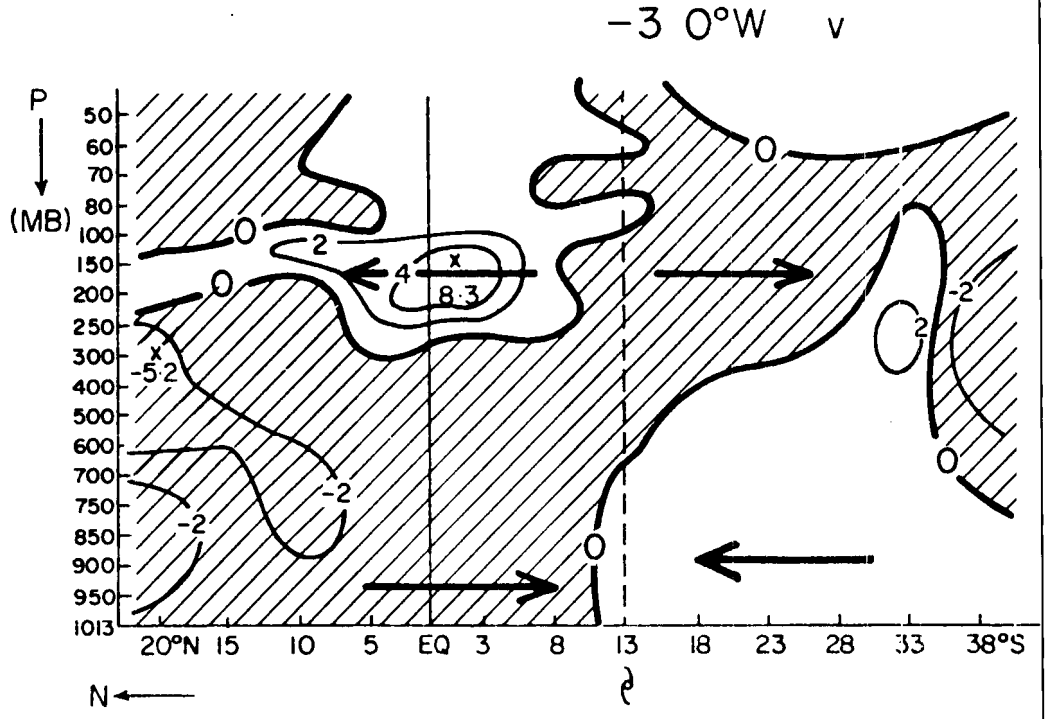

Fig. 92. Meridional wind field anomaly cross-section. -3 minus Q, at the genesis longitude for southern hemisphere genesis (m/s).

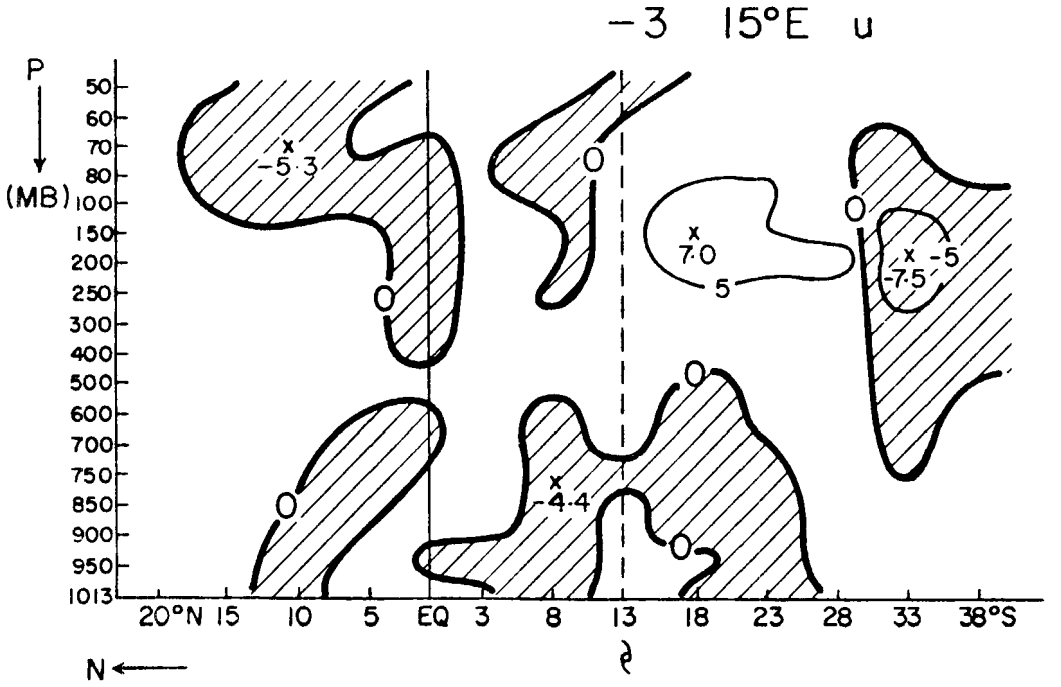

Fig. 93. Zonal wind field anomaly cross-section. -3 minus Q, 15° east of the genesis longitude, for southern hemisphere genesis (m/s).

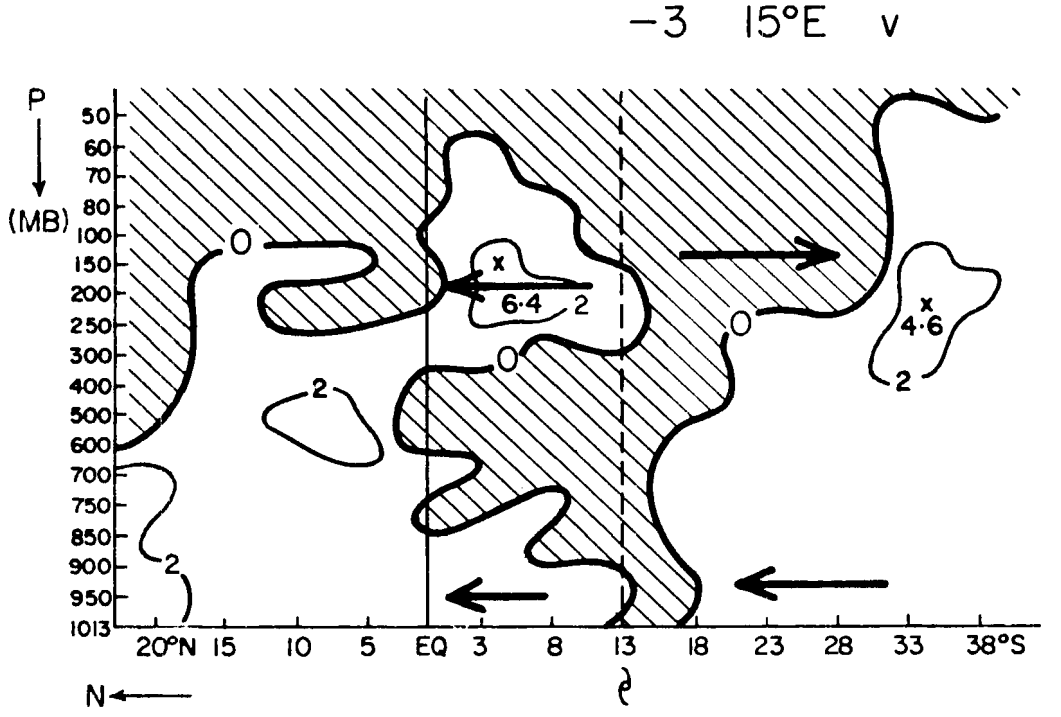

Fig. 94. Meridional wind field anomaly cross-section. -3 minus Q, 15° east of the genesis longitude, for southern hemisphere genesis (m/s).

15° west of the genesis longitude (Fig. 89) are:

(i) An increase in the low level equatorial westerlies and upper level midlatitude westerlies for the pregenesis cases maximized around 10° to 15° latitude from the storm.

(ii) An increase in the low level (trade) easterlies poleward of the disturbance and an increase in the upper level equatorial easterlies.

The net effect of these changes is to increase the surface to 150 mb westerly shear by around 7 m/s poleward of the genesis latitude and to increase the easterly shear by around 7 m/s equatorward of the disturbance.

Features of the meridional wind anomaly chart 15° west of the genesis longitude (Fig. 90) are:

(i) The entire troposphere from the equator to 20°N shows an increased equatorward wind component, maximized around 500 mb. This is suggestive of a deep layer surge, essentially barotropic in nature.

(ii) From the surface to 300 mb in the belt equator to 25°S the winds are more equatorward before storm genesis. An acceleration of the southeast trades is occurring at least three days before genesis.

(iii) Poleward of the genesis latitude, in the upper levels, there is increased poleward flow. This is most likely due to increased outflow from the anticyclone located above the inter-tropical convergence zone.

At the storm genesis longitude (140°E), the zonal wind anomaly cross-section (Fig. 91) shows:

(i) Similar shear increases north and south of the genesis latitude as in Fig. 89.

(ii) An increase in the winter hemisphere trade easterlies around 15°N to 20°N.

The 140°E meridional wind anomaly cross-section (Fig. 92) shows:

(i) An exceedingly strong (8 m/s) anomaly at 150 mb, representing a northward jet from southern to northern hemispheres existing in pregenesis situations.

(ii) A deep layer of increased southward flow from 20°N to 10°S most likely associated with cold surges.

(iii) Increased northward flow poleward of the developing disturbance, from 13°S to 38°S. Once again this feature is associated with the strengthened southeast trades and weakened westerlies poleward of the subtropical ridge.

At 15° east of the genesis longitude (155°E) the zonal wind anomaly chart (Fig. 93) shows:

(i) A much reduced westerly equatorial anomaly when compared with Figs. 89 and 91.

(ii) A pattern with a positive anomaly at 100 mb near 20°S and a negative anomaly near 30°S of roughly equal magnitude. This suggests that in the pregenesis situation, the subtropical jet east of the incipient disturbance has migrated 10° equatorward. Such circumstances would occur with an upper trough close to the genesis longitude.

The meridional wind anomaly chart at three days prior to southern hemisphere genesis, 15° east of the genesis longitude (Fig. 94) shows:

(i) Increased northward/decreased southward flow at all latitudes except fo an area around 10° (latitude) wide centered on the genesis latitude.

(ii) Increased south to north upper flow as seen in Fig. 92.

The one day before genesis minus the quiet period anomaly cross-sections show many similarities to the three before minus quiet anomaly charts and some significant differences.

The one day before genesis minus the quiet composite anomaly chart, 15° west of the genesis longitude (Fig. 95) shows:

(i) An easterly surface to 100 mb shear anomaly of 13 m/s 10° (latitude) equatorward of the genesis longitude and a poleward westerly shear anomaly of only 3 m/s.

(ii) The entire troposphere poleward of the genesis latitude shows a westerly anomaly. This indicates stronger

easterly trade winds to around 500 mb and a decreased westerly jet aloft.

The meridional wind anomaly chart 15° west of the genesis longitude (Fig. 96) shows:

(i) Stronger anomalies at 200 mb than on Fig. 90 indicating an increased divergence away from the area of the inter-tropical convergence zone.

(ii) The surface to 200 mb northern hemisphere negative anomaly has moved slightly equatorward than in Fig. 90 and become more intense in the lower layers.

The genesis longitude (140°E) zonal wind anomaly cross-section at one day before cyclone genesis (Fig. 97) shows:

(i) A stronger surface to 300 mb equatorial westerly anomaly than at three days before genesis. The anomaly is maximum around 700 mb where its of the order of 10 m/s. The quiet state winds are around 5 m/s easterly, indicating a major reversal of the flow prior to tropical cyclone genesis.

(ii) The weak positive anomaly at 33°S near 200 mb indicates the subtropical jet is impinging upon the upper, or that the uppers are spinning down as a result of the divergent outflow anticyclone

The meridional wind anomaly chart at the genesis longitude (Fig. 98) shows:

(i) Enhanced flow in the northern hemisphere, towards the southern hemisphere, at all levels below 250 mb with a strong narrow belt of enhanced return flow between 250 mb and 100 mb.

(ii) Meridional wind anomalies indicating enhanced poleward flow south of the developing disturbance.

The zonal wind anomaly chart for one day before genesis 15° east of the genesis longitude (Fig. 99) shows:

(i) A weak equatorial westerly wind enhancement.

(ii) A displacement of the southern hemisphere subtropical jet 10° (latitude) equatorward, as in Fig. 93.

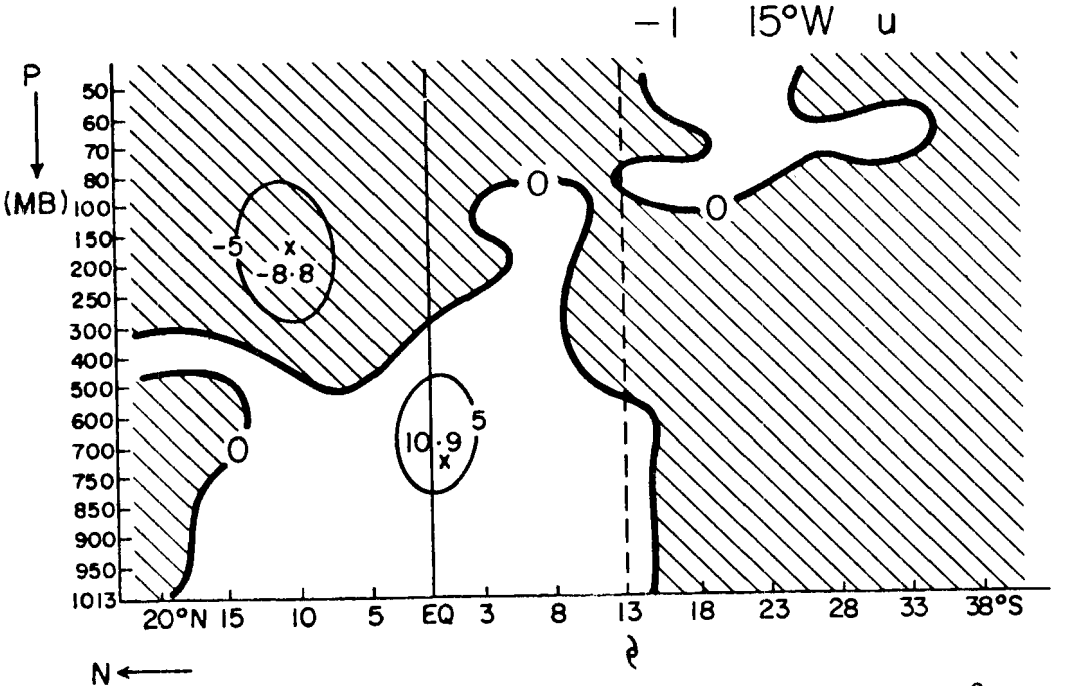

Fig. 95. Zonal wind field anomaly cross-section. -1 minus Q, 15° west of the genesis longitude for southern hemisphere genesis (m/s).

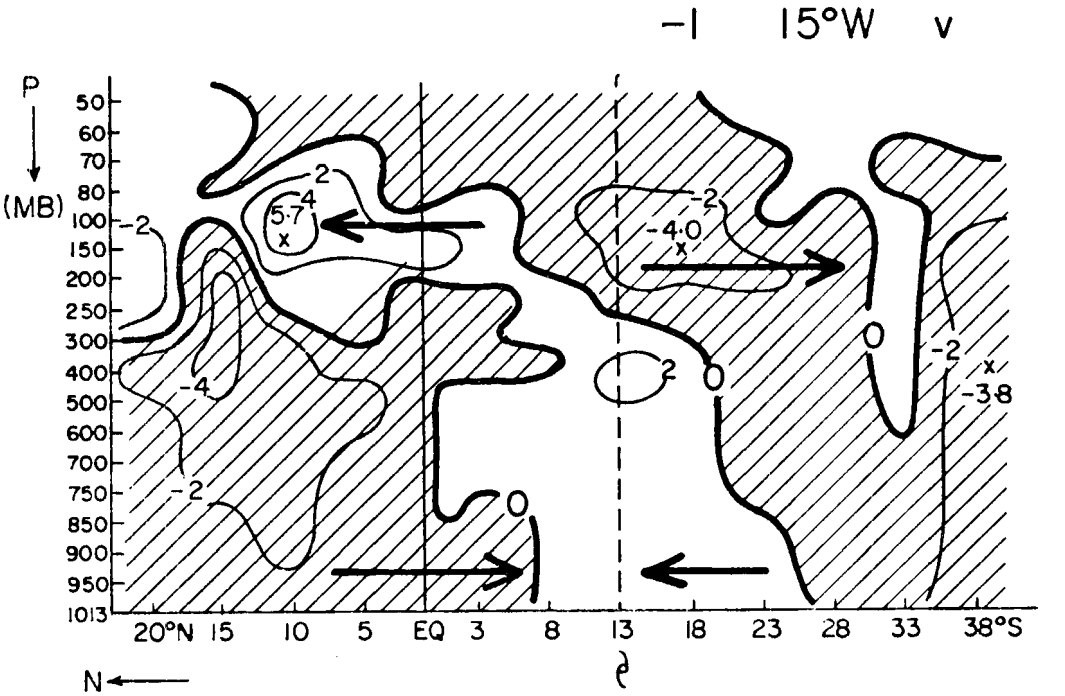

Fig. 96. Meridional wind field anomaly cross-section. -1 minus Q, 15° west of the genesis longitude for southern hemisphere genesis (m/s).

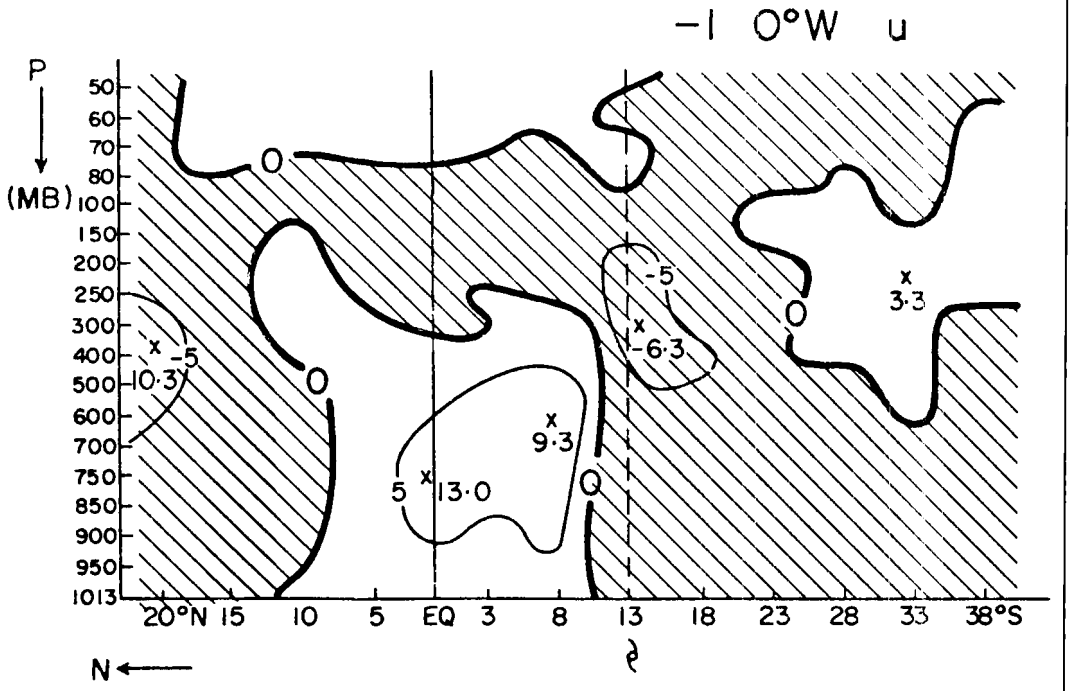

Fig. 97. Zonal wind field anomaly cross-section. -1 minus Q, at the genesis longitude for southern hemisphere genesis (m/s).

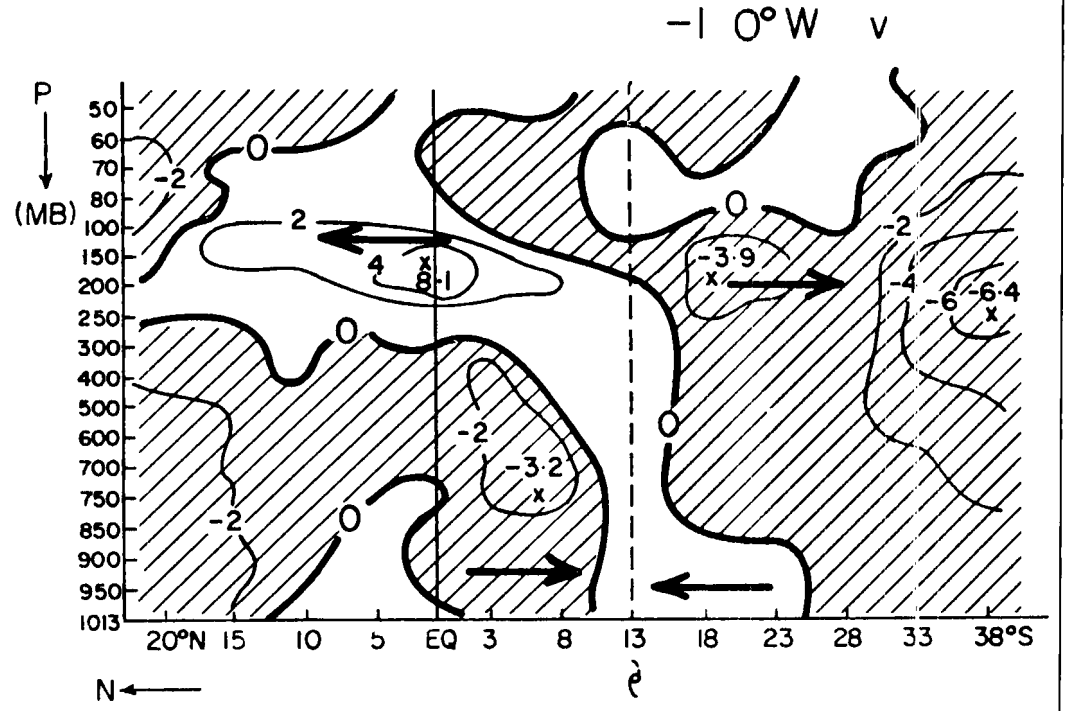

Fig. 98. Meridional wind field anomaly cross-section. -1 minus Q at the genesis longitude for southern hemisphere genesis (m/s).

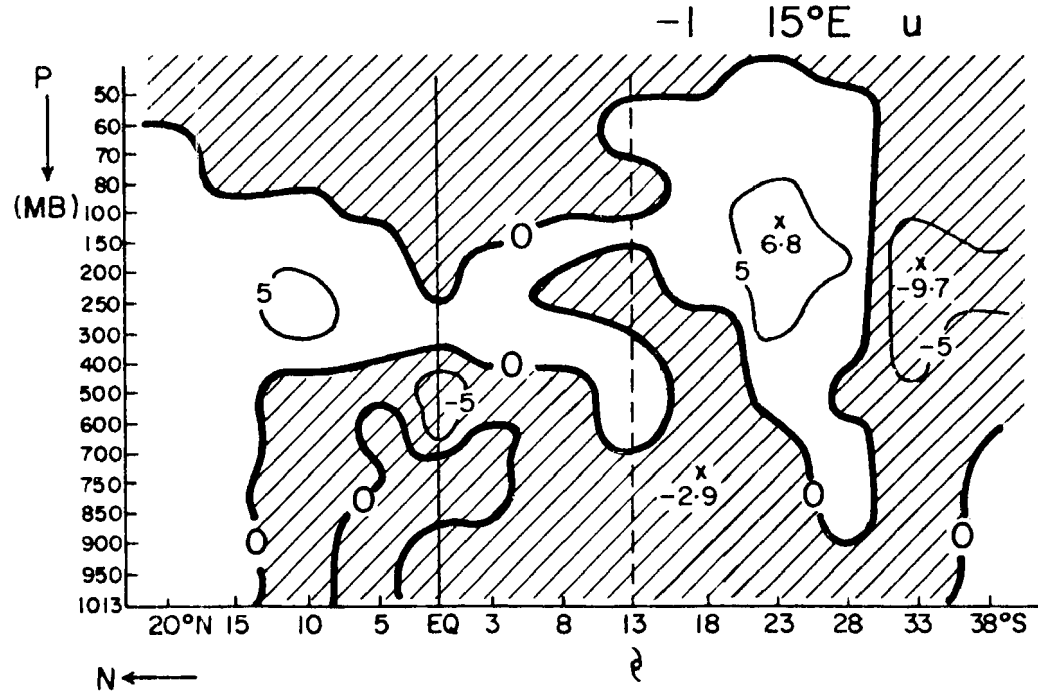

Fig. 99. Zonal wind field anomaly cross-section. -1 minus Q at the genesis longitude for southern hemisphere genesis (m/s).

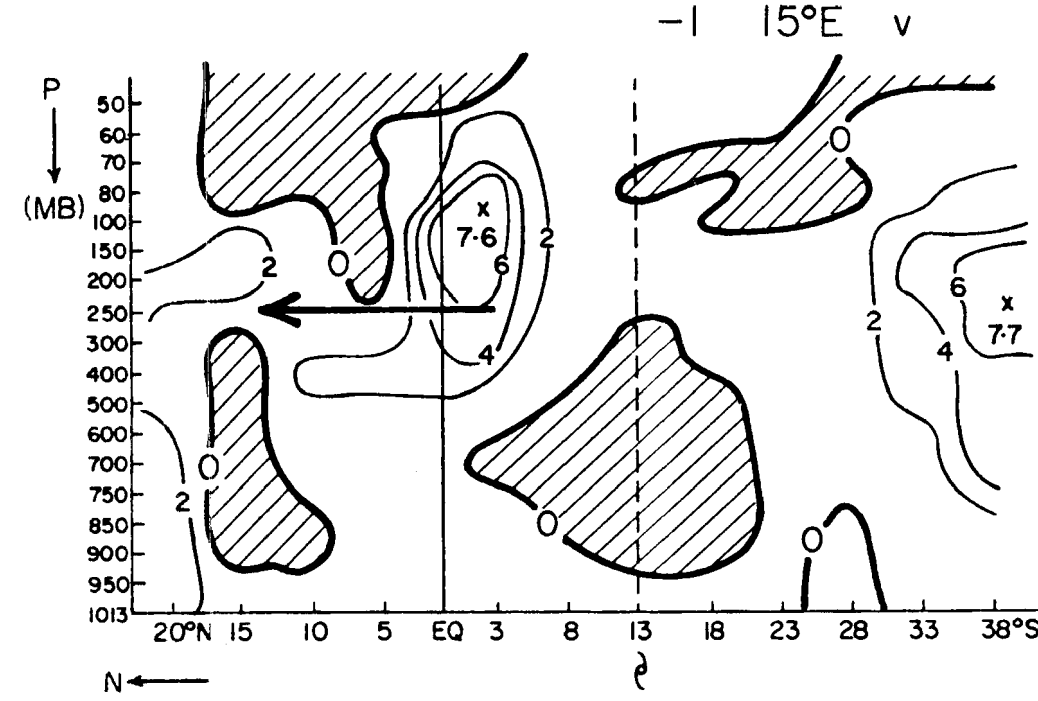

Fig. 100. Meridional wind field anomaly cross-section. -1 minus Q at the genesis longitude for southern hemisphere genesis (m/s).

The meridional wind anomaly chart 15° east of the genesis longitude (Fig. 100) shows:

(i) The largest anomalies in the upper levels with areas of enhanced southerly flow near 38°S and 3°S. The former anomaly indicates the presence of a composite trough to the east, the latter anomaly a return flow from southern to northern hemisphere above the low level monsoon.

(ii) Weak northerly (negative) anomalies below 400 mb. One near 13°S associated with the circulation of the developing cyclone. The second near 15°N associated with some weak surge activity.

6.6 Summary: Southern Hemisphere Genesis

Evolution of the large scale flow features before southern hemisphere genesis show:

(i) A large scale increase of easterly shear (in the vertical) equatorward of the cyclone genesis latitude.

(ii) A large scale increase of westerly shear poleward of the genesis latitude.

These tendencies in shear generation, in conjunction with the thermal wind relationship imply a warming of the ITCZ in pregenesis situations compared to the quiet conditions.

(iii) An increased southwards flow in the northern hemisphere at all levels below 200 mb, before southern hemisphere storm genesis. In the presence of the meridional temperature gradient found between 30°N and the equator, there must be significant cold air advection. Such conditions imply that the composite pregenesis situation contains a winter hemisphere cold surge.

(iv) An increased outflow from the upper levels above the inter tropical convergence zone. This outflow is located in the layer 250 mb to 100 mb. This feature combined with the increased low level convergence into the inter-tropical convergence zone implies a stronger Hadley cell prior to cyclone genesis.

These differences between the quiet period composite charts and the pregenesis composites have been summarized on Fig. 101 which contains the genesis longitude pregenesis minus quiet period cross-sections for

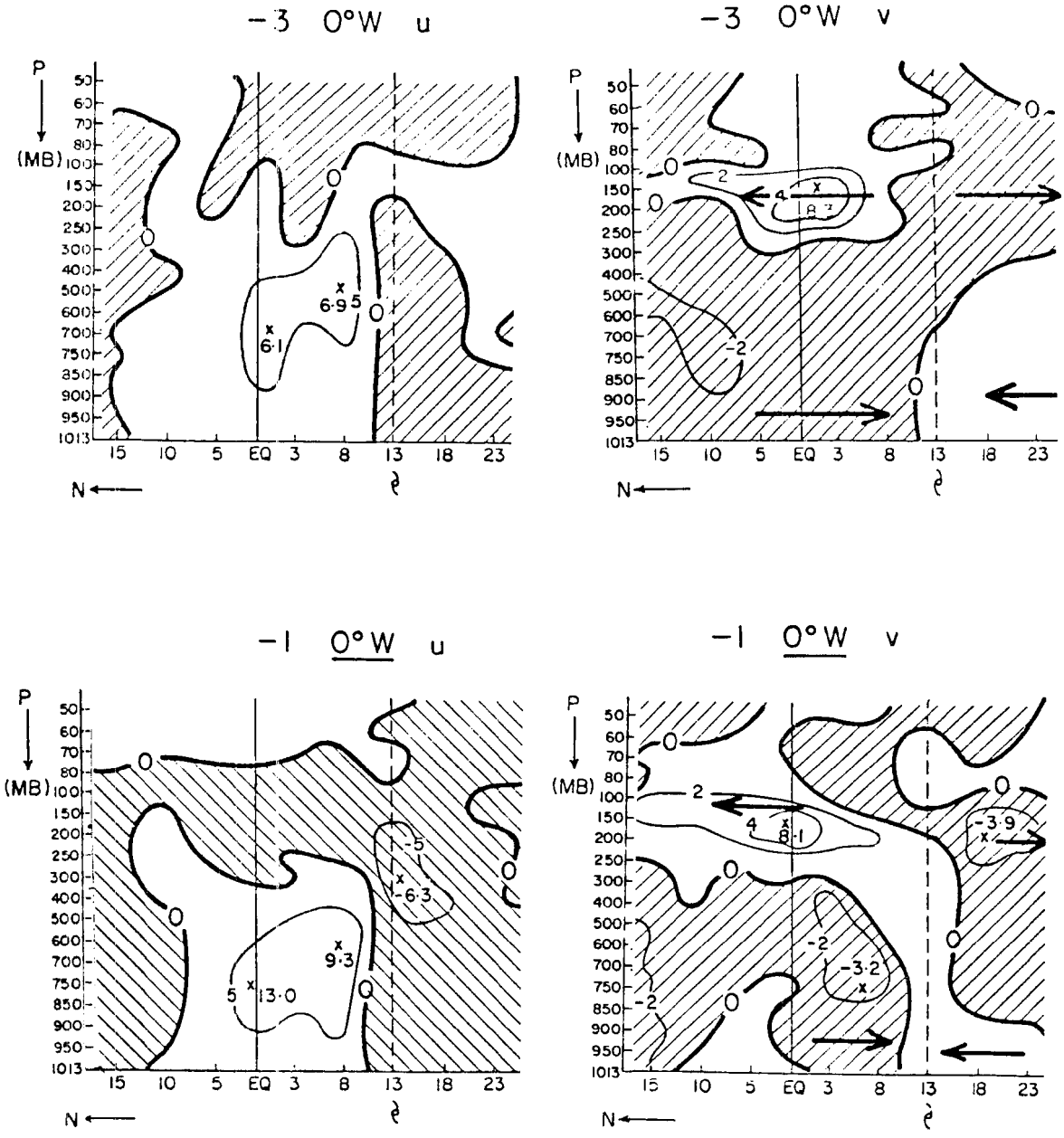

Fig. 101. Tropical strip pregenesis anomaly cross-section for southern hemisphere genesis. All cross-sections are on the genesis longitude (m/s).

the latitude belt 15°N to 25°S. At 3 days before genesis the differences between these composites and the quiet period are largely equatorwards of the storm. At one day before large differences are occurring in the southern hemisphere subtropics accompanied by an acceleration of the low level equatorial westerlies.

6.7 Northern Hemisphere Tropical Cyclone Genesis - Composite Wind Fields

Figures 102, 103 and 104 show the 1013 mb, 500 mb and 200 mb composite streamline/isotach analyses respectively one day before tropical cyclone genesis in the northern hemisphere. The composite genesis point is three degrees further poleward than for the southern hemisphere cases discussed in the previous section. The 1013 mb chart (Fig. 102) reveals a cyclonic circulation about 8° southeast of the composite genesis point. Reed and Recker (1971) give the mean speed of 18 northwest Pacific wave disturbances to be 7° longitude per day, indicating the composite pregenesis low in Fig. 102 to be moving in a normal fashion. This may be contrasted with the southern hemisphere pregenesis low which was located less than 2° west of the genesis point, indicating either that southern hemispheres systems move little or that they move erratically. Analysis of many charts indicates the latter is the most probable. Figure 102 also shows cross-equatorial winds, through the longitude belt 115°E to 155°E, converging into the pregenesis cluster. The 500 mb analysis (Fig. 103) shows most of the cross-equatorial infeed limited to the belt 105°E to 135°E, but once again the equatorial effects are through a deep layer. At 200 mb (Fig. 104) a tropical easterly jet with speeds in excess of 10 m/s appears downstream from the anticyclone overlying the incipient disturbance.

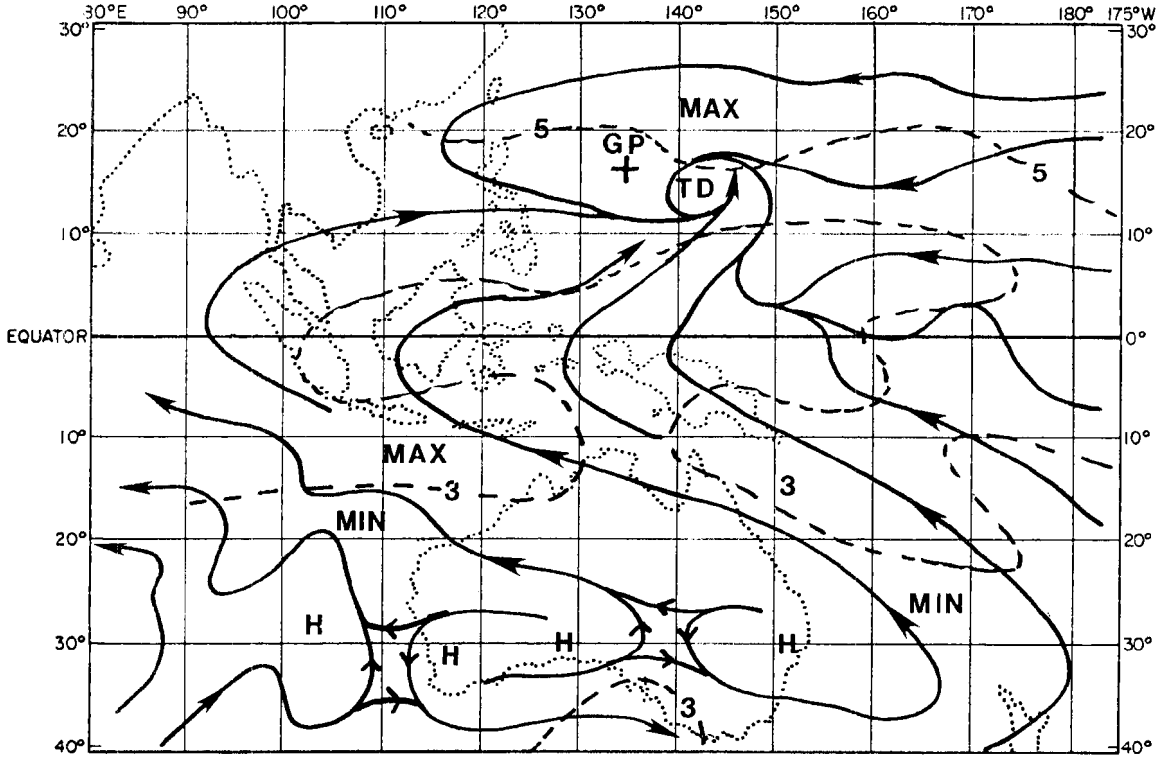

Fig. 102. 1013 mb composite streamline/isotach analysis one day before tropical cyclone genesis in the northern hemisphere (isotachs in m/s).

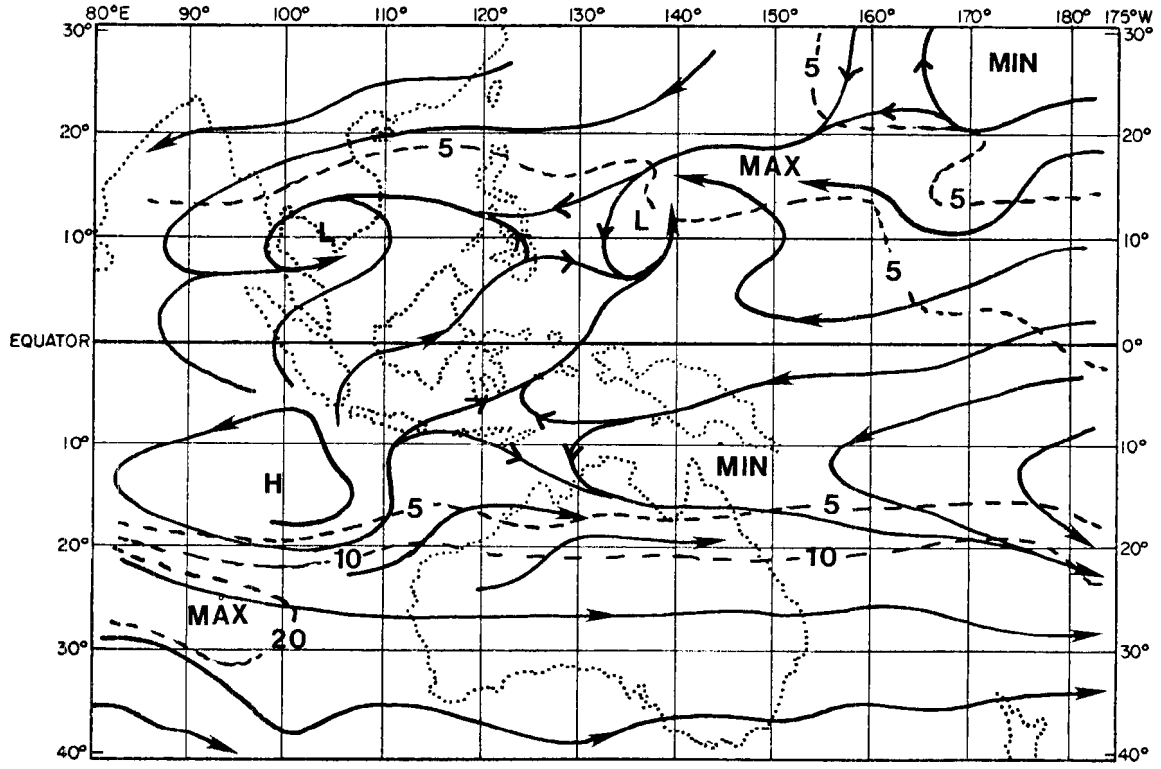

Fig. 103. 500 mb composite streamline/isotach analysis one day before tropical cyclone genesis in the southern hemisphere (isotachs in m/s).

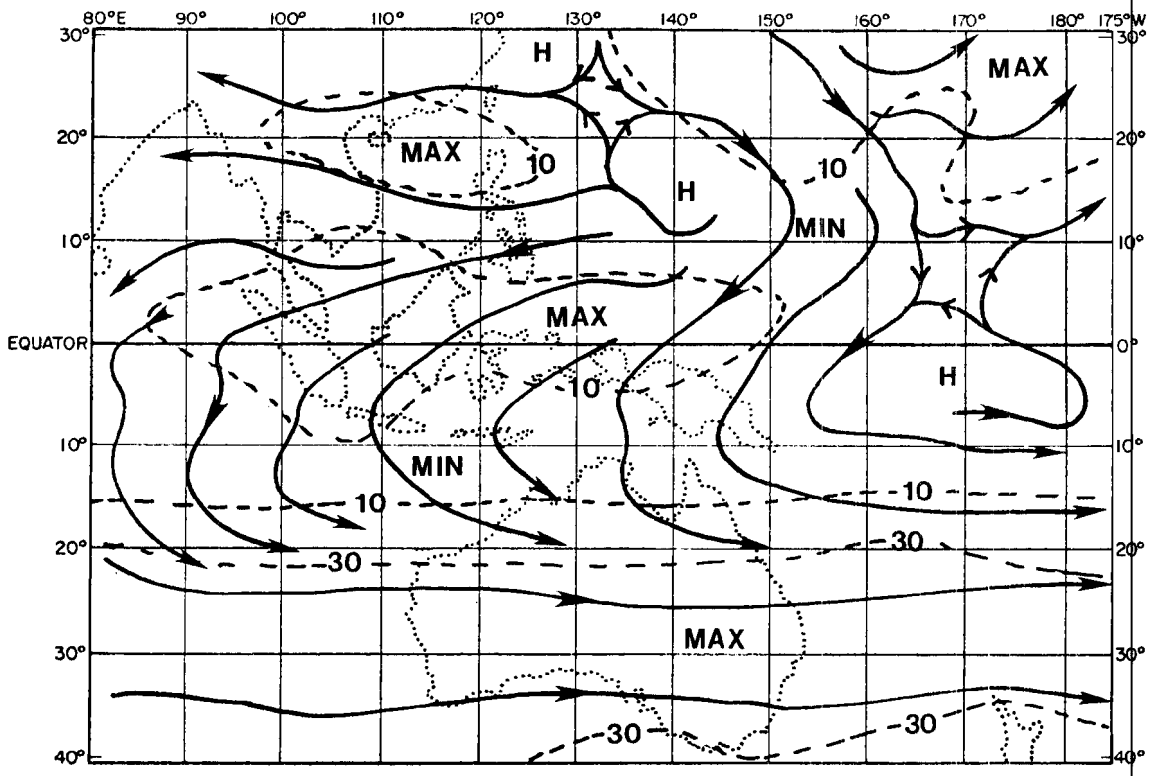

Fig. 104. 200 mb composite streamline/isotach analysis one day before tropical cyclone genesis in the southern hemisphere (isotachs in m/s).

There is also a weak indication of a tropical upper tropospheric trough immediately poleward of the disturbance.

6.8 Anomaly Cross-sections for Northern Hemisphere Genesis

There are structural similarities and differences between the northern hemisphere pregenesis anomaly cross-sections (Figs. 105 through 116 and their southern hemisphere counterparts. The westward motion of the north Pacific clusters leads to the important cold surges in the southern (winter) hemisphere being located further east relative to the genesis point than the corresponding northern (winter) hemisphere surges. The analyses also show the southern hemisphere surges to be less extensive longitudinally and generally located on the genesis longitude.

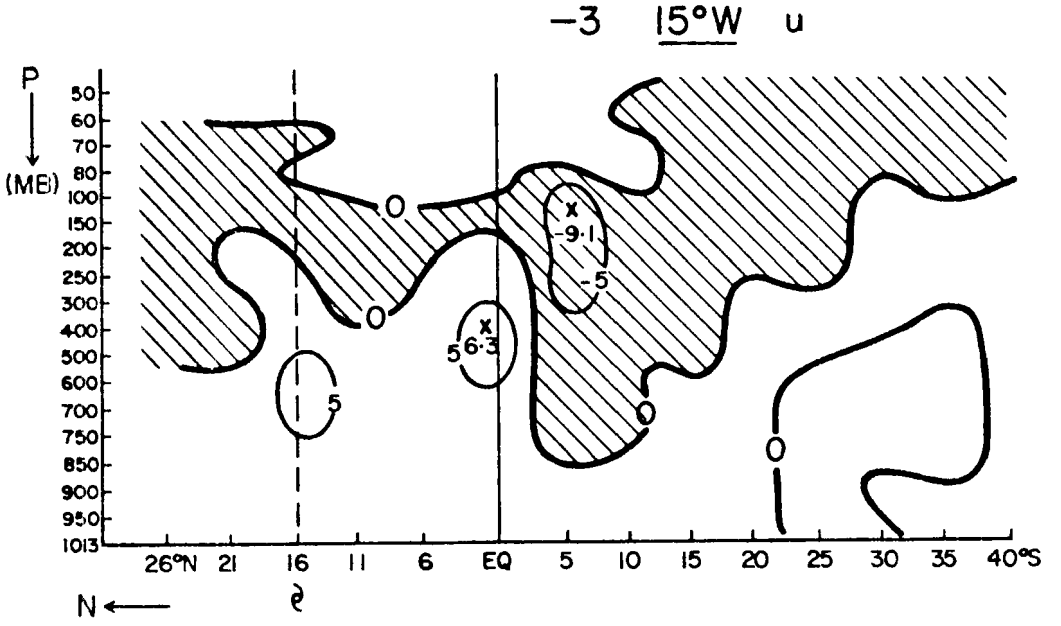

Fig. 105. Zonal wind field anomaly cross-section. -3 minus Q, 15° west of the genesis longitude, for northern hemisphere genesis (m/s).

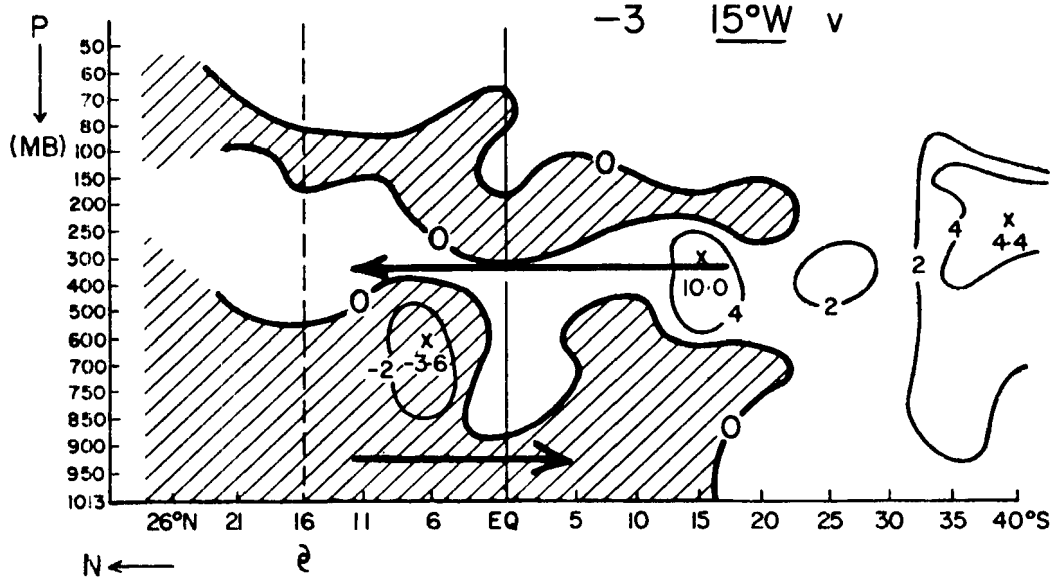

Fig. 106. Meridional wind field anomaly cross-section. -3 minus Q, 15° west of the genesis longitude, for northern hemisphere genesis (m/s).

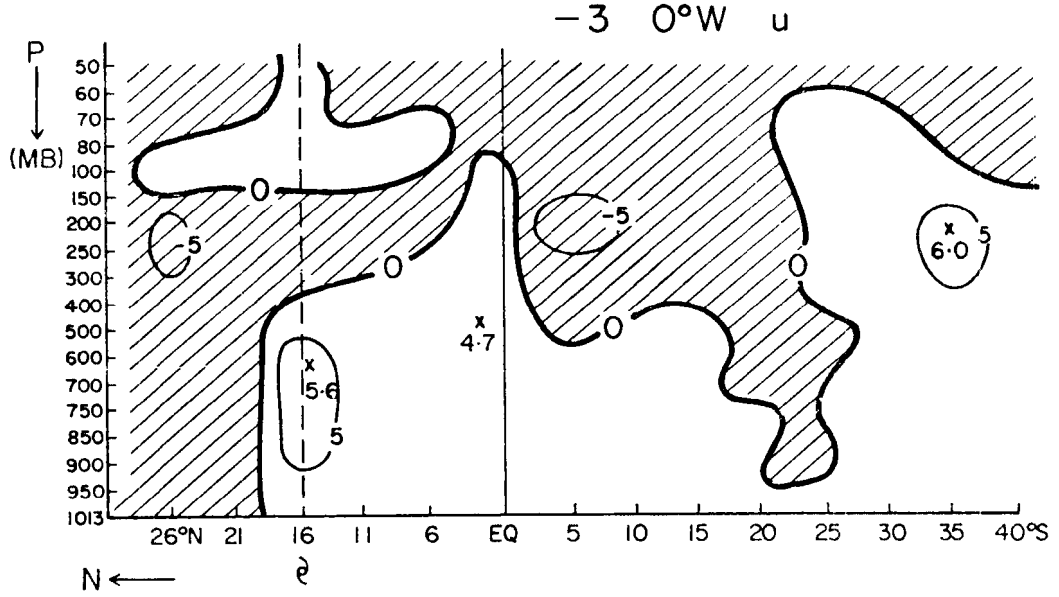

Fig. 107. Zonal wind field anomaly cross-section. -3 minus Q, at the genesis longitude, for northern hemisphere genesis (m/s).

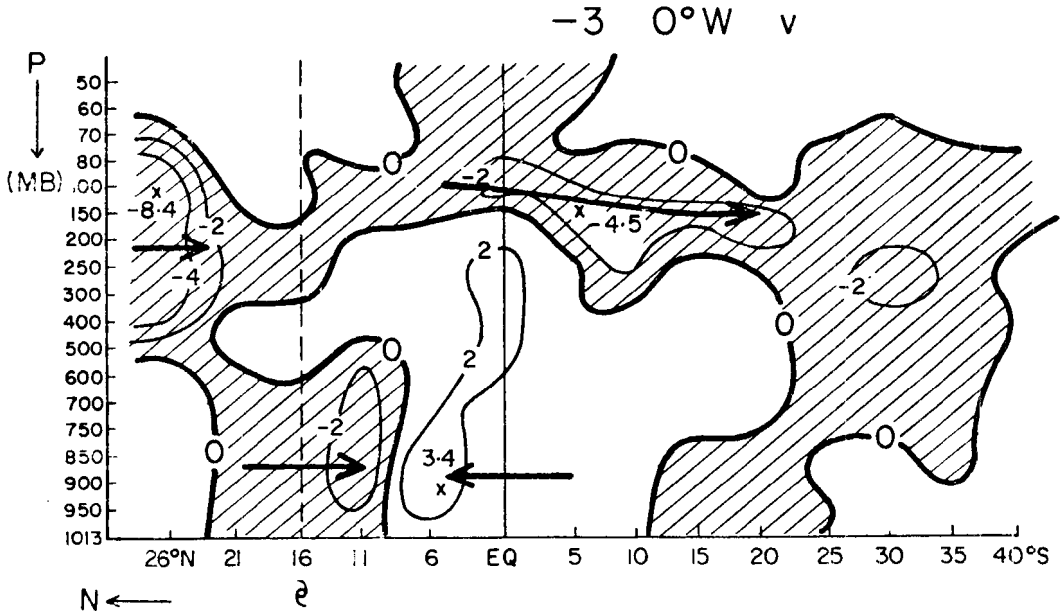

Fig. 108. Meridional wind field anomaly cross-section. -3 minus Q, at the genesis longitude, for northern hemisphere genesis (m/s).

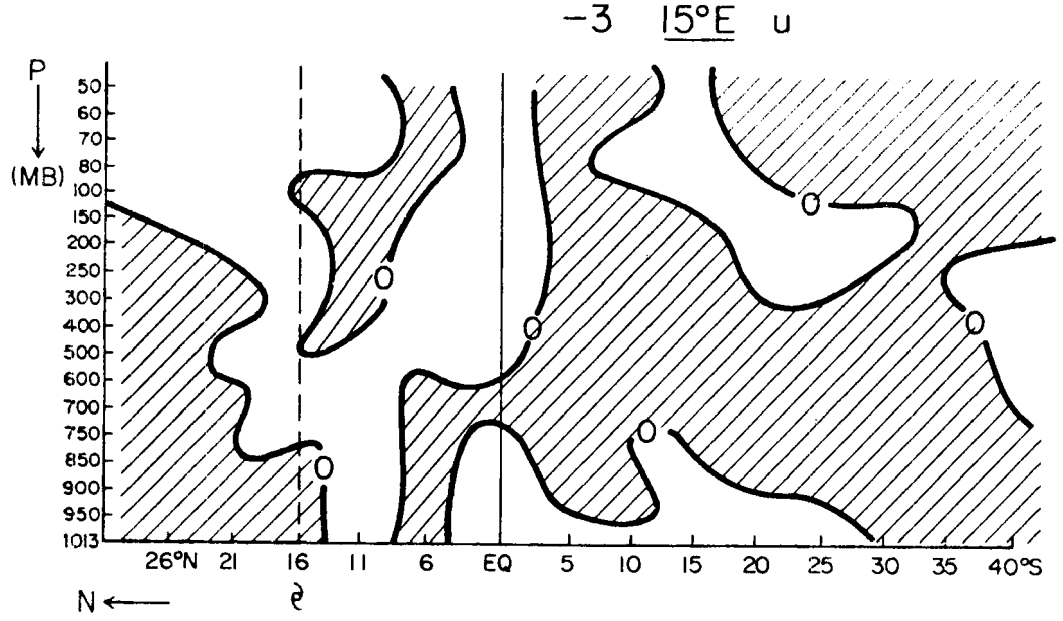

Fig. 109. Zonal wind field anomaly cross-section. -3 minus Q, 15° east of the genesis longitude, for northern hemisphere genesis (m/s).

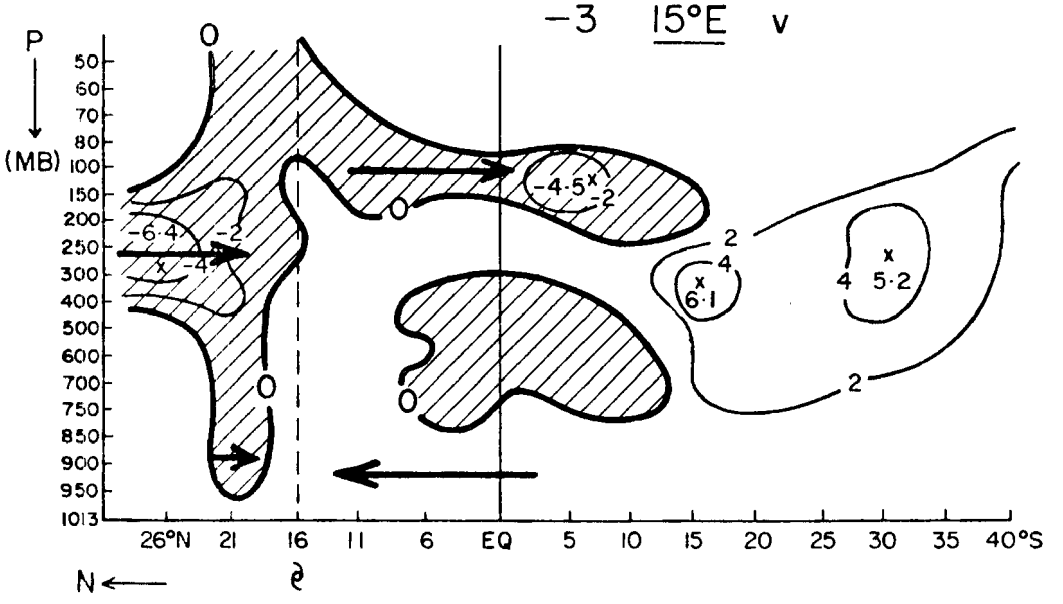

Fig. 110. Meridional wind field anomaly cross-section. -3 minus Q, 15° east of the genesis longitude, for northern hemisphere genesis (m/s).

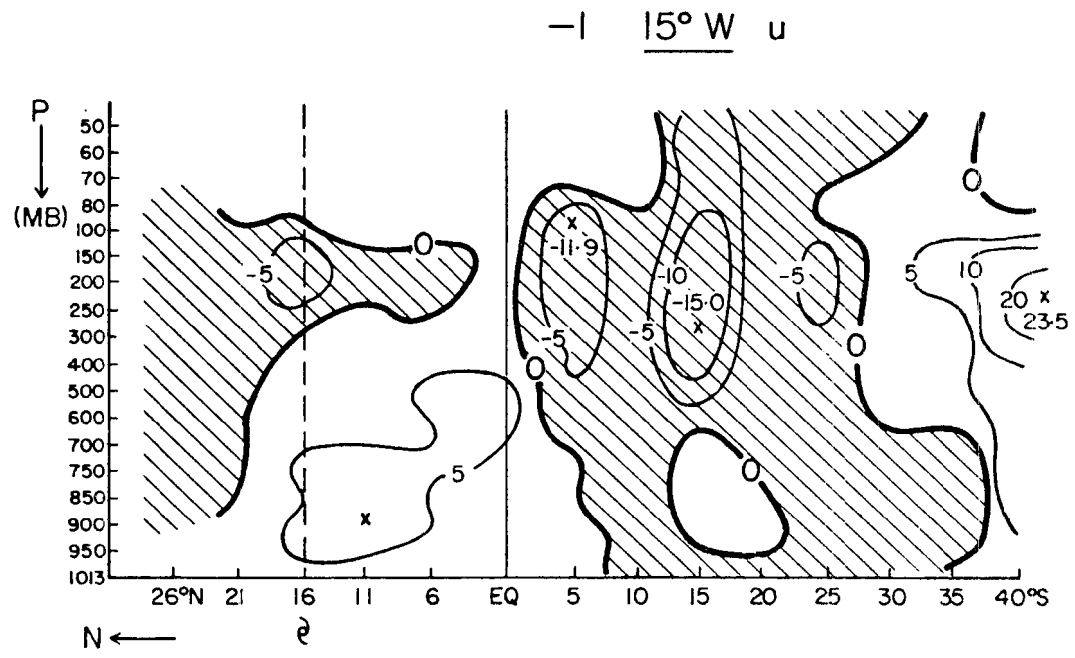

Fig. 111. Zonal wind field anomaly cross-section. -1 minus Q, 15° west of the genesis longitude, for northern hemisphere genesis (m/s).

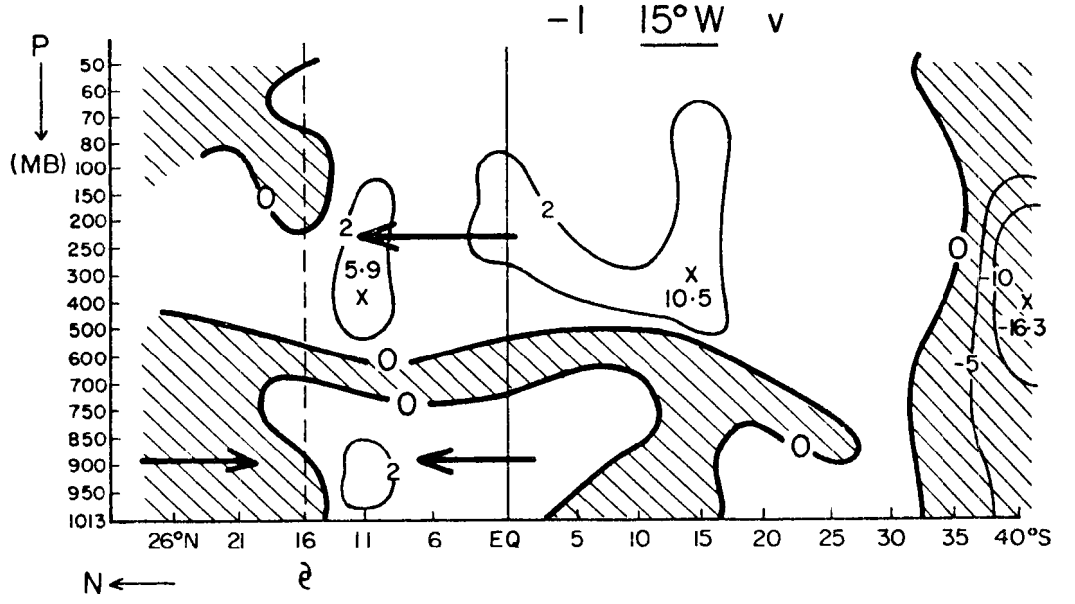

Fig. 112. Meridional wind field anomaly cross-section. -1 minus Q, 15° west of the genesis longitude, for northern hemisphere genesis (m/s).

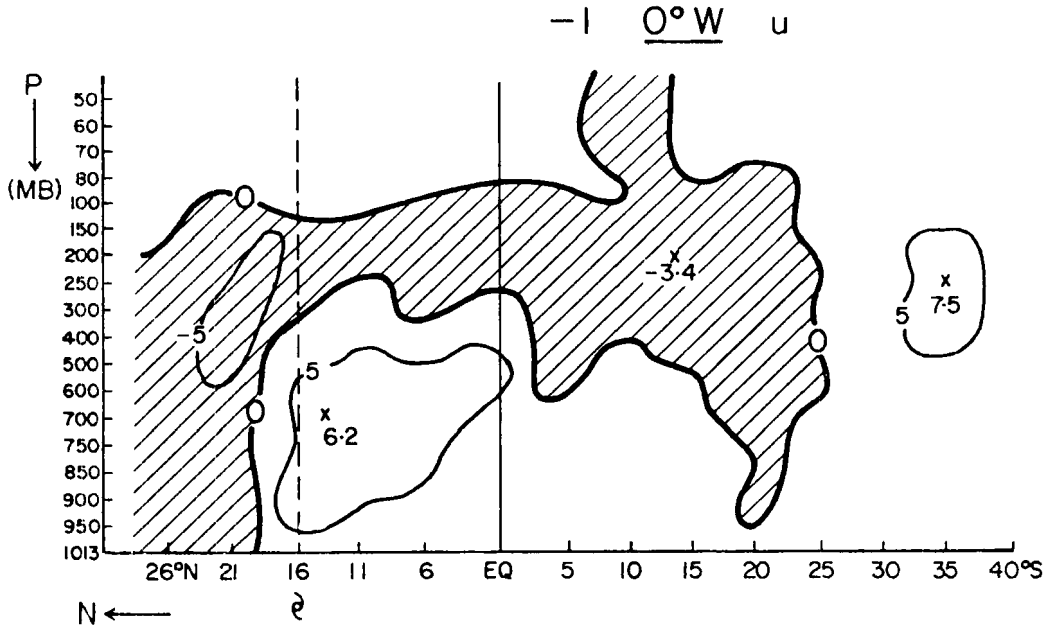

Fig. 113. Zonal wind field anomaly cross-section. −1 minus Q at the genesis longitude, for northern hemisphere genesis (m/s).

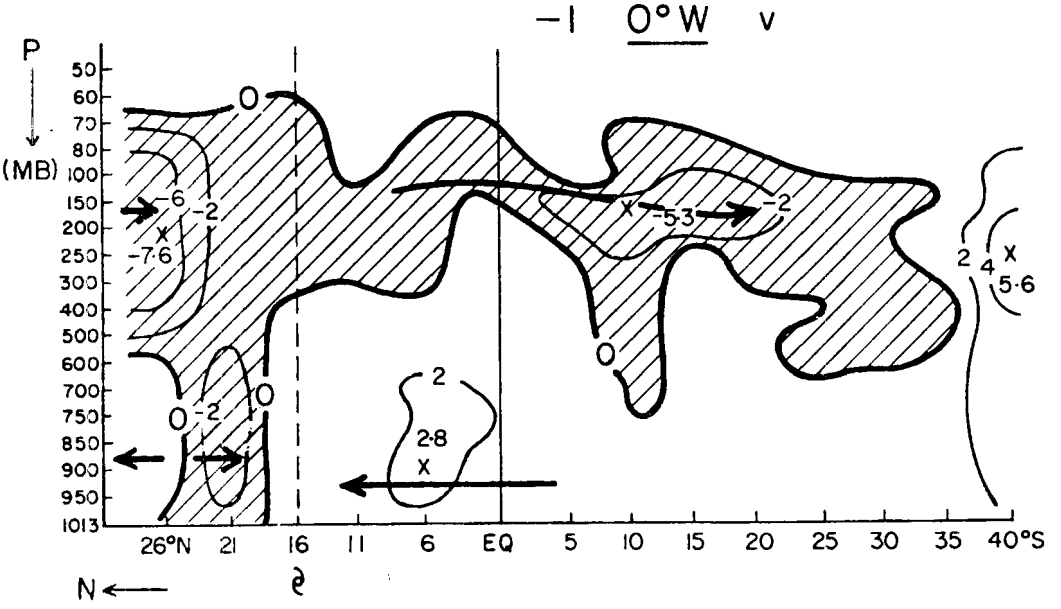

Fig. 114. Meridional wind field anomaly cross-section. −1 minus Q at the genesis longitude, for northern hemisphere genesis (m/s).

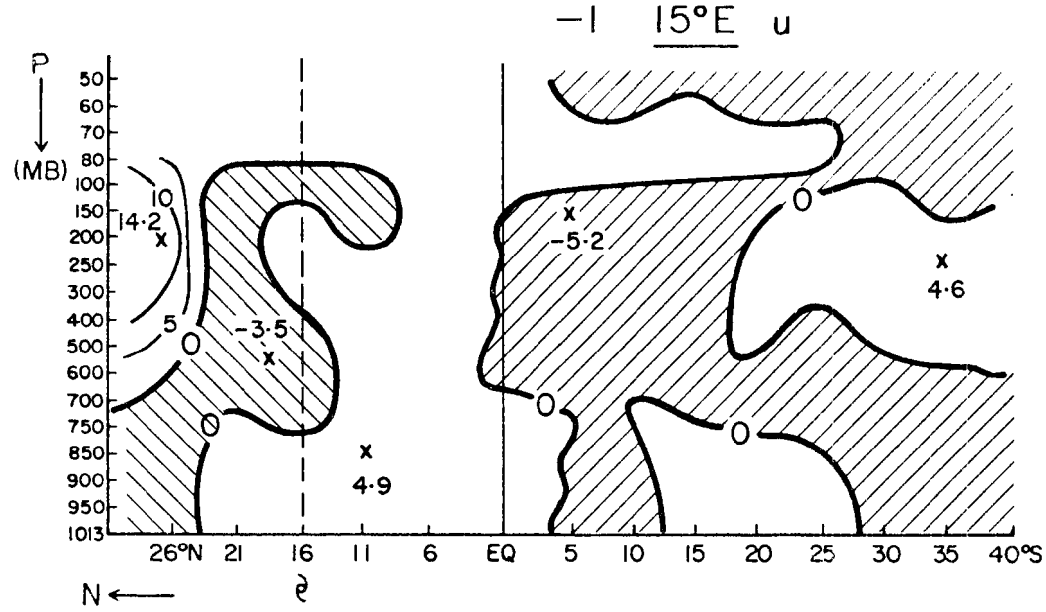

Fig. 115. Zonal wind field anomaly cross-section. −1 minus Q, 15° east of the genesis longitude, for northern hemisphere genesis (m/s).

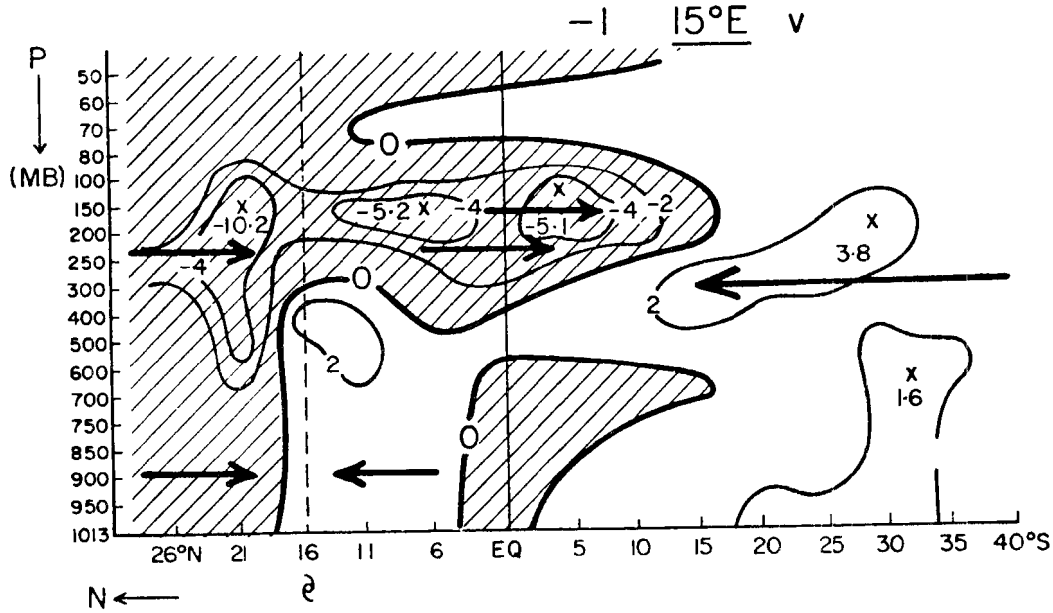

Fig. 116. Meridional wind field anomaly cross-section. −1 minus Q, 15° east of the genesis longitude, for northern hemisphere genesis (m/s).

The zonal and meridional wind anomaly charts 15° west of the genesis longitude, three days before northern hemisphere tropical cyclone genesis (Figs. 105 and 106 respectively) show enhanced equatorial westerly winds as seen in Fig. 94 but no deep layer of enhanced meridional flow in the southern hemisphere directed equatorwards.

The zonal and meridional cross-sections centered on the genesis longitude (135°E), three days before genesis (Figs. 107 and 108 respectively) show anomaly patterns representing many of the features seen in the southern hemisphere pregenesis cases. Figure 107, the zonal wind anomaly chart shows the enhanced westerly flow equatorward of the genesis latitude to be extensive in the latitudinal sense and from the surface to around 400 mb. The meridional wind anomaly chart (Fig. 108) reveals enhanced equatorward flow from 20°N to the equator from the surface to 250 mb with an anomolously large return flow from 250 mb to 100 mb. These features indicate that through the genesis longitude the Hadley cell circulation is enhanced three days before tropical cyclone intensity is reached.

At 15° east of the genesis longitude, the anomaly charts for three days before genesis of zonal (Fig. 109) and meridional wind (Fig. 110) reveal the surge effects seen at the genesis longitude to be displaced polewards and the equatorial westerly wind anomaly to be non existent. Figure 110 does show an enhanced outflow jet originating from the genesis latitude and flowing into the southern hemisphere. There is also an equatorward flow maximized at 26°N, 250 mb which is part of the tropical upper tropospheric trough seen in Fig. 108.

The zonal (Fig. 111) and meridional (Fig. 112) wind anomaly cross-section one day before northern hemisphere genesis 15° west of the genesis longitude show an area of enhanced westerly flow from the genesis latitude to 5°S below 300 mb. However, in the southern hemisphere there is no evidence of an equatorward (cold) surge, rather an antisurge. The upper westerlies are reduced in strength while the lower easterly trades have an area of westerly anomaly around 15°S.

The one day before genesis, zonal (Fig. 113) and meridional (Fig. 114) wind anomalies along the genesis longitude do indicate enhanced equatorward westerlies in the low levels and enhanced upper easterlies. The meridional winds show northward flow everywhere south of the genesis latitude to around the 400 mb level with enhanced southward flow from 400 to 100 mb, indicating a Hadley cell circulation in the pregenesis situations exceeding that of the quiet period. A negative anomaly is seen at 26°N, 250 mb indicating the cross-section is taken on the western side of pregenesis tropical upper tropospheric trough.

The one day before zonal (Fig. 115) and meridional (Fig. 116) wind anomaly cross-sections 15° east of the genesis longitude show little of the enhanced Hadley cell in the low levels, however, the meridional wind anomaly indicates a strong northern to southern hemisphere jet.

6.9 Summary

The anomaly charts depicting the evolution of the large scale flow patterns before northern hemisphere genesis (Figs. 105 through 116) revealed that before genesis an equatorward surge occurs in the southern hemisphere below 400 mb in the longitude belt 15° wide centered on the genesis longitude. There is a broad area of enhanced low level equatorial westerly flow before storm genesis existing from the equator

to the genesis latitude. In the relatively thin layer 250 mb to 100 mb a jet of flow returning to the southern hemisphere is well marked at the genesis longitude and to the east of it. The net effect of these changes is to increase the meridional overturning known as the Hadley cell in pregenesis periods when compared to quiet periods. This effect is to increase the vertical easterly shear equatorward of the intertropical convergence zone. The lack of data to the north of 16°N makes it difficult to determine whether there is an enhanced westerly shear around longitudes 26°N to 36°N before genesis, which, along with the enhanced Hadley cell would imply a warmer intertropical convergence zone as in the southern hemisphere case.

These data lead to the conclusion that the southern hemisphere cold surges are less intense or extensive than those in the northern hemisphere. Nevertheless, the same general large scale organization occurs before southern hemisphere storm genesis. Figure 117 contains a summary of the genesis longitude difference cross-sections. At three days before genesis the cross equator Hadley cell is more intense than the quiet period and at one day before this circulation has intensified.

6.10 Angular Momentum Transports for the Composite Tropical Disturbances

A fundamental role of the large scale environment surrounding an intensifying cloud cluster is to supply sufficient cyclonic angular momentum that surface frictional losses can be more than compensated. In this section the flux of absolute angular momentum through the 10° radius is evaluated for six composite circulation systems. The six systems are:

i) The southern and northern hemisphere tropical depressions three days before cyclone genesis.

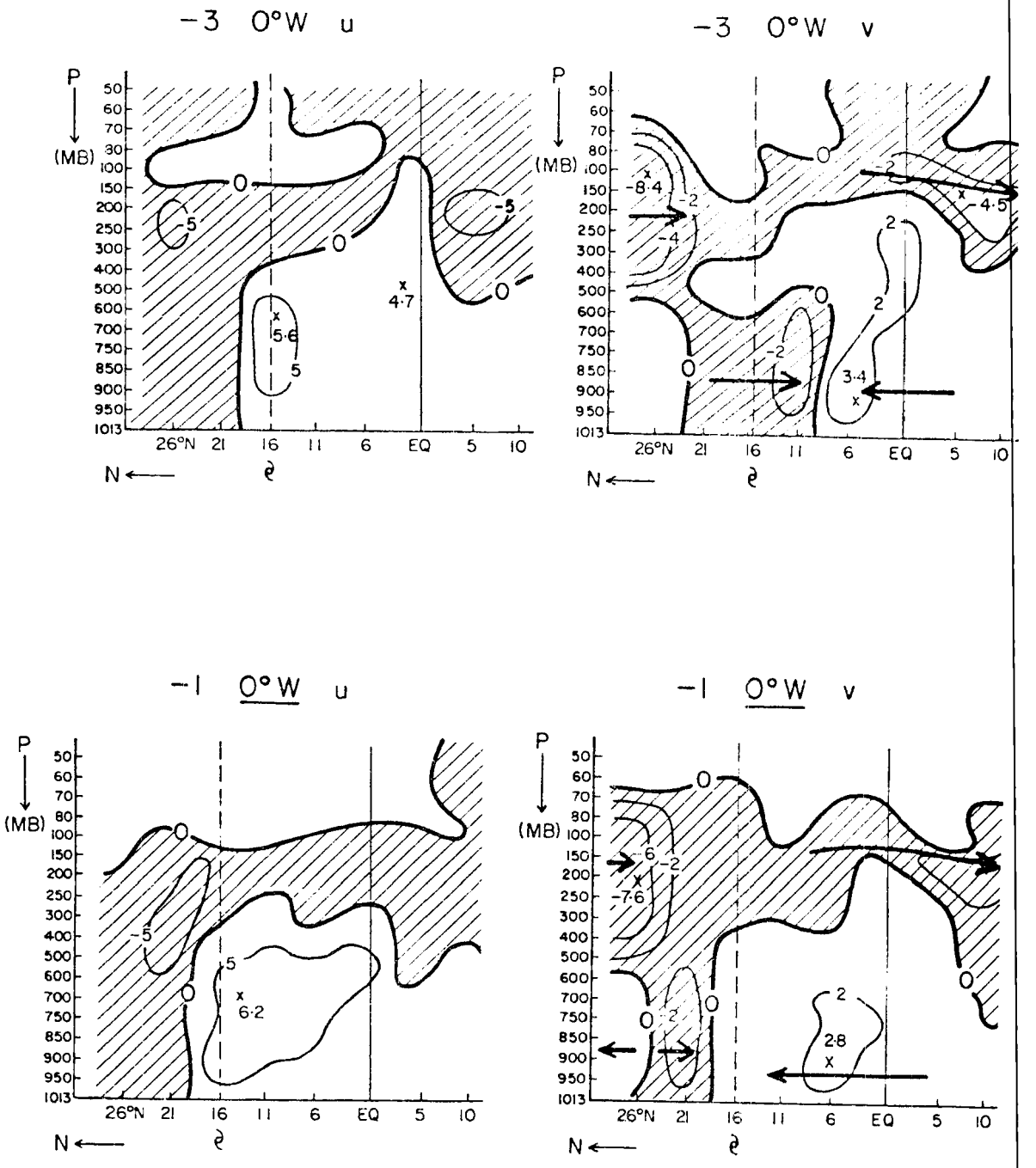

Fig. 117. Tropical strip pregenesis anomaly cross-section for northern hemisphere genesis. All cross-sections are on the genesis longitude.

ii) The southern and northern hemisphere tropical depression are day before cyclone genesis.

iii) The most prominent ITCZ depression in the northern and southern hemisphere quiet period composites.

The three day before depressions show the greatest rate of spin up the quiet period depressions a tendency to spin down.

Holland (1981) has shown that the flux of absolute angular momentum per unit mass through any circle of radius (r) about a vortex, in an Eulerian system, is given by:

$$F = \overline{V_R}\,\overline{V_T} + \overline{V'_R V'_T} + \overline{f' V_R} \qquad [7]$$

where $V_R = \overline{V}_R + V'_R$: is the radial wind

$V_T = \overline{V}_T + V'_T$: is the tangential wind

$f = f_o + f'$: is the Coriolis parameter

and the subscript R radial component of the wind

T tangential component of the wind

The primed quantities are deviations from azimuthal means denoted by the overbars and the Coriolis parameter at the vortex center is f_o.

The first term on the right hand side of Eq. 7 ($\overline{V}_R\overline{V}_T$) is the relative angular momentum flux by the mean radial circulation. A cyclonic spinup of the vortex will occur when the radial circulation imports high cyclonic momentum and exports lower cyclonic momentum air. Figure 118 depicts schematically a radial circulation which leads to cyclone spinup.

The $\overline{V'_R V'_T}$ term in Eq. 7 is the relative angular momentum flux by azimuthal eddies. The import of angular momentum occurs when there is a

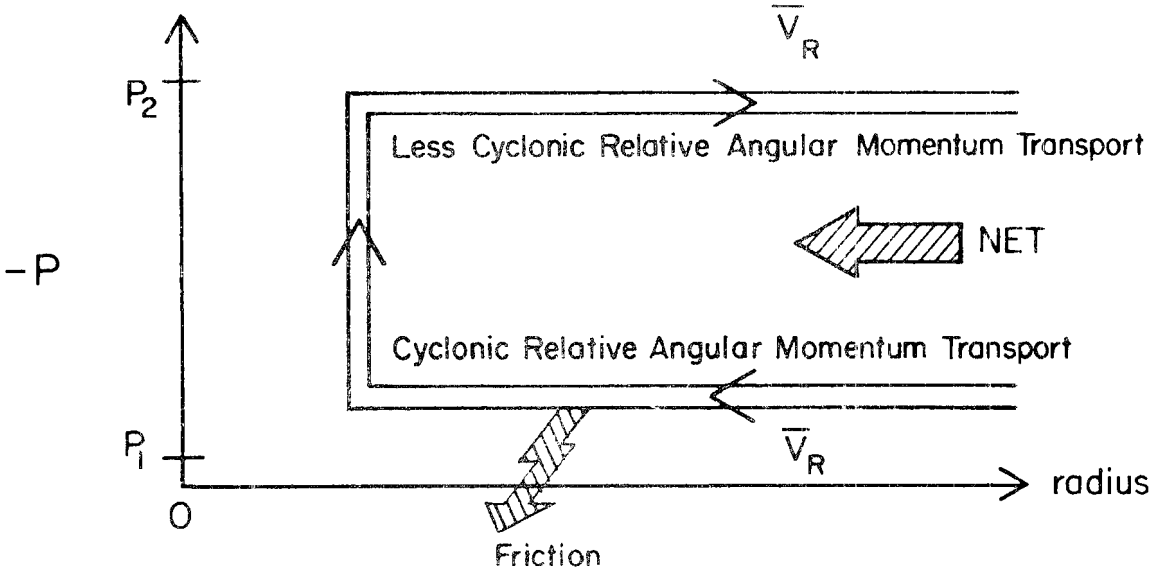

Fig. 118. An idealized radial circulation which would contribute to spinup of a vortex by way of the $\overline{V'_R V'_T}$ term.

correlation between high angular momentum air and inflow and lower angular momentum and outflow.

The $\overline{f'V_R}$ term in Eq. 7 gives the spinup of the cyclone by the eddy Coriolis torque. A net meridional flow through the vortex will result in an import of cyclonic momentum to the system through this term. Figure 119 depicts schematically such a situation.

Equation (6) may be evaluated at any radii less than about 15° (after which the earth's curvature makes the analysis doubtful) and for any number of layers in the composite analysis, to yield layer fluxes. By taking pressure weighted averages of the layer fluxes a mean spin up of a tropospheric column may be calculated. That is:

$$\text{Spinup} = \frac{1}{\sum_{i=1}^{n} \Delta P_i} \sum_{i=1}^{n} F_i \, \Delta P_i \qquad [8]$$

where F_i is the flux at level i. This spinup represents the solid body

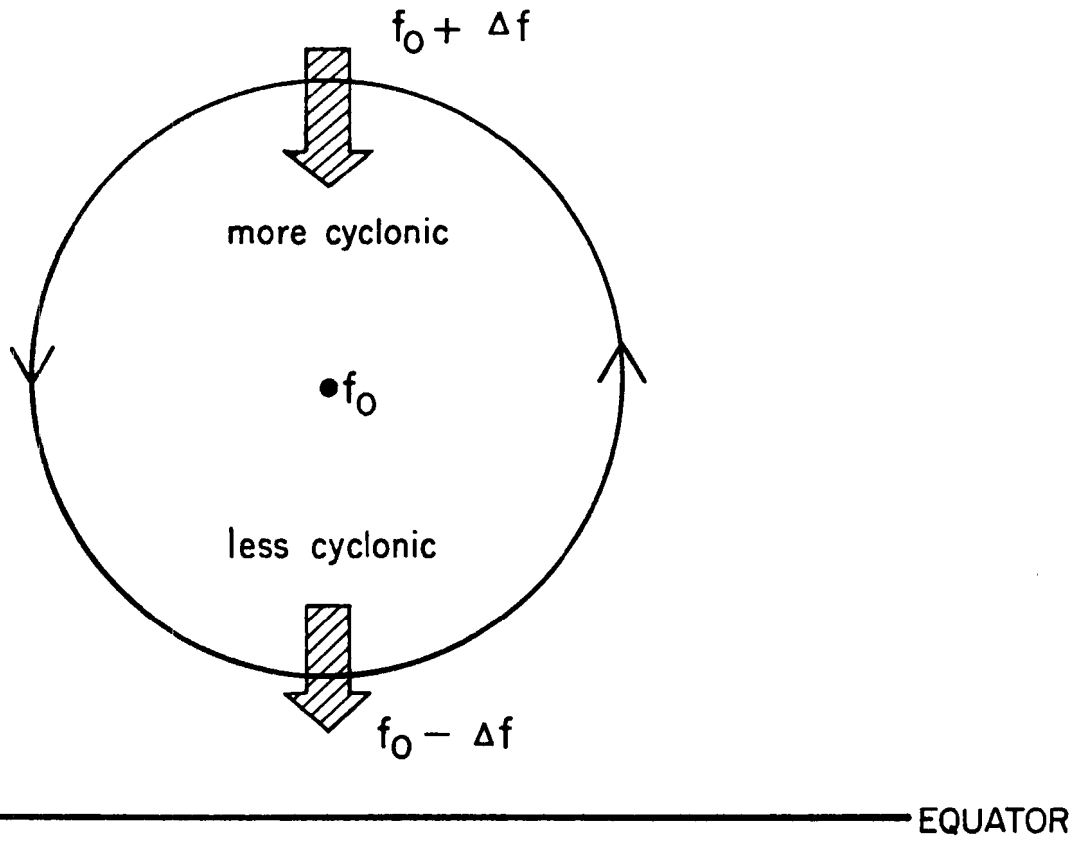

Fig. 119. A schematic of meridional flow through a vortex acting to spin it up by way of the $f'V_R$ term.

acceleration the cyclone would experience in m/s/d from the net angular momentum fluxes across the 10^o radius boundary.

As noted earlier, the supply of absolute angular momentum to the circulation within radius (r) is depleted by frictional losses at the surface. For each of the six cases the spin down due to frictional dissipation has been crudely estimated. The procedure used was as follows: A crude model depression was assumed with a radius of maximum winds at 50 km, with maximum wind speeds of 15 m/s for the one day before genesis depressions and 12.5 m/s for the quiet period and three days before genesis depressions. The wind field was assumed to increase from 0 m/s at the vortex center to its maximum value linearly and then decrease to 4^o radius with a profile of the form $v = c_2 r^{-x}$ where x typically lay between 0.4 and 0.6. From 4^o to 10^o radius the wind speed

was assumed to be a constant 5 m/s. Figure 120 shows a radius cross-section of this profile for the three days before and quiet period depressions. For the one day before depression V_{max} was increased to 15 m/s.

The piecewise expression for this profile is given by:

$$V = \begin{cases} c_1 r & r \leq 50 \text{ km} \\ c_2 r^{-x} & 50 \text{ km} < r \leq 4^o \\ c_3 & 4^o < r \end{cases} \qquad [9]$$

A constant inflow angle of 30^o was assumed for this surface wind profile along with a constant density ($\rho = 1.15$ kg/m^3) and drag coefficient ($C_D = 1.1 \times 10^{-3}$). Asymmetry of the wind within the 4^o radius was assumed due to the depression translation velocity (given by V_c). With some manipulation, it can be shown that,

$$F = \frac{-1.2\rho C_D 2\pi g}{\pi \Delta P (r_2^2 - r_1^2)\frac{r_1+r_2}{2}} \int_{r_1}^{r_2} r^2 \left(v^2 + \frac{1}{2}|V_c|^2\right) dr \qquad [10]$$

where ΔP denotes the depth of the atmosphere through which the friction is to be distributed. In all calculations, ΔP was set equal to 913 mb.

Tables 11 and 12 include the calculated spindown due to surface friction in m/s day for the six composite depressions.

In order to prepare absolute angular momentum budgets on the six distubances the fluxes were evaluated at 10^o radius for three levels, 850 mb, 500 mb and 200 mb. Assuming an atmosphere of the structure shown in Fig. 121 spinup rates in m/s per day are given in Tables 11 and 12 for the various terms in Eq. 8 and the frictional spindown.

The data presented in Tables 11 and 12 reveal that the mean relative angular momentum transport is consistently important in the

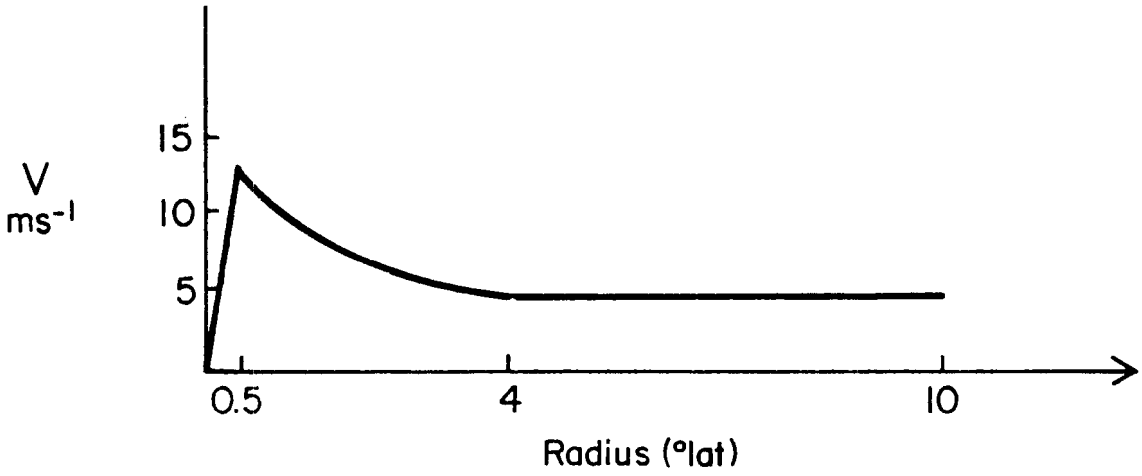

Fig. 120. Assumed surface tangential wind field of three days before and quiet period depressions.

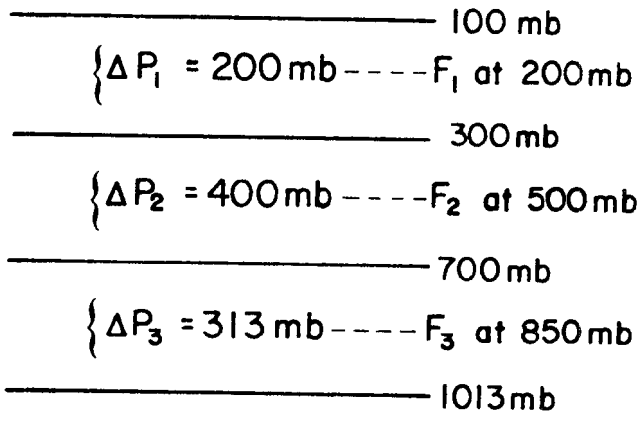

Fig. 121. Three layer structure of the troposphere assumed in calculations of tropospheric spinup by angular momentum fluxes.

TABLE 11

Cyclonic spinup (m/s per day) for three southern hemisphere composite systems. All fluxes evaluated at 10^{o} radius.

System Term	Minus Three Day Depression	Minus One Day Depression	Quiet Period Depression
$\overline{V}_R \overline{V}_T$	2.03*	1.91	-0.52
$\overline{V'_R V'_T}$	-0.91	-0.40	0.04
$\overline{f'V_R}$	0.95	-0.66	-0.08
Flux Total	2.08	0.85	-0.60
Friction	-0.50	-0.51	-0.50
Total	1.58	0.36	-1.10

*A positive number represents a flux of cyclonic relative angular momentum directed towards the vortex, through the 10^{o} radius.

TABLE 12

Cyclonic spinup (m/s per day) for three northern hemisphere composite systems. All fluxes are evaluated at the 10^{o} radius.

System Term	Minus Three Day Depression	Minus One Day Depression	Quiet Period Depression
$\overline{V}_R \overline{V}_T$	0.48	3.15	0.08
$\overline{V'_R V'_T}$	-0.01	-1.47	0.22
$\overline{f'V_R}$	0.65	0.19	0.31
Flux Total	1.12	1.86	.61
Friction	-0.54	-0.52	-0.50
Total	0.85	0.42	0.11

angular momentum budgets of intensifying systems. The eddy terms act to spin down intensifying systems and the Coriolis term, while contributing to spin up is generally smaller than the $\bar{V}_R\bar{V}_T$ term . The inclusion of the motion of the system merely alters slightly the frictional dissipation, increasing slightly the spin down in rapidly moving systems.

It is noteworthy that the minus three day composite depression is spinning up most rapidly in both oceans, the minus one less and the quiet period ITCZ system is decaying in the southern hemisphere and only slightly intensifying in the northern hemisphere. It may be that transports into the 10^o radius are important at very early stages of cluster development (three days before storm genesis) and then with increasing intensity, rearrangements within 10^o radius become of greater importance. Unfortunately with the crude resolution of these composites it is impossible to verify such a conjecture.

The angular momentum budgets show some consistencies between the ocean basins which indicate they are providing a reasonable estimate of the dynamic interaction between the cloud cluster and the large-scale circulation patterns. They also confirm that the interaction between the large scale and the vortex is critical in the very early stages of cluster development.

6.11 Conclusion: An Idealization of the Pregenesis Situation

In conjunction with the height anomaly charts of Chapter 4 of this paper an idealized scenario for a high percentage of ITCZ type tropical cyclone genesis cases could be described as follows:

(i) There is intense midlatitude cyclogenesis at about the genesis longitude in the winter hemisphere three days before genesis.

(ii) The strong anticyclogenesis in the wake of the developing winter hemisphere trough moves equatorward to reinforce the subtropical ridge near latitude 25^{o}.

(iii) A cold surge in the winter hemisphere propagates equatorward raising pressures throughout the subtropics to the equator in an area west of the genesis point.

(iv) With the establishment of east-west equatorial pressure gradients antitripic westerly winds occur equatorward of the intertropical convergence zone.

(v) Around the time of enhanced equatorial westerlies an anticyclone has moved slowly eastwards, polewards of the pregenesis cluster, intensifying the summer hemisphere trade easterlies.

(vi) Enhanced low level convergence into the intertropical convergence zone increases convection, with stronger outflow occurring aloft in the layer 250 mb to 100 mb.

(vii) The large scale vertical wind shears induced by the strengthened Hadley cell lead to warming of the core of the intertropical convergence zone. Such flows also allow the necessary transports of angular momentum to support an intensifying vortex.

This idealized picture has been depicted at three levels of the atmosphere, for southern hemisphere genesis in Figs. 122, 123 and 124. A similar series of schematics for northern hemisphere genesis is given in Figs. 125, 126 and 127.

The precise details of the intensification of the vortex within this environment are left to other workers with finer resolution in their data.

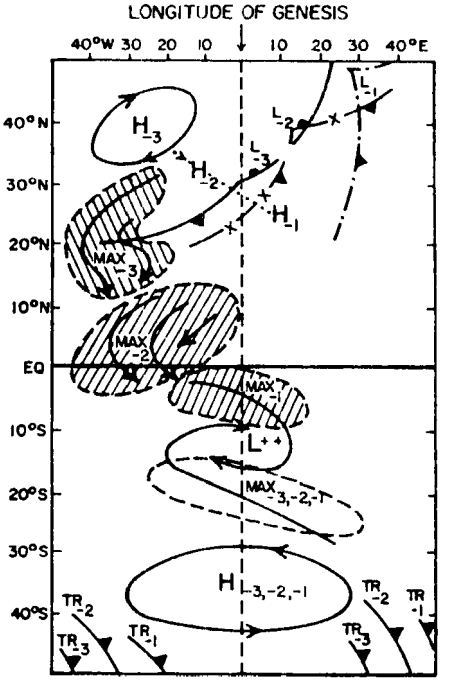

Fig. 122. Idealized gradient level streamline chart for three days preceding tropical storm genesis in the southern hemisphere. Subscripts -3, -2, -1 refer to the position of the synoptic system that number of days before genesis. The momentum burst (isotach maximum) has been shaded.

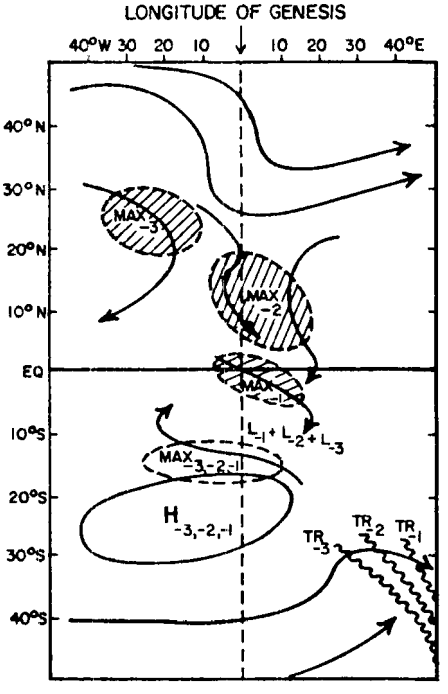

Fig. 123. Same as Fig. 122, except for 500 mb flow.

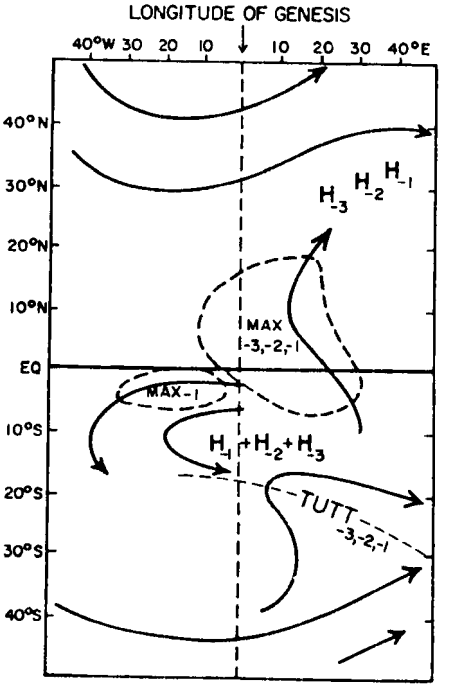

Fig. 124. Same as Fig. 123, except for 200 mb flow.

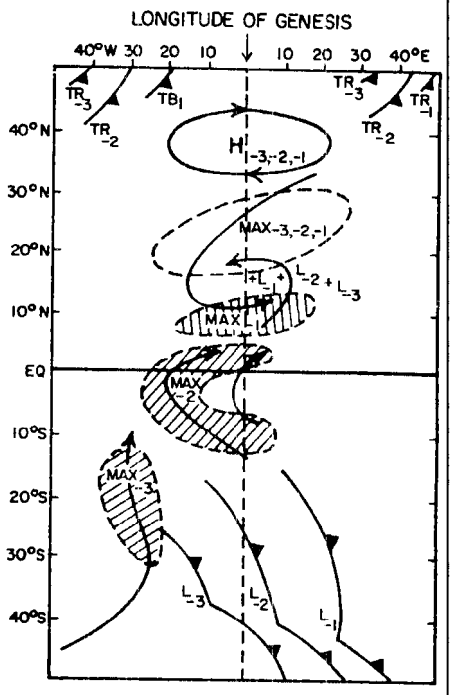

Fig. 125. Idealized gradient level streamline chart for three days preceding tropical storm genesis in the northern hemisphere. Subscripts -3, -2, -1 refer to the position of the synoptic system that number of days before genesis. The momentum burst (isotach maximum) has been shaded.

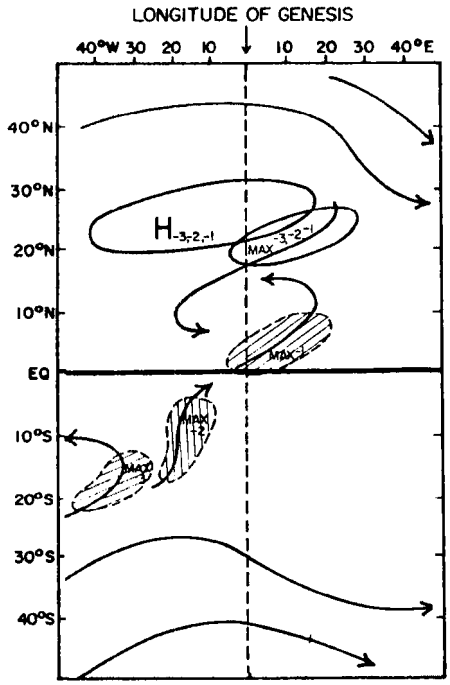

Fig. 126. Same as Fig. 125, except for 500 mb flow.

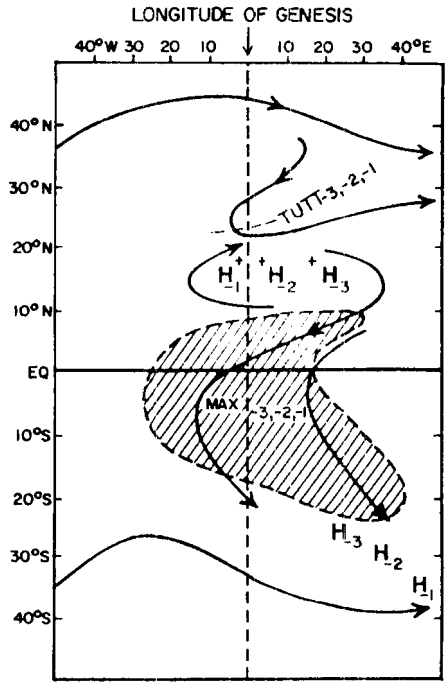

Fig. 127. Same as Fig. 125, except for 200 mb flow.

7. NUMERICAL MODEL DESCRIPTION

7.1 Introduction

The case studies and compositing work described in previous chapters have documented in great detail the tropical-midlatitude interactions occurring at times of cyclone genesis. There is a need to investigate the fundamental physics of this interaction. One direction in which an investigator could proceed would be to use a general circulation model to reproduce the phenomena observed. However, given the nonlinear effects included in such models, along with complex cumulus parameterization schemes required to drive the tropics, the investigator at the conclusion of a successful simulation cannot be sure he has not obtained the correct answer for the wrong reasons. Worse still, after an unsuccessful simulation he is faced with the daunting task of identifying the area of his model in which inadequate physics are crucially destructive.

The large scale tropics may be viewed as a system constantly attempting to achieve wind-pressure balance in the presence of a large number of unbalancing forcings. These forcing mechanisms cover all scales from turbulent heat fluxes at the earth-atmosphere interface to clouds, tropical waves, midlatitude-tropical interactions and differential radiational heating. When unbalanced the atmosphere radiates inertia-gravity waves which carry energy and momentum. The system will come to balance with both wind and mass fields changed from their initial state. The relative change of each field depends largely on the horizontal scale of the unbalancing perturbation and the background vorticity.

Rather than investigating the sum total of all of these forcings at once in a highly non linear general circulation model, the role the midlatitude forcings plays in unbalancing the tropical flow fields alone has been investigated. In order to understand more fully the physics of meridional energy propagation from midlatitudes to tropics, a linear model with extremely simple physics was used. The shallow water equations were solved; spherical geometry, time dependent forcing and realistic pole to pole profiles of the zonal component of the wind have been considered in their solution. In this way a qualitative appreciation of the physics and energetics of large scale gradient adjustment was obtained.

7.2 Earlier Investigations Using the Shallow Water Equations

In order to solve numerically the atmospheric prediction equations, the dependent variables may be represented in physical space by a series of orthogonal functions. Space derivatives may be calculated analytically in terms of a finite series of the same functions. The prediction equations may then be transformed to the system of ordinary differential equations for the expansion coefficients that depend on time. Such a method for solving the primitive equations is commonly referred to as a spectral technique.

In this section the barotropic primitive equations (shallow water equations) over a sphere are solved by spectral methods. The spectral form of the barotropic nondivergent vorticity equation over a sphere, with spherical harmonics as basis functions, was formulated by Silberman (1954). There have been many model simulations since 1954 using the primitive equations and spectral techniques, in this work the general formulation of Kasahara (1977 and 1980) is followed.

The physics of many meteorological phenomena have been explored by successful modeling of that phenomena, by the technique described above. Two observed features of the tropics which have been so treated are:

i) Zonally propagating waves of period 5 days and another class of waves of period 15 to 20 days

ii) Meridionally propagating disturbances from the midlatitudes which act to modulate the large-scale tropical flow fields.

Of the zonally propagating tropical waves, the five day period westward propagating wave was first documented by Deland (1964). The 16 to 20 day period westward propagating wave was documented by Eliassen and Machenhauer (1965, 1969). Madden (1978) hypothesized these planetary waves to be free oscillations of the external mode in an atmosphere of equivalent depth of 10 km. Kasahara (1980) has shown from theoretical considerations that the 5 day wave is little affected by the zonal flow whereas the 16 to 20 day waves are significantly affected. Solving the shallow water equations for an atmosphere of equivalent depth equal to 10 km, with the basic state at rest, reveals the free oscillations to have a period of only 12.3 days. For a realistic pole to pole zonal wind profile (representative of the 500 mb level) the period is 16.7 days in June and 18.4 days in January. This seasonal change in periodicity of the free oscillations is related to the intensity of the westerly wind maximum at 45^{o}N, the strongest winds corresponding to the longest period of oscillation. The smaller variation in the intensity of the southern hemisphere westerly jet between seasons leads to a strong correlation between period of free oscillation and northern hemisphere westerly wind speeds; however, there is no evidence to suggest that anomalously strong winds in the southern

hemisphere subtropical jet would not also act to modulate the tropical flow fields.

Observational evidence for meridionally propagating waves is not well documented, the work of Fujita (1969) illustrates how energy may propagate across the equator, leading to the formation of equatorial anticyclones. In the case study presented by Fujita, two hurricanes are observed interacting with the cross-equatorially forced anticyclone. However, there is no lack of theoretical work to suggest that under special circumstances meridional propagation of energy may occur from the midlatitudes to the tropics. The previous chapters of this paper indicate that such propagation does occur.

The problem of meridional energy propagation is discussed in Eliassen and Palm (1961). In Charney (1969) the following argument is advanced to indicate that energy may propagate from the midlatitudes to the deep tropics only when the intervening winds are westerly: writing the perturbation form of the conservation equation as,

$$\left(\frac{\partial}{\partial t} + V \cdot \nabla_h \right) q = 0 \qquad [11]$$

where

$$V = k \times \nabla_h \psi$$

$$q = \nabla_h^2 \psi + \beta_o y + \frac{f_o^2}{\rho_o} \frac{\partial}{\partial z} \left[\frac{\rho_o}{N_o^2} \frac{\partial \psi}{\partial z} \right]$$

$$\psi = \frac{P - P_o}{\rho_o f_o} \qquad N_o^2 = g \frac{\partial \ln \theta}{\partial z}$$

$$f_o = 2\Omega \sin \phi_o \qquad \beta_o = \frac{\partial f_o}{\partial y}$$

then substituting

$$\psi = \psi(y,z)e^{ik(x-ct)} \qquad [12]$$

into Eq. 11 gives

$$\frac{\partial^2\psi}{\partial y^2} + \frac{f_o^2}{\rho_o}\frac{\partial}{\partial z}\left[\frac{\rho_o}{N_o^2}\frac{\partial\psi}{\partial z}\right] + \left[\frac{\partial q_o/\partial y}{u_o - c} - k^2\right]\psi = 0 \qquad [13]$$

Now assuming u_o and $N^2{}_o$ are independent of y and z then substituting for

$$\Phi = \left[\frac{\rho_o}{N_o^2}\right]\psi \qquad [14]$$

enables Eq. 13 to be rewritten as,

$$\frac{\partial^2\Phi}{\partial y^2} + \frac{f_o^2}{N_o^2}\frac{\partial^2\Phi}{\partial z^2} + \left[\frac{\beta_o}{u_o - c} - k^2 - \lambda^2\right]\Phi = 0 \qquad [15]$$

where

$$H_o = R\frac{T_o}{g} \qquad [16]$$

and

$$\lambda^2 = \psi\frac{H_o^2 N_o^2}{f_o^2} \qquad [17]$$

When

$$0 < (u_o - c) < \frac{\beta_o}{k^2+\lambda^2} \qquad [18]$$

the coefficient of Φ in Eq. 15 is positive the Green's Function for 15 is oscillatory. When the coefficient of Φ is negative the Green's Function is exponentially damped. Equation 18 states that energy

propagation only becomes possible if c exceeds the local Rossby phase velocity $u_o - \beta_o/(k^2 + \lambda^{-2})$ but is less than the zonal velocity. Thus, propagation becomes possible in an easterly regime only if the phase velocity is more easterly. The energy is such waves in the middle latitudes is small.

Within the preceding analysis are the assumptions that the tropical flow fields, in the absence of deep convection, are to a first approximation nondivergent and that the flow is in geostrophic balance. Additional assumptions have been made that the beta plane approximation is appropriate and the horizontal scale of the waves is smaller than that of the belt of easterlies with which they interact.

Following this analysis by Charney, Mak (1969) and Bennett and Young (1969) use nondivergent models with the beta plane approximation to elegantly confirm in greater detail the qualitative conclusion of Charney presented above.

More recently Hoskins et al. (1977) have shown that significantly different results may be obtained by replacing the beta plane approximation with spherical geometry. There is more meridional energy propagation in the spherical earth simulations, and with realistic tropical easterly flow fields appreciable cross-equatorial energy flows occur for zonally elongated vorticity sources.

This investigation describes the solution of the shallow water equations with spherical geometry, time dependent forcing of an arbitrary nature and realistic zonal wind profile. Particular emphasis is placed on the sensitivity of meridional energy propagation to:

1) Background (zonal) wind field,

2) The time scale of the forcing,

3) The length scale of the forcing, and

4) The geographical orientation of the perturbation.

Experiments were performed using the so called 'external' mode of the shallow water equations.

7.3 The Horizontal Structure

The shallow water equations over a sphere have been given by Kasahara (1980) as:

$$\frac{du}{dt} - \left(f + \frac{u}{a}\tan\phi\right) v + \frac{g}{a\cos\phi}\frac{\partial z}{\partial \lambda} = 0 \qquad [19]$$

$$\frac{dv}{dt} + \left(f + \frac{u}{a}\tan\phi\right) u + \frac{g}{a}\frac{\partial z}{\partial \phi} = 0 \qquad [20]$$

$$\frac{dz}{dt} + \frac{z}{a\cos\phi}\left[\frac{\partial u}{\partial \lambda} + \frac{\partial}{\partial \phi}(v\cos\phi)\right] = 0 \qquad [21]$$

the total derivative in spherical coordinates may be written:

$$\frac{d}{dt} = \frac{\partial}{\partial t} + \frac{u}{a\cos\phi}\frac{\partial}{\partial \lambda} + \frac{v}{a}\frac{\partial}{\partial \phi} \qquad [22]$$

substituting Eq. 22 into 19, 20 and 21 gives:

$$\frac{\partial u}{\partial t} + \frac{u}{a\cos\phi}\frac{\partial u}{\partial \lambda} + \frac{v}{a}\frac{\partial u}{\partial \phi} - \left[f + \frac{u}{a}\tan\phi\right] v + \frac{g}{a\cos\phi}\frac{\partial z}{\partial \lambda} = 0 \qquad [23]$$

$$\frac{\partial v}{\partial t} + \frac{u}{a\cos\phi}\frac{\partial v}{\partial \lambda} + \frac{v}{a}\frac{\partial v}{\partial \phi} + \left[f + \frac{u}{a}\tan\phi\right] u + \frac{g}{a}\frac{\partial z}{\partial \phi} = 0 \qquad [24]$$

$$\frac{\partial z}{\partial t} + \frac{u}{a\cos\phi}\frac{\partial z}{\partial \lambda} + \frac{v}{a}\frac{\partial z}{\partial \phi} + \frac{z}{a\cos\phi}\left[\frac{\partial u}{\partial \lambda} + \frac{\partial}{\partial \phi}(v\cos\phi)\right] = 0 \qquad [25]$$

It is assumed that the wind field consists of a latitude dependent mean zonal flow $\bar{u}(\phi)$ and perturbations in both x and y directions, called u' and v'. The height field is broken into three components, an equivalent depth h_e, a latitudinally varying constant deviation from h_e, given by $H(\phi)$ (which is determined by assuming gradient balance) and finally h' the perturbation in the height field. Giving:

$$u = \bar{u}(\phi) + u'(\lambda,\phi,t) \qquad [26]$$

$$v = v'(\lambda,\phi,t) \qquad [27]$$

$$z = h_e + H(\phi) + h'(\lambda,\phi,t) \qquad [28]$$

substituting 26, 27, 28 into 23, 24 and 25 gives:

$$\frac{\partial u'}{\partial t} + \frac{\bar{u}}{a\cos\phi}\frac{\partial u'}{\partial \lambda} + \frac{v'}{a}\frac{\partial \bar{u}}{\partial \phi} - \left[f + \frac{\bar{u}}{a}\tan\phi \right] v' + \frac{g}{a\cos\phi}\frac{\partial h'}{\partial \lambda} = 0 \qquad [29]$$

$$\frac{\partial v'}{\partial t} + \frac{\bar{u}}{a\cos\phi}\frac{\partial v'}{\partial \lambda} + f\bar{u} + fu' + \frac{2\bar{u}u'}{a}\tan\phi + \frac{u^{-2}}{a}\tan\phi + \frac{g}{a}\frac{\partial H}{\partial \phi} + \frac{g}{a}\frac{\partial h'}{\partial \phi} = 0 \qquad [30]$$

$$\frac{\partial h'}{\partial t} + \frac{\bar{u}}{a\cos\phi}\frac{\partial h'}{\partial \lambda} + \frac{v'}{a}\frac{\partial H}{\partial \phi} + \frac{1}{a\cos\phi}\left[\frac{\partial u'}{\partial \lambda} + \frac{\partial}{\partial \phi}(v'\cos\phi)\right]$$

$$+ \frac{H}{a\cos\phi}\left[\frac{\partial u'}{\partial \lambda} + \frac{\partial}{\partial \phi}(v'\cos\phi)\right] = 0 \qquad [31]$$

where products of perturbation terms have been neglected as small compared to the other terms:

Assuming that the mean zonal flow is in gradient balance:

$$f\bar{u} + \frac{\bar{u}^2}{a}\tan\phi + \frac{g}{a}\frac{\partial H}{\partial \phi} = 0 \qquad [32]$$

allows Eq. 30 to be rewritten as:

$$\frac{\partial v'}{\partial t} + \frac{\bar{u}}{a\cos\phi}\frac{\partial v'}{\partial \lambda} + fu' + \frac{2\bar{u}u'}{a}\tan\phi + \frac{g}{a}\frac{\partial h'}{\partial \phi} = 0 \qquad [33]$$

Defining nondimensional variables,

$$\tilde{u} = \frac{u}{\sqrt{gh_e}}, \quad \tilde{v} = \frac{v}{\sqrt{gh_e}}, \quad \tilde{h} = \frac{h}{h_e}, \quad \tilde{t} = 2\Omega t \qquad [34]$$

Equations 29, 31 and 33 become:

$$2\Omega\sqrt{gh_e}\frac{\partial \tilde{u}'}{\partial \tilde{t}} + \frac{gh_e}{a\cos\phi}\overline{\tilde{u}(\phi)}\frac{\partial \tilde{u}'}{\partial \lambda} + \frac{gh_e}{a}\tilde{v}'\frac{\overline{\partial \tilde{u}}}{\partial \phi} - \sqrt{gh_e}f\tilde{v}'$$

$$- \frac{gh_e}{a}\bar{\tilde{u}}\tilde{v}'\tan\phi + \frac{gh_e}{a\cos\phi}\frac{\partial \tilde{h}'}{\partial \lambda} = 0 \qquad [35]$$

$$2\Omega\sqrt{gh_e}\frac{\partial \tilde{v}'}{\partial \tilde{t}} + \frac{gh_e}{a\cos\phi}\bar{\tilde{u}}\frac{\partial \tilde{v}'}{\partial \lambda} + \sqrt{gh_e}f\tilde{u}'$$

$$+ \frac{2gh_e}{a}\bar{\tilde{u}}\tilde{u}'\tan\phi + \frac{gh_e}{a}\frac{\partial \tilde{h}'}{\partial \phi} = 0 \qquad [36]$$

$$2\Omega\, h_e \frac{\partial \tilde{h}'}{\partial \tilde{t}} + \frac{h_e\sqrt{gh_e}}{a\cos\phi}\,\bar{\tilde{u}}\,\frac{\partial \tilde{h}'}{\partial \lambda} + \frac{h_e\sqrt{gh_e}}{a}\,\tilde{v}'\,\frac{\partial \tilde{H}}{\partial \phi}$$

$$+ \frac{h_e\sqrt{gh_e}}{a\cos\phi}\,\frac{\partial \tilde{u}'}{\partial \lambda} + \frac{\sqrt{gh_e}}{a\cos\phi}\,\frac{\partial}{\partial \phi}\,(\tilde{v}'\cos\phi) \qquad [37]$$

$$+ \frac{h_e\tilde{H}\sqrt{gh_e}}{a\cos\phi}\,\frac{\partial \tilde{u}'}{\partial \lambda} + \frac{h_e\tilde{H}\sqrt{gh_e}}{a\cos\phi}\,\frac{\partial}{\partial \phi}(\tilde{v}'\cos\phi) = 0$$

All equations following this will be dimensionless, so dropping the tildes and assuming that for each equation a forcing acts, and letting

$$\gamma = \sqrt{gh_e}/2\Omega a \quad \text{and} \quad f = 2\Omega\sin\phi \qquad [38]$$

35, 36 and 37 become:

$$\frac{\partial u'}{\partial t} + \frac{\gamma}{\cos\phi}\,\bar{u}\,\frac{\partial u'}{\partial \lambda} + \gamma v'\,\frac{\partial \bar{u}}{\partial \phi} - v'\sin\phi - \gamma\bar{u}v'\tan\phi$$

$$+ \frac{\gamma}{\cos\phi}\,\frac{\partial h'}{\partial \lambda} = F_u \qquad [39]$$

$$\frac{\partial v'}{\partial t} + \frac{\gamma}{\cos\phi}\,\bar{u}\,\frac{\partial v'}{\partial \lambda} + u'\sin\phi + \gamma 2\bar{u}u'\tan\phi + \gamma\,\frac{\partial h'}{\partial \phi} = F_v \qquad [40]$$

$$\frac{\partial h'}{\partial t} + \frac{\gamma}{\cos\phi}\,\bar{u}\,\frac{\partial h'}{\partial \lambda} + \gamma v'\,\frac{\partial H}{\partial \phi} + \frac{\gamma}{\cos\phi}\left[\frac{\partial u'}{\partial \lambda} + \frac{\partial (v'\cos\phi)}{\partial \phi}\right]$$

$$+ \frac{\gamma H}{\cos\phi}\left[\frac{\partial u'}{\partial \lambda} + \frac{\partial}{\partial \phi}\,(v'\cos\phi)\right] = F_z \qquad [41]$$

Rearranging 39, 40 and 41 such that the advective terms are on the right hand sides:

$$\frac{\partial u'}{\partial t} - v'\sin\phi + \frac{\gamma}{\cos\phi}\frac{\partial h'}{\partial \lambda} = \frac{-\gamma}{\cos\phi}\left[\bar{u}\frac{\partial u'}{\partial \lambda} + v'\frac{\partial \bar{u}\cos\phi}{\partial \phi}\right] + F_u \qquad [42]$$

$$\frac{\partial v'}{\partial t} + u'\sin\phi + \gamma\frac{\partial h'}{\partial \phi} = \frac{-\gamma}{\cos\phi}\left[\bar{u}\frac{\partial v'}{\partial \lambda} + 2\bar{u}u'\sin\phi\right] + F_v \qquad [43]$$

$$\frac{\partial h'}{\partial t} + \frac{\gamma}{\cos\phi}\left[\frac{\partial u'}{\partial \lambda} + \frac{\partial (v'\cos\phi)}{\partial \phi}\right] = \frac{-\gamma}{\cos\phi}\left[\bar{u}\frac{\partial h'}{\partial \lambda} + v'\frac{\partial (H\cos\phi)}{\partial \phi}\right] + H\left(\frac{\partial u'}{\partial \lambda} + H\cos\Theta\frac{\partial v'}{\partial \phi}\right] + F_z \qquad [44]$$

Equations 42, 43 and 44 may be represented in vector form by:

$$\frac{\partial W}{\partial t} + L\,W + F = 0 \qquad [45]$$

where F contains the nonlinear and forcing terms and,

$$W = \begin{bmatrix} u'(\lambda,\phi,t) \\ v'(\lambda,\phi,t) \\ h'(\lambda,\phi,t) \end{bmatrix} \qquad [46]$$

$$L = \begin{bmatrix} 0 & -\sin\phi & \frac{\gamma}{\cos\phi}\frac{\partial}{\partial \lambda} \\ \sin\phi & 0 & \gamma\frac{\partial}{\partial \phi} \\ \frac{\gamma}{\cos\phi}\frac{\partial}{\partial \lambda} & \frac{\gamma}{\cos\phi}\frac{\partial}{\partial \phi}([]\cos\phi) & 0 \end{bmatrix} \qquad [47]$$

$$F = \frac{\gamma}{\cos\phi} \begin{bmatrix} \bar{u}\frac{\partial u'}{\partial \lambda} + v'\frac{\partial \bar{u}\cos\phi}{\partial \phi} - F_u \\ \bar{u}\frac{\partial v'}{\partial \lambda} + 2\bar{u}u'\sin\phi - F_v \\ \bar{u}\frac{\partial h'}{\partial \lambda} + v'\frac{\partial (H\cos\phi)}{\partial \phi} + H\frac{\partial v'}{\partial \lambda} \\ \quad + H\cos\phi\frac{\partial v'}{\partial \phi} - F_z \end{bmatrix} \quad [48]$$

Neglecting the term F in Eq. 45 yields

$$\frac{\partial W}{\partial t} + L W = 0 \quad [49]$$

which is Laplace's tidal equation. The solutions to this have been discussed by Longuet-Higgins (1968) and more recently by Kasahara (1976) and Silva Dias and Schubert (1978). For a specified equivalent depth, the solution to Eq. 49 may be written as:

$$W(\lambda,\phi,t) = H_{m,n}(\lambda,\phi)\, e^{i\sigma_{m,n}t} \quad [50]$$

where $H_{m,n}$ represents the horizontal structure of normal modes with (m) the wavenumber in the zonal direction and (n) the meridional index. $\sigma_{m,n}$ is the dimensionless frequency of the normal modes. The longitudinal dependence of $H_{m,n}$ is given by:

$$H_{m,n}(\lambda,\phi) = \Theta_{m,n}(\phi)\, e^{im\lambda} \quad [51]$$

where $\Theta_{m,n}$ is the Hough vector

$$\Theta_{m,n} = \begin{bmatrix} U_{m,n}(\phi) \\ -iV_{m,n}(\phi) \\ h_{m,n}(\phi) \end{bmatrix} \quad [52]$$

The completeness of the eigenfunctions $\Theta_{m,n}(\phi)$ in the interval (-1, +1) and the completeness of $e^{im\lambda}$ in the interval (0. 2π) allows for the expansion of any arbitrary function $A(\lambda,\theta,t)$ with the series

$$A(\lambda,\phi,t) = \sum_{m=0}^{\infty} \sum_{n=0}^{\infty} a_{m,n}(t)\, \Theta_{m,n}(\phi) e^{im\lambda} \qquad [53]$$

with

$$a_{m,n} = \langle A_m(\phi) , \Theta_{m,n}(\phi) \rangle \qquad [54]$$

where

$$A_m(\phi) = \frac{1}{2\pi} \int_0^{2\pi} A(\lambda,\phi)\, e^{im\lambda} d\lambda \qquad [55]$$

and

$$\langle A_m(\phi) , \Theta_{m,n}(\phi) \rangle = \int_{-1}^{1} A_m(\phi)\, \Theta^*_{m,n} d\phi \qquad [56]$$

Accordingly W and F in Eq. 45 may be rewritten (approximately) as:

$$W(\lambda,\phi,t) \quad \sum_{m=0}^{M} \sum_{n=0}^{N} \omega_{m,n}(t)\, \Theta(\phi)\, e^{im\lambda} \qquad [57]$$

and

$$F(\lambda,\phi,t) \simeq \sum_{m=0}^{M} \sum_{n=0}^{N} f_{m,n}(t)\, \Theta(\phi)\, e^{im\lambda} \qquad [58]$$

Substituting Eqs. 57 and 58 into Eq. 45 and multiplying the result by $\Theta^*_{m,n}(\phi)$ and integrating over the whole domain (from $\sin\theta = -1$ to $+1$ and $\lambda = 0$ to 2π) yields:

$$\frac{d}{dt} \omega_{m,n}(t) + i\sigma_{m,n}\, \omega_{m,n}(t) = f_{m,n}(t) \qquad [59]$$

For any given (m) and (n) a one dimensional equation of the form:

$$\frac{d}{dt} \omega(t) + i\sigma\, \omega(t) = f(t) \qquad [60]$$

may be written. Multiplying both sides of Eq. 60 by $e^{i\sigma t}$,

$$\frac{d}{dt}\left(e^{i\sigma t}\omega(t)\right) = f(t)e^{i\sigma t} \qquad [61]$$

Integrating both sides of Eq. 61 for some time interval ($2\Delta t$) about (t) yields:

$$e^{i\sigma(t+\Delta t)}\,\omega(t+\Delta t) - e^{i\sigma(t-\Delta t)}\,\omega(t-\Delta t) = \int_{t-\Delta t}^{t+\Delta t} f(t')\, e^{i\sigma t'} dt' \qquad [62]$$

if $f(t)$ is considered to be slowly varying with respect to Δt, then the right hand side of Eq. 61 may be rewritten as:

$$= f(t) \int_{t-\Delta t}^{t+\Delta t} e^{i\sigma t'} dt' \qquad [63]$$

and with some manipulation the following expression may be obtained:

$$\omega(t+\Delta t) = \left[\, 1-e^{-2i\sigma t_{\Delta t}} \,\right] \frac{f(t)}{i\sigma} + \omega(t-\Delta t)\, e^{-2i\sigma\Delta t} \qquad [64]$$

Through the use of Eq. 63 and a prescribed forcing, the vector $\omega_{m,n}$ may be evaluated at $(t + \Delta t)$ given that it was known at $(t - \Delta t)$.

This scheme for integrating the shallow water equations was first described by Daley (1980) as being suitable for treating the fast gravity waves. In the series of simulations which follow, this scheme has been used for all waves. A feature of this scheme is an unrealistic dampening of the very fastest gravity waves. Application of a leapfrog scheme to Eq. 60 yields the expression:

$$\omega(t + \Delta t) = 2f(t)\Delta t e^{-i\sigma\Delta t} + e^{-2i\sigma\Delta t}\omega(t + \Delta t) \qquad [65]$$

The ratio of difference in the forcing term between Eq. 64 and Eq. 65

is:

$$\left(\frac{\sin\sigma\Delta t}{\sigma\Delta t} - 1 \right) \qquad [66]$$

For $\sigma\Delta t = 0.8$, the spurious damping due to this term is approximately 10%. In the simulations which follow $\sigma\Delta t = 1.67$ for the fastest gravity wave, with a resultant damping of 40% occurring fo this wave.

The energy projected onto the fast gravity modes in these simulations is small and the change between simulations of time steps of 20, 30 and 40 minutes are extremely small. That this should be the case can be seen from an inspection of Eq. 47, the physical space representation of f(t). The forcing terms $F_{u,\ v,\ z}$ all contain an e-folding time of many days and from the work of Schubert et al. (1980) the excitation of gravity waves by these forcing terms will be small. The remaining terms of Eq. 47 represent an advection of the perturbation by the basic state flow. The basic state is in gradient balance and unchanging, its energy is projected onto the Rossby modes alone. The perturbation terms contain energy in all wave modes, however the gravity modes have approximately two orders of magnitude less energy than the Rossby modes. Hence, the forcing terms may be visualized as large amplitude, long period Rossby waves with extremely small amplitude gravity wave perturbations superimposed. The spurious damping of these very high frequency gravity modes (in which we are not particularly interested) does not apparently change the simulation results for a doubling of the time step.

The advantage of Eq. 64 is that it allows for time steps greater than $\sigma\ \Delta t \leq 1$ without the computational instability occurring which would arise using the leapfrog scheme. The disadvantage is the spurious

damping of the extremely small amplitude highest frequency gravity waves.

Time splitting for such a scheme may be expected to occur (Lilly, 1965), however for less than 200 time steps, the difference in domain kinetic energy for odd and even time steps can be expected to be less than 10% (Lilly, 1964, pg. 22).

The procedure by which the shallow water equations were solved for a time dependent forcing was as follows:

i) The model was initialized with a prescribed zonal wind profile in gradient balance.

ii) The amplitude in physical space (x,y space) of the advective and forcing terms is evaluated at time (t)

iii) The spectral representations of the forcings (F) and the W vector were determined through the application of expressions like Eq. 54.

iv) The spectral form of $\omega_{m,n}$ for the truncated series m=1,...21 n=1,...60, at time (t + Δt) was determined through the use of Eq. 64.

v) The $\omega_{m,n}$ vector was transformed back in physical space through the use of Eq. 57. Step (ii) through (v) were then repeated for as many time steps as was needed.

Time steps of 20 min, 40 min and 60 min were used with no apparent change in solutions. A conservative time step of 40 minutes was used in all simulations and the model was integrated forward for ten days.

7.4 Vertical Structure

In order to proceed with the solution of the set of horizontal structure equations, an equivalent depth (h_e) must be specified. To obtain an insight into the role of equivalent depth in the model, and thus select an appropriate value for it, it is necessary to inspect solutions of the vertical structure equation.

Kasahara (1976) describes the separation of the perturbation equations, on a sphere, into the horizontal and vertical dependent parts and uses an isothermal atmosphere to demonstrate the role of the vertical structure. Fulton (1980) presents a solution of the vertical structure equation for a constant static stability atmosphere which closely resembles Jordan's (1958) mean summertime temperature sounding for the West Indies area. Fulton's treatment differs from Kasahara in that he uses the beta plane approximation and the different thermodynamic profile. The choice of geometry is irrelevant to the solution of the vertical structure equation, the thermodynamic profile crucial. As this investigation is particularly concerned with adjustment processes in the tropics, the work of Fulton is of great relevance.

Fulton (1980) defines the vertical coordinate by:

$$z^* = \ln\left(\frac{P_o}{P}\right) \qquad [67]$$

the static stability parameter by:

$$\Gamma(z^*) = \frac{d\bar{T}(z^*)}{dz^*} + \frac{R}{c_p}\bar{T}(z^*) \qquad [68]$$

and shows that the vertical structure equation may be written as:

$$\frac{d}{dz^*}\left[\frac{e^{-z^*}}{R\Gamma}\frac{dz}{dz^*}\right] + \frac{e^{-z^*}}{c^2}z = 0 \qquad [69]$$

where

$$W^* = \frac{dz^*}{dt} \quad \text{and} \quad W = \frac{dz}{dt} \qquad [70]$$

With appropriate boundary conditions, Eq. 69 forms an eigenvalue problem with eigenvalue c^{-2} and eigenfunction $Z(z^*)$. $Z(z^*)$ is referred to as

the vertical structure function. Taking as an upper boundary condition $W^* = 0$ at $Z^* = Z^*_T$ and a lower boundary condition $W = 0$ at $Z^* = 0$ yields a countably infinite phase speed spectrum, (where c is the phase speed). Finally, recognizing that $c^2 = gh_e$, allows the computation of the equivalent depth for each phase speed c_n $n = 0,1,2,....$.

Figure 128 (from Fulton, 1980) shows the vertical structure functions for the constant static stability atmosphere for $n = 0,1....4$. Table 13 (also from Fulton, 1980) shows the phase speeds the first 10 modes. The $n = 0$ mode is commonly referred to as the barotropic divergent mode (or external mode) as there is no level of nondivergence between $Z^* = 0$ and $Z^* = Z^*_T$. Mode 1 has a single level of nondivergence around 400 mb and each higher mode of order n has n levels of nondivergence.

Bradley and Wiin-Nielsen (1968) extensively observed the vertical structure of the transient large scale motions in the midlatitude troposphere. They found modes 0, 1 and 2 explained 70-90%, 10-20% and 1-10% of the variance respectively. It may be concluded from these data that in midlatitude forcing of the atmosphere a considerable amount of energy is projected onto both external and first internal modes. In cold surge forcing the observed large thickness changes in the midlatitudes and subtropics suggest a large partitioning of energy to the first internal mode. However, the near simultaneity of midlatitude and equatorial pressure rises (for stations on the same longitude), reported in Chapter 4 of this paper, implies that extremely rapid energy propagation over large distances is occurring. Such observations would be consistent with an appreciable partitioning of energy to the external mode. Furthermore, the observation of an extremely deep layer of

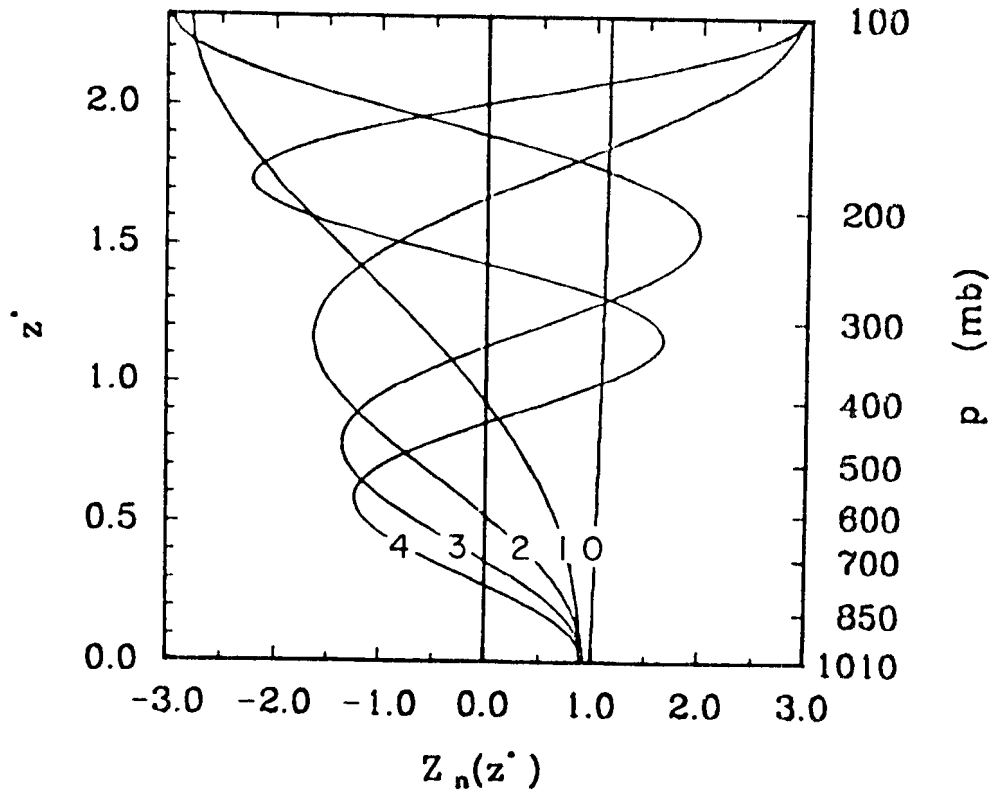

Fig. 128. The vertical structure functions for the constant static stability atmosphere for n = 0, 1....4. (After Fulton, 1980).

TABLE 13

Exact and approximate values of the phase speeds of the constant static stability atmosphere. (From Fulton, 1980).

n	c_n (ms^{-1})	
	exact	approximate
0	287.00	279.70
1	56.28	60.84
2	29.79	30.42
3	20.09	20.28
4	15.13	15.21
5	12.13	12.17
6	10.12	10.14
7	8.68	8.69
8	7.59	7.60
9	6.75	6.76
10	6.08	6.08

meridional wind anomaly (surface to 200 mb) in the winter hemisphere in Figs. 101 and 117, suggests a forcing which is at least partly barotropic in nature. Accordingly one set of experiments describing the response of the system with an equivalent depth of 10 km (C_o = 313 m/s) will serve to illustrate the role of the external mode in large scale adjustment processes. As it is desired to understand some of the physics of the adjustment of the large scale flow fields to midlatitude surge type forcing, where there is little convection, the absence of a convective parameterization was not felt to be too unrealistic.

It must be stressed that this modelling is extremely qualitative in nature, much of the physics of the atmospheric surges being neglected. It is hoped that a model with modes 0, 1 and 2 (at least) interacting, forced by a baroclinicity unstable midlatitude wave, could be used to more realistically simulate this cold surge phenomena.

8. MODELING RESULTS

8.1 Introduction

The model described in the previous section has been used to investigate the adjustment processes which occur when a forcing is applied on the planetary scale. The results of a number of simulations are described in this chapter.

The case study data described in Chapter 3 clearly showed the existence of strong anticyclogenesis events in the midlatitudes which were accompanied by a wind surge in the subtropical regions. In this chapter, winter hemisphere cold surges are crudely simulated and the resulting adjustment processes studied. Particular emphasis has been placed on evaluating the role of the background wind field, shape, and latitudinal positioning of the forcing and time scale of the forcing in producing an adjusted state in the model.

The work of Silva Dias and Schubert (1978), Schubert et al. (1979) and Fulton and Schubert (1980) is reviewed to provide a conceptual framework within which these experimental results may be better understood.

8.2 Geostrophic Adjustment - A Brief Review

Two important concepts in the understanding of adjustment processes are:

i) The speed of propagation of energy, or group velocity of various wave models.

ii) The partitioning of energy between the gravity and Rossby modes for a given disturbance.

Silva Dias and Schubert (1978), following the work of Hoskins (1977) describe the group velocity of free waves on a sphere with imposed zonal periodicity. Table 14 gives the time of reinforcement (in days) for two waves of specified meridional wavenumber (ℓ) and of zonal

wavenumbers S_1 and S_2 in specified ranges (either $1 \leq S \leq 3$ or $5 \leq S \leq 7$). It gives the apparent group velocity of energy dispersion by waves of these characteristics (c) given in degrees longitude per day. The h_e = 8.8 km corresponds to the external mode used in the experiments described.

For the external mode, from Table 14, it can be seen that the time between wave reinforcement for Rossby waves is very long and the apparent group velocity small. For the shorter waves $\ell \sim 8$ the group velocity is about 1^o longitude/day and the time between reinforcement about 20 days. These waves appear stationary. For the gravity waves, however, the apparent group velocity is of the order of 200^o longitude/day which closely approximates the phase velocity of the waves. Accordingly they appear nondispersive.

So in summary, the Rossby waves appear stationary for both external and first internal modes, particularly the shorter waves around $1 \sim 6$. Gravity waves for the external mode have a group velocity close to their phase velocity, energy projected onto these waves will be seen to disperse rapidly.

The partitioning of energy between available potential and kinetic forms, for the various wave modes on a sphere, has been discussed by Longuet-Higgins (1968), Kasahara (1976) and Silva Dias and Schubert (1978). Silva Dias and Schubert investigated the adjustment processes when either the wind or mass fields are forced at the initial instant and then allowed to adjust with time towards a geostrophically balanced state. It is found that the Rossby radius of deformation (R.r.d.) plays a fundamental role in determining the response of the system. Considering first a perturbation in the geopotential field, it is noted

TABLE 14

Time interval between reinforcement points (days) and implied group velocity (degrees per day) for the Mixed Rossby Gravity Wave (MRGW) and various Rossby Waves (RW) and East and West Gravity Waves (EGW) and (WGW) on the sphere. Equivalent depth equals 8.8 km. (After Silva Dias and Schubert, 1979).

		$1 \leq S \leq 3$	$5 \leq S \leq 7$
MRGW ($\ell = 0$)	$\Delta t_{1,2}$ (days)	1.0	1.9
	$C_{1,2}$ (^{o}/day)	62	14
RW ($\ell = 1$)	$\Delta t_{1,2}$ (days)	6.6	3.1
	$C_{1,2}$ (^{o}/day)	-13	7
RW ($\ell = 2$)	$\Delta t_{1,2}$ (days)	11.8	4.6
	$C_{1,2}$ (^{o}/day)	-11	3
RW ($\ell = 8$)	$\Delta t_{1,2}$ (days)	104.1	22.6
	$C_{1,2}$ (^{o}/day)	-4	-1
WGW ($\ell = 0$)	$\Delta t_{1,2}$ (days)	0.7	1.5
	$C_{1,2}$ (^{o}/day)	-140	-215
WGW ($\ell = 7$)	$\Delta t_{1,2}$ (days)	0.2	0.2
	$C_{1,2}$ (^{o}/day)	-220	-222
EGW ($\ell = 1$)	$\Delta t_{1,2}$ (days)	0.9	1.1
	$C_{1,2}$ (^{o}/day)	204	224
EGW ($\ell = 9$)	$\Delta t_{1,2}$ (days)	0.2	0.2
	$C_{1,2}$ (^{o}/day)	219	222

S gives a range of zonal wavenumber

ℓ gives a meridional wavenumber

that for an e-folding radius larger than the R.r.d. a more significant percentage of energy goes into the Rossby waves. With energy in the long Rossby modes the system is slowly dispersed westwards and the wind field tends to adjust to the mass field. If, however, the initial disturbance were small compared with the R.r.d. then most of the energy is partitioned to gravity waves and little to the slowly

dispersive Rossby waves. Furthermore, Rossby modes of shorter wave length have more energy in the wind field (see Kasahara, 1976, page 683, Fig. 13) and thus the initial mass field perturbation is very much reduced. The mass field can be said to have adjusted to the wind field.

For those experiments where the wind field was initially perturbed by the presence of a vortex, adjustment proceeded in the opposite fashion. For a small vortex (compared with the R.r.d.) the bulk of the energy is in the Rossby modes and, since these are slowly dispersive and contain more information in the wind field we can say the wind field perturbation remains, becoming balanced by changes in the mass field. The mass field has adjusted to the wind field. The state of quasi-balance is said to be reached when the gravity waves leave the vicinity of the perturbation. For a large scale vortex more energy is contained in the gravitational modes which disperse leaving little energy in the Rossby waves. The wind field thus adjusts to the mass field tending towards a state of no perturbation.

Finally, it should be noted that the time for adjustment T_a can be defined as (Silva Dias and Schubert, 1978)

$$T_a = r_e/C_g$$

where C_g is the characteristic group velocity of the gravity waves, and r_e is the e-folding radius of the amplitude of the disturbance.

8.3 Sensitivity Experiments

An equivalent depth 10 km has been specified. As mentioned earlier, studies by Bradley and Wiin-Nielsen (1968) reveal 70-90% of the variance in the observed vertical structure of the transient large scale motions of the atmosphere can be explained by this mode. Silva Dias and

Schubert (1978) provide a discussion of how the external mode may be physically interpreted.

The external mode may be interpreted as a one layer model. The fluid is incompressible and homogeneous with a free surface in hydrostatic balance. A high pressure area may be thought of as a 'bump' on the fluid surface with mass diverging away from the column of fluid below that point, at the same rate at every level.

In those experiments where the wind field is perturbed, a time dependent forcing of the form:

$$\mathbf{F}(x,y,t) = (\alpha^2 - \alpha^3 t)e^{-\alpha t} \begin{bmatrix} (\pm)\exp(-[\frac{(x-x_o)^2}{r_{ex}^2} + \frac{(y-y_o)^2}{r_{ey}^2}]) \\ (\pm)\exp(-[\frac{(x-x_o)^2}{r_{ex}^2} + \frac{(y-y_o)^2}{r_{ey}^2}]) \\ 0 \end{bmatrix} \quad [71]$$

For a perturbation in the height field, the form:

$$\mathbf{F}(x,y,t) = (\alpha^2 - \alpha^3 t)e^{-\alpha t} \begin{bmatrix} 0 \\ 0 \\ (\pm)\exp(-[\frac{(x-x_o)^2}{r_{ex}^2} + \frac{(y-y_o)^2}{r_{ey}^2}]) \end{bmatrix} \quad [72]$$

These expressions (Eqs. 71 and 72) allow the positioning of a vortex (in the case of Eq. 71) or a geopotential perturbation (in the case of Eq. 72) at any specified location (x_o, y_o) with e-folding

distances in the x and y directions of r_{ex} and r_{ey} respectively. By judicious choice of sign a cyclonic, anticyclonic, high or low disturbance may be placed in either hemisphere. The time dependence allows, through choice of α, a variable length of time where the amplitude of the disturbance exceeds 1/e times its maximum amplitude. The form of the time dependence gives the result that integrating the forcing for an infinite time will yield the same energy input into the system regardless of the choice of α.

That is

$$\int_0^\infty \alpha^2 t e^{-\alpha t} dt = 1 \qquad [73]$$

In all the experiments performed, for every cyclonic vortex or low there is an anticyclonic vortex or high of identical geometry. In this way, for all simulations, no mass was generated or dissipated within the model domain. However, the presence of a forcing in a non dissipative system led to an increase in total energy in every simulation. There are 64 grid points in the zonal direction. For a wavenumber 6 forcing (6 high and 6 lows) each disturbance is spread over a width of 5 grid points except the last two disturbances (one high one low) which occupy 7 grid points each. Because of this feature when 2 times the wavenumber does not evenly divide into 64, irregularities appear.

The philosophy guiding each experiment has been to assess the impact on the southern hemisphere of an unbalancing of the wind and pressure fields in the northern hemisphere. As the model contains no topography the basic adjustment processes for the forcing of the southern hemisphere by the northern hemisphere are the same for the

southern hemisphere forcing the north, the simulations have only been made for this case of north to south forcing.

In order to assess the sensitivity of the adjustment process to the background wind field three simulations using a wavenumber one forcing were made. Table 15 gives a summary of the differences and similarities for each experiment. The wind profiles labeled Active and Quiet are shown in Fig. 129, these are the only differences between the experiments. These wind profiles have been derived from a blend of composite data in the tropical areas and Crutcher's (1961) and Von Loon's (1971) mean monthly wind data.

An interesting feature of the active and quiet wind profiles is the absence of easterly winds in the northern hemisphere tropics for the active profile. This is slightly unusual but does occur for brief period, usually during times of strong equatorward surges from the winter hemisphere. In the previous chapter the work of Charney (1969) was discussed which indicated that the meridional propagation of energy should show a great sensitivity (and damping) to easterly wind regimes in the tropics. Such has not been the case in these experiments.

It is to be expected that the differences between the experiments will be a result of the same perturbation being imposed on a different background wind field. The important parameter in determining how the energy of the perturbation is partitioned between Rossby and gravity waves is the R.r.d. For this series of experiments the R.r.d. may be defined (following Schubert et al., 1980).

$$\text{R.r.d.} = \frac{c}{[f(f-\partial\bar{u}/\partial y)]^{1/2}} \qquad [74]$$

TABLE 15

Values of some important parameters in experiments A, B and C.

Experiment	A	B	C
u (ϕ)	0	Quiet	Active
e-folding time (day)	5	5	5
Wave number	1	1	1
R_{ex} (^{o} longitude)	33.25	33.25	33.25
R_{ey} (^{o} latitude)	11.75	11.75	11.75
Latitude of Y_o	36	36	36
Type of focing (WF - wind field) (PF - pressure field)	PF	PF	PF
h_e	10 km	10 km	10 km

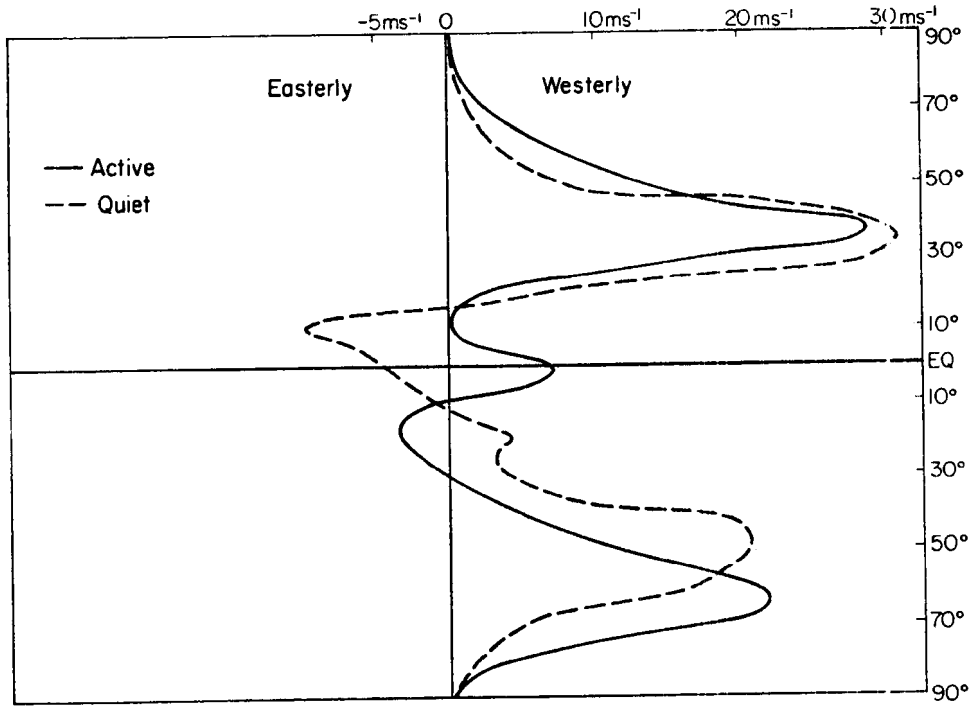

Fig. 129. Quiet and active period zonal wind profiles, north pole to south pole (m/s).

However, within a distance of one Rrd from the equator Eq. 74 should be replaced by the beta plane approximation, $\text{Rrd} = (\frac{c}{\beta})^{1/2}$. Since the basic state vorticity shear is of the order of beta, the shear has been incorporated by the approximation

$$\text{Rrd} = \left[\frac{c}{\beta - d^2\bar{u}/dy^2}\right]^{1/2} \qquad [75]$$

Table 16 shows the variation of R.r.d. with latitude in the northern hemisphere midlatitudes and subtropics for experiments A, B and C.

The results equatorward of 35° have been computed using Eq. 72, the remainder using Eq. 71.

Unfortunately in the application of both Eq. 71 and Eq. 72 to real atmospheric data problems arise. Obviously, neither is defined when the denominator equals zero and in Eq. 72 when the anticyclonic shear of the basic state exceeds β the Rrd becomes imaginary. This does occur for some points within the QUIET period profile leaving the author in a quandry as to how geostrophic adjustment should proceed. It is noteworthy that a necessary condition for barotropic instability is

$$\beta - \frac{d^2\bar{u}}{dy^2} = 0 \qquad \text{(Holton, 1979).}$$

It must then be concluded that barotropic instability may arise in the quiet basic state simulations. No such instability has been observed in the simulations, most probably because the e-folding times of even the shortest waves (around 1600 km at latitude 15°N) are too long for changes to be observed in five day integrations. The theoretical work

TABLE 16

The variation of Rossby radius of deformation with latitude for the basic states used in 'external mode' experiments.

Latitude	Rossby radius of deformation (km). h_e = 10 km		
	Resting Basic State	Active Shear	Quiet Shear
45°N	2981	3135	3262
35°N	3675	3675	3675
25°N	3884	10,480	3160
15°N	3762	4364	imaginary
5°N	3705	4749	3269
EQ	3697	2913	3573

of Nitta and Yanai (1968) indicates from the use of Marshall Islands 1000 mb data for 1958, the shortest e-folding time for barotropically unstable waves is 10 days.

Inspection of Table 16 reveals no systematic differences in Rrd with latitude between the three experiments. However, both non resting basic state simulations show a latitude equatorward of the disturbance where the Rrd becomes large or imaginary, as the longitudinal shear of the anticyclonic shear vorticity of $\bar{u}$ approaches the value of β. As both non resting basic states show greater energy transmission to the Southern Hemisphere it may be concluded that advection of the perturbations by the basic state plays an important role in these simulations.

Since the intention of these experiments is to assess the role of meridional energy propagation, a good measure of the southern hemisphere response is to be found in the ratio of the amplitude of the major

height perturbation in the southern hemisphere to that in the northern hemisphere. Figure 130 shows this ratio for experiments A, B and C. A ratio of two means that the southern hemisphere height field perturbations is twice that in the northern hemisphere. The Rest simulation shows the smallest southern hemisphere response. There is some support for the Charney (1963) hypothesis that an easterly wind belt will meridional damp energy propagation, as the southern hemisphere response is greater in the Active simulation than in the Quiet.

An examination of the perturbation height and wind fields (with the basic state removed) at 12, 48 and 72 hours for experiment C shows a typical sequence of development. These are presented in Figs. 131 through 136. The initial height field response in the southern hemisphere is in the equatorial regions. With increasing time height anomalies develop in the vicinity of the maximum cyclonic shear vorticity in the southern hemisphere and by 72 hours, Fig. 136 shows that a number of vortices have developed in the wind field. It is noteworthy that the initial wind response in equatorial regions is to develop a belt of westerly winds between high and low pressure regions. Such a result also indicates how planetary scale adjustment proceeds. Given a midlatitude high/low pair there is a need to shift mass from the high to the low to restore the system to its lowest available potential energy state. In the midlatitudes, with a high value of the Coriolis parameter the flow tends to be rotational. Close to the equator zonal flows can be established which perform zonal mass transports in an attempt to wipe out the perturbations.

Having assessed that a background wind field is important to the experiments and given the crudity of the simulation which follow, it is

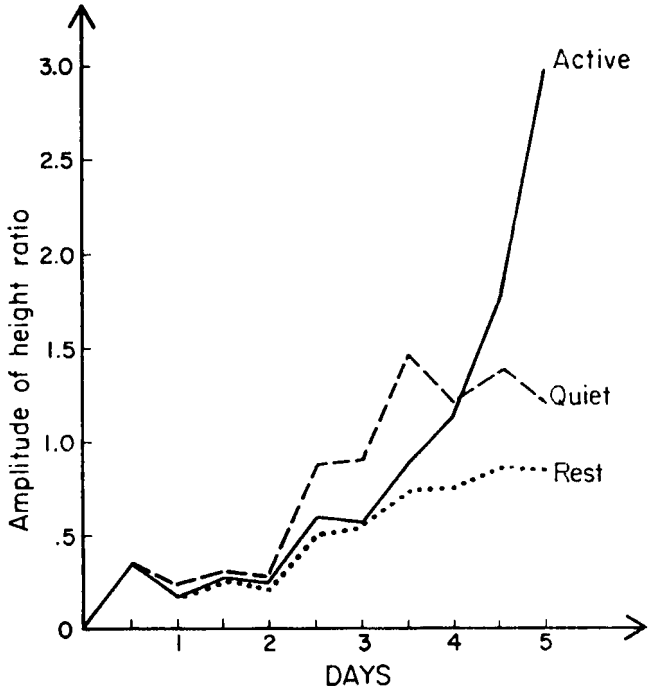

Fig. 130. Ratio of maximum height field perturbations in the southern hemisphere to that in the northern hemisphere for experiments A, B and C for the five days of integration.

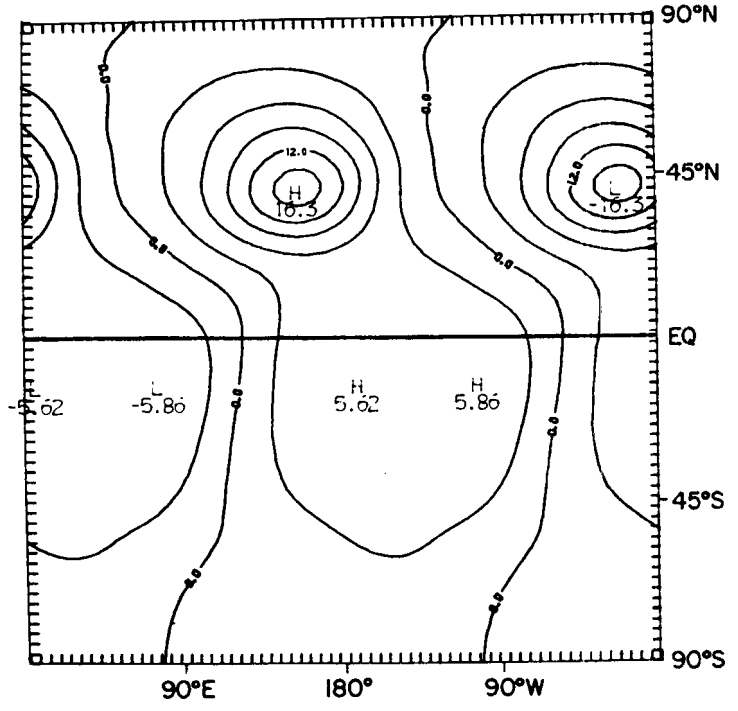

Fig. 131. Perturbation height field for experiment C after 12 hours of model integration.

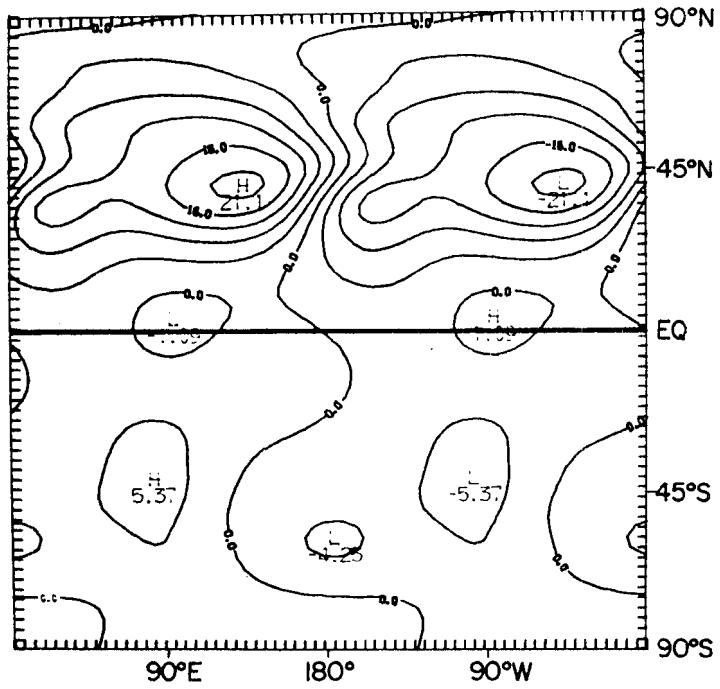

Fig. 132. Perturbation height field for experiment C, after 48 hours of model integration.

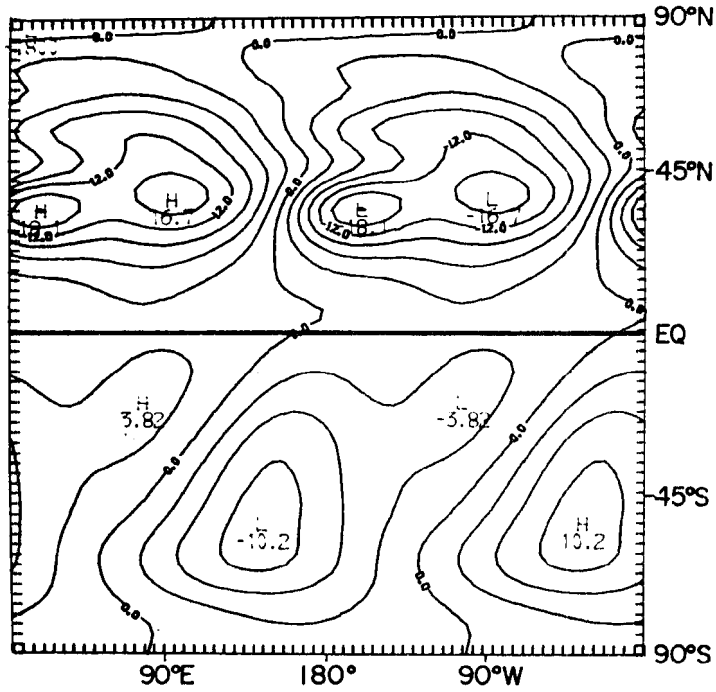

Fig. 133. Perturbation height field for experiment C, after 72 hours of model integration.

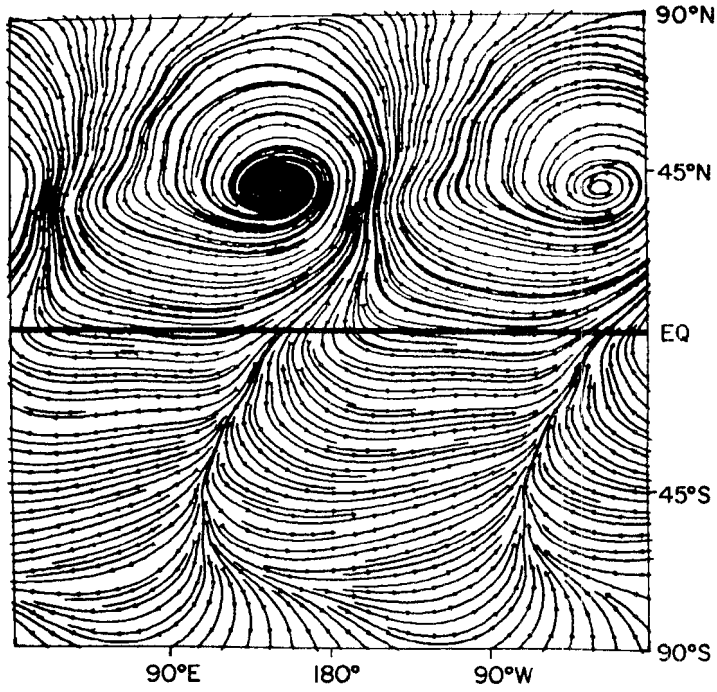

Fig. 134. Perturbation wind field streamline analysis for experiment C, after 12 hours of model integration.

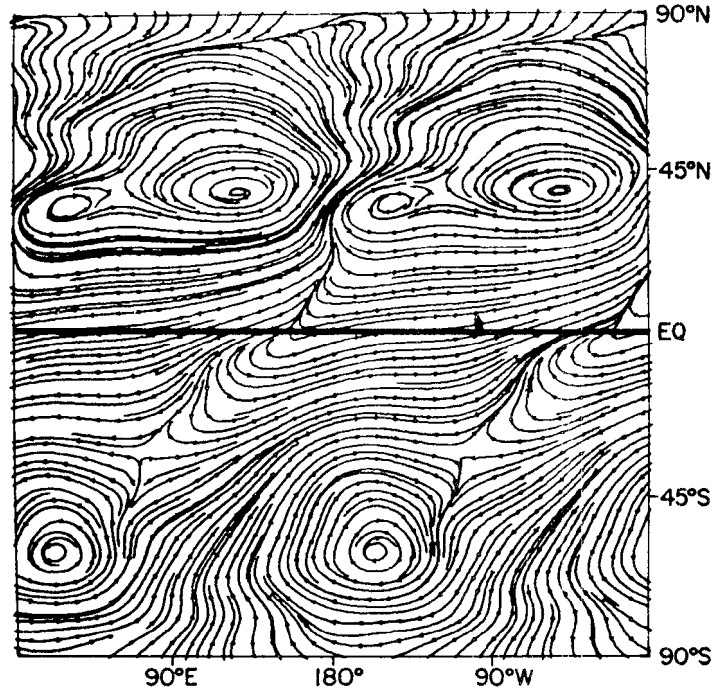

Fig. 135. Perturbation wind field streamline analysis for experiment C, after 48 hours of model integration.

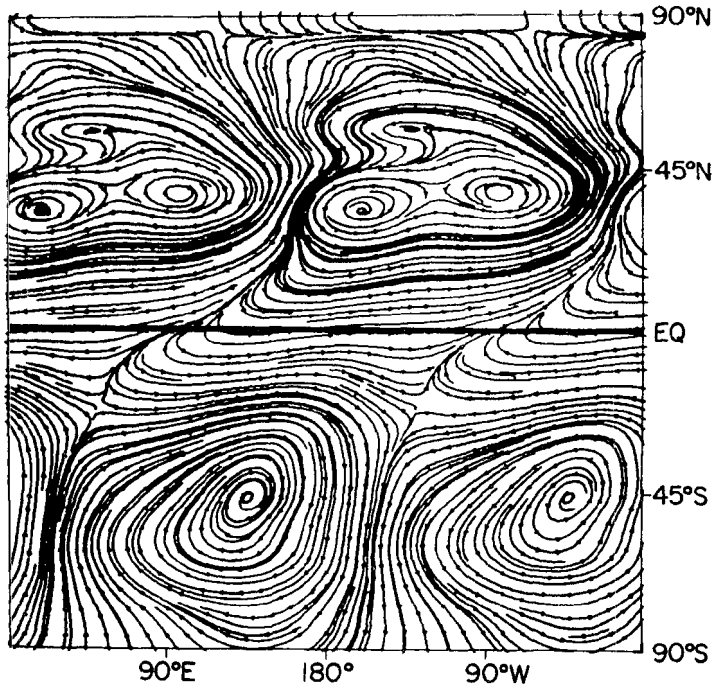

Fig. 136. Perturbation wind field streamline analysis for experiment C, after 72 hours of model integration.

felt that the 500 mb active wind profile should be used in all further simulations.

8.4 Mass vs. Wind Field Forcing, Midlatitudes and Subtropics

As was seen in the case study data of section 3, an intensifying cyclone moving polewards and eastwards in the midlatitudes was accompanied by strong anticyclogenesis commencing around 35^{o} latitude and moving equatorward in the succeeding days. Behind the front trailing into the subtropics was observed a belt of accelerated easterly winds with an equatorward component. The composite meridional wind anomaly cross-sections around 10^{o} to 20^{o} from the equator in the winter hemisphere, show a forcing prior to the active periods which acts from the surface to 200 mb rather than concentrated in a shallow layer. In the equatorial regions the winds prior to cluster genesis show an

increased westerly component in the low layers and increased easterly component aloft.

In order to investigate whether it is the strong mass field forcing (through intense anticyclogenesis) at 35°N or the wind field forcing at 20°N (or neither) a series of experiments were performed with equivalent depths of 10 km and 320 m with the forcing in both wind and mass fields at both 20°N and 35°N. The response of the southern height field perturbation and the evolution of wind and height fields through the experiments have been monitored to ascertain which is the most realistic response. In each experiment wavenumber 6 was used in the forcing, with e-folding distances of 22.5 degrees longitude in the east-west and 8.4 degrees latitude in the north-south. The e-folding time was 5 days with a maximum amplitude after 42 hours. Table 17 summarizes some details of these experiments.

Plotting perturbation kinetic energy within the model domain against time for these series of experiments yields the sets of curves given in Fig. 137. For these cases, applying the forcing in the wind field on a scale which is smaller than the R.r.d. yields a maximum impact. In experiment D the perturbation is smallest with respect to the R.r.d. and the kinetic energy is the greatest. These responses are in accordance with the reasoning of Silva Dias and Schubert (1978) discussed earlier.

Plotting the ratio of southern to northern hemisphere height field perturbation against day through the integration provides an indication of how localized the kinetic energy may be. Figure 138 shows such a plot for experiments D, E, F, G. From Fig. 138, it can be seen that there is a 'burst' of energy into the southern hemisphere in the first

TABLE 17

Values of some important parameters in experiments D, E, F and G.

Experiment	D	E	F	G
$u(\phi)$	Active	Active	Active	Active
e-folding time (day)	5	5	5	5
Wave number	6	6	6	6
R_{ex} (^{o} longitude)	22.5	22.5	22.5	22.5
R_{ey} (^{o} latitude)	8.4	8.4	8.4	8.4
Latitude of Y_o	35	35	20	20
Type of focing (WF - wind field) (PF - pressure field)	WF	PF	WF	PF
h_e	10 km	10 km	10 km	10 km

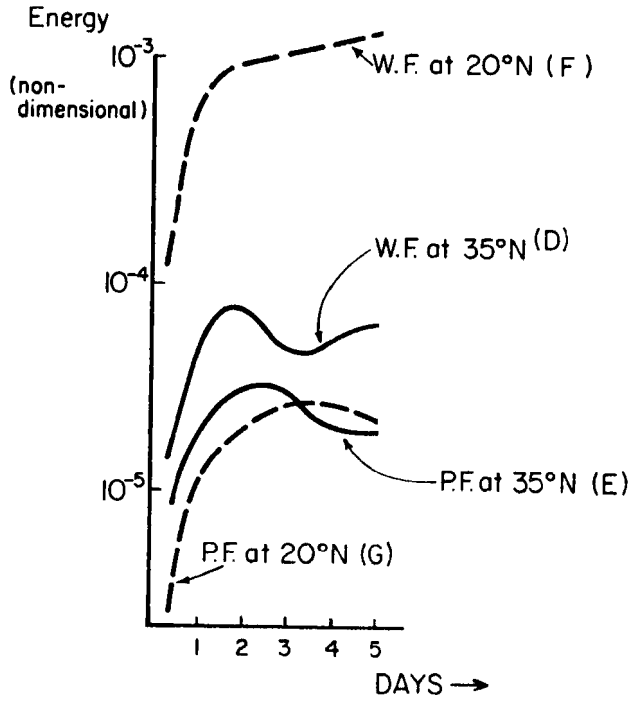

Fig. 137. Perturbation kinetic energy (non dimensional units) in the model domain through the five day integration for experiments D, E, F and G.

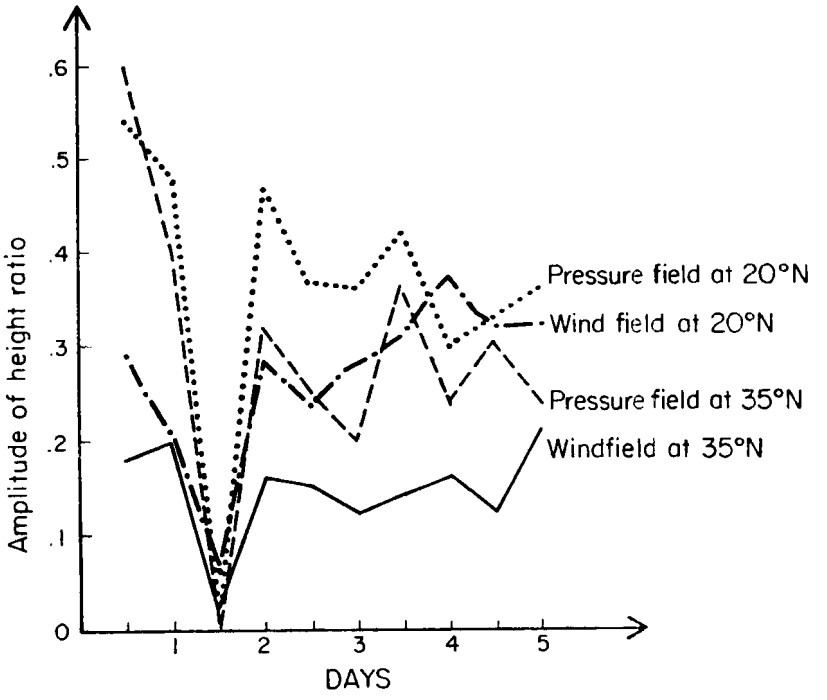

Fig. 138. Ratio of maximum height field perturbation in the southern hemisphere to that in the northern hemisphere for experiments D, E, F and G.

thirty six hours. This southern hemisphere response is most probably due to energy transmission by the fast moving mixed Rossby-gravity modes. At thirty-six hours, in all four experiments (D, E, F, G) there is a minimum in southern hemisphere response, probably the result of destructive interference between the southern hemisphere mixed Rossby-gravity modes. Thereafter, a steady increase in the ratio of height perturbation is seen. The maximum ratio for each experiment is somewhere between .5 and 1.0. Comparison of Fig. 138 with Fig. 131 reveals that for the wavenumber one experiments the southern hemisphere response is approximately an order of magnitude greater than in the wavenumber six experiments.

8.5 Conclusions

Gradient adjustment on a planetary scale has been crudely investigated using a barotropic model. Figures 139a, b and 140 a, b depict schematically the response of the model to wavenumber one forcing. Poleward of the perturbations, the earth's rotation, acting on fluid diverging from the high, (and converging into the low) leads to rotation and consequently minimizes divergence/convergence. Equatorward of the high perturbation the air is free to diverge in a region of low (and decreasing) Coriolis parameter. Associated with this divergence is a high (or bump on the upper free surface of the fluid). With time this high moves rapidly southwards as shown on Fig. 139b. At 24 hours the southward travelling high and low upper free surface perturbations have travelled deep into the Southern Hemisphere. Figure 140a shows the schematic streamline height chart and Fig. 140b the cross-section through the parent high in the Northern Hemisphere and ridging it has generated both on the equator and in the Southern Hemisphere.

Of the imposed forcings, from Fig. 138, it could clearly be seen that a mass field forcing which is equivalent barotropic in nature can effeciently generate equatorial east-west pressure gradients, on a time scale of one to two days. From the earlier study of cold surge data, a suggested atmospheric analog to this type of forcing would be anticyclogensis through the entire troposphere. It should, however, be recognized that in the atmosphere, anticyclogenesis occurs from 40^{o}N to 20^{o}N, with a wind surge from 35^{o}N to 10^{o}N, so both wind and mass fields are being forced simultaneously.

The energy propagation from the midlatitudes to the deep tropics appears sensitive to the presence of a background wind in so much as it

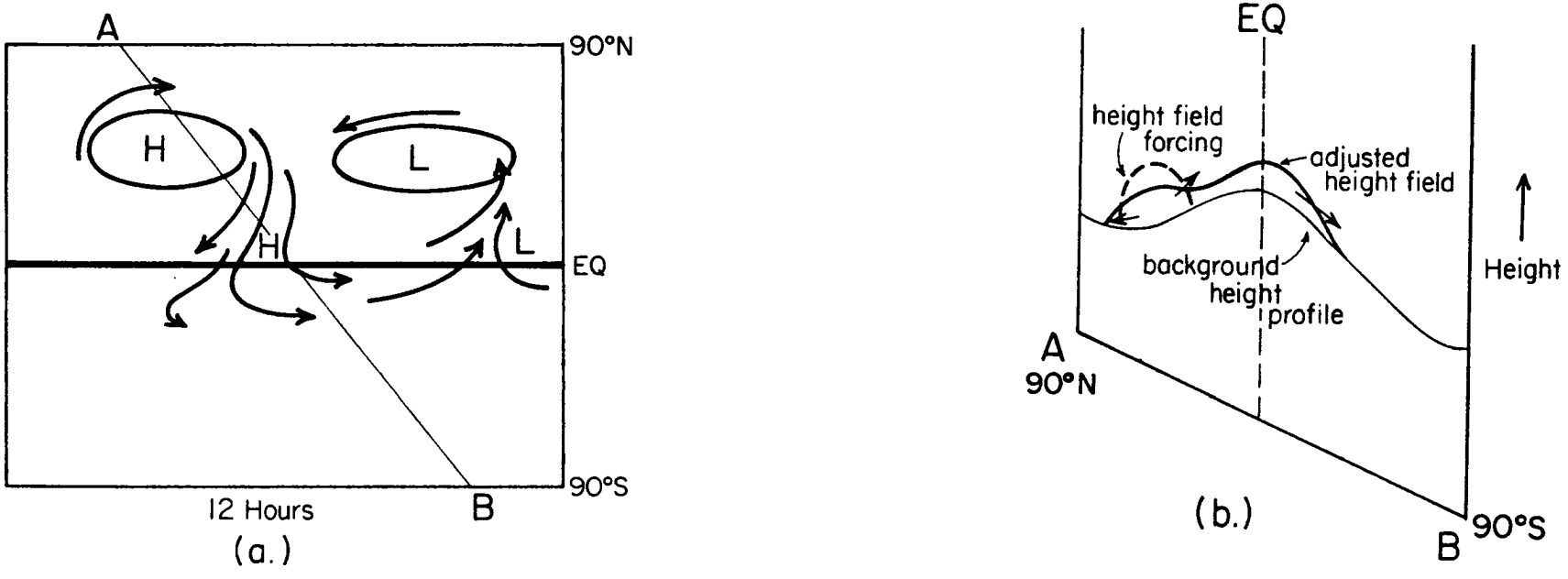

Fig. 139a-b. (a) Schematic plan view of the streamline and height perturbation fields after 12 hours of integration in experiment C. (b) Schematic cross-section of the height field for experiment C at 24 hours.

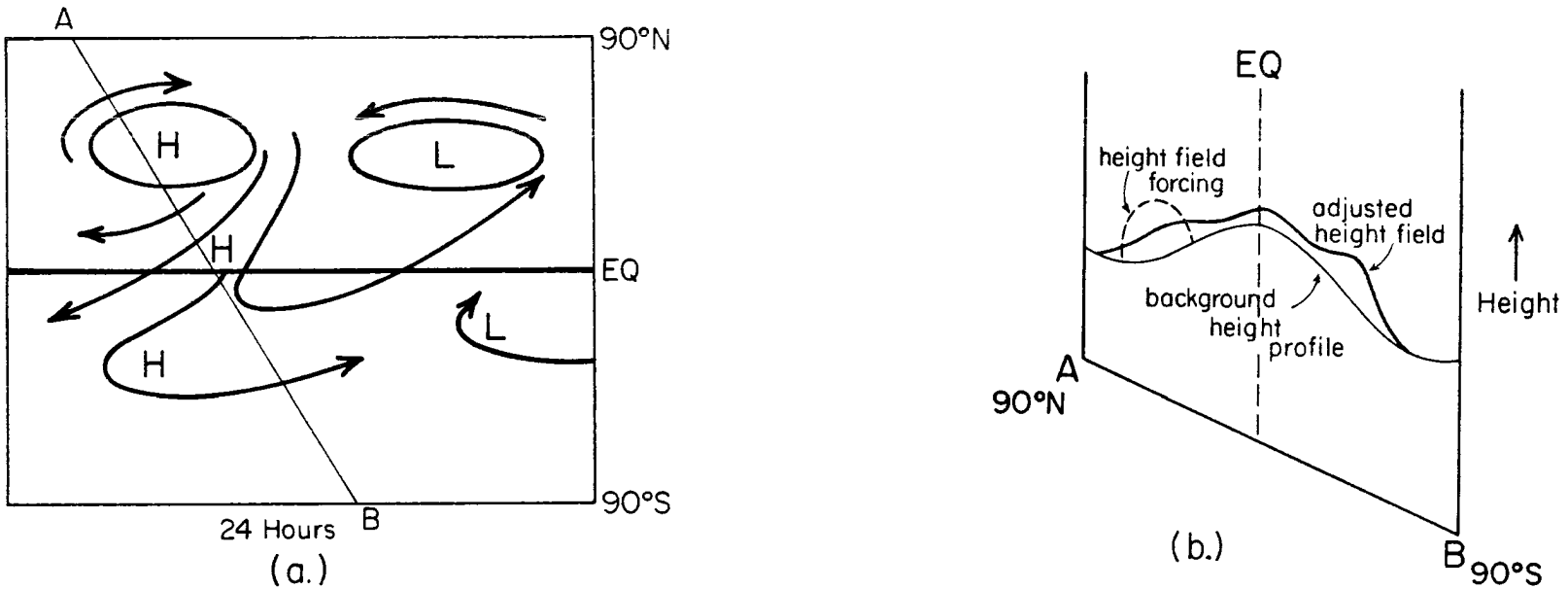

Fig. 140a-b. (a) Schematic streamline and height perturbation fields for experiment C at 24 hours. (b) Schematic cross-section of the height field for experiment C at 24 hours.

modifies the Rossby radius of deformation. Easterly winds do not appear to form critical areas through which energy may not propagate. The reason for this result, which is at variance with Charney's (1969) hypothesis, may be that the assumptions in his model were overly restrictive and unrepresentative of the atmosphere. In particular, the assumptions of non divergence and a constant background wind profile (u_o) of infinite extent are not consistent with observed cold surge characteristics.

This series of simulations have answered a number of questions which the data posed. Can energy propagate from the midlatitudes of the winter hemisphere to the tropics, such that planetary scale Rossby waves are excited? Can easterly background winds prevent such interactions? Is it reasonable to postulate midlatitude anticyclogenesis as a tropical forcing mechanism? Can pressure rises be sustained on the equator? There are, of course, many questions raised by the crudity of these simulations. Perhaps the most pressing is what is the role of convection. Convection acts to 'link' the upper and lower levels in the tropics, giving rise to a two layer structure in the atmosphere, with upper ouflow anticyclones above surface low pressure areas. Is it then reasonable to use this model to justify the generation of equatorial east-west pressure gradients when it is known that accompanying such surges is deep, active monsoonal convection. Perhaps not, but until the important question of how the cumulus scale interacts with synoptic scale in the tropics is answered, such simulations do serve to illustrate how the atmosphere may respond to a forcing of the type observed.

9. CONCLUDING DISCUSSION

9.1 Summary

The essence of this paper is that the large scale circulation patterns play an important role in determining the likelihood of a tropical cloud cluster intensifying to become a cyclone. To understand completely the dynamics of tropical cyclone genesis, an understanding of the interactions between the cloud cluster (of radius $\simeq 4^{o}$) and its environment must be obtained. The data considered in this paper indicate that the interacting environment extends to at least 40^{o} either side of the cluster longitude and from the subtropical ridge in the winter hemisphere to the subtropical ridge in the summer hemisphere.

In order to demonstrate the role of the planetary scale flow fields during tropical cyclone genesis, data on a variety of time and space scales have been considered. A study of the climatology of storm genesis on a global basis revealed that for any ocean basin, the year to year variability in where genesis occurs, and how often, is quite great. Only changes on the general circulation scale can lead to such large scale systematic variations in genesis locations. Data were assembled for two very different years in an attempt to investigate which general circulation parameters showed the most variation between seasons. There were small variations in the thermodynamic parameters and larger changes in dynamic parameters. The McBride (1981b) vorticity shear parameters showed the largest changes between the seasons in a fashion which could explain the changing climatology. This was surprising in that McBride developed the parameter from a consideration of individual genesis events, but reassuring in that it relates to the essential physics of genesis.

From consideration of case study data it was noted that before genesis occurs in the summer hemisphere, there is often a cold surge towards the equator in the winter hemisphere, associated with anticyclogenesis behind polar fronts. These cold surges appeared to lead to pressure rises in the equatorial regions, most probably through cold air advection. This process proceeded very rapidly with strong pressure rises usually being observed simultaneously (or as close to as was resolvable using the data available) through the whole winter hemisphere equatorward and westward of the baroclinic trough. In the equatorial regions pressure rises of around one to two millibars were observed on a scale of 20^{o} to 30^{o} longitude by 10^{o} latitude. The westerly monsoon winds appeared to adjust to this mass field forcing by undergoing a 'down the pressure gradient' acceleration. The data showed the enhanced westerlies to be through a deep layer of the atmosphere (at least surface to 500 mb). Aloft a strengthened return flow from summer to winter hemisphere, in a layer 300 mb to 100 mb was observed during surges.

A number of criteria were proposed by which a surge capable of influencing ITCZ disturbances could be identified. Many storms were preceded by a winter hemisphere surge, however, it was obvious that storm genesis could proceed without apparent forcing from the winter hemisphere (about 20% of the cases). The criteria proposed pertained only to surface charts as they contain the most detailed information available to forecasters. The need for favorable upper flow patterns is seen in the case studies, however, a surface based forecast method would no doubt have the greatest utility. A similar survey of non-developing depressions is required to establish how often these enhanced monsoon

westerlies preceed dissipation of clusters. Without such a survey a reliable forecast technique cannot be developed. It is planned to build a non-developing depression data set and carry out such a survey.

By compositing midlatitude height fields for quiet and active periods for a large number of days, it was possible to determine which midlatitude flow features typically preceded tropical cyclone genesis. Some of the important conclusions drawn from this work were that the forcing from northern to southern hemisphere during the southern hemisphere summer is quite similar to that operating in the other direction six months later. A minimum of baroclinic action poleward of the developing disturbance is favorable with an upper level (200 mb) tropical upper tropospheric trough type disturbance impinging on it. Baroclinic action pushing relatively close to the equator in the winter hemisphere appears to be a consistent feature of these composites, which agrees well with the observations of highly mobile winter hemisphere troughs in the case study data. Furthermore, strong anticyclogenesis can be seen developing through the troposphere (surface to 200 mb) poleward and west of the trough. Because of data deficiencies equatorward of 20^{o} latitude, it was difficult to draw conclusions concerning pressure tendencies in locations where it would be highly informative to do so.

A study of composite tropical wind fields revealed flow anomalies between quiet and active periods which indicated the two cases treated in Chapter 3 were representative of those situations generaly preceding tropical cyclone genesis. The composite pre genesis situation contains a more intense Hadley cell between winter and summer hemisphere subtropical ridges and the ITCZ. Using a wind field only data set in

the Atlantic Ocean basin, similar results have been obtained. Once again between three and one day before tropical cyclone genesis the greatest changes in the large scale flow fields occur at large distances from the cloud cluster, on the equatorial side. These results will be described more fully in a forthcoming report.

The angular momentum transports into the composite tropical depressions three days before tropical cyclone genesis demonstrated a supply of cyclonic angular momentum, through the 10^{o} radius, exceeding frictional dissipation. The data indicate these systems were spinning up at around 1 m/s/d. The composite depressions one day before genesis were diagnosed as spinning up at around 0.5 m/s/d. The southern hemisphere quiet period depression was spinning down at 1 m/s/d while for the northern hemisphere quiet period depression the net import of cyclonic angular momentum was very nearly balanced by frictional losses, indicating that no intensification could be expected. Analysis of these angular momentum transports at 10^{o} radius further reinforced the belief that favorable interaction between the cluster and its environment is crucial if genesis is to occur.

In Chapters 7 and 8 a change of approach to the problem was employed. The observational data clearly show the wind and mass fields in the winter hemisphere to be undergoing strong forcing during periods of intense baroclinic activity. In order to obtain an insight into how the energy derived from baroclinic action in the westerlies may propagate equatorward, driving subtropical and equatorial wind and mass fields out of balance, the shallow water equations using spherical geometry, were solved. Experiments showed that external mode simulations, with mass field forcing in the winter hemisphere, most

closely match the short time scale of southern hemisphere response, observed in the data. The induced wind field perturbations act to increase the westerly wind in equatorial regions and then planetary scale wind and mass perturbations are established in the southern hemisphere.

When perturbations in the thickness field were established on and near the equator in the first internal mode simulations, the shear in the wind field established was in the same sense as that observed in the data. That pressure rises can be maintained in equatorial regions, through mass field forcing, without a total partitioning of energy to gravity waves, reinforces the belief that the observed equatorial pressure rises are significant.

In summary, both the observations and the modeling work support the hypothesis that events in the winter hemisphere baroclinic zones can strongly influence the wind fields equatorward of the ITCZ. The composite analyses also reveal the need for a favorable summer hemisphere subtropical environment for incipient depressions.

9.2 Suggestions for Future Work

The central theme of this paper has been to document the role the large scale circulation patterns play in tropical cyclone genesis. In doing so a number of questions have arisen which have not been fully answered. From a forecasting point of view the most pressing is, how often do tropical cloud clusters experience accelerated monsoon flow equatorward and not intensify. A survey of non-developing depressions in both the northwest Pacific and Australian region is necessary and it is hoped it will be performed. However, it should be noted that such a survey would in some sense repeat the work of McBride (1981b). In a

study of both non-developing and developing depressions it was found that upper to lower level vorticity shear was an excellent genesis forecast tool. The accelerated monsoon flow is causally linked to increasing low level cyclonic vorticity in the ITCZ region, and so increasing the upper to lower level vorticity shear.

There also is a need to document more fully the meridional teleconnections or energy exchanges, which operate between the midlatitudes and deep tropics. These teleconnections have been briefly touched on within this paper but require further study, particularly those cloud bands which appear to originate around the equator and propagate polewards in the summer hemisphere.

The composite study presented in Chapter 6 was incomplete due to the lack of thermodynamic parameters available. A data set is presently being built which will allow for the further investigation of the magnitude of east-west equatorial pressure gradients and the degree of balance between wind and mass fields in the midlatitude and tropics during surges.

Finally, an attempt should be made to simulate the effects of winter hemisphere cold surges on the Hadley cell in a multilayer numerical model which contains a realistic heating parameterization. Care should be taken in such a simulation to leave within the model a full wave spectrum to enable adjustment to external forcings to be as realistic as possible.

ACKNOWLEDGEMENTS

Without the support, guidance and encouragement of Prof. William M. Gray this research would never have been performed. The author deeply appreciates this educational experience given to him by William Gray over the past three years.

The author has also been fortunate to have had invaluable scientific assistance from Dr. J. Tribbia and Mr. G. J. Holland. Joe Tribbia willingly made the numerical model, described in Chapter 7, available to the author and spent many hours describing its operation in order that the author could modify it for his own use. Greg Holland provided the programs to compute the angular momentum fluxes and many challenging discussions.

The author would also like to acknowledge the assistance given him by Rex Falls and Bruce Neal, two gentlemen who helped make this study program possible.

The author is also deeply appreciative of the fine technical support provided by Barbara Brumit, Edwin Buzzell, Grant Burton, Cindy Schrandt, Norine Halley and many others who have worked for Prof. Gray over the past three years.

The author has also gained much from discussions with all the students and research associates associated with Prof. Gray's project: Cheng Shang Lee, Johnny Chan, Ken Dropco, Bob Merrill, Jianmin Xu, Dev Sikka, Bill Fingerhut, Edwin Nunez and John McBride.

During the course of this research a great deal of data has been analyzed. Many people have contributed to making it available. Some of those in Australia have been: Mark Williams, Helen Pearce and Terry Skinner. In America: all of those associated with Roy Jenne's section

at the National Center for Atmospheric Research, Boulder, Colorado, Dr. U. Radok and Scott Woodruff at CIRES, Boulder, Colorado and also Yi-Hui Ding of Colorado State University.

The author would also like to thank his committee, Dr. W. Schubert, Dr. D. Stevens, Dr. R. Johnson and Dr. P. Brockwell, for scientific guidance and reviewing the manuscript.

Finally, the author would like to thank Narelle for her infinite patience.

This research has been primarily supported by the US National Science Foundation No. ATM-7923591 with supplementary support from the Australian Bureau of Meteorology.

REFERENCES

Atkinson, G. D., 1971: Forecasters guide to tropical meteorology. Tech. Report No. 240, Air Weather Service (MAC), United Air Force, 297 pp.

Arnold, C. P., 1977: Tropical cyclone cloud and intensity relationships. Atmos. Sci. Paper No. 277, Colo. State Univ., Ft. Collins, CO, 154 pp.

Ballenzweig, E. M., 1956: Seasonal variations in the frequency of north Atlantic tropical cyclones related to the general circulation. Proceedings from the tropical cyclone symposium, Brisbane, Dec. 10-16, Director of Meteorology, Melbourne, Australia, 37-70.

Bennett, J. R. and J. A. Young, 1971: The influence of latitudinal wind shear upon large scale wave propagation into the tropics. Mon. Wea. Rev., 99, 202-214.

Bjerknes, J., 1969: Atmospheric teleconnections from the equatorial Pacific. Mon. Wea. Rev., 97, 162-172.

Carlson, T. N., 1969: Hurricane genesis from disturbances formed over Africa. Mar. Wea. Log., 13, 197-202.

Carlson, T. N., 1971: Apparent relationship between sea surface temperature of the tropical Atlantic and the development of African disturbances into storms. Mon. Wea. Rev., 99, 309-310.

Chang, C. P., 1977: Some theoretical problems of the planetary scale monsoons. J. Pure Appl. Geophys., 115, 1089-1109.

Chang, C. P., J. E. Erikson and K. M. Lau, 1979: Northeasterly cold surges and near equatorial disturbances over the winter MONEX area during December 1974: Part I: Synoptic aspects. Mon. Wea. Rev., 107, 812-829.

Chang, C. P. and K. M. Lau, 1980: Northeasterly cold surges and near equatorial disturbances over the winter MONEX area during December 1974: Part II: Planetary-scale aspects. Mon. Wea. Rev., 108, 298-312.

Charney, J. G., 1963: A note on large scale motions in the tropics. J. Atmos. Sci., 20, 607-609.

Charney, J. G., 1969: A further note on large scale motions in the tropics. J. Atmos. Sci., 26, 182-185.

Charney, J. G. and P. G. Drazin, 1961: Propagation of planetary-scale disturbances from the lower into the upper troposphere. J. Geophys. Res., 66, 83-109.

Charney, J. G. and A. Eliassen, 1964: On the growth of the hurricane depression. J. Atmos. Sci., 21, 68-74.

REFERENCES (cont'd)

Cressman, G., 1959: An operational objective analysis system. Mon. Wea. Rev., 87, 367-374.

Crutcher, H. L., 1961: Meridional cross-sections of upper winds over the northern hemisphere. Tech. Paper No. 41, US Weather Bureau, Dept. of Commerce, Washington, DC, 307 pp.

Deland, R. J., 1964: Traveling planetary waves. Tellus, 16, 271-273.

Ding, Yi-Hui and E. R. Reiter, 1980a: A preliminary study of the variability in the frequency of typhoon formation over the west Pacific Ocean. Environmental Research Paper 28, Colo. State Univ., Ft. Collins, CO, 15 pp.

Ding, Yi-Hui and E. R. Reiter, 1980b: A further study of the variability in the frequency of tyhoon formation over the west Pacific Ocean. Environmental Research Paper 27, Colo. State Univ., Ft. Collins, CO, 23 pp.

Ding, Yi-Hui and E. R. Reiter, 1981: A climatological study of some dynamical conditions influencing the variability in typhoon formation over the west Pacific Ocean. Environmental Research Paper 28, Colo. State Univ., Ft. Collins, CO, 15 pp.

Eliassen, A. and E. Palm, 1961: On the transfer of energy in stationary mountain waves. Geofysiske Publikasjoner, 22, 23 pp.

Eliassen, E. and B. Machenhauer, 1965: A study of the fluctuations of the atmospheric planetary flow patterns represented by spherical harmonics. Tellus, 17, 220-238.

Eliassen, E. and B. Machenhauer, 1969: On the observed large scale atmospheric wave motion. Tellus, 21, 149-166.

Fingerhut, W. A., 1980: Tropical cyclone genesis - numerical modeling inferences. Atmos. Sci. Ph.D. Thesis, Colo. State Univ., Ft. Collins, CO, 155 pp.

Flohn, H. and H. Fleer, 1975: Climatic teleconnections with the equatorial Pacific and the role of ocean-atmosphere coupling. Atmosphere, 13, 99 pp.

Frank, W. M., 1977a: The structure and energetics of the tropical cyclone, I: Storm structure. Mon. Wea. Rev., 105, 1119-1135.

Frank, W. M., 1977b: The structure and energetics of the tropical cyclone, II: Dynamics and energetics. Mon. Wea. Rev., 105, 1136-1150.

REFERENCES (cont'd)

Fujita, T. T., K. Watanabe and T. Izawa, 1969: Formation and structure of equatorial anticyclones caused by large-scale cross-equatorial flows determined by ATS-I photographs. J. Appl. Meteor., 8, 649-667.

Fulton, S. R. and W. H. Schubert, 1980: Geostrophic adjustment in a stratified atmosphere. Atmos. Sci. Paper No. 326, Colo. State Univ., Ft. Collins, CO, 97 pp.

Gauntlett, D. J., R. S. Seaman, W. R. Kininimonth and J. C. Langford, 1972: An operational evaluation of a numerical analysis-prognosis system for the southern hemisphere. Aust. Met. Mag., 20, 61-82.

Gorshkov, S. G., 1974: World ocean atlas. S. G. Goshkov (Ed.), Pergamon Press, 640 pp.

Gray, W. M., 1967: Global view of the origin of tropical disturbances and storms. Mon. Wea. Rev., 96, 55-73.

Gray, W. M., 1973: Cumulus convection and large scale circulations, I: Broadscale and meso-scale considerations. Mon. Wea. Rev., 101, 839-855.

Gray, W. M., 1975: Tropical cyclone genesis. Atmos. Sci. Paper No. 234, Colo. State Univ., Ft. Collins, CO, 121 pp.

Gray, W. M., 1979: Hurricanes/their formation, structure and likely role in the tropical circulation. Supplement to Meteorology Over the Tropical Oceans. Published by RMS, James Glaisher House, Grenville Place, Bracknell, Berkshire, RG 12 1BX, D. B. Shaw, ed., 155-218.

Gray, W. M., 1981: Recent advances in tropical cyclone research from rawinsonde composite analysis. World Meteorological Organization Report, Geneve, Switzerland, 407 pp.

Gustafon, A. F. and J. E. McDonell, 1965: The derivation of first guess fields for objective analyses, 1000 mb to 500mb. NMC Tech. Memo No. 31, 6 pp.

Hack, J. J. and W. H. Schubert, 1980: The role of convective-scale processes in tropical cyclone development. Atmos. Sci. Paper No. 330, Colo. State Univ., Ft. Collins, CO, 206 pp.

Haggard, N. H., 1965: Climatological-synoptic patterns associated with north Atlantic tropical cyclogenesis. Geo. Intern., 5, 97-113.

Holland, G. J., 1981: Angular momentum transports in tropical cyclones. Atmos. Sci. Paper, Colo. State Univ., Ft. Collins, CO, (in preparation).

REFERENCES (cont'd)

Holton, J. R., 1979: An introduction to dynamic meteorology. 2nd Ed., Academic Press, 391 pp.

Hoskins, B. J., A. J. Simmons and D. G. Andrews, 1977: Energy dispersion in a barotropic atmosphere. Quart. J. Roy. Meteor. Soc., 103, 553-567.

Hoskins, B. J. and D. Karoly, 1981: The steady, linear response of a spherical atmosphere to thermal and orographic forcing. J. Atmos. Sci., 38, (in press).

Huschke, R. E., (ED), 1959: Glossary of Meteorology. American Meteorological Society, 45 Beacon Street, Boston, MA, 02108, 638 pp.

Jordan, C. L., 1958: Mean soundings for the West Indies area. J. Meteor., 15, 91-97.

Julian, P. R. and R. M. Chervin, 1978: A study of the southern oscillation and Walker Circulation phenomenon. Mon. Wea. Rev., 106, 1433-1451.

Kasahara, A., 1976: Normal modes of ultralong waves in the atmosphere. Mon. Wea. Rev., 104, 669-690.

Kasahara, A., 1977: Numerical integration of the global barotropic primitive equations with Hough harmonic expansions. J. Atmos. Sci., 34, 687-701.

Kasahara, A., 1980: Effect of zonal flows on the free oscillations of a barotropic atmosphere. J. Atmos. Sci., 37, 917-929.

Lee, C. S., 1981: Vertical rearrangement of tangential momentum in tropical cyclones. Atmos. Sci. Paper, Colo. State Univ., Ft.Collins, CO, (in preparation).

Lilly, D. K., 1965: On the computational stability of numerical solutions of time-dependent non-linear geophysical fluid dynamics problems. Mon. Wea. Rev., 93, 11-26.

Longuet-Higgins, M. S., 1968: The eigenfunctions of Loplace's tidal equations over a sphere. Phil. Trans. Roy. Soc. London, A262, 511-607.

Madden, R., 1978: Further evidence of traveling planetary waves. J. Atmos. Sci., 35, 1605-1618.

Mahrt, L. J., 1972: A numerical study of the influence of advective accelerations in an idealized low latitude, planetary boundary layer. J. Atmos. Sci., 29, 1477-1484.

REFERENCES (cont'd)

Mak, Man Kin, 1969: Laterally driven stochastic motions in the tropics. J. Atmos. Sci., 26, 41-64.

Malkus, J. S. and H. Riehl, 1960: On the dynamics and energy transformations in steady state hurricanes. Tellus, 12, 1-20.

McBride, J. L., 1981a: Observational analysis of tropical cyclone formation, Part I: Basic description of data sets. J. Atmos. Sci., 38, 1117-1131.

McBride, J. L. and R. Zehr, 1981b: Observational analysis of tropical cyclone formation, Part II: Comparison of non-developing versus developing systems. J. Atmos. Sci., 38, 1132-1151.

McBride, J. L., 1981c: Observational analysis of tropical cyclone formation, Part III: Budget analysis. J. Atmos. Sci., 38, 1152-1166.

Morgan, M. R., 1965: Outbreaks of Antarctic air in relation to the hurricane season 1962. Dept. of Transport, Meteorology Branch, Canada, CIR 4235, TEC 571, 23 pp.

McDonell, J., 1962: An objective analysis system used at the national meteorological center. Tech. Memo. No. 23, US National Meteorological Center, Suitland, MD, 31 pp.

Namias, J., 1969: On the cause of the small number of Atlantic hurricanes in 1968. Mon. Wea. Rev., 97, 346-348.

Namias, J., 1973: Hurricane Agnes: An event shaped by large scale air-sea systems generated during antecedent months. Quart. J. Roy. Meteor. Soc., 99, 506-519.

Nitta, T. and M. Yanai, 1968: Barotropic instability of the equatorial easterly current. Proceedings WMO/IUGG Symposium on Numerical Weather Prediction, Japan Meteor. Agency Tech. Report No. 67, III, 1-4.

Nunez, E., 1980: Tropical cyclone structure and intensity change. Atmos. Sci. Ph.D. Thesis, Colo. State Univ., Ft. Collins, CO, 192 pp.

Ooyama, K. V., 1964: A dynamical model for the study of tropical cyclone development. Geofis. Int., 4, 187-198.

Ooyama, K. V., 1979: Numerical simulation of the life cycle of tropical cyclones. J. Atmos. Sci., 26, 3-40.

Palmen, E., 1948: On the formation and structure of tropical hurricanes. Geophysica (Helsinki), 3, 26-38.

REFERENCES (cont'd)

Palmen, E. and H. Riehl, 1957: Budget of angular momentum and energy in tropical storm. J. Meteor., 14, 150-159.

Pelissier, J. M., 1979: Operational techniques for forecasting tropical cyclone intensity and movement. WMO Report No. 528, J. M. Pelissier (Ed.), Secretariat of the World Meteorological Organization, Geneve, Switzerland, 127 pp.

Pfeffer, R. L., 1958: Concerning the mechanics of hurricanes. J. Meteor., 15, 113-120.

Ramage, C. S., 1974: Monsoonal influences on the annual variation of tropical cyclone development over the India and Pacific Oceans. Mon. Wea. Rev., 102, 745-753.

Reed, R. J. and E. E. Recker, 1971: Structure and properties of synoptic scale wave disturbances in the equatorial western Pacific. J. Atmos. Sci., 28, 1117-1133.

Riehl, H. and J. S. Malkus, 1961: Some aspects of hurricane Daisy, 1958. Tellus, 13, 181-213.

Saucier, W. J., 1955: Principles of meteorological analysis. The Univ. of Chicago Press, 438 pp.

Schaefer, J. T. and C. A. Doswell, 1980: The theory and practical application of antitriptic balance. Mon. Wea. Rev., 108, 746-756.

Schubert, W. H., J. J. Hack, P. L. Silva Dias and S. R. Fulton, 1980: Geostrophic adjustment in an axisymmetric vortex. J. Atmos. Sci., 37, 1464-1484.

Seaman, R. S., R. L. Falconer and J. Brown, 1977: Application of a variational blending technique to numerical analysis in the Australian region. Aust. Met. Mag., 25, 3-23.

Silberman, I., 1954: Planetary waves in the atmosphere. J. Meteor., 11, 27-34.

Silva Dias, P. L. and W. H. Schubert, 1979: The dynamics of equatorial mass-flow adjustment. Atmos. Sci. Paper No. 312, Colo. State Univ., Ft. Collins, CO, 203 pp.

Van Loon, H., J. J. Taljaard, R. L. Jenne and H. L. Crutcher, 1971: Climate of the upper air: Southern hemisphere, Vol. II: Zonal geostrophic winds. NAVAIR 50-IC-56, National Climatic Center, Federal Building, Asheville, NC, 28801.

Walker, G. T. and E. W. Bliss, 1932: World Weather V. Mem. Roy. Meteor. Soc., 4, 53-84.

REFERENCES (cont'd)

Wallace, J. M. and D. S. Gutzler, 1981: Teleconnections in the geopotential height field during the northern hemisphere winter. Mon. Wea. Rev., 109, 784-812.

Webster, P. J., L. Chou and K. M. Lau, 1977: Mechanisms effecting the state, evolution and transition of the planetary scale monsoon. J. Pure Appl. Geophys., 115, 1463-1491.

Webster, P. J. and K. M. Lau, 1977: A simple ocean-atmosphere climate model: Basic model and a simple experiment. J. Atmos. Sci., 34, 1063-1084.

Whitaker, W. D., 1967: Quantitative determination of heat transfer from sea to air during passage of hurricane Betsy. M.S. Thesis, Texas A and M Univ., College Station, TX, 65 pp.

Williams, K. T. and W. M. Gray, 1973: A statistical analysis of satellite observed trade wind cloud clusters in the western north Pacific. Tellus, 21, 313-336.

Williams, M., 1981: Interhemispheric interaction during winter MONEX. Paper presented at FGGE/MONEX Conference, Tallahassee, FL, 12-17 January, 4 pp.

Yanai, M., S. Esbensen and J. H. Chu, 1973: Determination of bulk properties of tropical cloud clusters from large scale heat and moisture budgets. J. Atmos. Sci., 30, 611-627.

Zehr, R., 1976: Tropical disturbance intensification. Atmos. Sci. Paper No. 259, Colo. State Univ., Ft. Collins, CO, 91 pp.

APPENDIX A

The following figures portray the 1977-1975 difference fields for the five tropical cyclone genesis parameters along with the areas (shaded) where those parameters exceed the critical level specified in Chapter 3 of this paper.

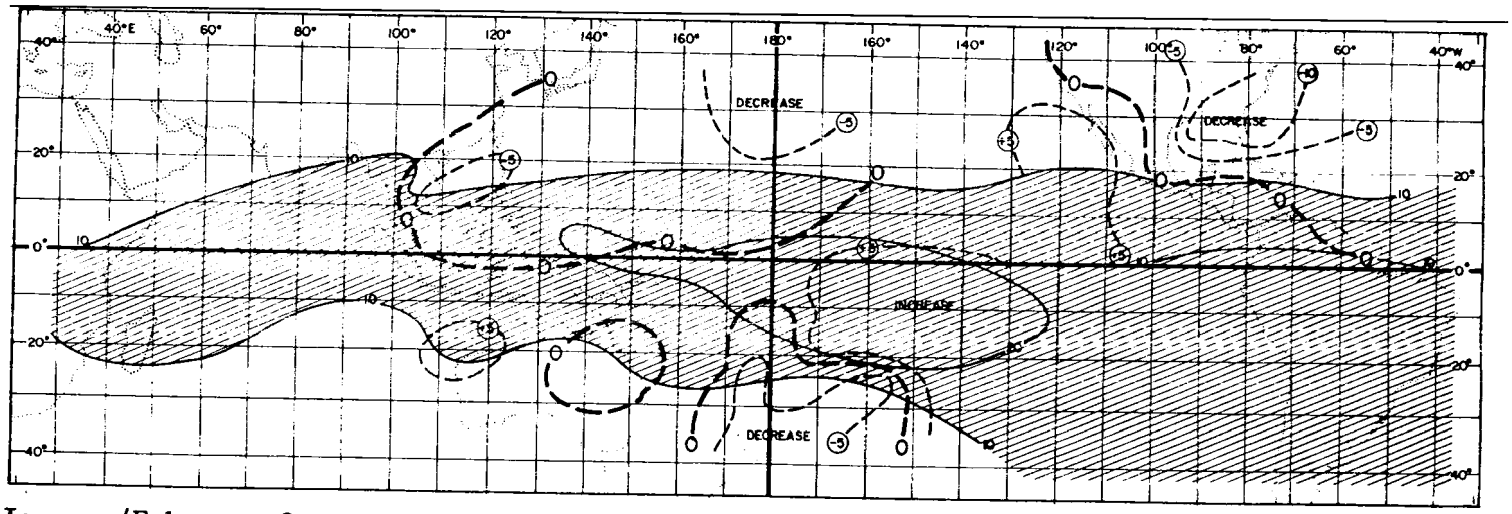

Fig. A1. January/February θ_e gradient difference chart, 1977 minus 1975 (^{o}K). The shaded areas had a θ_e gradient favorable for genesis in 1977 (^{o}K).

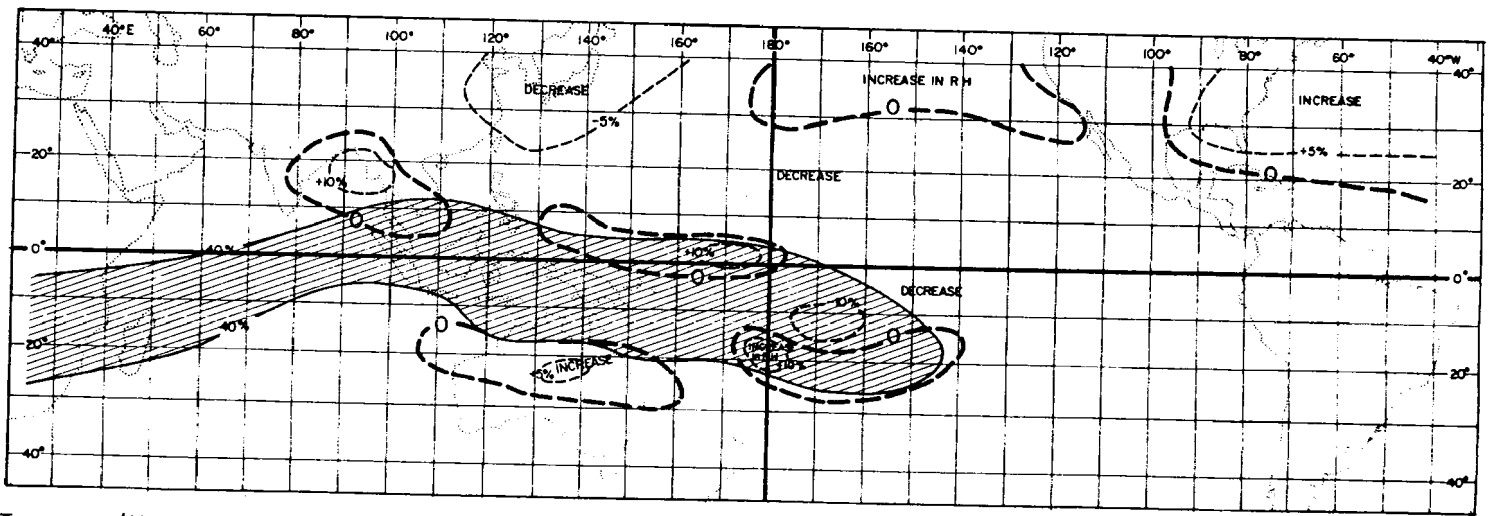

Fig. A2. January/February RH difference chart, 1977 minus 1975. The shaded areas had a favorable RH in 1977 (%).

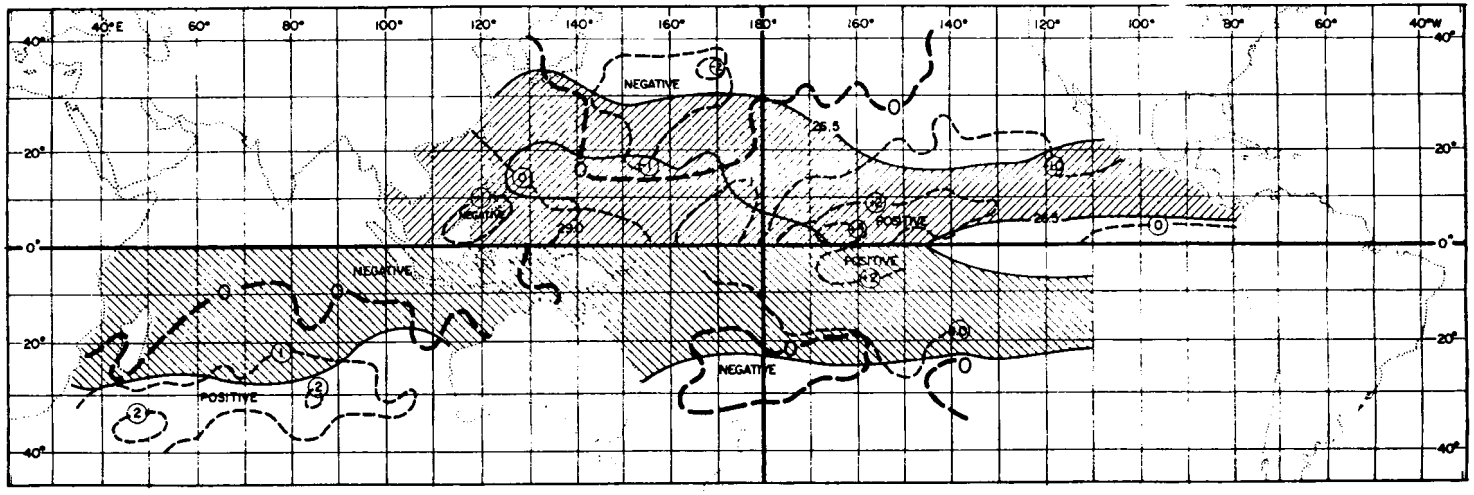

Fig. A3. Sea surface temperature difference chart 1977 minus 1975 (dashed curves). The southern hemisphere is for the January/February bimonthly means, the northern hemisphere the July/August means. The shaded areas had sea surface temperatures exceeding 26°C in the 1977 summers (°C).

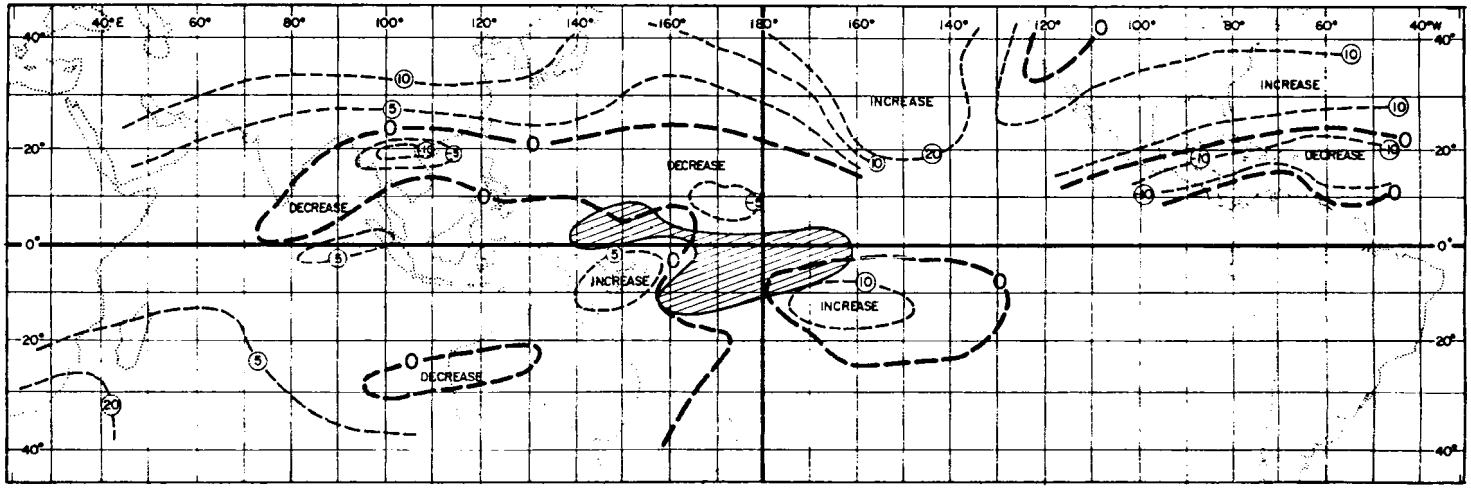

Fig. A4. January/February shear difference chart 1977 minus 1975 (dashed). The shaded areas had shear less than 5 m s^{-1}/650 mb in 1977 (m s^{-1}/650 mb).

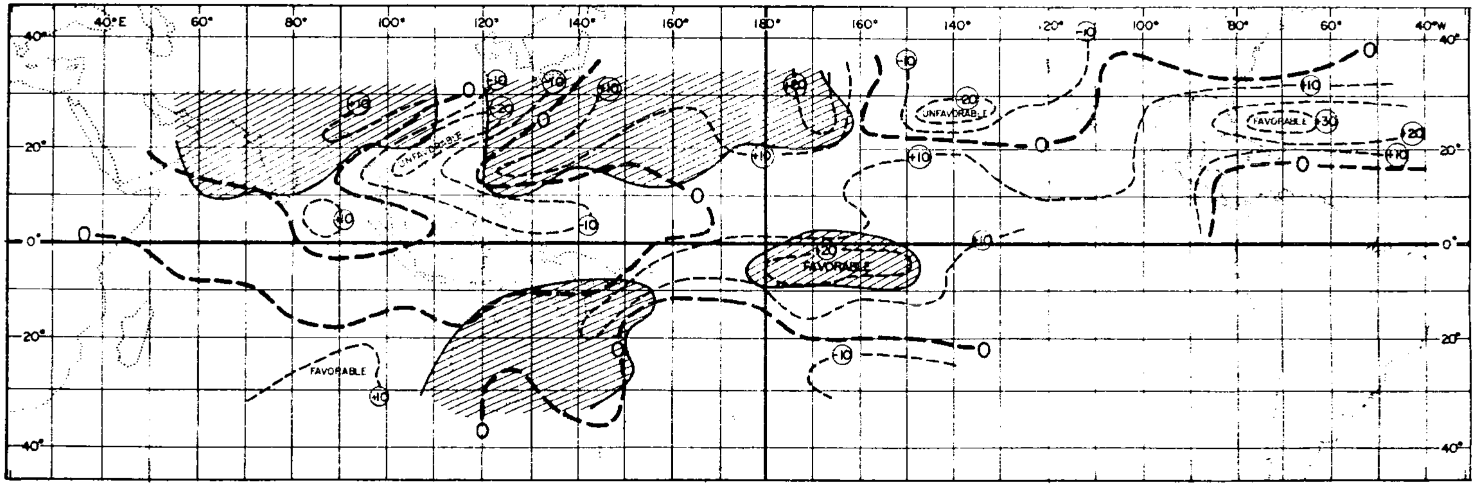

Fig. A5. January/February genesis potential difference chart, 1977 minus 1975 (dashed). The shaded areas had a genesis potential exceeding 15 x 10^{-6} s^{-1} in 1977 ($10^{-6}s^{-1}$).

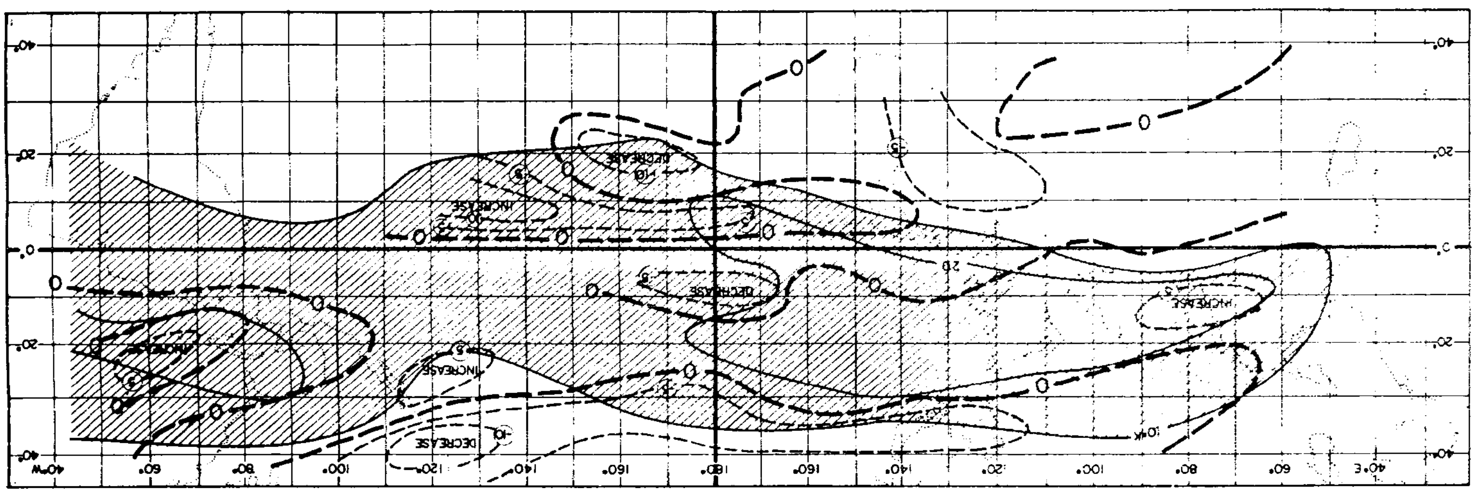

Fig. A6. July/August θ_e gradient difference chart, 1977 minus 1975 (dashed). Shaded areas had a favorable θ_e gradient in 1977 (^{o}K).

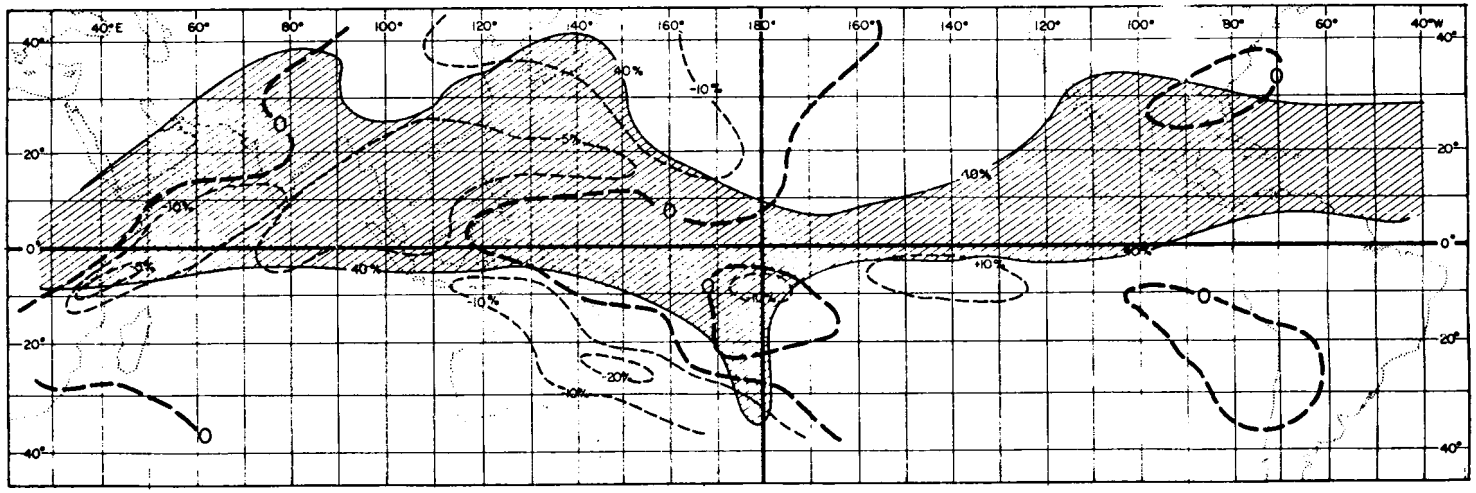

Fig. A7. July/August RH difference chart, 1977 minus 1975. Shaded areas had a favorable RH in 1977 (%).

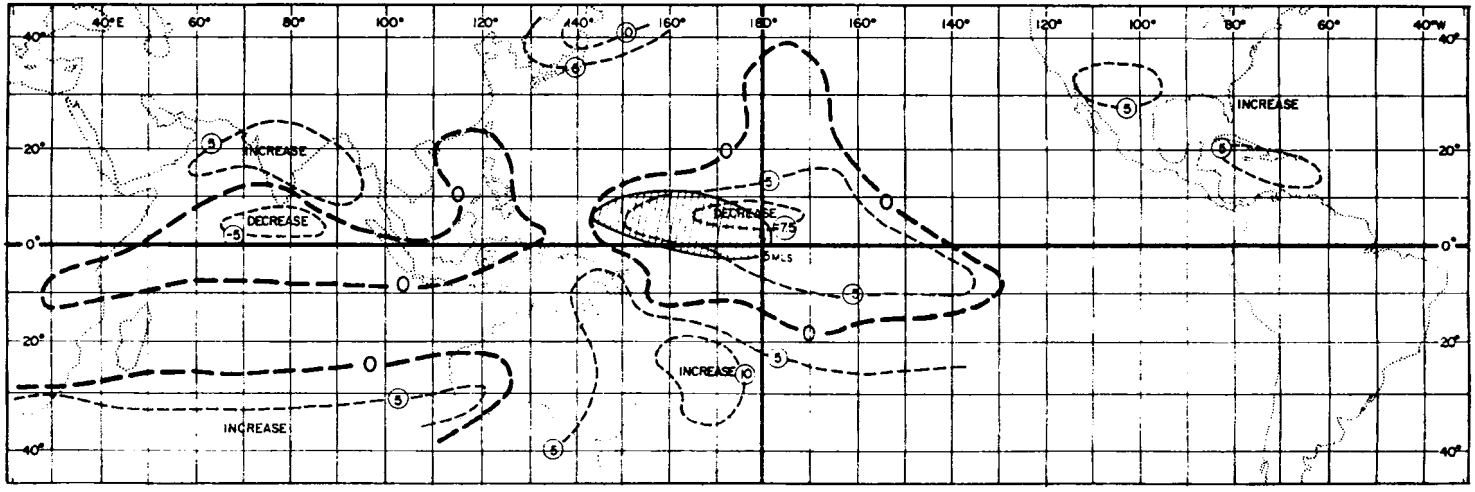

Fig. A8. July/August shear difference chart, 1977 minus 1975. Shaded areas had a favorable shear in 1977 ($m\ s^{-1}$ per 650 mb).

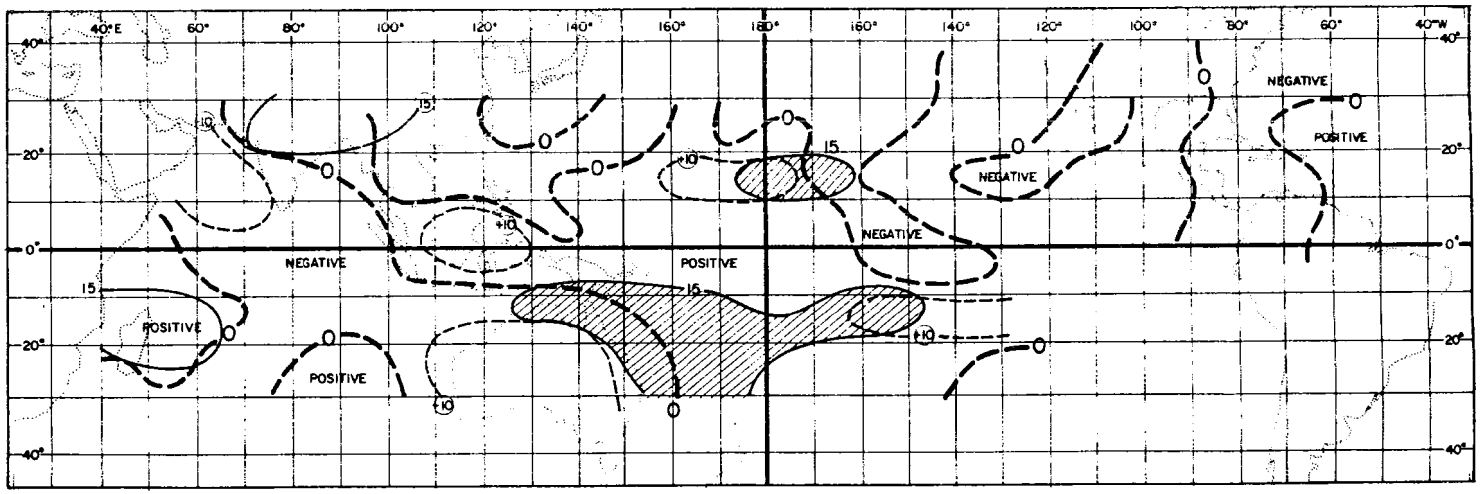

Fig. A9. July/August genesis potential parameter difference chart, 1977 minus 1975. Shaded areas had a favorable genesis potential in 1977 (10^{-6} s^{-1}).